Sensorimotor control of *Drosophila* copulation

A thesis submitted for the degree of

Doctor of Philosophy at the University of Oxford

by

Matthew Robertson Herbert

Wolfson College

Michaelmas 2020

Author’s declaration

I hereby declare that all the work reported in this thesis is my own, unless otherwise stated in the text. None of the work has been previously submitted for any other degree at any other institution. All sources are indicated by reference.

Matthew R. Herbert

For my parents

Abstract

Dipteran insects show a wide range of species-specific mating postures, and interspecific differences in the postures they adopt may reflect sexual selection acting on these traits. As with most sequences of motor action, mechanosensory inputs have long been thought to be important for the male to achieve and maintain this position, although until now we have understood very little about the function or properties of the sensory neurons involved.

In *Drosophila,* the conserved transcription factor *doublesex* (*dsx)* is required for the specification of both male and female sexual identity. One of the key roles played by *dsx* is regulating the development of a sexually dimorphic nervous system and recent work has shown that *dsx* is expressed in external mechanoreceptor neurons that adorn the male genitalia (herein termed male terminal sensilla; MTS). Targeted manipulation of these MTS neurons may help to elicit a deeper understanding of the functional organisation of sensorimotor circuits that aid in the maintenance of body posture, but so far these manipulations have proved difficult to achieve with a reasonable level of specificity due to the broad expression domain of developmental genes such as *dsx*.

To address this issue, in this thesis I have screened a number of both publicly available and novel genetic driver lines with the aim of establishing spatially restricted genetic access to MTS neurons. By identifying those lines labelling our cells of interest, not only can we develop a genetic toolkit for manipulating their function, but we can also gain insights into their properties by identifying, for example, the expression of mechanosensitive ion channels such as *nompC* or the excitatory neurotransmitter *ChAT*. After identifying a sufficient number of useful lines, I then developed a series of novel split-GAL4 hemidriver lines that when combined with another driver - for example dsx^{DBD} - reveal expression that is closely restricted to MTS neurons.

Following on from this, using the most suitable drivers that I have identified, I have performed a series of manipulations on MTS function in freely behaving male flies to quantify the effects on courtship and copulation. These results show clearly how sensory feedback from MTS neurons is important for mating posture, as even animals with only a small subset of MTS neurons being manipulated exhibit marked changes in mating posture. Effects on the likelihood and duration of copulation were also a common phenotype we identified in these manipulations, but we could not however identify any obvious effect of the aberrant mating posture on reproductive success.

Lastly, taking insight from our behavioural experiments, we have leveraged genetically encoded calcium indicators and the transsynaptic labelling technology; trans-*Tango,* to identify and visualize connections between sensory MTS neurons and upstream circuits in an attempt to establish a view of how body movement can be coordinated via communication between many independent proprioceptive organs. Altogether, the data presented herein represents the characterisation of a relatively simple circuit for the control of body posture that shows some remarkable capabilities to receive input from other regions of the body and ultimately feed into centres for higher order processing in the brain.

Table of Contents

Table of tables

Table of figures

Acknowledgements

Throughout my short career as a scientist I have been blessed to be able to surround myself with supportive and inspirational colleagues, mentors, and friends. It goes without saying that without the Goodwin group I would not have been able to complete this endeavour, but I also thank the McGregor and Nunes labs at Oxford Brookes for the support they showed me early on. I must also acknowledge my family, who this thesis is dedicated to. Although I'm sure they couldn't tell you what exactly any of my work is 'about', they have shown me unbelievable support through thick and thin to get to this point.

Whilst no amount of words can quite convey my gratitude, I would like to thank each member of the lab individually.

First and foremost, to my supervisor Stephen F. Goodwin, for giving me the opportunity to join his lab and pursue my interests in a supportive environment. Whilst I am sure that it cannot have been easy at points, his generosity and willingness to assuage my feelings of doubt and impostor syndrome were instrumental in the completion of this thesis.

To Megan Goodwin, your ace molecular skills taught me a lot in the early days and your willingness to cut through the faff in countless reports and talks has been vital for me. It didn't take me long to realise that you are the 'oracle' of the lab with a fantastic memory for obscure publications or reagents that had long been forgotten. Perhaps most importantly I learnt that if Megan thought something was a cool idea, then I could convince Stephen too!

To Aaron – I have always believed that the only way to get good at something is to surround yourself with people better than yourself. Working physically alongside you in the office was proof of this and I was regularly amazed at your technical proficiency, intellect, wit, and critical assessment of whatever topic we happened to be discussing in that moment. Perhaps most importantly though, you provided me a great friend to blow off some steam in the pub with, and reassurance in times of doubt that it will be alright in the end.

To Sebastian. It was fantastic having another PhD student in the lab with which to share the ups and downs of life in the lab. The way in which you proactively organise your thoughts was inspirational to me and I have filled many a notebook in an attempt to copy your methods (perhaps unsuccessfully). I will always remember the fun we had in Groningen together, the trips to the Uni club for drinks after an exhausting Friday (albeit rather early in the afternoon on some occasions), dancing in the various bad clubs of Oxford, and our jokes about whatever strange sexual innuendo Stephen might have made that day.

To Annika, your support with calcium imaging experiments reported here was indispensable, but more importantly your willingness to meet with me at odd times to discuss our experiments and your ability to pull together a quick matlab or python script to help with my analysis, was indispensable. I could not have presented all of

the data shown in chapter 5 without your help. Lastly, I always appreciated how you never answered off-the-cuff, but took a moment to pause and think deeply about whatever issue I might be facing before offering sound advice.

To Tetsuya, the human encyclopaedia of *Drosophila* neuroanatomy. Your knowledge was indispensable when writing up many of the results of this thesis. Your complete dedication to your work was both inspirational and at times daunting, but most importantly I thank you for always being willing to help me in the lab and generally offer your input whenever I needed it. Even once I have long been away from fly-work I don't believe I'll ever lose the ability to dissect a fly brain after being taught by such a master.

Deniz, although we didn't overlap in the lab for as long as some of the others, I always appreciated our conversations in the lab, often fly-pushing on a Saturday afternoon. What's more, I found that you brought a fresh breath of air into the group having just moved from the US and what I must imagine is a slightly different system than in the UK. I have a long list of biotechs to invest in, and places to visit in Seattle since we began our conversations!

And to Ammerins. Technicians are so often the unsung heroes of research groups but there is no doubt in my mind that the work you do is the glue that keeps the whole thing from falling apart. Your technical expertise is second to none in the wet lab and you have shown that here, as much of the credit for *R23F02-LexA* belongs to you. What I will remember most though is your brilliant, dry, Dutch sense of humour and your love of Rick and Morty posters for scolding newbies in the lab.

Lastly, I would like to thank my internal examiners; Professor Clive Wilson and Professor Scott Waddell for taking the time to discuss my project and length and provide constructive feedback whenever needed. The opportunity to discuss your science like this is often overlooked but it was an honour and invaluable experience.

Glossary

Anatomical Terms

Abdominal Ganglion	Abg
Abdominal nerve trunk	AbNT
Abdominal segment 9	A9
Anal sensory neuron	ASN
Antennal mechanosensory and motor centre	AMMC
Anterior optic tubercle	AOTU
Central nervous system	CNS
Dendritic arborization	da
Gnathal ganglion	GNG
Male terminal sensilla	MTS
Muscle of Lawrence	MOL
Sensory organ precursor	SOP
Superior lateral protocerebrum	SLP
Superior medial protocerebrum	SMP
Ventral nervous system	VNS
Ventrolateral protocerebrum	VLP

Genetic Terms

Abdominal-B	*Abd-B*

Acetylcholine	Ach
Activation domain	AD
Basic helix-loop-helix	bHLH
Canton-Special	CS
Channelrhodopsin-2	ChR2
Choline acetyltransferase	*ChAT*
Curly of Oster	*CyO*
decapentaplegic	*dpp*
Degenerin/epithelial sodium channel (protein family)	DEG/ENaC
DNA binding domain	DBD
doublesex	*dsx*
Doublesex isoforms (male/female)	Dsx^{M}/Dsx^{F}
ebony	*e*
embryonic lethal, abnormal vision	*elav*
engrailed	*en*
Enhanced green fluorescent protein	eGFP
Flippase recognition target	FRT
Flippase site-specific recombinase	FLP
fruitless	*fru*
Fruitless (protein)	Fru

Fruitless (male isoform)	Fru^M
G protein coupled receptor	GPCR
Genetically encoded calcium indicators	GECIs
GFP reconstitution across synaptic partners	GRASP
Glutamic acid decarboxylase 1	*Gad1*
Green Fluorescent Protein	GFP
head involution defective	*hid*
hedgehog	*hh*
Humeral	*Hu*
inactive	*iav*
Membrane-bound mouse lymphocyte marker CD8	mCD8
mini-white	*mw*
Minos-mediate integration cassette	MiMIC
nanchung	*nan*
neuronal Synaptobrevin	*nSyb*
no mechanoreceptor potential C	*nompC*
pickpocket	*ppk*
Pigment-dispersing factor (neuropeptide)	Pdf

Position effect variegation	PEV
Purinergic receptor P2X	$P2X_2$
Recombinase mediated cassette exchange	RMCE
Red fluorescent protein	RFP
RNA interference	RNAi
Serrate	*Ser*
Sex-lethal (gene)	*Sxl*
Sex-lethal (protein)	Sxl
shibire	*shi*
Stubble	*Sb*
Tetanus toxin	TNT
transformer (gene)	*tra*
Transformer (protein)	Tra
transformer-2 (gene)	*tra-2*
Transfomer-2 (protein)	Tra-2
Transient receptor potential channels (protein family)	TRP
Tryptophan hydroxlase	Trh
Upstream Activating Sequence	*UAS*
Vesicular Glutamate transporter	VGlut

Vesicular monoamine transporter	Vmat
white	*w*
Wild-type	WT
wingless	*wg*
Yeast Transcriptional Activator GAL4	GAL4
yellow	*y*

Measurements

Base pair	bp
Degrees Centigrade	°C
Hertz	Hz
Hour	hr
Kilobases	kb
Kilogram	Kg
Melting temperature	Tm
Microgram	µg
Microlitre	µL
Micrometre	µm
Micromolar	µM
Milliliter	mL
Millimolar	mM/mmol

Millinewton	mN
Millivolt	mV
Minute	min
Molar	M
Nanogram	ng

Behavioural Parameters

Courthsip Index	CI
Interpulse interval	IPI
Wing index	WI

Chemicals

7,11-heptacosadiene	7,11-HD
7,11-nonacosadiene	7,11-ND
Adenosine triphosphate	ATP
Carbon Dioxide	CO_2
Deoxyadenosine triphosphate	dATP
Deoxyribonucleic acid	DNA
Ethidium Bromide	EtBr
Ethylenediaminetetraacetic acid	EDTA
Messenger RNA	mRNA
Normal goat serum	NGS

Paraformaldehyde	PFA
PBS with 10% NGS	PTN
PBS with Triton-X	PBT
Phosphate buffered Saline	PBS
Ribonucleic acid	RNA

Computing and statistical terms

Analysis of variance	ANOVA
Audo video interleave file	.avi
DeepLabCut	DLC
Janelia Automatic Animal Behaviour Annotator	JAABA
Leica image file format	.lif
micro-fly movie format	.ufmf/µfmf
Standard error of the mean	sem

Miscellaneous

Bloomington *Drosophila* stock centre	BDSC
Caltech Multiple Walking Fly Tracker	Ctrax
Cuticular hydrocarbon	CHC
Environmentally controlled room	ECR
Heat shock	hs
P transposable element	P-element

Polymerase chain reaction	PCR
Portable Network Graphics format	.png
RNA interference	RNAi
Room temperature	RT
Temperature sensitive	ts
Ultraviolet	UV

1 Introduction

The ability of animals to navigate within complex environments and flexibly adapt their motor programmes to novel or dynamic situations, relies on the integration of sensory information. This feedback is paramount, as the unpredictable nature of the world means that both the environment, the animal itself, and other animals or objects within the environment are continually changing. Therefore, a given motor command will not always produce the same outcome. Similarly, as motor programmes of behaviour are typically progressive actions, the internal reference frame must constantly update due to, for example, the movement of a body part, thus necessitating the use of closed-loop sensory feedback to continually update motor control centres with the correct information to inform the next step in the sequence.

The sensory system most commonly linked with motor control is mechanosensation. Unsurprisingly the ubiquity of mechanical stimuli has driven the evolution and diversification of both internal and external mechanoreceptors – specialised sensory organs that respond to mechanical forces generated both within the body, such as those produced as the result of moving a limb, and also externally - for example as a result of some contact with the external environment. These sensory organs then modulate the action of motor neurons to produce an appropriate response in a continuous loop.

In recent years, the applications of studying these mechanisms have increased drastically, with both therapeutic and robotic systems employing mechanical sensors to provide real-time control of motor systems (Ijspeert 2014). However, the flexibility of biological motor systems is still unparalleled, so investigating the organisational principles of such circuits has the potential to progress our knowledge and abilities in a plethora of applications.

The compact neural circuits of insects such as *Drosophila melanogaster* provide an excellent testbed on which to investigate these adaptive motor circuits, and at the same time, researchers can apply a wealth of knowledge relating to the development of these animals to examine the underlying principles by which motor control circuits form during development and specialise in various regions of the animal's body depending on their function.

However, even though *D. melanogaster* nervous systems are relatively simple compared to say the mouse or humans, understanding the processes by which information from the external environment is perceived and then incorporated into the nervous system to produce an appropriate response is a complex process that requires many steps. One strategy is to first identify genes or genetic loci which influence the development or function of the neural circuitry underlying these behaviours. Following this, one can identify the contribution of these loci to the nervous system throughout development and pinpoint which neurons are required for normal behaviour to occur. Finally, once candidate neural cells have been identified, they must be manipulated - ideally *in vivo* - so that the contribution of those neurons to the behavioural phenotype can be measured. Once all these steps have been accomplished, both the necessity and sufficiency of particular elements within a motor control circuit can be examined in order to elucidate the common and-or critical features required to achieve highly adaptable motor programmes, that are resilient to the variability of natural environments.

Within this thesis, I will present a series of data which aims to identify methods for genetically targeting external mechanoreceptors, before then using these methods to test their function in freely behaving animals. Ultimately, I will draw a circuit diagram

that describes how a motor circuit for the attachment of the male genitalia during copulation is modulated by external mechanical stimuli to provide robust and highly adaptive motor control. Importantly, as this particular motor sequence is so strongly linked with the reproductive behaviour of the fly and the sexually dimorphic structures of the male genitalia, several drivers and intersectional methods I have used to target and manipulate these sensory cells will leverage earlier work relating to sex determination in the fly (see section 1.6). In particular, the terminal transcription factors of the sex determination hierarchy; *doublesex* and *fruitless*, have both been engineered to provide split-Gal4 hemidriver variants (Pavlou *et al*. 2016; Rideout *et al*. 2010), so these may be used as intersectional tools alongside drivers identified in later sections of this work.

Before presenting these data, I will first discuss, with some historical context, the study of animal behaviour, and provide context for the analysis of courtship behaviour that will later be used to test the importance of these sensory systems for copulation.

1.1 Behaviour

Behaviour can be broadly defined as a reaction or response to an internal or external stimulus. The form that a given behaviour takes is unique to the organism that exhibits it, but most behaviours can be loosely organised along a spectrum between innate and learned.

Despite this categorisation being useful in many respects, it is important to remember that most behaviours are inherently complex and contain varying levels of both innate and learned components. Examples of such complexity include innate behaviours that

can be refined and modified by experience, or learned behaviours that rely in part on innate pathways. Nonetheless, by understanding the genetic and developmental underpinnings of behaviours such as courtship and copulation that are in large part developmentally determined, we can enable the study of higher levels of behavioural complexity, including learned behaviours, and the higher processing/integration of information into other circuits in the nervous system.

Nikolaas Tinbergen (1963) appropriately summed up the different approaches to understanding behaviour when he proposed the following four questions of ethology, all of which can be assessed with respect to any given behaviour through the lens of behavioural genetics:

Proximate questions

Causation – i.e. Mechanism. Mechanistic explanations of how aspects of an animals' physiology contribute to behaviour. For example, identification of genes or neurons contributing to behaviour.

Ontogeny – i.e. Development. Developmental explanations of how behaviour develops over an animals' lifetime.

Ultimate Questions

Adaptive Significance – Functional explanations of the utility of behaviour with regard to increasing an organisms' lifetime reproductive success.

Evolution – What is the phylogenetic history of this behaviour? What selective pressures have shaped this behaviour?

1.2 Neurogenetics

The field of neurogenetics endeavours to identify the underlying developmental and mechanistic genetic factors which underpin a given behaviour, before then using this information to gain insight into the adaptive functions of that behaviour.

To achieve this, researchers have employed both forward and reverse genetic strategies.

In the former, one aims to identify genes or loci related to a known phenotype. While in the latter, one seeks to identify phenotypes associated with known genes or loci. By then leveraging various genetic methods to manipulate the function of the associated genes, or the cells expressing them, one can examine the resulting behavioural effects and begin to understand the functional significance of different neural circuits.

Undoubtedly, most complex behaviours and the neural circuitry underlying them are under the control of complex gene regulatory networks, but by identifying individual genes contributing to a behaviour, one can leverage this insight to identify new approaches (e.g. novel driver lines) that provide genetic access to the cells underlying a phenotype. For this work, I have used a forward genetic approach.

As will be highlighted in chapter two, I have focused on candidate gene driver lines with known roles in mechanosensation or the development of mechanosensory bristles, thereby drastically increasing the likelihood of identifying drivers that label cells involved in my phenotype of interest. After sufficient genetic access has been achieved, these drivers can be used to visualise cellular anatomy and manipulate cell or gene function. Furthermore, by interrogating neurons contributing to behaviour through artificial activation or inhibition, not only can we begin to understand the developmental and contextual requirements for these neurons in specifying the

behaviour of interest, but we can also utilise several different methods to identify circuit organisation.

It is by this progressive expansion of a circuit model that we can begin to understand the complex organisation that allows a stereotypical sequence of behaviours to retain a degree of plasticity in response to short- and long-term changes in the environment. For example, as will be discussed later, through the integration of sensory information from other circuits or via the perception of external stimuli through peripheral sensory neurons.

1.3 Tools for Neurogenetics

1.3.1 Binary Expression Systems

The last two decades have seen enormous expansions to the repertoire of tools available for gaining genetic access to target cells, and the rapidity of these enhancements is especially noticeable in *Drosophila melanogaster,* where the study of neural circuits often requires genetic access to small, reproducible sets of neurons. One of the most widely applicable methods that has been developed for use in *Drosophila* is the binary expression system GAL4/UAS (Brand and Perrimon 1993; Viktorinova and Wimmer 2007), which allows the researcher to control the spatial and/or temporal expression of almost any coding sequence. By using this system to alter the gene expression profile of a given cell(s), one can readily visualise its morphology and induce changes in cell fate and physiology.

Since the development of GAL4/UAS, two orthogonal binary expression systems, the LexA/LexAop and QF/QUAS systems have also been developed to provide further

flexibility to gene expression manipulations (del Valle Rodriguez *et al*. 2012; Lai and Lee 2006; Potter *et al*. 2010)

GAL4 is an 881 amino acid *Saccharomyces cerevisiae* transcriptional activator protein (Laughton and Gesteland 1984). It binds a complex of four 17 bp recognition sites forming an **u**pstream **a**ctivation **s**equence, or UAS. The GAL4 protein has no endogenous binding sites in the *Drosophila* genome and is therefore able to specifically activate the expression of transgenes under the control of the UAS element (Figure 1-1A; Brand and Perrimon 1993; Fischer *et al*. 1988). Furthermore, the driver and responder elements (GAL4 and UAS, respectively) can be maintained in separate, stable lines, allowing for the maintenance of responder stocks carrying potentially toxic gene products, as they will remain silent until driver and responder are combined into one animal. The stability of lines carrying either driver or responder transgenes, has been a major driving factor in the formation of several independent stock centres that maintain a curated selection of stocks (Cook *et al*. 2010; Yamamoto 2010).

By inserting the GAL4 coding sequence into a genomic position where it is under transcriptional control from the surrounding genome, for example by using homologous recombination to target GAL4 insertion to an intron or exon, expression of the *GAL4* protein in the same spatiotemporal pattern as the target gene (*X-GAL4*) can be achieved (Rideout *et al*. 2010). In these cases, where the endogenous local environment governs transactivator expression, these lines are termed enhancer traps.

Alternatively, promoter fusion lines function by fusing cloned putative regulatory regions, with a strong promoter that is synthetic or from another gene. In this way, one can identify smaller subdomains of expression governed by a handful of enhancers in these regions and identify regulatory elements of a gene (Bellen *et al*. 1989; Bier *et al*. 1989).

The later addition to this system of expressing (under the control of a separate promotor) the inhibitor GAL80, enables further restriction of responder expression by negatively regulating GAL4 (Figure 1-1B). This negative regulation occurs by binding to 30 amino acids within the GAL4 C-terminus (Ma and Ptashne 1987; Suster *et al*. 2004).

The *LexA/LexAop* system utilises a conceptually similar approach by fusing the *E.coli* repressor; LexA, with the GAL4 activation domain (GAL4-AD; Figure 1-1C). The *LexA* protein specifically binds to the *LexAop* sequence, bringing the activation domain into proximity with the transgene to drive expression. *LexA* fusions with the GAL4-AD are sensitive to GAL80 inhibition, but alternative methods where *LexA* is fused with the herpes simplex activation domain; VP16AD, provide a GAL80 insensitive variant (Brent and Ptashne 1985; Lai and Lee 2006).

Finally, the third expression system, known as the ‘Q system’ is derived from genes in the *qa* cluster of the bread fungus *Neurospora crassa* (Potter *et al*. 2010) and operates similarly to GAL4/UAS. The system has three parts; the QF transcription factor, the QUAS responder, and the inhibitor QS, that are analogous to GAL4, UAS and GAL80, respectively.

1.3.1.1 Ternary Expression Systems

To refine the expression of engineered transgenes, one can adopt a variety of ternary expression systems. There are many ternary approaches, some of which will be covered in more depth later in this work, but most importantly, the split-GAL4 method (Figure 1-1D) has been adopted widely in the lines that I have screened in chapter 2, and the novel lines developed in chapter 3.

As indicated by the use of its activation domain in the *LexA* system, GAL4 contains two functional domains – the DNA-binding domain (DBD), which binds in a sequence-specific manner to the responder, and a trans-activation domain (AD) that locally activates transcription through its interaction with basic transcription factors (Keegan *et al*. 1986; Ma and Ptashne 1987). By placing each of these functional domains under the control of independent enhancers, fused with a heterodimerizing leucine zipper (Luan *et al*. 2006), the expression pattern of the responder can be further restricted to cells where both halves are co-expressed and the AD and DBD domains can be reconstituted into a functional transcriptional activator (Figure 1-1D).

The split-*LexA/LexAop* system utilizes this same approach by driving LexA under the control of one promoter, and either the VP16 activation domain (VP16AD) or GAL4 transactivation domain under another (Ting *et al*. 2011). Both of these hybrid LexA proteins bind the LexA operator (LexAop) to effectively drive transgene expression in *Drosophila*, although it is generally accepted that VP16 is a more potent activator (Brent and Ptashne 1985; Lai and Lee 2006; Mellert *et al*. 2010).

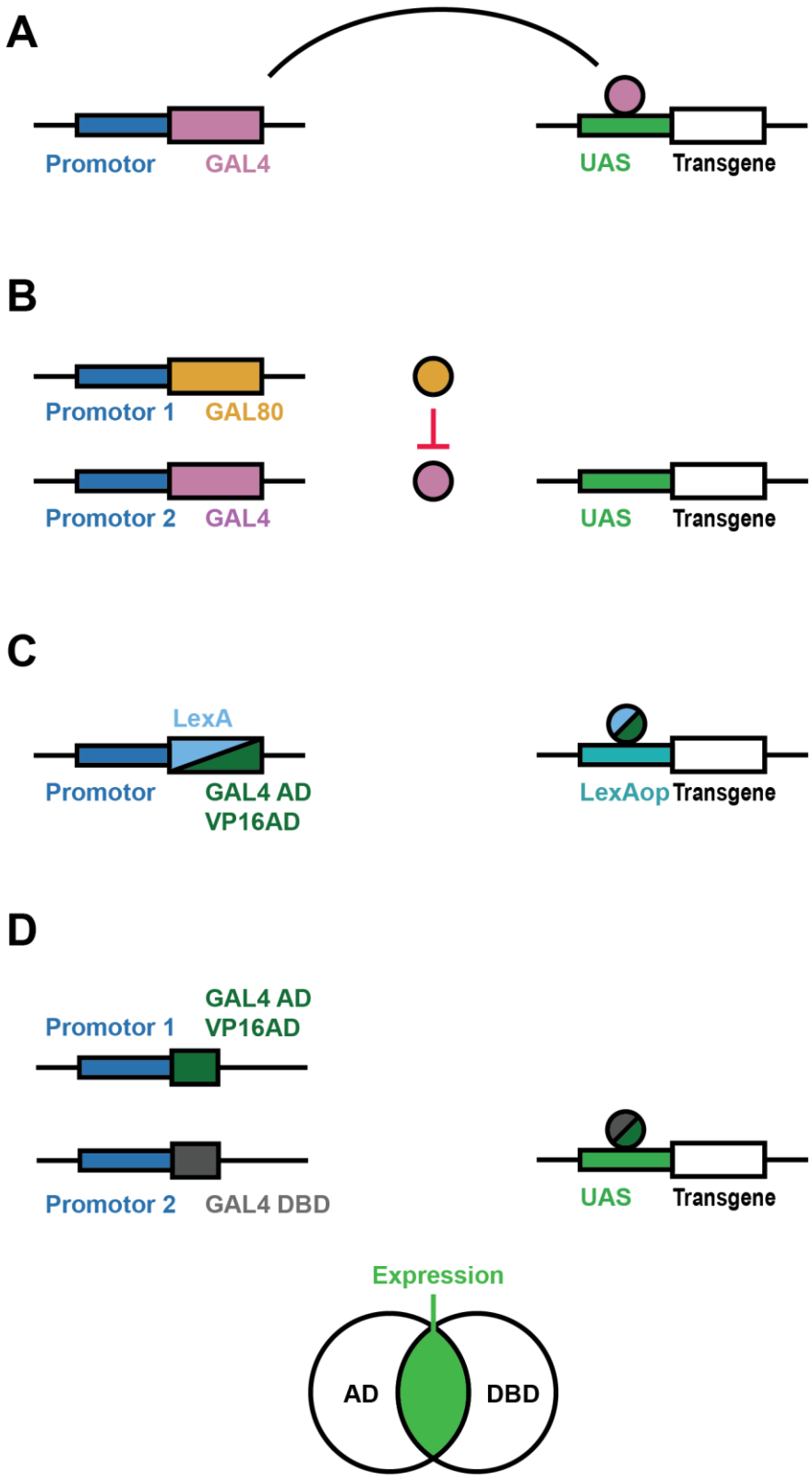

Figure 1-1: Binary and Ternary Expression Systems.
(A) The GAL4/UAS system is a binary expression system in which all cells expressing GAL4 will also express any transgene under UAS control. **(B)** GAL80 acts to repress GAL4 function by binding to its' C-terminus. **(C)** LexA/LexAop system utilizes the DNA binding capacity of *E. coli* LexA and either a GAL4 or VP16 activation domain. **(D)** The split-GAL4 system (and split-LexA) requires that both functional halves are driven by separate promotors. In cells were both promotors are active, the halves will reform by binding through a leucine zipper domain to then promote transgene expression.

1.3.1.2 Further Refinements

The final obstacle in achieving precise and reproducible expression of driver and responder resources, relates to the epigenetic effects of the host chromatin surrounding them (Markstein *et al*. 2008; Wallrath and Elgin 1995). As traditional methods for the creation of transgenic lines relied on the random integration of P-elements, the influence of so-called position effects can be highly variable, or in the case of enhancer trap lines, they may only capture a subsection of a gene's total expression pattern. Attempting to counteract these effects, researchers have identified and engineered methods to either, a) target the insertion of constructs to increase the likelihood that the element comes under gene or even isoform-specific control, or b) isolate promoter fusion and responder transgenes from the influence of the surrounding chromatin.

One tool in the geneticist's arsenal when attempting to diminish position effects is to target the integration of transgenes into loci (or 'landing sites') that lie in well-characterised locations, or in proximity to a gene of interest. Thereby reducing the need to screen random p-element insertions. In *Drosophila,* exploiting φC31 site-specific integration offers an excellent tool to achieve this. The φC31 phage integrase acts autonomously to mediate recombination between bacterial (*attB)* and phage (*attP)* attachment sites, a process which can be leveraged for the efficient integration of DNA plasmids containing *attB* sites into *attP* 'landing sites' (Groth and Calos 2004). To aid in the development of novel driver lines, a library of attP landing sites throughout the *Drosophila* genome has been generated and optimised to express transgenes in the nervous system (Markstein and Perrimon, 2008). These efforts allow researchers to choose an appropriate landing site for their study and then continue to integrate constructs into that site for improved reproducibility. Most of the promoter fusion

constructs described in this thesis have been inserted into one of two sites – attP2 or attP40, on the 3rd and 2nd chromosomes, respectively, due to the low level of basal, but highly inducible expression from transgenes inserted at these locations.

In recent years, the utility of φC31 recombination has been further improved with the advent of recombination-mediated cassette exchange (RMCE; Bateman *et al*. 2006). With this technology, insertion cassettes and landing loci are both flanked by recognition sites, enabling a clean exchange of target and donor sequences and an efficient means to target the integration of transgenes *in vivo* with minimal constraints (Groth *et al*. 2004; Markstein *et al*. 2008). Newer technologies such as the RMCE-mediated MiMIC system (see chapter 3; Venken *et al*. 2011) leverage this efficient replacement of cassettes to develop lines with transgenes inserted directly into a gene, providing excellent recapitulation of the endogenous expression pattern.

1.3.2 Visualising Neural Architecture

When attempting to visualise neuroanatomy, fluorophores like green and red fluorescent proteins (GFP and RFP, respectively) under UAS control are indispensable. Furthermore, the development of 3D registration software makes it possible to map a series of individual images onto a standard reference brain, allowing for the visualisation and digital comparison of distinct cellular populations (Cachero *et al*. 2010; von Philipsborn *et al*. 2011; Yu *et al*. 2010). This technique has become a powerful tool for inferring sexual dimorphism in neural anatomy (Kohl *et al*. 2013) and for the formation of putative circuit diagrams between genetically defined populations.

1.3.3 Neural Inhibition

One method to abolish neuron function once genetic access has been achieved, is to target the expression of the cell death genes *head involution defective* (*hid*) and *reaper* (*rpr*) using binary expression systems (McNabb *et al*. 1997), but this results in irreversible ablation that cannot be temporally controlled. Similarly, targeted expression of the inwardly rectifying potassium ion channel Kir2.1, which reduces neural activity by hyperpolarising the cell (Baines *et al*. 2001) and the bacterial tetanus toxin (TNT), which cleaves the vesicle protein synaptobrevin and thus halts neurotransmitter exocytosis (Sweeney *et al*. 1995), also provide a means by which a defined population of neurons can be irreversibly silenced.

Alternatively, by expressing a temperature sensitive allele of the *Drosophila* dynamin ortholog *shibire* – *shibire*^{ts} – one can transiently block vesicle endocytosis, and therefore synaptic transmission, at restrictive temperatures of 30°C and above (Kitamoto 2001). In this thesis I have performed experiments in which MTS neurons are silenced to determine necessity using both *UAS-TNT* and UAS-*shibire*^{ts}. In earlier experiments I used UAS-TNT in order to maximise the likelihood of seeing a loss-of-function phenotype, but in later experiments I utilised *UAS-shibire*^{ts} due to the ability to temporally control inactivation if needed, but also due to concerns that permanently silencing synaptic transmission throughout the lifetime of the animal may result in adverse developmental effects that could confound our results.

1.3.4 Neural Activation

The use of tools for artificially activating neurons provides a method to test the sufficiency of those cells for a behavioural output. Unlike methods for artificial inactivation however, temporal control is extremely important when activating neurons

as constant activation can lead to the depletion of neurotransmitter within the cell, and ultimately result in the neuron becoming permanently inactive (Peabody *et al*. 2009). The development of optogenetic technologies that evoke action potentials via a flash of light provide an unparalleled level of temporal control and enable researchers to activate neurons at specific points in a behavioural sequence, or in combination with neural imaging to identify downstream synaptic partners to the activated cell. Optogenetic technologies like transgenes encoding the ATP-gated ion channel $P2X_2$ (Clyne and Miesenbock 2008; Lima and Miesenbock 2005; Zemelman *et al*. 2003), or the green algae derived monovalent cation channel, Channelrhodopsin-2 (ChR2) provided the first methods to control neural activity with photo-stimulation (Boyden *et al*. 2005; Nagel *et al*. 2003). These systems do have their drawbacks however, for example, $P2X_2$ requires the delivery of caged ATP via microinjection, an invasive and often harmful process, and whilst ChR2 only requires food supplementation of the co-factor retinal, these earlier approaches oftentimes suffered from low light penetration of the tissue and/or unintended activation from ambient light sources. More recently, optogenetic channels like CsChrimson (CsChR), which are 45nm red-shifted compared to other known channelrhodopsins (Klapoetke *et al*. 2014) have further improved tissue penetration and reduced responses in the visual system. For the neural activation experiments that I have reported in this thesis, I opted to use *UAS-CsChrimson* as I reasoned that red light had the highest likelihood of reaching bristle neurons which are obscured during copulation.

1.4 Why the fly?

Drosophila melanogaster has been a model organism for studying the basis of behaviour for more than 100 years (Carpenter 1905), and its' prominence continues to this day, with researchers using the fly to study complex behaviours including, but not limited to, aggression (Asahina *et al*. 2014), learning and memory (Dubnau and Tully 1998; Felsenberg *et al*. 2017), circadian rhythms (Konopka 1987), proprioception (Mamiya *et al*. 2018; Tuthill and Wilson 2016) and both male and female reproductive behaviour (Clough *et al*. 2014; Manoli *et al*. 2005; Pavlou and Goodwin 2013; Pavlou *et al*. 2016; Rezaval *et al*. 2012; Rezaval *et al*. 2014; von Philipsborn *et al*. 2011).

Drosophila is particularly well suited to these studies as the level of cellular diversity within the nervous system is intermediate between other model species like the nematode *Caenorhabditis elegans* and mammalian models like the mouse (*Mus musculus*), allowing for a reasonable level of extrapolation from flies to vertebrates when aiming to identify the underlying principles of nervous system development and function. Ultimately though, the utility of the fly lies in the sophisticated genetic tools available in this organism. Visible genetic markers, balancer chromosomes (Ashburner *et al*. 2005), binary and ternary expression systems like GAL4/UAS and split-GAL4, the ability to carry out large-scale mutagenic screens, mobilise transposable elements for the development of thousands of new transgenic lines (Venken *et al*. 2011), a fully sequenced genome (Adams *et al*. 2000), and methods to target the integration of transgenic constructs, have all augmented our ability to perform both forward and reverse genetic screens (reviewed in Olsen and Wilson 2008; Venken and Bellen 2005). Additionally, recent applications of high-throughput 'next-gen' technologies such as single-cell transcriptomic profiling of the nervous system (Allen *et al*. 2019; Croset *et al*. 2018), have begun to provide an incredible depth of information for

understanding the development of cellular diversity in the nervous system, as well as new avenues for the discovery of intersectional tools.

In the case of innate behaviours, for example, courtship and copulation in the fly, which are under explicit evolutionary constraints and thought to be almost entirely inherited (Billeter *et al*. 2006b), there is a clear benefit to using genetic methods to examine the nervous system organisation underlying them as they are in large part genetically determined. However, it should be noted that in some cases, *Drosophila* sexual behaviours can be modified by experience (reviewed in; Griffith and Ejima 2009).

1.5 Sexual behaviour of *Drosophila melanogaster*

Drosophila melanogaster has a rich repertoire of behaviour. Alongside sleep, and learning and memory, courtship is a classic paradigm that has received significant attention for many decades (reviewed in Sokolowski 2001). The innate and sexually dimorphic nature of courtship behaviours makes them particularly amenable to genetic studies as two distinct variants, male and female, can be compared. Due to this and the utility of the genetic tools discussed above, courtship behaviour provides an indispensable lens through which researchers can study and quantify both the genetic basis of behaviour and the developmental origins of sexually dimorphic nervous systems.

1.5.1 Male Courtship Behaviour

In the fly, male courtship behaviours are mainly innate, meaning that even males reared in total isolation will display the entire courtship repertoire when exposed to a female for the first time (Villella and Hall 2008). However, it is also important to note that courtship conditioning experiments have shown that males can learn to depress courtship displays to new females when previously exposed to unreceptive mated females—suggesting that this innate behaviour is modifiable by experience (McRobert *et al*. 2003; Siegel and Hall 1979; Siwicki *et al*. 2005).

When first encountering a potential mate, visual, olfactory and auditory cues cause arousal in the male, leading to him orienting towards and following the female (Figure 1-2A; Markow 1987; Tompkins *et al*. 1983). Once in proximity, the male will tap the female abdomen with his foreleg, enabling him to sense cuticular hydrocarbons such as 7,11-heptacosadiene (7,11-HD) and 7,11-nonacosadiene (7,11-ND) from the female abdomen via chemosensory bristles on the forelegs (Ferveur 2005; Jallon 1984). After ‘tasting’ the female pheromone profile, the male will unilaterally extend the wing closest to the female and vibrate it, forming a species-specific courtship song made up from two components: Sine-song and pulse-song (Figure 1-2B; Schilcher 1976b; Shorey 1962). In *D. melanogaster*, pulse-song is comprised of one or two repeated trains of ~176 Hz pulses (Riabinina *et al*. 2011). The time between these trains, the inter-pulse interval (IPI), differs across species and acts as a critical factor in species recognition (Sawamura and Tomaru 2002). Pulse-song is interrupted, typically for a few seconds, by bouts of low frequency (~127 Hz) sine-waveform tones, known as sine-song (Riabinina *et al*. 2011). This sine-song is known to increase female receptivity (Schilcher 1976a, 1976b). If the males’ initial courtship display has been successful in stimulating the female into becoming receptive to copulation, she will

slow down, reduce rejection behaviours, and allow him to lick her genitalia, providing the male with additional information about her mating status through the action of gustatory sensory neurons in the labellum (Fan *et al*. 2013; Isono and Morita 2010; Thistle *et al*. 2012; Tompkins *et al*. 1983). At this point, the male will attempt copulation by engaging his leg muscles to propel forwards whilst curling his abdomen towards the female. In the same movement he thrusts his head and thorax between the female's wings to spread them, before grasping with the sex combs on his forelegs. At the same time, his genitalia align with the females (Figure 1-2D), and his epandrial posterior lobes insert into pockets under the female's 8th and 9th abdominal tergites (Kamimura and Mitsumoto 2011; Robertson 1988) before he grasps the female oviscape valves to open them with his surstyli - a pair of symmetric lobes bearing many bristles – to achieve intromission (Eberhard and Ramirez 2004). If successful, the male will copulate with the female and transfer a package of sperm and seminal fluid to both fertilise her and to modulate ovulation, locomotion, feeding activity, and receptivity to courtship from other males (Carvalho *et al*. 2006; Hasemeyer *et al*. 2009; Kubli 2008; Liu and Kubli 2003; Yang *et al*. 2009). Lastly, male-specific anti-aphrodisiac pheromones are transferred to the female through both the seminal fluid and contact with the male abdomen, which act to repel other males which may later court the female (Ejima *et al*. 2007).

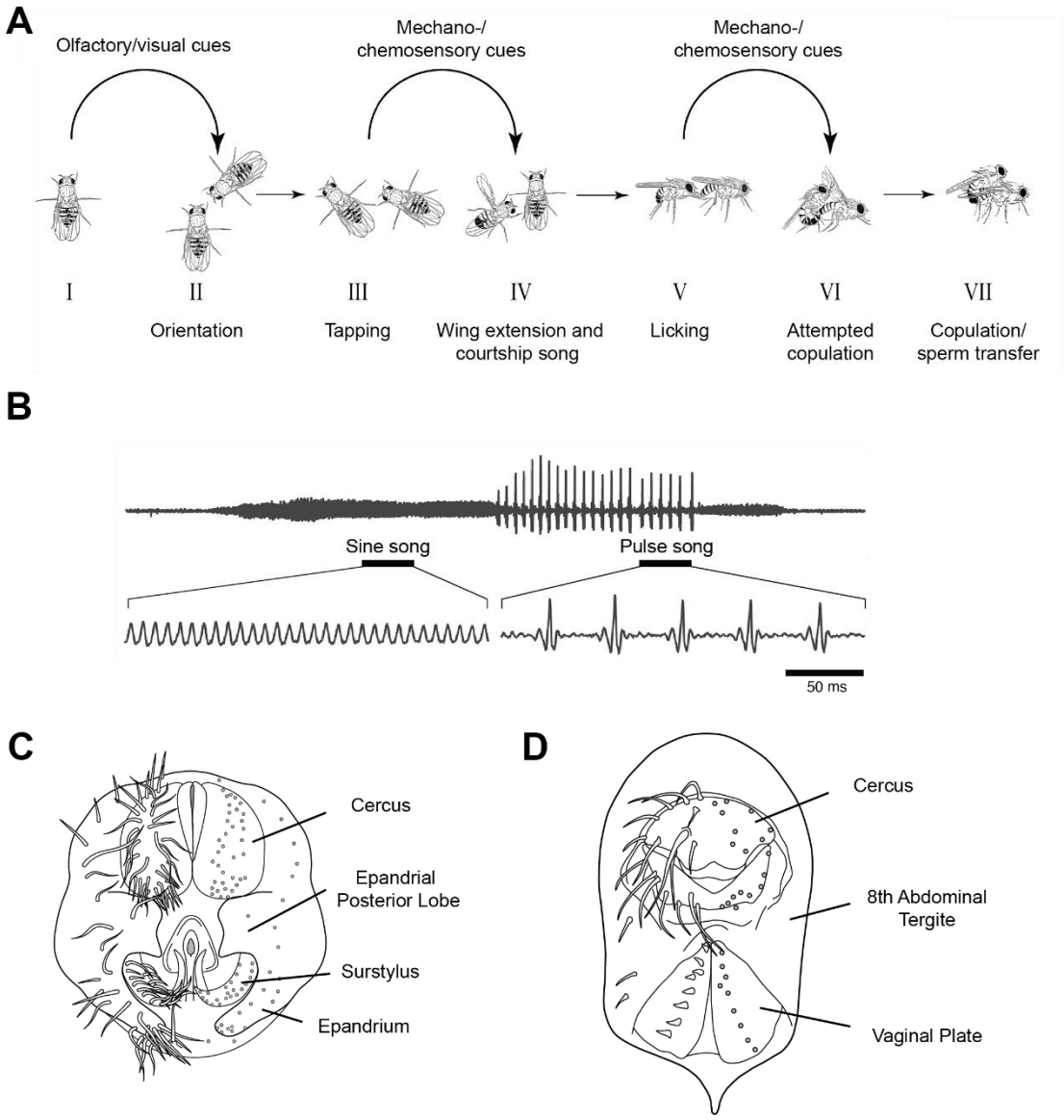

Figure 1-2: *Drosophila* male courtship behaviour, courtship song structure and exterior genitalia. **(A)** The distinct sequence of male courtship behaviour progresses from orientation through to attempted copulation and relies on sensory input from a range of distinct modalities including mechanosensory inputs. Figure adapted from Billeter *et al*. (2006a). **(B)** Male courtship song has two components; sine song and pulse song. The time between pulses, the interpulse interval (IPI) reflects the species identity. Figure adapted from Clyne and Miesenbock (2008). **(C)** The exterior male genitalia of *Drosophila melanogaster* indicating cercus, epandrium and surstylus. Left side shows approximate bristle morphology whilst right side shows the location of underlying cell bodies. The epandrial posterior lobes which are inserted under the female abdominal tergites are also shown. **(D)** Female genitalia showing morphology and bristle location as in C. Figure adapted from Pavlou *et al.* (2016).

1.5.2 Female Courtship Behaviour

Although our understanding of female behaviour during courtship is less developed than that of the male, it is clear that the female must assess the stimuli provided by the courting male in order to determine both the species identity and the fitness of any potential mates (Kyriacou and Hall 1980; Ritchie *et al*. 1999). If the female is unreceptive, then she will exhibit rejection behaviours such as wing flicking, kicking, and ovipositor extrusion (Connolly and Cook 1973; Ejima *et al*. 2001). If she is receptive, then she will allow the male to copulate by slowing her locomotion, ceasing to exhibit any rejection behaviours, and opening her vaginal plates to allow intromission (Spieth 1974). The specific stimuli which trigger female acceptance or rejection behaviours come from many sensory modalities, and their relative contributions to the sensory 'goldilocks zone' for copulation success may not be fully understood. What is apparent, however, is that several specific molecules such as the pheromonal compounds 7,11-heptacosadiene, 7,11-nonacosadiene, 7-tricosene and cVA play vital roles in signalling both species identity, mating status and mate quality, and that as well as the ability of the male to coerce a female, there is a strong element of female choice in granting successful copulation (for a thorough review of the roles of pheromonal compounds in *Drosophila* reproduction, see: van der Goes van Naters, 2014). If a successful mating does occur, then the pair will remain almost stationary for a period of 20-30 minutes, although it has been shown that matings of as little as 8 minutes are sufficient for the transfer of sperm and seminal fluids into the female reproductive tract (Gilchrist and Partridge 2000). Once transferred, this complex package will not only fertilise her, but also engender post-mating behavioural changes to her receptivity, egg production, oviposition, and innate immune responses (Carvalho *et al*. 2006; Hasemeyer *et al*. 2009; Kubli 2008; Liu and Kubli 2003; Ram and Wolfner

2007; Yang *et al*. 2009). Altogether, the likelihood of a successful mating relies on both the quality of the male courtship display, as well as the reproductive status of the female and her willingness to mate. As a final point, it has been noted that persistent males can overcome the rejection behaviours of both mated and virgin females, suggesting that the evolution and development of male traits to counteract female rejection behaviours is driven by sexually antagonistic coevolution (Cordero and Eberhard 2003; Yoshitaka Kamimura 2010; Y. Kamimura 2012). While there is evidence to support this evolutionary arms race, for example the identification of thick cuticular 'pouches' in the female abdomen to protect against wounding *in copulo* (Yassin and Orgogozo 2013) and preferential sperm storage (Bloch Qazi and Wolfner 2003; Bressac and Hauschteck-Jungen 1996; Schnakenberg *et al*. 2012), the relative contributions of pre- and post-copulatory mate selection mechanisms is not yet fully understood.

1.6 *Drosophila melanogaster* Sex Determination

Sexual dimorphism can be defined as any difference between the sexes, whether they are differences in the interior or exterior anatomy and morphology, physiology, neural architecture, or behaviour. In *Drosophila*, genes comprising the sex-determination hierarchy orchestrate the development of sex-specific and sexually dimorphic cells and tissues, including neural cells which have been implicated in all aspects of sexual behaviour.

Sex determination in the fly acts cell-autonomously, that is to say that within each cell the X chromosome to autosome ratio (X:A) specifies the sex of that cell by activating the gene *Sex lethal (Sxl)* in females (XX) and suppressing it in males (XY; see Figure 1-3; Billeter *et al*. 2006a; Camara *et al*. 2008), resulting in functional Sxl products in

females only, where it acts as an RNA splicing factor (Bell *et al*. 1988). Sxl then regulates the female-specific splicing of *transformer (tra)* mRNA, resulting in the expression of functional Tra protein (Inoue *et al*. 1990; Nagoshi *et al*. 1988). In males, the lack of Sxl results in the absence of Tra proteins. The presence or absence of Tra, alongside the ubiquitous non-sex-specific Tra-2, determines the sex-appropriate isoform expression of the two key transcription factors at the bottom of the sex-determination cascade, Dsx and Fru. Through alternative splicing, Dsx is expressed as either a male or female-specific isoform, while Fru proteins are only fully expressed in males, as female Fru is truncated and non-functional. These two terminal transcription factors ultimately determine all aspects of male and female dimorphism, both in terms of their morphology and behaviour (for select examples, see; Chan and Kravitz 2007; Rezaval *et al*. 2012; Rideout *et al*. 2010; von Philipsborn *et al*. 2011). The male-specific proteins, Fru^{M} and Dsx^{M}, determine the morphological and neural characteristics that underly the complete male-specific behavioural repertoire, while the equivalent processes in the female rely on the function of the female-specific Dsx^{F} and the absence of Fru (Billeter *et al*. 2006a; Billeter *et al*. 2006b; Kimura *et al*. 2005; Kimura *et al*. 2008; Rezaval *et al*. 2012; Rideout *et al*. 2007; Rideout *et al*. 2010; Villella and Hall 1996).

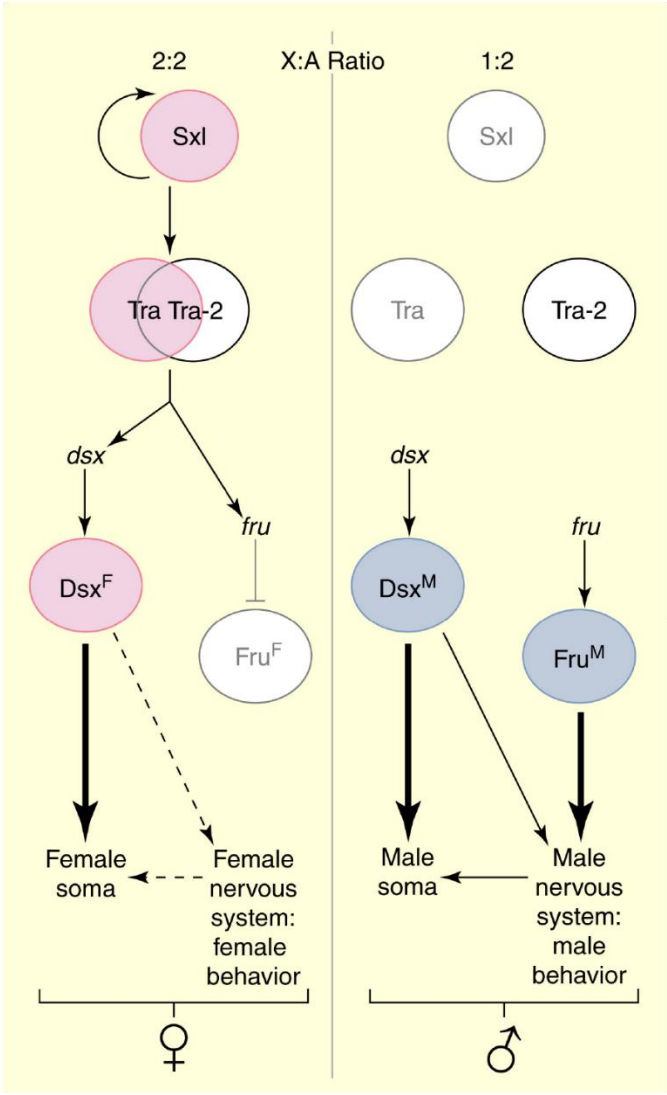

Figure 1-3: The *Drosophila* sex determination hierarchy. Image from Billeter *et al*. (2006a). In females (left side) which have 2X chromosomes and 2 autosomal chromosomes per cell, *Sex lethal* positively autoregulates its own expression and can sex-specifically splice *transformer* to give rise to functional protein. The combined action of female Tra alongside Tra-2 results in the production of female *doublesex* isoforms and no *fruitless*. In males, the 1:2 X to autosome ratio means that Sxl expression is insufficient to result in splicing of Tra. Therefore, Tra and Tra-2 do not influence *doublesex* and *fruitless* expression, leading to male isoforms of both.

1.6.1 Fruitless

The *fruitless* locus spans approximately 140kb of the right arm of the third chromosome and encodes a BTB (Broad-complex/Tramtrack/Bric-a-brac) zinc finger transcription factor (Ito *et al*. 1996). The gene itself is transcriptionally complex with multiple different

isoforms and has two primary functions. Male-specific *fru* isoforms are necessary for the control of male sexual behaviour, while the other isoforms are important for the viability of both sexes (Billeter *et al*. 2006b; Demir and Dickson 2005; Goodwin *et al*. 2000; Ito *et al*. 1996). Alternative splicing at both the 5' and 3' ends of *fru* produce a variety of transcription factors proteins from four distinct promotors (P1-P4). These proteins all contain a common BTB N-terminal domain that enables protein:protein interactions - and due to alternative splicing - one of three alternative DNA-binding zinc finger domains in the C-terminus (A-C; nomenclature as per Billeter *et al*. 2006b). Transcripts from the most distal promoter, P1, are sex-specifically spliced by the female Tra/Tra-2 protein complex, such that in females these transcripts contain a premature stop codon (Billeter *et al*. 2006a). In males, the absence of the Tra/Tra-2 complex leads to the production of functional, male-specific, P1 transcripts which are collectively referred to as Fru^{M} (Billeter *et al*. 2006a; Goodwin *et al*. 2000; Ryner *et al*. 1996). Fru^{M} isoforms each contain an additional 101 bp sequence upstream of the BTB domain and one zinc finger domain (A-C). As such they are referred to as Fru^{MA}, Fru^{MB} and Fru^{MC}.

The first mutation in *fru* (*fru^{1}*) was identified via an X-ray induced mutation screen (Gill 1963). Behavioural analysis of this mutant revealed that the underlying cause for the sterility was abnormal courtship behaviour, including the courting of males and females indiscriminately, and failure to attempt copulation (Gailey and Hall 1989). Several *fru* mutant alleles have since been generated to investigate the requirement for *fru* in the manifestation of male courtship behaviours, and several behavioural effects have been identified. These include reduced or absent courtship towards females, increased male-male courtship, abnormal or absent courtship song, and the failure to attempt copulation (Gailey and Hall 1989; Hall 1979). The morphology of *fru* mutant males

appears normal with the noted exception of the muscle of Lawrence (MOL) which is missing or incomplete in the absence of *fru* (Anand *et al*. 2001; Billeter *et al*. 2006a; Gailey *et al*. 1991; Villella *et al*. 1997). Interestingly, *fru* mutations in the female have little to no effect on female behaviour or morphology (Villella *et al*. 1997), a fact which has helped to shape our understanding of *fru* function and its importance for specifying male behaviour (Demir and Dickson 2005).

1.6.2 Doublesex

The *dsx* locus spans ~50kb on the right arm of the third chromosome. It encodes a transcription factor belonging to the Dmrt family (*doublesex and mab-3-related transcription factors*), and unlike Fru, it is structurally and functionally conserved throughout the animal kingdom (Kopp 2012). Male and female Dsx (Dsx^M and Dsx^F, respectively) isoforms contain a shared 66-amino-acid N-terminal segment that mediates sequence-specific DNA binding via a DM domain and protein:protein interactions via an oligomerization domain (OD1; An *et al*. 1996). Due to alternative sex-specific splicing, the carboxyl termini of the Dsx^F and Dsx^M proteins contain divergent oligomerization domains ($OD2^F$ and $OD2^M$) which mediate further dimerization and protein:protein binding (An *et al*. 1996; Burtis and Baker 1989; Cho and Wensink 1997; Erdman *et al*. 1996). The differential binding of cofactors to these sex-specific C-termini (Ghosh *et al*. 2019; Williams *et al*. 2008) helps to expand the range of the sex-specific functions of Dsx isoforms.

Dsx proteins are known to be involved, alongside Fru, in the specification of neural clusters within the nervous system that are vital for normal sexual behaviour, but most notably they are required for the specification of sexual dimorphism in external

morphology (Kimura *et al*. 2008; Rideout *et al*. 2007; Rideout *et al*. 2010). For example, the development of the male-specific sex combs, male and female pigmentation patterns and the morphology of the exterior genitalia have all been linked to the action of *doublesex* and can be completely or partially transformed via the ectopic expression of Dsx^F or Tra (Mellert *et al*. 2010; Rideout *et al*. 2010; Robinett *et al*. 2010).

Hypomorphic alleles of *doublesex* cause both males and females to differentiate into intersex animals with male-like pigmentation, ambiguous internal reproductive organs and incomplete sex combs on the legs (Burtis and Baker 1989; Jursnich and Burtis 1993; Rideout *et al*. 2010; Waterbury *et al*. 1999). These mutant phenotypes are the result of the loss of both positive and negative regulation of the many different genes targeted by *doublesex,* giving testament to the complexity of regulation that can be achieved by this one sex-specifically spliced protein in conjunction with many different cofactors.

Genetic access to *dsx*-expressing cells, in particular neurons, was established by the generation of a dsx^{GAL4} allele (Rideout *et al*. 2010; Robinett *et al*. 2010). By observing the neuronal morphology that is labelled by dsx^{GAL4}, it is clear that there are two different modes of dimorphism. Some neural clusters like SN, TN1 and TN2 clusters are present in males only. In the case of TN1 and TN2, these neurons act to specify male-specific wing extension and courtship song (Rideout *et al*. 2007; Rideout *et al*. 2010; Robinett *et al*. 2010; von Philipsborn *et al*. 2011). On the other hand, clusters such as pC1 and pC2 are present in both sexes but exhibit differences in cell number between male and female (Rideout *et al*. 2010).

Testing the behavioural function of dsx^{GAL4} neurons, Rideout *et al*. (2010) demonstrated that disruption of *dsx* circuitry via the constitutive expression of *UAS-TNT* (dsx^{GAL4} > *UAS-TNT)* resulted in aberrant behaviour and sterility in both males

and females. Silencing all *dsx*-positive neurons in males caused a drastic reduction in courtship behaviours, increased latency to copulation and the complete abolition of attempted copulation (Rideout *et al*. 2010). Conversely, silencing *dsx* circuitry in virgin females impaired their ability to assess courtship displays and provide acceptance responses. In cases where copulation did occur, this effect manifested in much higher-than-expected movement and increased rejection behaviours. Secondly, although sperm and seminal fluids were transferred during these matings, females with silenced *dsx* circuitry laid no eggs, readily re-mated and did not suppress the courtship advances of other males, indicating that *dsx* neurons are critical for both pre- and post-copulatory female behaviour (Rideout *et al*. 2010).

More recently, the development of a *dsx* split-GAL4 allele (dsx^{DBD}) by homologous recombination (Pavlou *et al*. 2016) has enabled identification and functional manipulation of subsets of *dsx* expressing cells by intersecting against a plethora of neurotransmitter and gene specific hemi-drivers. The expression pattern of this novel allele has been shown to faithfully recapitulate that of the earlier dsx^{GAL4} when combined with a pan-neuronally expressed activation domain *(dsx^{DBD}/$elav^{VP16AD}$),* and when these cells were silenced by combining the two hemidrivers to drive TNT, both males and females exhibit the same aberrant behavioural phenotypes as previously reported (Pavlou *et al*. 2016; Rideout *et al*. 2010).

1.7 Insect mechanosensation, adaptive motor control, and behaviour

Until recently, the majority of work surrounding insect motor control has been undertaken in the ‘big insect’ models such as locusts, crickets and stick insects. More

recently however, *Drosophila* has gained traction in the field, as the availability of genetic tools in the fly, as well as various other benefits outlined in section 1.4, provide easy access to many specific cell types, thus enabling the precise study of neural correlates of behaviour.

The different types of insect mechanoreceptors are often classified into two functional groups: exteroceptors and proprioceptors. Exteroceptors directly detect external mechanical forces, whilst proprioceptors detect the position and movement of body parts. This distinction is in some sense artificial however, as exteroceptors can be stimulated by self-generated movement, and proprioceptors can be stimulated by external forces. Nevertheless, tactile hairs – which as outlined in the following section are particularly important to this work - are typically classified as exteroceptors, whilst other mechanosensory organs in the fly are considered proprioceptors. These hairs (often called bristles) are the most abundant mechanosensory structure on the adult *Drosophila* and belong to a morphological class of structures called trichoid sensilla. They exhibit some marked differences in size and shape across the flies' body (for examples see section 1.7.1) but can broadly be classified as microchaetes or macrochaetes depending on their size.

Each bristle is in fact a compact organ, comprised of a hollow shaft rooted in a cuticular socket. The base of the shaft is attached to the dendritic tip of a sensory neuron, upon which the shaft acts as a lever arm that exerts and amplifies mechanical perturbations onto the sensory neuron dendrite. Here, mechanosensitive ion channels such as *no mechanoreceptor potential C* (*nompC*) are localised and sense these deflections (Lee *et al*. 2010; Yan *et al*. 2013). The bristle is typically oriented at an acute angle relative to the cuticle, providing a directional selectivity where the bristle is most sensitive to deflections which push the bristle closer to the cuticle (Corfas and Dudai 1990; Walker

et al. 2000). Once deflected, the sensation of this stimulus is projected directly via the sensory neuron axons to the nervous system, where anatomical studies suggest they are systematically organised depending on mechanoreceptor type, position, and tuning to form a somatotopic map (Murphey *et al*. 1989; Tsubouchi *et al*. 2017).

In flies, stimulation of as little as one or two mechanosensory bristles has been shown to be sufficient to elicit complex grooming behaviours (Hampel *et al*. 2017; Seeds *et al*. 2014; Vandervorst and Ghysen 1980), often generating complex motor patterns entirely from thoracic circuits (Vandervorst and Ghysen 1980).

Furthermore, links between mechanosensory organs and sexual development are clear, although much of the focus so far has been on proprioceptors such as the chordotonal organs which are comprised of ~100 or more sensory neurons which span a flexible junction such as the tibia/fibia joint and respond in functional groups to movement in all directions (Mamiya *et al.* 2018). Firstly, classical studies have shown that bristles and the neurons innervating them are developmentally influenced by the sex determination hierarchy (Figure 1-3), with *tra-2* mutant females forming male genitalia and also the correct pattern of male bristles, with the appropriate male-like organisation of neural projections from these bristles in the abdominal ganglion (Taylor 1989).

Secondly, experiments in females for example, have shown that mechanosensory bristles are utilised in concert with chemosensory bristles found in the antennae and labellum to select appropriate oviposition sites (Zhang *et al*. 2020). In males, on the other hand, experiments have shown that ablating a singular bristle on the surstyli can lead to aberrant mating posture (Acebes 2003), highlighting the possibility, which we will investigate in much greater depth, that the rapid sensory feedback provided by these bristles is a vital component of normal mating behaviour.

1.7.1 Peripheral Sensilla - Development

The bristles which adorn the exterior of the flies thorax, legs, and wings can be loosely defined as microchaetes or macrochaetes, depending on their size (see Figure 1-4A). They have been used as the primary model for investigating cell fate determination and the sensory roles of bristles due to their accessibility, stereotyped spatial pattern and synchronous development (Lai and Orgogozo 2004). While the bristles of the male and female genitalia are almost morphologically identical to these bristles, their size and position significantly increases the difficulty of experimental observation, particularly electrophysiological recordings. As such, much of what is known more generally about peripheral sensilla relates to bristles on the legs and thorax, while information directly pertaining to genital bristles is in some cases lacking.

Nonetheless, the ontogeny of these bristles is conceptually similar to that all of all exterior sensory organs (Reviewed in; Jan and Jan 1993): Within a field of undifferentiated epithelial cells, groups of adjacent cells called proneural clusters acquire neural potential via the action of basic helix-loop-helix (bHLH) transcription factors of two classes; the Ato class (Atonal and Amos) and the AS-C class (Achaete, Scute and Lethal of Scute). External mechanoreceptors across the animal are specified from proneural clusters of Achaete and Scute expressing cells (Lai and Orgogozo 2004). The potential for neural differentiation is restricted to one of the cells in the cluster (termed sensory organ precursor, SOP) via the Notch (N) signalling pathway, and once stably specified, this cell undergoes two rounds of asymmetric cell division to form four cells; the socket cell, shaft (bristle), sheath and neuron (reviewed in Lai and Orgogozo 2004).

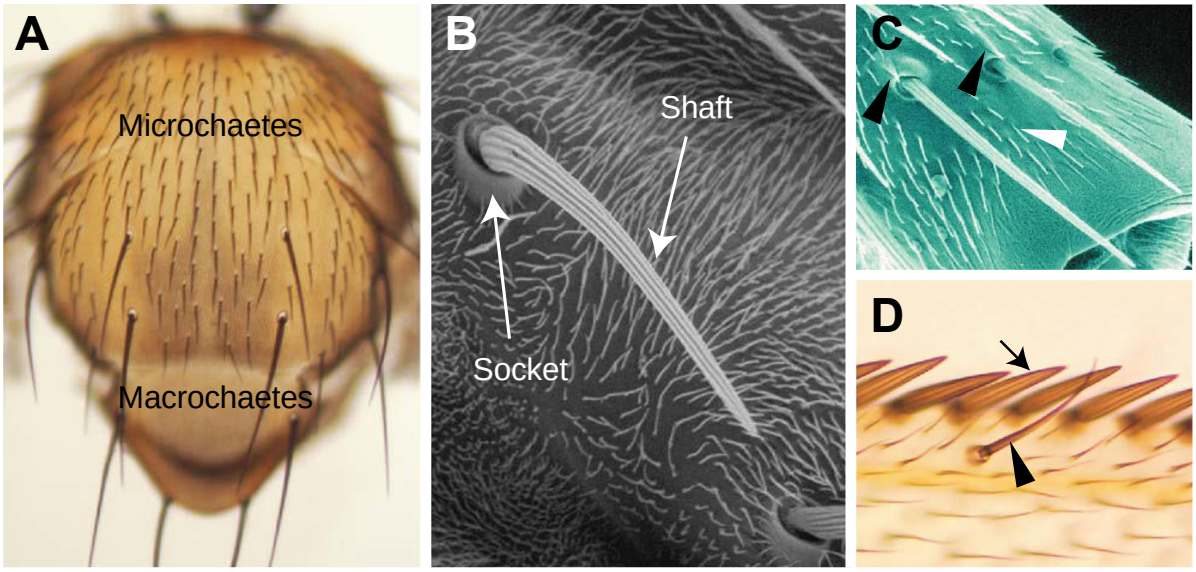

Figure 1-4: Microchaete and macrochaete sensory bristles.
(A) Bristles on the thorax and the rest of the animal can be classified based on size as microchaetes and macrochaetes. **(B)** Scanning electron micrograph showing the two exterior cells of mechanosensory bristles; socket and shaft. **(C)** Leg mechanosensory bristles are associated with a bract cell (black arrowheads). Epidermal cells also produce non-sensory trichomes (white arrowhead). **(D)** Anterior wing margin showing stout mechanosensory bristles (black arrow) and long slender mechanosensory bristles (black arrowhead). Images adapted from Lai and Orgogozo (2004).

The existence of this four cell sensory lineage results from the asymmetric division of Notch and Delta proteins, as well as signalling elements like Numb. After the first division of the SOP, two distinct cells are formed; Notch-positive *pIIa* cells which will subsequently give rise (again through asymmetric division of Notch components) to the shaft and socket, and Notch-negative *pIIb* cells that will give rise to the neuron and sheath cell (Rhyu *et al*. 1994). This method of developing cellular diversity from a small pool of undifferentiated epithelial cells has been shown to be Notch-dependent through the ectopic expression of Notch or Numb in SOPs, which in the extreme cases results in the development of four socket cells (Notch gain of function/Numb loss of function) or four neural cells (Notch loss of function/Numb gain of function; Hartenstein and Posakony 1990; Parks and Muskavitch 1993; Rhyu *et al*. 1994; Schweisguth *et al*. 1996).

While understanding the early development of peripheral sensilla may not immediately uncover precise spatially restricted intersection of genital bristles due to the diverse roles of the Notch signalling pathway, understanding that the sensory neurons themselves are derived from epithelial tissue provides an excellent avenue of exploration to look for bristle expressing lines. For example, as we will discuss more in section 2.5.6, the genital imaginal disc which gives rise to the adult genitalia (Estrada *et al*. 2003) is an excellent candidate region in which to identify lines for this screen, as this disc contains all the epithelial cells that will later be specified as SOPs and ultimately the sensory neurons innervating genital bristles.

1.8 Nomenclature for the Male Genitalia

To describe the results of this thesis in a manner that is consistent with future studies, I will report each result using the terminology defined by Rice *et al.* (2019), although it is worth nothing that several research papers use the term ‘claspers’ to refer to the surstyli. Figure 1-5 highlights the periphallic substructures of the male genitalia and updated nomenclature from Rice *et al.* (2019).

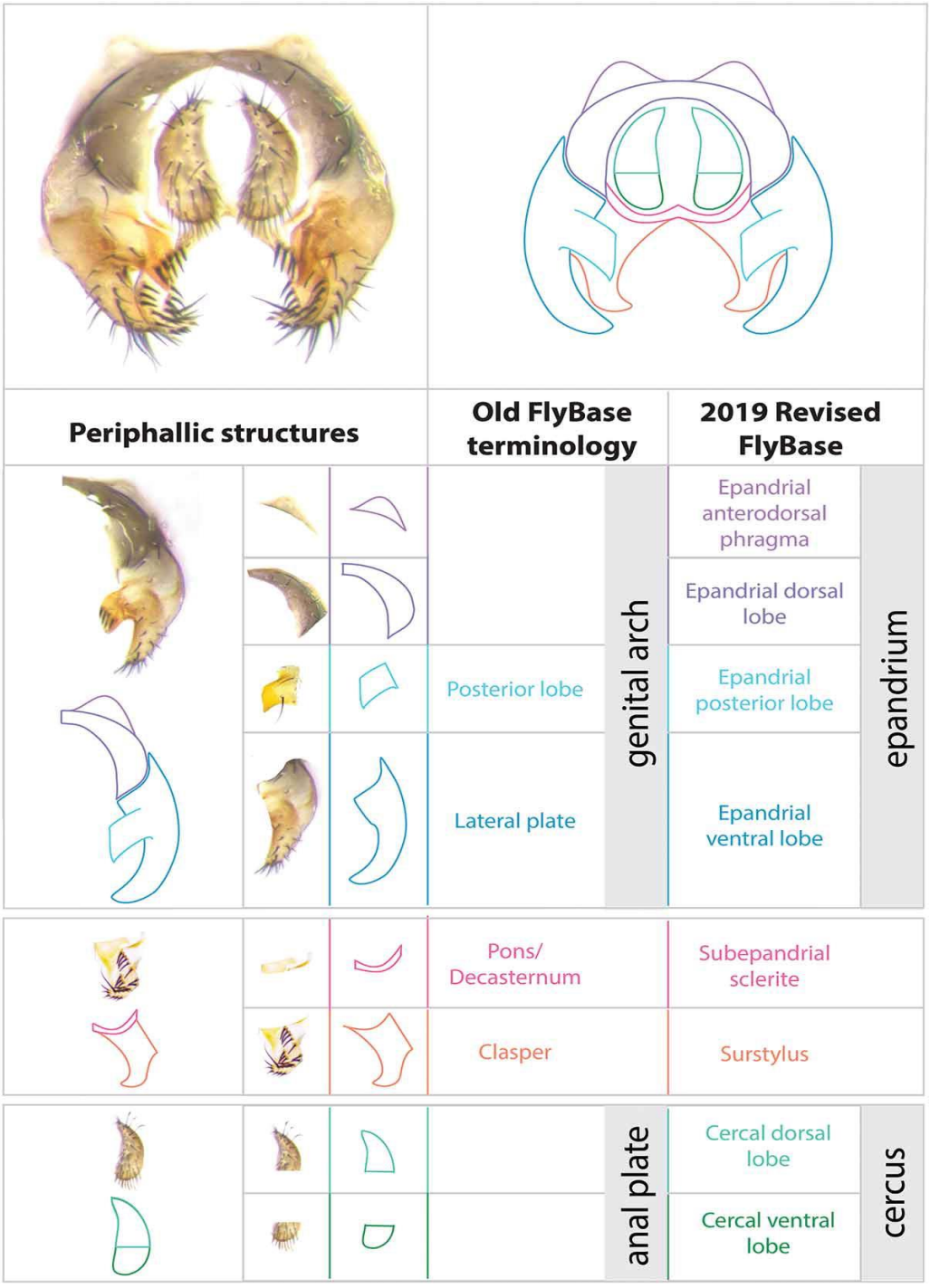

Figure 1-5: Visual atlas of *Drosophila melanogaster* male terminalia.
Light microscopy images of *Canton-S* strain and diagrams representing the division of substructures within the epandrium and cercus. Images are oriented so dorsal is to the top and ventral towards the bottom. Previous terms are shown on the left and updated terms from Rice *et al*. (2019) are on the right. Image from Rice *et al.* (2019).

1.9 A Circuit for Male Attachment

The work presented within this thesis will develop upon previous research from our lab published by Pavlou *et al*. (2016). Using a dsx^{DBD} driver developed for their study, Pavlou and colleagues were able to intersect *dsx*-positive neurons on the basis of their neurotransmitter usage. When combined with $OK371^{VP16AD}$ that is expressed in all glutamatergic neurons (Daniels *et al*. 2004), and $Gad1^{p65AD}$ which marks GABAergic neurons (Erlander and Tobin 1991), they unearthed a sexually dimorphic motor circuit in the Abg that appears to control the coordinated sequence of motor actions required for successful copulation (Pavlou *et al*. 2016).

This circuit is formed of three parts, first, *dsx*∩*VGlut* motor neurons innervate all genital muscles, including both protractor and retractor muscles, which are contracted to enable the male to clasp the female oviscapt and achieve intromission (Kamimura 2010). Activating *dsx*∩*VGlut* neurons *in copulo* resulted in a complete inability to detach due to the chronic contraction of genital musculature, whilst activating these neurons pre-copulation abolished the male's ability to attach.

Second, these motor neurons are inhibited by the action of $dsx \cap Gad1^{p65AD}$ abdominal ganglion interneurons to control both the timing of copulation termination, as well as to prevent the indiscriminate protraction of the copulatory organs. This role is supported by the observation that activating $dsx \cap Gad1^{p65AD}$ neurons *in copulo* results in the immediate termination of copulation. Conversely, activation pre-copulation results in no attachment being formed.

Lastly, the third component of this circuit is sensory feedback, a hallmark of all motor circuits which must coordinate fine motor outputs. Whilst they were not able to test the behavioural implications of altering sensory feedback to this circuit, Pavlou and

colleagues showed strong evidence using retrograde dye-fills and calcium imaging which suggest that this circuit receives sensory input from mechanosensory bristles found on the genitalia. These sensory bristles likely provide information relating to the male body position and the grasp of the surstyli on the female genitalia. During copulation, this sensory information is provided passively through contact, but they may also be used in an exploratory way pre-copulation, where the male purposefully makes movements to acquire sensory inputs, a process termed active sensing (Gomez-Marin and Louis 2012; Schroeder *et al*. 2010).

Whilst there is some anatomical evidence to support the notion that these MTS neurons signal to the Abg motor circuit described by Pavlou *et al*. (2016), it is yet unclear to what extent sensory feedback from these bristles is required for copulation. For example, are they only required for the initial steps of copulation where the male grasps the female and attempts intromission, or are they required for more fine-grain control throughout copulation where a dynamic balance between excitation and inhibition is required to achieve copulation and maintaining a proper mating posture. In the following chapters I will describe novel reagents and behavioural tests that will examine the role of feedback from mechanosensory MTS for copulation.

1.10 Aims

As I have outlined, *Drosophila* courtship behaviour provides an excellent model for studying the neurogenetics of behaviour due to both the wealth of previous studies examining genetic determinants of behaviour, and the more recent development of methods to assist in targeting and manipulating neural cells. In this thesis, I will present my efforts to establish causal relationships between distinct populations of sensory

bristle neurons in the peripheral nervous system of *Drosophila melanogaster* and a defined set of reproductive behaviours – i.e. attachment and detachment during copulation – controlled by a neural circuit first identified by Pavlou *et al*. (2016).

The defining characters of this circuit are; it is made up of opposing glutamatergic (excitatory) and GABAergic (inhibitory) neuron populations, it is sexually dimorphic, and the cells comprising it express the gene *doublesex* (*dsx),* that is required for the sexual differentiation of both neural and non-neural tissues in the fly. The cell bodies of the neurons that comprise this attachment circuit are located within the abdominal ganglion (Abg), the most posterior ganglion of the fly ventral nervous system (Power 1948) and can be functionally subdivided into two distinct populations via intersectional labelling of *doublesex* and *VGlut* (*dsx*∩*VGlut*), or *doublesex* and *Gad1* (*dsx*∩*Gad1*) expressing cells. In their work, Pavlou *et al*. (2016) were able to identify that this circuit played a necessary and sufficient role in controlling the initiation and termination of genital attachment. Yet, our understanding of how this circuit adapts to exterior stimuli remains unclear.

This thesis posits that MTS mechanosensory neurons and others similar to them provide sensory feedback to the circuit previously identified by Pavlou *et al*. (2016) in the context of copulation and attempted copulation, and will attempt to show this through a series of anatomical and behavioural investigations.

To examine this hypothesis, I asked:

1) Does the artificial activation or inactivation of MTS neurons produce an analogous phenotype to that reported by Pavlou *et al*. (2016)?
2) Is there anatomical and physiological evidence to support a circuit connection between MTS neurons and motor circuits in the Abg?

To this end, using insights from the available literature, I screened several published genetic driver lines to identify those which can be used to precisely label my cells of interest. In many cases, I then generated novel transgenic tools based on these drivers to enable precise and reproducible genetic access to subsets of genital sensilla. The details of this screen and the development of these novel transgenic lines will form the basis of the second and third chapters of this thesis, respectively.

After establishing a sufficient genetic toolkit, I then focussed on a handful of hemidriver combinations that allowed me to intersect bristle neurons in the most precise manner. The influence of these manipulations on male reproductive behaviour was examined via a series of established and novel behavioural paradigms. These data will be presented in chapter 4.

2 A Screen for Tools to Facilitate Genetic Access to Genital Sensilla

2.1 Introduction

As I alluded to in Chapter 1, there are a plethora of tools available in *Drosophila* to gain genetic access to a spatially restricted population of neurons and test their function. These methods can be loosely defined as either binary or ternary expression systems and by identifying and leveraging these tools to both visualise neuroanatomy and manipulate neural function, one can build a framework linking genes, the neural circuitry in which these genes act, and their behavioural outputs.

In this chapter, I will present a targeted screen with the aim of identifying driver lines that will facilitate genetic access to MTS neurons. I primarily screened enhancer traps associated with genes with known roles in peripheral sensilla. Then, in selected cases, I identified promoter fusion lines to subdivide their expression pattern further. In particular, I have focused on genes which are active in mechanosensory sensilla, as the results of Pavlou *et al*. (2016) indicate that the circuit for male attachment is modulated by mechanosensory inputs. I have also focussed on drivers associated with genes like *dsx* and *fru* that are vital for the specification of sexually dimorphic structures like the genitalia, where the sensilla of interest are located.

Ultimately these lines will lay the foundation from which I will manipulate MTS function in freely behaving males. However, as the first port of call, they will allow me to describe the architecture and underlying properties of sensilla covering the male genitalia.

While this approach has its drawbacks in the sense that it is biased towards specific drivers and may not identify all the available resources, the labour required to establish a ‘genetic toolkit’ which can later be used for the development of novel split-hemidrivers

and behavioural assays is drastically reduced. This approach offers more time investigating and developing drivers that may allow us to parse out broader expression domains to more restricted patterns and therefore, fewer cells. It is important to note, however, that the targeted nature of this screen was not intended to limit the number of lines which we looked at, and to this end, I have also included lines relating to genes involved in the early development of the bristles, the genitalia themselves, and specific neurotransmitters. In combination, the results of these screening efforts serve to identify resources for the functional manipulation of MTS neurons, and as a method to describe their underlying physiology. These dual outcomes mesh neatly with both the proximate and ultimate questions of ethology, as outlined in chapter 1: They offer insights into the mechanism and development of mechanosensory bristles by describing genes expressed in these structures, and the ultimate questions of the adaptive significance and evolutionary pressures underlying their evolution by examining their role in behaviour.

To identify lines labelling our cells of interest, I first took a baseline measurement of the number of bristles on the surface of the male and female genitalia to compare cell counts against, I then identified a list of candidate genes that may be expressed in genital sensilla, and from this list I collected a published driver line for each gene and examined their expression pattern in the genitalia and other peripheral tissues.

Results

2.2 *CantonS* 'Wild-type' Bristle Distribution and Morphology

In adult *CantonS Drosophila melanogaster,* the genitalia are densely covered by sensory bristles, often termed sensilla. In males the total number of sensilla per side of the genitalia is 79±4 (n=20, median ± half the range, Figure 2-1), with an average of 24±2, 36±4 and 20±3 adorning the surstyli, cercus and epandrium, respectively (Figure 2-1). All the cells covering the epandrium and cercus resemble the slender mechanosensory bristles on the legs and wings, although they are noticeably smaller than leg bristles (Figure 1-4; Lai and Orgogozo 2004). These male terminalia sensilla (MTS) are not accompanied by a non-lineally related bract cell as is the case in the legs (del Alamo *et al*. 2002; Held 2002). MTS on the surstyli are more similar to the stout anterior wing margin bristles, and are sometimes termed surstylar teeth (Figure 1-4D; Lai and Orgogozo 2004). These surstylar teeth are arranged in a curved band towards the distal tip of the surstylus, although there is a handful (typically 4 or 5) located beneath the epandrial posterior lobes. Positioned centrally on the distal tip of the surstylus is a longer and more slender bristle that extends outwards to cross the opening of the aedeagus (Figure 2-1). This is known as the surstylar long bristle. Interestingly, bilateral ablation of these surstylar long bristles significantly reduces the chances of mating but does not affect attachment, detachment or mating posture (Acebes 2003). Unilateral ablation of surstylar long bristles, however, did not result in reduced mating rate, latency or duration, but caused males to adopt a striking asymmetric mating position where the male would lean to one side of the female's body. The direction of this lean was contralateral to the ablation – right-side ablation resulted in a left-leaning male (Acebes 2003).

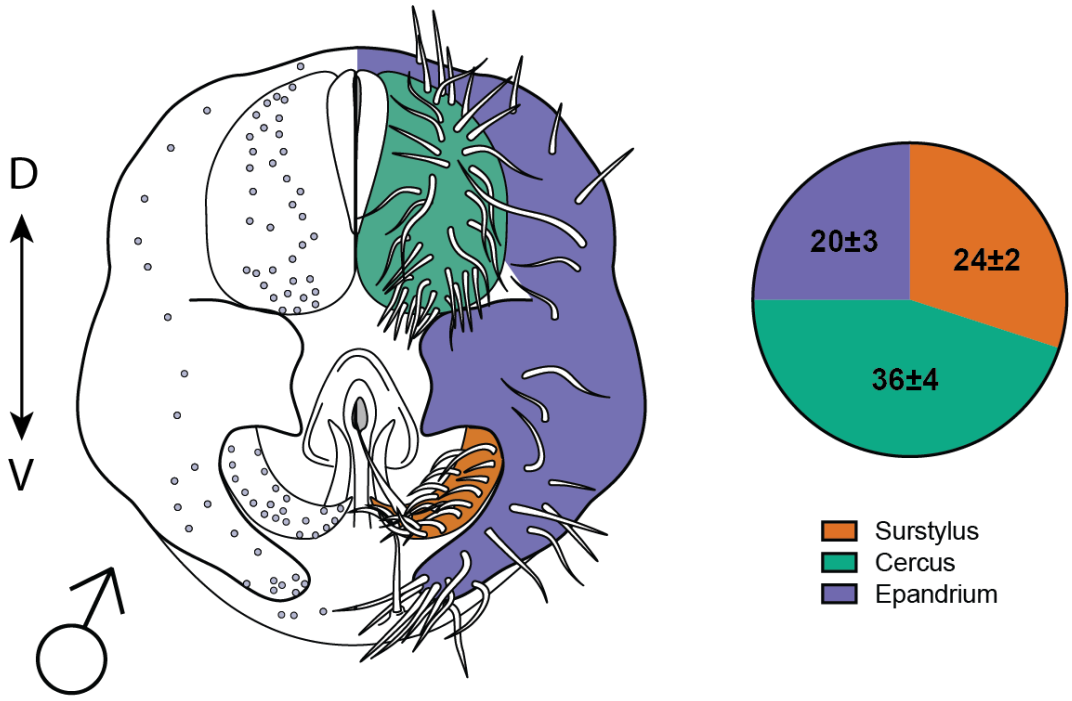

Figure 2-1: Cartoon of Drosophila melanogaster male genitalia.
For clarity, right side shows the bristles whilst left side shows typical bristle position. The average bristle number per side (n=20) is indicated by colour. Note the longer surstylar bristle. Figure adapted from Pavlou *et al*. (2016). D – Dorsal, V – Ventral.

In females, the total number of bristles is less at 36±3 bristles per side of the genitalia, with an average of 18±2, 15±2 and 4±1 bristles on the anal plate, vaginal plate and 8th abdominal tergite, respectively. The anal plate and abdominal tergite bristles are long and slender, akin to the epandrial and cercal bristles of the male, while the bristles associated with the vaginal plate are shorter, more rigid and arranged in a line running parallel to the central opening of the vagina. These vaginal plate bristles (often termed vaginal teeth) more closely resemble basiconic chemosensory sensilla which often house one or more gustatory sensory neurons and a single mechanosensory neuron (Falk *et al*. 1976). This configuration suggests that females may be able to respond to gustatory cues, perhaps when selecting an oviposition site in response to nutrients, as has been shown for other species (Rice, 1977).

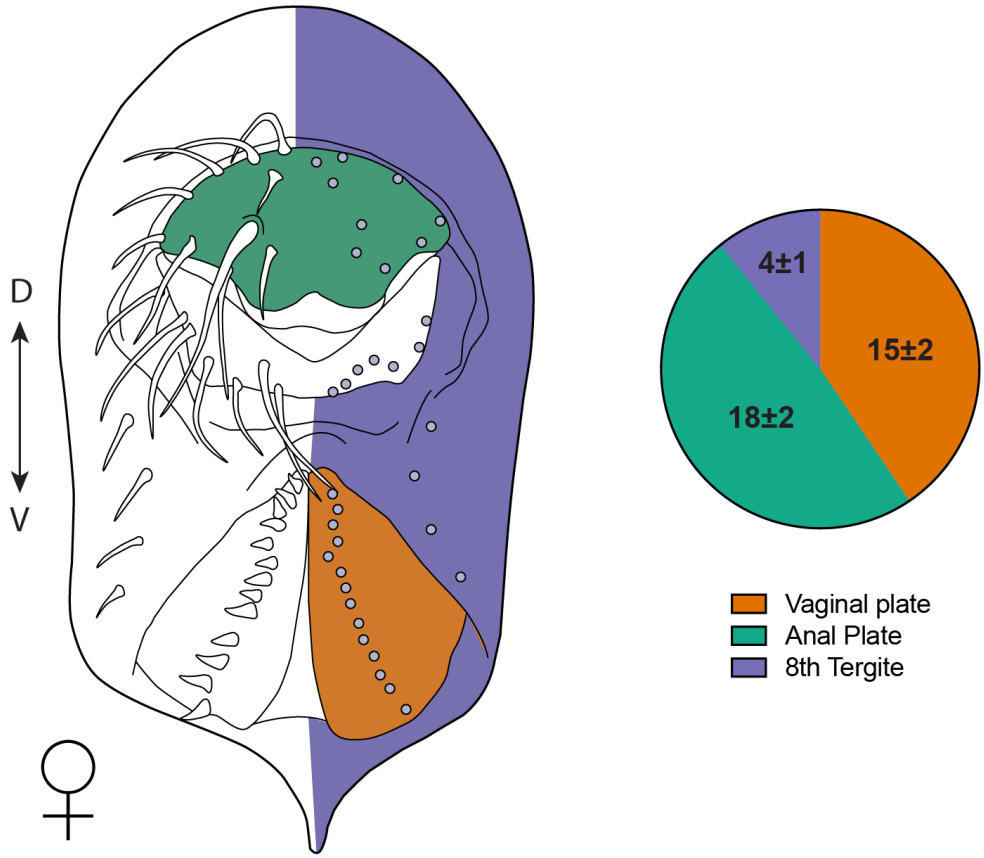

Figure 2-2: Cartoon of *Drosophila melanogaster* female genitalia.
For clarity, left side shows the bristles whilst right side shows typical bristle position. The average bristle number per side (n=20) is indicated by colour. Image adapted from Taylor (1989). D – Dorsal, V – Ventral.

2.3 Neurotransmitter Usage of Genital Sensilla

One useful avenue for intersecting these cells and describing their qualities is to identify their neurotransmitter usage, as one would expect that cells which are capable of transducing external stimuli onto internal motor circuits are likely excitatory cells.

The primary excitatory neurotransmitter in *Drosophila* is acetylcholine (Ach). As such, when driving a membrane-bound *UAS-mCD8::GFP* under the control of *ChAT* - an enzyme that is required for Ach biosynthesis - the majority of mechanosensitive neurons known in the fly are labelled (Tuthill and Azim 2018). For this reason, I

surveyed the expression of *ChAT-T2A-GAL4* driving *UAS-mCD8::GFP* (Diao and White 2012). Imaging of these animals revealed extensive labelling of bristle neurons in the cercus, epandrium and surstyli of the male genitalia, and the vaginal plates, anal plates and 8th abdominal tergite of the female genitalia (Figure 2-6). More specifically, the median number of *ChAT-T2A-GAL4* labelled cells was 51±5 per side (median ± (range/2), n=20) amounting to a significantly smaller number of neurons (64.5%) than exterior bristles in CS males (Figure 2-6C). This underrepresentation of innervated sensilla was found in all regions of the male genitalia, with 18±3 bristles in the surstyli, 18±2 in the cercus and 16±4 bristles in the epandrium (see Figure 2-6 figure legend for statistical comparison). In females, we identified a similar trend, with *ChAT-T2A-GAL4* driving expression in a total of 30±1 neurons per side, a significantly smaller number than that of the total cuticular bristles (Figure 2-6D). More specifically, *ChAT-T2A-GAL4* marked 10±1 bristle neurons in the vaginal plates, 17±1 bristle neurons in the anal plates and 3±1 bristle neurons in the 8th abdominal tergite (see figure legend for statistical comparison). Intriguingly, these results suggest that not every external bristle is innervated by a sensory neuron and the location of these innervated bristles may be functionally relevant with a higher density of neurons visible in the surstyli and ventral cercal lobes, the two regions which come into the most contact with a copulatory partner (Jagadeeshan and Singh 2006). However, it is important to consider that some variation in the number of labelled cells could be a result of genetic variation between the driver lines or in body size between individuals.

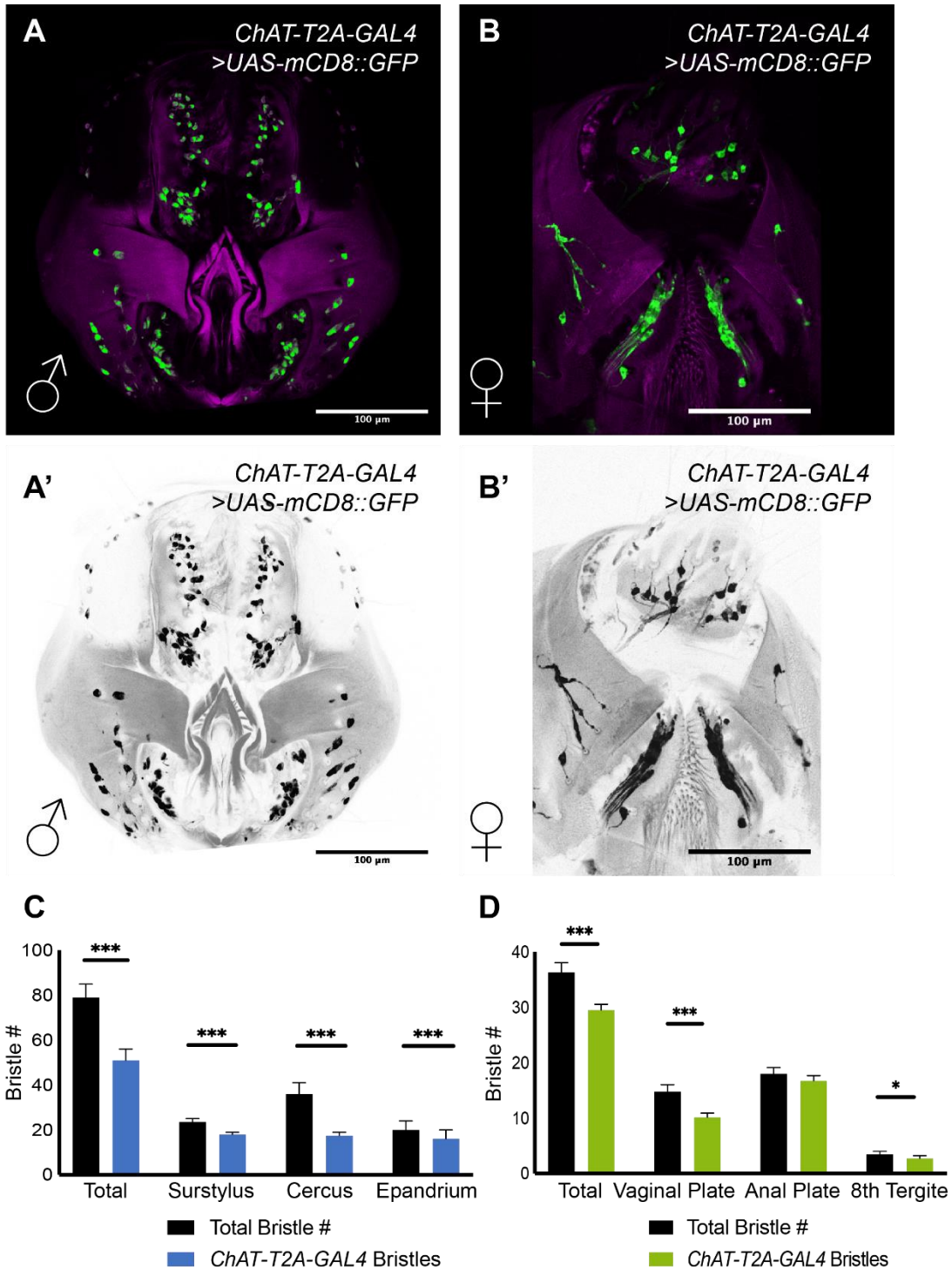

Figure 2-3: *ChAT-T2A-GAL4>UAS-mCD8::GFP* labels genital sensilla in male and female genitalia.

Maximal Z-projection of male and female *ChAT-T2A-GAL4* genitalia show extensive labelling of bristle neurons. **(A&A')** Male expression labels 18±3 surstylar bristles, 18±2 cercal bristles and 16±4 epandrial bristles. **(B&B')** Female expression labels 10±1 vaginal plate bristles, 18±1 cercal bristles and 3±1 bristles on the 8th abdominal tergite. **(C)** Comparing the number of *ChAT-T2A-GAL4* labelled cells in males against the total number of exterior bristles reveals there are a significantly smaller number of cholinergic neurons than exterior bristles, both in terms of total number (per side); $t(18)=23.69$, $p<0.0001$, and in specific regions, i.e. the surstylus ($t(18)=8.88$, $p<0.0001$), cercus ($t(18)=20.84$, $p<0.0001$), and epandrium ($t(18)=6.33$, $p<0.0001$). **(D)** We identified a similar trend when examining *ChAT-T2A-GAL4* in the female terminalia for the total number of labelled cells; $t(18)=8.5$, $p<0.0001$, vaginal teeth; $t(18)=8.28$, $p<0.0001$, and the 8th abdominal tergite; $t(18)=2.44$, $p=0.031$, but we did not

see any significant difference in number in the anal plate ($p>0.05$). N=10 for all count data. $P<0.05$ (*), $P<0.01$ (**), $P<0.0001$ (***). Error bars are standard error of the mean.

To verify that these labelled cells are indeed innervating the bristle of the male terminalia, I imaged this line from a lateral view. This image reveals the characteristic dendritic morphology that is common to bristle neurons (Figure 2-7; Tuthill and Wilson 2016).

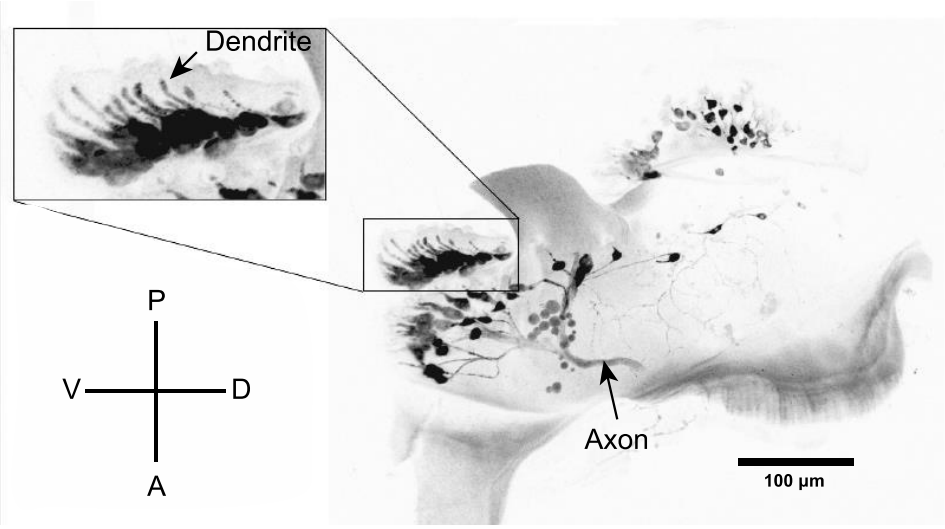

Figure 2-4: *ChAT-T2A-GAL4* neuron morphology supports their role in innervating genital sensilla.
The dendritic projections of neurons innervating surstylar teeth (enlarged view in box) indicates that they innervate the base of hollow bristles, a morphology that is characteristic of mechanosensory neurons. This same morphology is also apparent in the dendrites of neurons innervating all regions of the male genitalia. Axonal projections are combined into a large nerve fibre which projects anteriorly into the ventral nervous system. A – Anterior, P – Posterior, V – Ventral, D – Dorsal.

These results indicate that the neurons innervating male and female terminal sensilla are excitatory cholinergic neurons, suggesting a hypothesis that they are poised to provide real-time sensory feedback to motor circuits for the control of attachment, detachment, and mating posture.

2.4 Mechanosensitive Ion Channel Expression in Genital Sensilla

To confirm whether MTS neurons express the necessary ion channels to perceive mechanical stimuli, I surveyed a collection of GAL4 drivers for the mechanosensitive channels *nompC*, *Piezo, pickpocket*, *nanchung* and *inactive* (Table 2-1).

Table 2-1: Mechanosensory ion channel lines screened for MTS expression.
Name, related gene and source of mechanosensory GAL4 drivers screened for this thesis.

Line	Gene	Reference
nompC-GAL4	*nompC*	Cheng *et al*. (2010)
Piezo-GAL4	*Piezo*	Kim *et al*. (2012)
iav-GAL4	*inactive*	Kwon *et al*. (2010)
nan-GAL4	*nanchung*	Kim *et al*. (2003)
ppk-GAL4	*pickpocket*	Grueber *et al*. (2007)

2.4.1 nompC-GAL4

nompC is a mechanosensory pore-forming subunit in the TRP family. It is considered a 'gentle touch' channel and provides sensitivity to mechanical deflections of as little as 10μm in otherwise non-mechanosensory neurons or S2 cells (Yan *et al*. 2013; Zhang *et al*. 2015). Mutant analysis reveals that the gating of mechanical disturbances onto the pore requires tethering of ankyrin repeat domains to tubulin microtubules (Zhang *et al*. 2015), and it has previously been implicated in behaviours surrounding food texture detection (Sanchez-Alcaniz *et al*. 2017), locomotion (Cheng *et al*. 2010) and hearing (Effertz *et al*. 2011).

nompC-GAL4 is a fusion line derived from 1.5kb of regulatory sequence located immediately upstream of the first exon of *nompC* (Cheng *et al*. 2010). Its expression reliably labels adult leg chordotonal organs and bristle-associated neurons (Figure 2-5 B-F).

Examining *nompC-GAL4>UAS-mCD8::GFP* in the male terminalia revealed labelling of 49±3 bristle neurons per side, making up ~62% of the total exterior bristles. These bristles included 19±2 cercal bristle neurons, predominantly on the ventral side, 14±1 ventral epandrial bristle neurons and 16±2 surstylar bristle neurons at the distal tip, including the long surstylar bristles (Figure 2-5 A). While *nompC-GAL4* expresses in the larval nerve cord, no expression was observed in the adult brain or VNS (Cheng *et al*. 2010). This restricted pattern which completely encompasses the complement of *ChAT*-positive bristle neurons (see Figure 2-6), highlights *nompC* as a potential intersectional partner for drivers labelling MTS neurons, but which also have broader central nervous system expression.

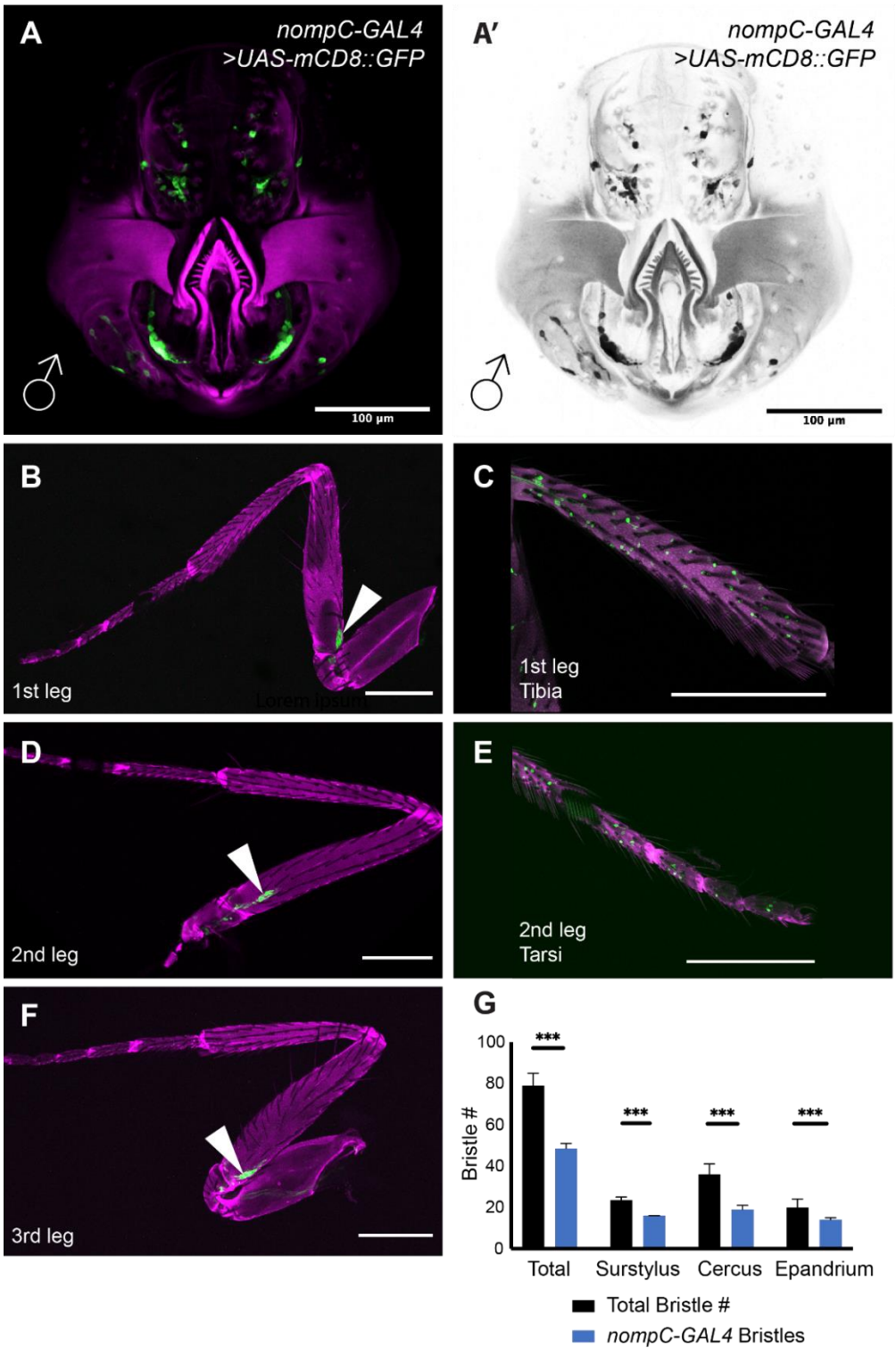

Figure 2-5: *nompC-GAL4* expression in the male genitalia, leg chorodotonal organs and bristle neurons.
(A) *nompC-GAL4* labels 19±2 cercal, 16±2 surstylar and 14±1 epandrial bristle neurons in the male genitalia, **(B, D, F)** leg chordotonal organs (arrowheads) and **(C & E)** leg bristle neurons. Scalebar in A is 100µm, and 200µm in B-F. **(G)** Comparing the number of bristles innervated by *nompC* neurons against the number of external bristles reveals this number is significantly lower both in total number; $t(18)=28.59$, $p<0.0001$, and in each separate region of the genitalia: surstylus; $t(18)=37.34$, $p<0.0001$, cercus; $t(18)=17.17$, $p<0.0001$ and epandrium; $t(18)=12.60$, $p<0.0001$. n=10 for count data. P<0.05 (*), P<0.01 (**), P<0.0001 (***).

2.4.2 Piezo-GAL4

The cation channel *Piezo* is the only member of the protein family by the same name that is encoded by the *Drosophila* genome. Commonly expressed alongside the degenerin/epithelial sodium channel (DEG/ENaC) family member *pickpocket* in larval multidendritic neurons, *Piezo* is considered a ‘painful’ touch, or nociceptive channel that responds most strongly to forces above 45 millinewtons (mN; Kim *et al*. 2012). When examining *Piezo-GAL4* expression the male genitalia and other peripheral tissues (*Piezo-GAL4>UAS-mCD8::GFP;* Figure 2-6), labelling of bristle neurons in the cercus, epandrial lobes and surstyli was visible. Interestingly *Piezo-GAL4* labels 50±3 bristle neurons, indicating that it may be co-expressed in all *nompC* neurons in the male genitalia. This similarity in cell number is uniform across all regions of the genitalia; surstyli bristle neurons - 16±2, cercal bristle neurons - 21±2 and epandrial bristle neurons - 16±2. *Piezo-GAL4* was also extremely broad in other regions of the peripheral nervous system, particularly in leg chordotonal organs and other external bristles (Figure 2-6 B-D).

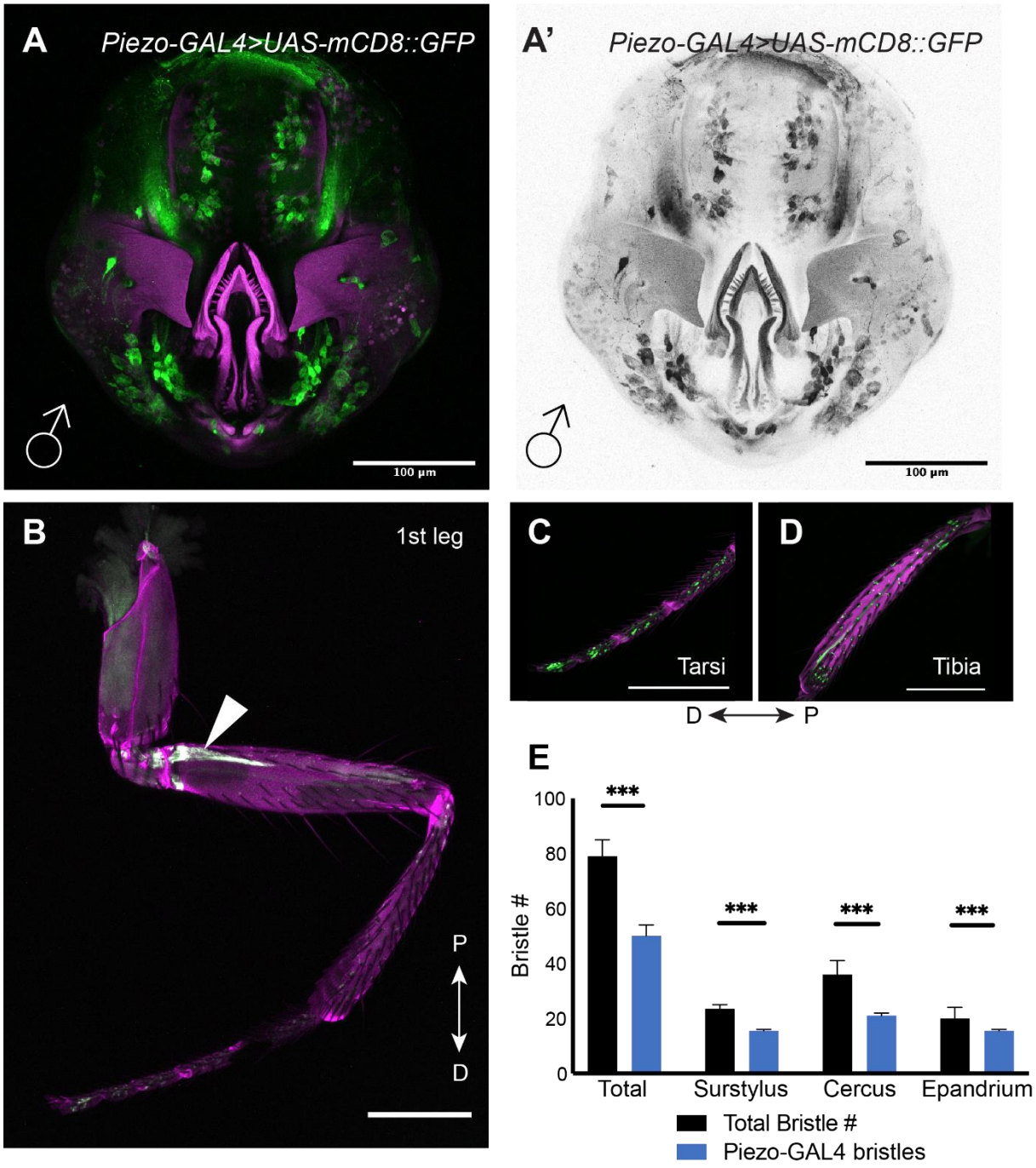

Figure 2-6: *Piezo-GAL4* expression in male genitalia and peripheral sensory neurons.

(A) *Piezo-GAL4* expression in male genitalia showing labelling of 16±2 surstylar bristle neurons, 21±2 cercal bristle neurons, and 16±2 epandrial bristle. Also labelled are **(B)** femoral chordotonal organs (arrowhead, 1st leg shown for illustration) and **(C-D)** leg bristle neurons. **(E)** Comparing the number of Piezo-expressing bristle neurons to the total number of exterior bristles revealed a significant underrepresentation both the total number; $t(18)=17.7$, $p<0.0001$, and in all regions of the male genitalia. Surstylus; $t(18)=10.37$, $p<0.0001$, cercus; $t(18)=10.97$, $p<0.0001$, and epandrium; $t(18)=6.80$, $p<0.0001$. Scale bar = 100µm in panel A and 200µm in B-D. N=10 for all count data. P – proximal, D – distal. $P<0.05$ (*), $P<0.01$ (**), $P<0.0001$ (***).

2.4.3 *iav-GAL4* and *nan-GAL4*

inactive and *nanchung* expression is generally considered to be restricted to larval and adult chordotonal organs, but we screened expression of both *iav-GAL4* and *nan-GAL4* to more completely characterize the complement of mechanosensory organs in the male genitalia. When used to drive *UAS-mCD8::GFP* we did not identify any expression in the male genitalia of either line (Figure 2-7), and only identified expression in femoral chordotonal organs as previously described (Figure 2-7 C-G).

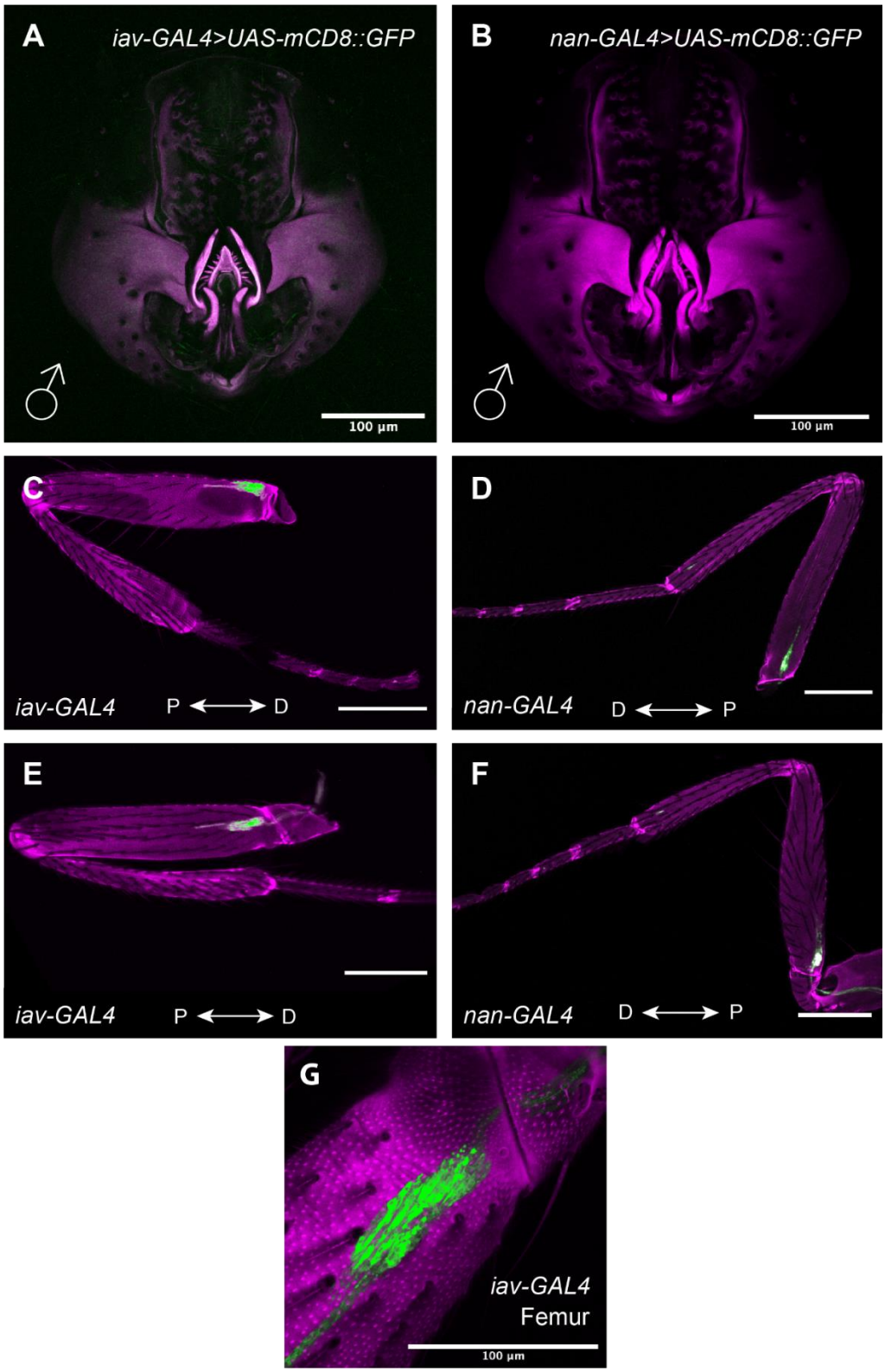

Figure 2-7: *iav-GAL4* and *nan-GAL4* expression in male genitalia and leg chordotonal organs.

(A) Male genital expression of *iav-GAL4* and **(B)** *nan-GAL4* does not label MTS neurons. **(C-F)** Femoral chordotonal organs are reproducibly labelled by both lines with *inactive* labelling a larger number of chordotonal neurons than *nanchung* **(G)**. Scalebar = 100µm in panels A, B and G, and 200µm in panels C-F.

2.4.4 ppk-GAL4

Lastly, the epithelial sodium channel *pickpocket (ppk)* is expressed in class I-IV dendritic arborization (da) neurons in the larvae and adult, contributing to both mechanical nociception and dendritic pruning during metamorphosis (Shimono *et al*. 2009). Behaviourally, *pickpocket* expression in the peripheral nervous system has been associated with feeding behaviour (Kuraishi *et al*. 2015), and *fru*/*dsx*-positive *pickpocket* cells have been shown to be necessary and sufficient for inducing sex peptide induced female postmating behaviour (Hasemeyer *et al*. 2009; Rezaval *et al*. 2012; Yang *et al*. 2009). However, descriptions of *pickpocket* expression in genital sensilla are at best limited.

To identify whether *ppk-GAL4* expression could provide a useful tool for intersecting MTS neurons, I examined it's expression in the male genitalia with the membrane-bound *UAS-mCD8::GFP.* Examining this pattern revealed that *ppk-GAL4* does not label any bristle sensilla but does label class IV multidendritic da neurons with extensive projections beneath the genital cuticle (Figure 2-8).

I also identified expression in a single neuron near the anus that does not exhibit the characteristic dendritic projection of bristle neurons (Figure 2-8 arrowhead). Curiously there is no bilaterally symmetric partner to this neuron, which may identify it as the anal sensory neuron (ASN) - a *pickpocket*-positive neuron that is stochastically positioned to one side of the midline but has symmetrical arbors covering the body wall around the anal slit and extending along the anal sphincter to detect opening and closing (Zhang *et al*. 2014).

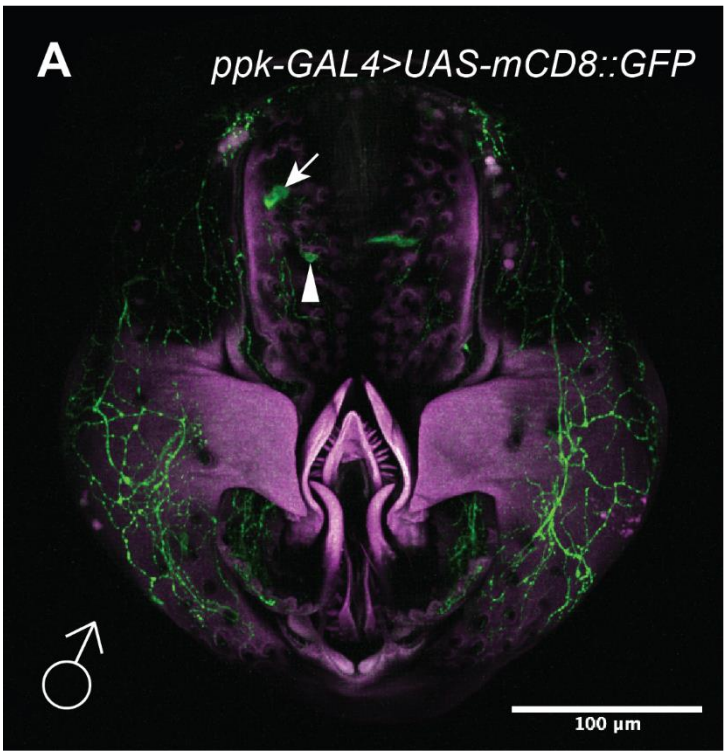

Figure 2-8: *ppk-GAL4* expresses in multidendritic neurons and anal sensory neuron.

Ppk-GAL4 expression the male genitalia does not label neurons innervating bristles, but does label multidendritic class IV da neurons under the cuticle wall. Arrowhead indicates a unilateral neuron positioned near the anus which may be the anal sensory neuron described in Zhang *et al*. (2014). Arrow indicates a da neuron cell body.

2.5 Developmental Gene Expression in Adult Terminalia

The imaginal discs of *Drosophila* are groups of epithelial cells that are set aside to remain quiescent during embryonic development, proliferate during the larval period and then differentiate during metamorphosis to give rise to the adult legs, wings, halteres, eyes, antennae and genitalia (Cohen *et al*. 1991). The genital disc is of particular interest as its development is regulated in three distinct manners. The *decapentaplegic, hedgehog, wingless* and *engrailed* signalling pathways convey positional boundaries to cells within the disc, whilst Hox genes such as *Abdominal-B (Abd-B)* inform anterior-posterior segmental identity within the whole animal. Lastly, as discussed in chapter one, the terminal transcription factor in the sex determination

pathway - *doublesex* - is required for the sex-specific morphology of the genitalia. Therefore, I reasoned that targeting my screening towards lines associated with genes in these three groups would best serve me in identifying novel drivers to MTS.

To identify whether drivers relating to any of these genes might provide robust genetic access to MTS neurons, I first surveyed the expression of *doublesex* and *fruitless* in the male genitalia and then moved towards examining the expression of *Abd-B* and *engrailed* drivers. Lastly, I attempted to subdivide the expression domain of some of these lines by examining FlyLight driver lines which tile promising loci in the hope of isolating specific enhancers to my region of interest (Jenett *et al*. 2012; Jory *et al*. 2012; Pfeiffer *et al*. 2008).

2.5.1 *doublesex* Labels a Subset of Terminal Sensilla.

To functionally identify sub-populations of *dsx* neurons with differing neurotransmitter profiles, Pavlou *et al.* (2016) generated a dsx^{DBD} split-GAL4 hemidriver by homologous recombination. Combined with the pan-neuronal split-hemidriver, $elav^{VP16AD}$ (Luan *et al*. 2006), they identified sexually dimorphic patterns of *dsx*-expression in several bilateral clusters of mechanosensory neurons of the male and female adult terminalia. They also observed expression in the forelegs and labellum of both sexes. In males, *dsx* neurons in the terminalia are associated with bristles of the clasper teeth, lateral plates and anal plates, and are cholinergic. In females, they are associated with bristles of the anal plates, vaginal plates, and 8th abdominal tergite.

To better quantify the expression of *dsx*^{DBD} in genital bristle neurons and assess its' utility for further intersection, we utilised this same hemi-driver combination *(dsx*^{DBD}∩*elav*^{VP16AD}*)* with a membrane bound GFP (*UAS-mCD8::GFP*). Examination of *dsx*^{DBD}∩*elav*^{VP16AD}*>UAS-mCD8::GFP* animals revealed labelling of bristle neurons in all regions of the male and female genitalia (Figure 2-9). In males, a total of 43±7 bristle neurons were labelled per side. Within these, 16±2 innervate surstylar teeth, 14±3 innervate cercal bristles and 13±4 innervate epandrial bristles.

Much like *ChAT-T2A-GAL4* (

Figure 2-3*), dsx*^{DBD}*∩elav*^{VP16AD}*>UAS-mCD8::GFP labels a little over half the total* number of bristles that we identified on the exterior male genitalia, although this percentage is dependent on the region, with as high as 67% of surstylar bristle neurons being labelled (Figure 2-9).

Interestingly, comparing the number of MTS labelled by *dsx*^{DBD}∩*elav*^{VP16AD} to the number labelled by *ChAT-GAL4, nompC-GAL4* and *Piezo-GAL4*, suggests that the full complement of surstylar and epandrial bristles express *doublesex, ChAT, nompC* and *Piezo*, but in the cercal lobes, significantly fewer cells are marked by *doublesex* than the other three drivers (Figure 2-9E). This may indicate that a small number of cercal bristle neurons do not express *doublesex* and may not be directly under the influence of the sex determination pathway. Alternatively, *doublesex* expression in these cells may not continue into adult stages of development. These results suggest that while not all exterior bristles are sensory or *dsx*-positive, the majority of innervated MTS are partnered with neurons that express *ChAT*, *nompC* and *Piezo*.

In females, a total of 31±6 bristles per side are labelled by *dsx*^{DBD}∩*elav*^{VP16AD}*>UAS-mCD8::GFP,* totaling 86.1% of the total bristles we identified in CS females (Figure 2-9 B&D). 12±3 vaginal plate bristles, 16±2 cercal bristles and 3±1 8th abdominal tergite bristles are labelled.

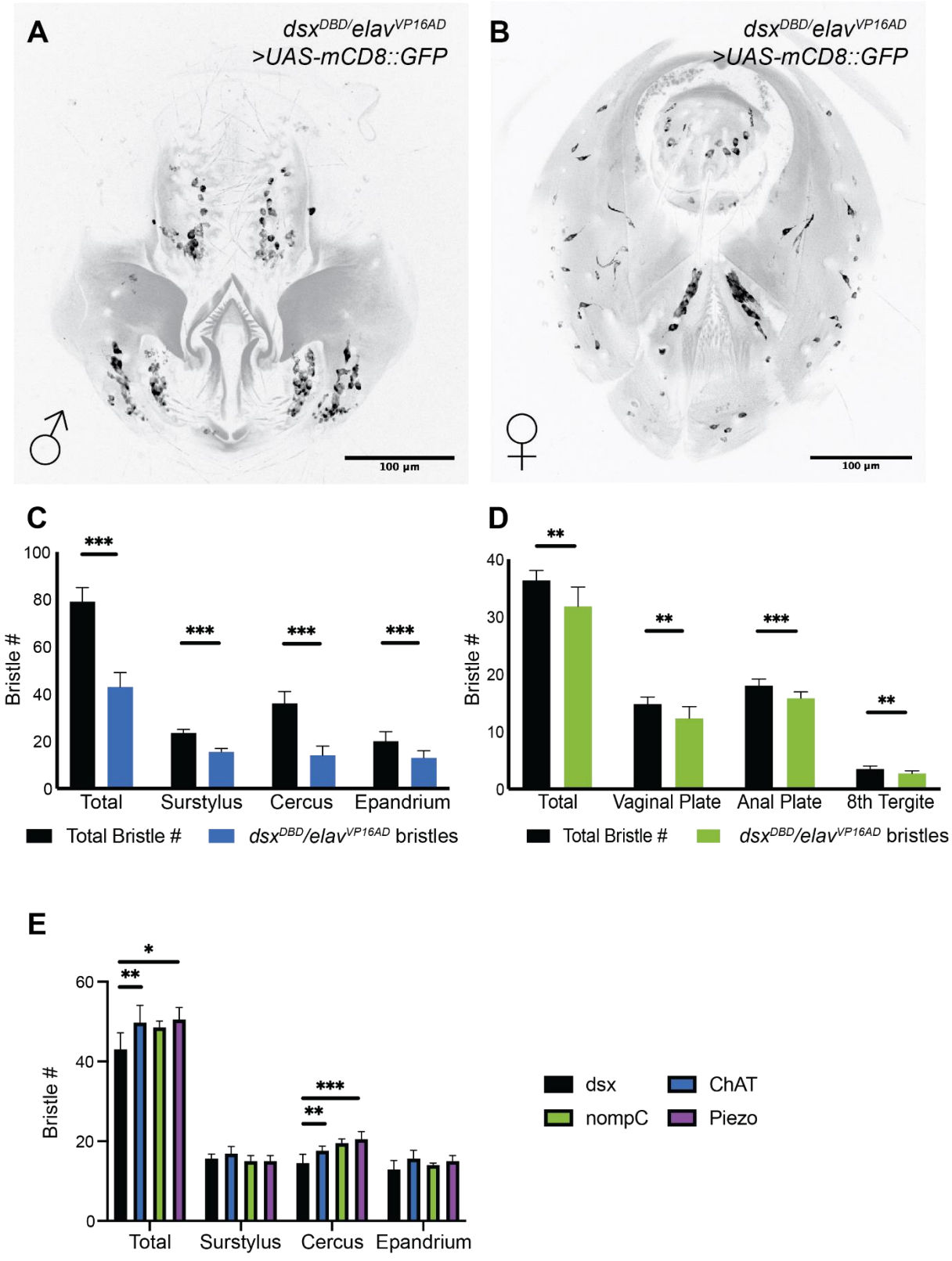

Figure 2-9: *dsx^{DBD}∩elav^{VP16AD}>UAS-mCD8::GFP* labels male and female genital bristles.

(A) Maximal Z-projection of *dsx^{DBD}∩elav^{VP16AD}>UAS-mCD8::GFP* male genitalia marks a total of 43±7 bristle neurons per side, 16±2 of these innervate surstylar teeth, 14±3 innervate cercal bristles and 13±4 innervate epandrial bristles. **(B)** In females *dsx^{DBD}∩elav^{VP16AD}>UAS-mCD8::GFP* marks an average total of 31±6 bristles per side, comprising 86% of the bristles in that region. 12±3 vaginal plate bristles, 16±2 cercal bristles and 3±1 8th abdominal tergite bristles are labelled. **(C)** In males *dsx^{DBD}∩elav^{VP16AD}*

neurons labelled ~54% of the bristles present on the cuticle (t(18)=23.37, p<0.0001). This trend was seen throughout all regions of the male genitalia: surstylus (t(18)=13.62, p<0.0001), cercus (t(18)=20.22, p<0.0001), and epandrium (t(18)=9.18, p<0.0001). **(D)** In the female, a greater but still significantly small proportion of bristles are innervated by $dsx^{DBD} \cap elav^{VP16AD}$ neurons (t(18)=3.75, p=0.0015). This underrepresentation is common for all regions of the female genitalia: vaginal plate (t(18)=3.30, p=0.004), anal plate (t(18)=4.30, p=0.0004), and 8th abdominal tergite (t(18)=3.54, p=0.0023). **(E)** Comparing the number of $dsx^{DBD} \cap elav^{VP16AD}$ neurons against ChAT-GAL4, *nompC-GAL4,* and *Piezo-GAL4* labelled neurons reveals that these drivers label the same complement of neurons in all regions but the cercus, where *dsx* marks a significantly smaller proportion of cells than all three other lines; *ChAT-GAL4* (one-way ANOVA with Bonferroni correction, p=0.0014), *nompC-GAL4* (p<0.0001), and *Piezo-GAL4* (p<0.0001), suggesting that as well as not all bristles being sensory, a small subset do not express *doublesex*, although we cannot exclude the possibility that this is due to genetic variation or differences in body size. N=10 for all count data. P<0.05 (*), P<0.01 (**), P<0.0001 (***).

While it is possible that sensory neurons still innervate bristles on the male and female genitalia that are not marked by *ChAT-T2A-GAL4* or $dsx^{DBD} \cap elav^{VP16AD}$ (Diao and White 2012; Pavlou *et al*. 2016), the master regulatory role of *doublesex* in orchestrating genital development, and the role of acetylcholine as the primary neurotransmitter of peripheral sensory organs makes this unlikely. What is perhaps more likely is that the position of $dsx^{DBD} \cap elav^{VP16AD}$ cells are concentrated towards the distal tips of the surstyli and the ventral side of the cercal lobe, two regions that contact the female the most during genital attachment, and so would provide the greatest amount of sensory feedback (Jagadeeshan and Singh 2006). A more detailed analysis is required to identify whether these potentially non-sensory bristles induce a neuron through the same Notch/Delta dependent mechanism as the innervated bristles (Lai and Orgogozo 2004), which then undergoes cell death, or whether these bristles develop without an associated neuron. Using a marker for all neurons, such as *elav* or *nSyb-GAL4* and checking for the presence of neurons innervating these bristles at different timepoints in development will help to answer this question.

In general, the large proportion of cells marked by *dsx*^{DBD}∩*elav*^{VP16AD} and the reliability of the *dsx*^{DBD} hemidriver make this an excellent intersectional partner to combine with lines I have identified later in this thesis. However, to assess which other lines may give equal or better genetic access to these cells, I continued to screen other driver lines, beginning with *fru*^{GAL4} (Stockinger *et al*. 2005).

2.5.2 *fruitless* also Marks a Subset of Genital Bristle Neurons

To identify *fruitless* expression in male and female genital sensilla, I utilised *fru*^{GAL4} developed by Stockinger *et al*. (2005). Examination of *fru*^{GAL4} driven GFP expression (*fru*^{GAL4}*>UAS-mCD8::GFP)* revealed labelling of genital sensilla in the male and female genitalia (Figure 2-10).

In males, the total number of labelled cells per side (27±2) is only 34% of the total number of bristles we counted on CS male genitalia. Of these, 9±1 were neurons innervating surstylar teeth – approximately one-third of the total number of bristles we scored in this region and 34% of the total exterior bristles. In females, *fru*^{GAL4} labels an average of 17±2 genital bristle neurons, ~44% of the total female exterior bristles (Figure 2-10 B).

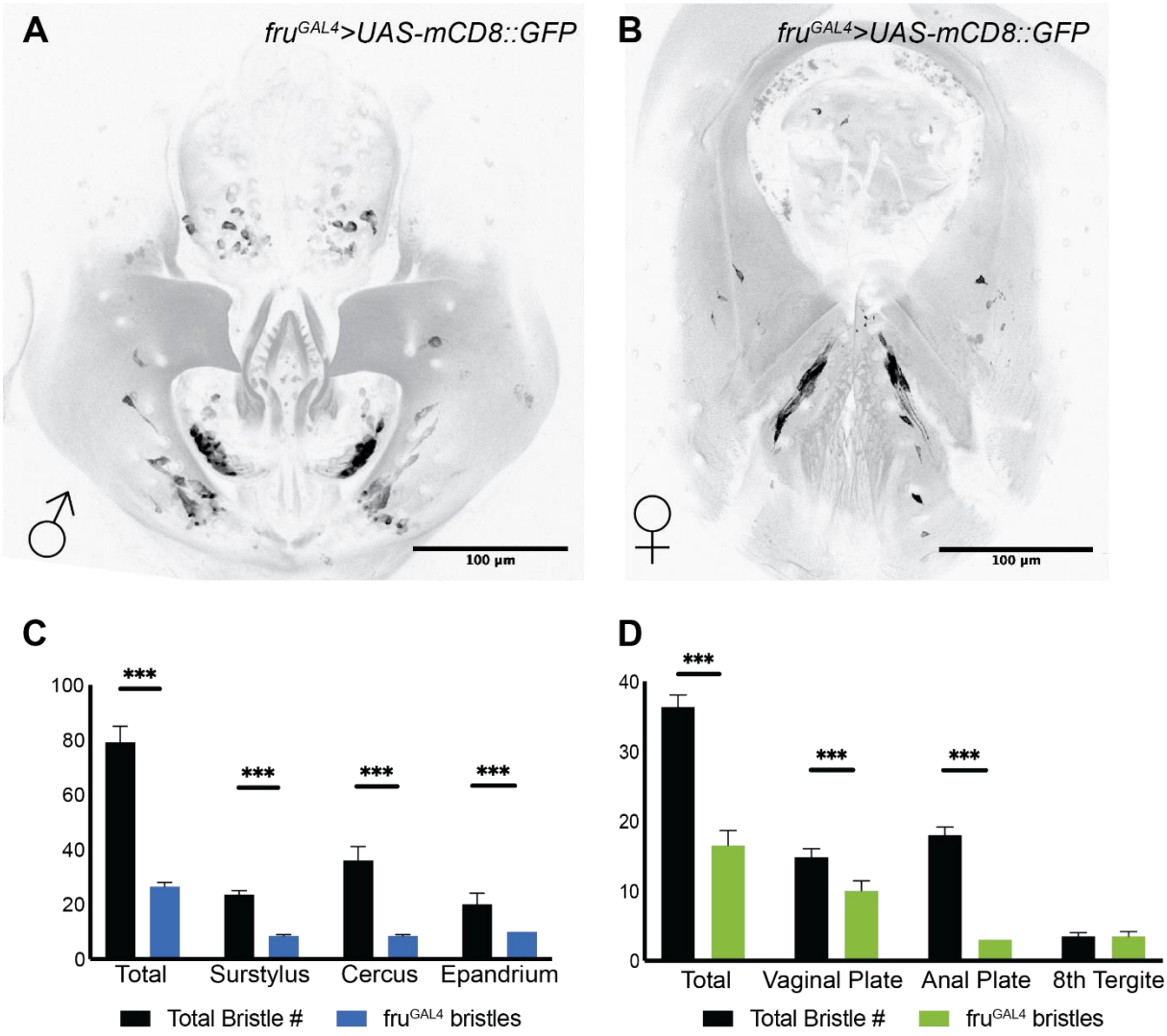

Figure 2-10: *fru^{GAL4}* expression in male and female genitalia.

(A) Maximal Z-projection of male genitalia reveals labelling of sensilla neurons in the surstyli (9±1), cercus (9±1) and epandrium (10±0). **(B)** Female labelling reveals sensory neurons in the vaginal teeth (10±1), 8th abdominal tergite (4±1) and cercus (3±0). **(C)** *fru^{GAL4}* labels a small proportion of the total male bristles in the surstyli ($t(18)=20.70$, $p<0.0001$), cercus ($t(18)=20.72$, $p<0.0001$), and epandrium ($t(18)=14.73$, $p<0.0001$). **(D)** In females this trend is also present in the vaginal plate ($t(18)=4.96$, $p=0.0006$) and anal plate ($t(18)=17.68$, $p<0.0001$), but not the 8th abdominal tergite ($t(18)=0$, $p=1$) N=10 for all count data. $P<0.05$ (*), $P<0.01$ (**), $P<0.0001$ (***).

These results show that *fru^{GAL4}* labelled bristle neurons are primarily located in either the distal tip of the surstyli, the ventral cercal lobe and the ventral epandrial lobe. These findings are consistent with those of Manoli *et al*. (2005) who independently developed *fru^{P1}-GAL4* to capture the expression of Fru^{M} products and were able to identify labelling of putative mechanosensory neurons in the surstyli, cercus and epandrium.

Although the expression of *fru*^{GAL4} in MTS makes it a potentially useful tool for spatially restricting expression to genital sensilla, the broader expression of *fru* in the central nervous system and the lower proportion of labelled cells means that for this thesis I have focused on intersecting against *dsx* rather than *fru.* However, to achieve the most precise intersection of MTS possible for behavioural analysis - ideally targeting only peripheral sensilla and not any CNS neurons which express *dsx* – I next asked whether the broader expression domain of *dsx* could be further subdivided.

In an attempt to achieve this, I utilised promoter fusion lines from the Janelia FlyLight collection (Jenett *et al*. 2012; Jory *et al*. 2012; Pfeiffer *et al*. 2008) and focused on their expression in the male terminalia.

2.5.3 *doublesex* Promoter Fusions Label Smaller Bristle Subsets

To separate smaller numbers of cells which are labelled by *dsx,* I utilised the FlyLight collection of enhancer trap lines (Jenett *et al*. 2012; Jory *et al*. 2012; Pfeiffer *et al*. 2008). I selected 14 lines which tile ~48 kb of the *dsx* locus and cover all introns, exons and ~5kb upstream of the transcription start site. Each of these lines name, stock number and genomic position as per the Flybase genome release 6.32 is listed in Table 2-2. GAL4 stocks were visualised in combination with *UAS-mCD8::GFP* and LexA drivers were combined with *LexAop-mCD8::GFP.* Split-hemidriver stocks were imaged in combination with *dsx*^{DBD} and *UAS-mCD8::GFP* to visualise *bona fide dsx*-positive cells.

Table 2-2: Driver stocks for identifying subsets of *doublesex*-positive genital bristles.

Stock numbers relate to the Bloomington *Drosophila* Stock Centre (BDSC). Numbers given as 'N/A' indicate that these lines have been removed from stock centre collections since this screening took place. Sequence locations are from FlyBase *D.melanogaster* release 6.32 and are for the loci which were cloned to develop the drivers. For examination, all transgenes are inserted into the third chromosome insertion site attP2 (Markstein *et al*. 2008).

Driver	Stock #	Genitalia Expression	Sequence Location	Nature of line
40F04	50094	no	3R:7,970,268..7,973,286	GAL4 driver
42B01	69894	no	3R:7,967,735..7,971,550	p65AD hemidriver
42C06	50150	no	3R:7,962,625..7,966,507	GAL4 driver
39E06	50051	no	3R:7,960,790..7,962,578	GAL4 driver
40F03	47355	no	3R:7,956,762..7,959,777	GAL4 driver
42D04	47588	no	3R:7,953,942..7,957,854	GAL4 driver
41A01	39425	no	3R:7,951,729..7,954,994	GAL4 driver
42A11	N/A	no	3R:7,949,001..7,952,795	GAL4 driver
68D03	N/A	no	3R:7,946,411..7,949,735	GAL4 driver
41F06	47584	no	3R:7,944,266..7,947,896	GAL4 driver
42D02	41250	yes	3R:7,941,579..7,945,482	GAL4 driver
41D01	50123	no	3R:7,938,919..7,942,427	GAL4 driver
42G02	61540	yes	3R:7,930,618..7,934,708	LexA driver
40A05	48138	yes	3R:7,925,287..7,927,810	GAL4 driver

Of these 14 lines, only three; 40A05, 42D02 and 42G02 showed expression in the genitalia.

42D02 expression appeared to be restricted to subcuticular cells, potentially cells which are involved in secretion of the cuticle itself, but was not found to have any expression in MTS neurons (Figure 2-11).

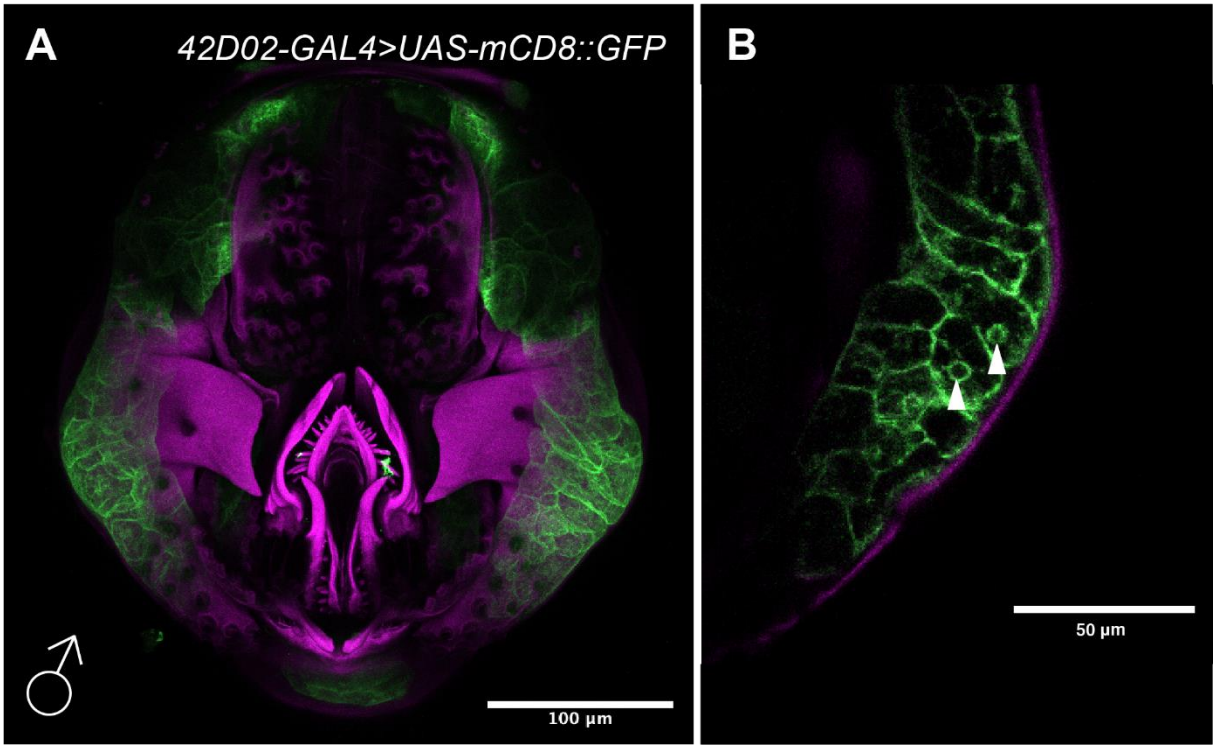

Figure 2-11: *42D02-GAL4>UAS-mCD8::GFP* labels subcuticular cells of the male terminalia.

(A) Maximal Z-projection of *42D02-GAL4* male genitalia showing lack of neuronal labelling but with extensive expression in subcuticular cells. **(B)** Enlarged view of epandrium cross-section showing subcuticular cells. White arrows indicate nuclei. Green = GFP, Magenta = Cuticle.

On the other hand, 40A05 and 42G02 drivers both labelled MTS neurons (Figure 2-12). 40A05 labelled an average of 22±2 cells per side with 8±0 of these being located in the distal tip of the surstyli (n=10, Figure 2-12A), whilst 42G02 labelled an extremely small number of surstylar bristles, typically only one or two per side in the male (Figure 2-12B) and did not label neurons in the female terminalia (data not shown).

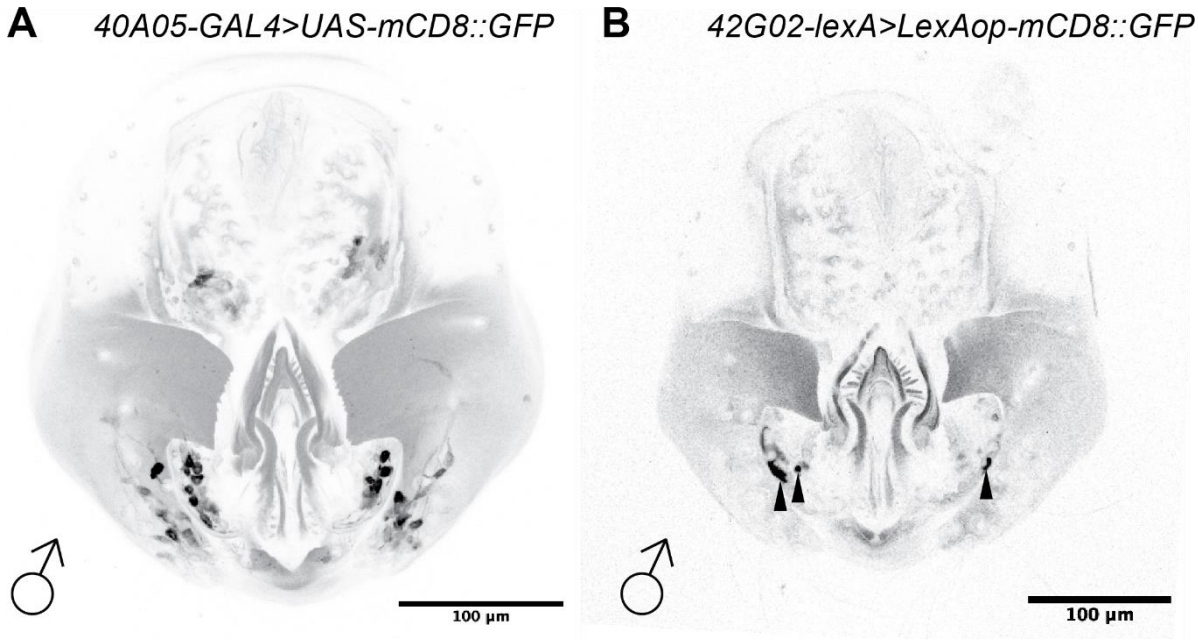

Figure 2-12: MTS labelling with *40A05-GAL4* and *42G02-LexA.*

(A) Maximal Z-projection of *40A05-GAL4>UAS-mCD8::GFP*, reveals labelling of MTS in surstyli (8±0), epandrium (10±1) and cercus (5±0). **(B)** Maximal Z-projection of *42G02-LexA>LexAop-mCD8::GFP* reveals limited labelling of surstylar bristles (indicated by black arrows). N=10 for all counts.

2.5.4 The Hox Gene *Abd-B* Labels a Restricted Population of Surstylar Bristles

Positional information at both the whole organism level and within individual appendages is vital for proper development in *Drosophila.* At the whole organism level, the anterior-posterior axis is specified by homeodomain-containing Hox genes (reviewed in; Akam 1998). The most posteriorly expressed Hox gene – *Abd-B* – is required for the proper specification of abdominal segments 5-9 (Sanchez-Herrero *et al*. 1985; Tiong *et al*. 1985) which in theory may provide genetic access to cells in all regions of the male genitalia except for the cercus which develops from abdominal segment 10.

To assess whether *Abd-B* drivers provide a useful level of restricted access to MTS, I surveyed the expression of *Abd-B^{LDN}-GAL4,* an enhancer trap lying 242 bp upstream of the *Abd-B^{m}* transcription start site (Bussell *et al*. 2014; de Navas *et al*. 2006; Estrada *et al*. 2002; Zavortink and Sakonju 1989). Imaging this line revealed expression that was limited in males to 15±1 neurons innervating surstylar bristles, including the long surstylar bristles, and one epandrial bristle per side (N=10, Figure 2-13 A). *Abd-B^{LDN}-GAL4* also labelled peripheral sensilla in the posterior abdominal wall, but did not label peripheral cells more anterior than abdominal segment 5 (A5, data not shown).

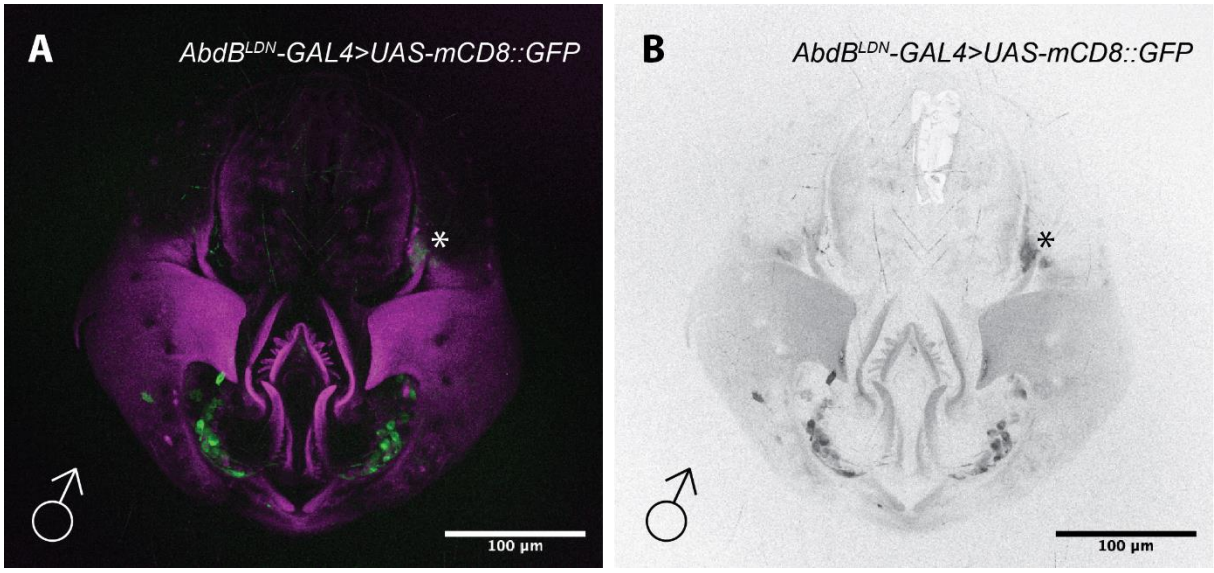

Figure 2-13: *Abd^{LDN}-GAL4* expression in the male genitalia.

(A) Maximal Z-projection of *Abd^{LDN}-GAL4* expression shown in colour, and **(B)** black and white for contrast. Asterisk marks green autofluorescence which is not related to neurons. On average, *Abd^{LDN}-GAL4* labels 15±1 surstylar bristles per side and one epandrial bristle per side. N=10. In (A), green indicates GFP expression under *Abd^{LDN}-GAL4* control, magenta marks the cuticle.

Investigating the central nervous system expression of this line revealed a large number of cell bodies in the Abg only (Figure 2-14 C & C'). Projections via the abdominal nerve trunk (AbNT; Court *et al*. 2017) are visible, presumably including the ascending axons of surstylar bristles (Pavlou *et al*. 2016; Taylor 1989). Also clearly

visible are projections ascending through the midline of the VNS, from the Abg and into the cervical connective to the brain (Figure 2-14 C & C'). These projections into the brain ramify extensively throughout the gnathal ganglia (GNG), ventrolateral protocerebrum (VLP), superior lateral protocerebrum (SLP) and superior medial protocerebrum (SMP. Figure 1-13 A-B'; Nomenclature as per Ito *et al*. 2014).These projections are located centrally and on the posterior surface of the brain (Figure 2-14 B & B'), only extending onto the anterior surface of the brain (Figure 2-14 A & A') to innervate the anterior VLP and GNG.

The lack of cell bodies outside of the Abg and genitalia highlight this line as a potentially useful tool that could be further developed into a split-GAL4 hemi-driver. Theoretically, if intersected against a line which does not express in Abg neurons but has many cell bodies elsewhere and in the surstyli – such as *nompC-GAL4*, one could restrict transgene expression to just the behaviourally relevant surstylar bristles.

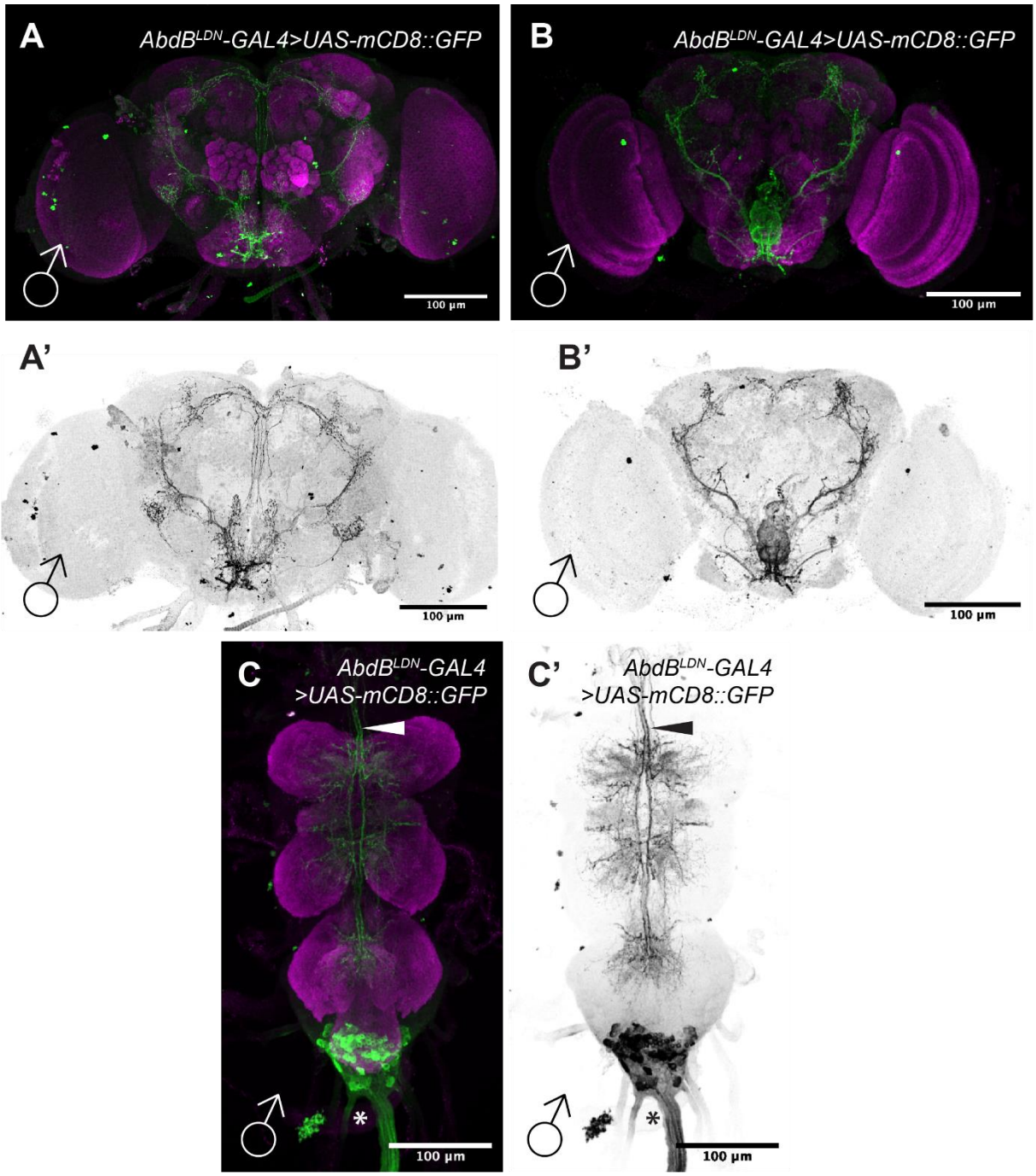

Figure 2-14: *AbdB^{LDN}-GAL4* projections in the brain and VNS of male *Drosophila.*

Maximal Z-projections of **(A & A')** anterior and **(B & B')** posterior brain of *AbdB^{LDN}-GAL4>UAS-mCD8::GFP* males. In A and B, green represents GFP expression and magenta is neuropil staining with nC82. **(C & C')** Ventral nervous system expression labels projections in the abdominal nerve trunk (asterisk), midline projections and ascending projections via the cervical connective (arrowhead). Scalebar is 100µm in all panels.

2.5.5 An *engrailed* Promoter Fusion Labels Surstylar Bristles

Appendages which develop from imaginal discs not only receive positional information at an organismal scale via Hox genes, but also more locally through the action of transcription factors like *engrailed (en), hedgehog (hh), wingless (wg),* and *decapentaplegic (dpp)* that act to specify distinct compartments within the developing discs (Emerald and Roy 1998; Morimura *et al*. 1996; Royet and Finkelstein 1997).

The activation of *engrailed* sets up the boundary between anterior and posterior founder cells in every abdominal segment by negatively regulating *dpp* in the posterior compartment (Kornberg *et al*. 1985; Sanicola *et al*. 1995). Importantly, *en* is expressed early in the specification of abdominal segment 9 (A9), which gives rise to the epandria and surstyli (Estrada *et al*. 2003). We reasoned that an *engrailed* driver might predominantly label cells in the surstyli, as they are the most posterior structures derived from this segment.

To exploit the posterior expression of *engrailed* to target surstylar bristles, we identified a promoter fusion termed *R94D09-GAL4* that lies ~30kb upstream of the *engrailed* transcription start site. Intriguingly, combining *R94D09-GAL4* with *UAS-mCD8::GFP* revealed minimal but repeatable expression in 6 surstylar bristle neurons per side (N=20, Figure 2-15), accounting for ~33% of the total number of cholingergic neurons in the surstyli. We reasoned that *R94D09* only labels a more distal subset of MTS neurons due to the role of *engrailed* in specifying posterior domains within a structure.

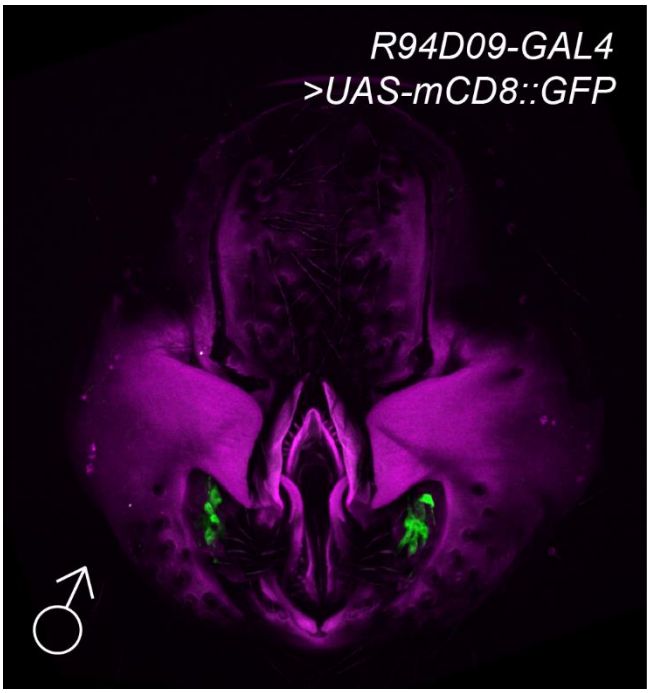

Figure 2-15: *R94D09-GAL4* expression in the male genitalia labels surstylar bristles exclusively. When combined with *UAS-mCD8::GFP*, *R94D09-GAL4* reliably marks 6 surstylar bristle neurons per side.

Closer inspection of the peripheral and central nervous system expression of *R94D09-GAL4* indicates that as well as expressing in the surstyli, *R94D09* labels projections throughout the VNS and brain, with cell bodies in the Abg, GNG and VLP (Figure 2-16 A&A').

This broader expression pattern of *R94D09-GAL4* in the central nervous system and in peripheral tissues like the legs (Figure 2-16 B-D) limits the utility of the GAL4 variant of this line. However, the future development of a split-GAL4 variant of *R94D09* that can then be combined with another split-GAL4 hemi-driver (e.g., a *nompC* hemi-driver) should provide an excellent means for specific perturbation of these sensilla.

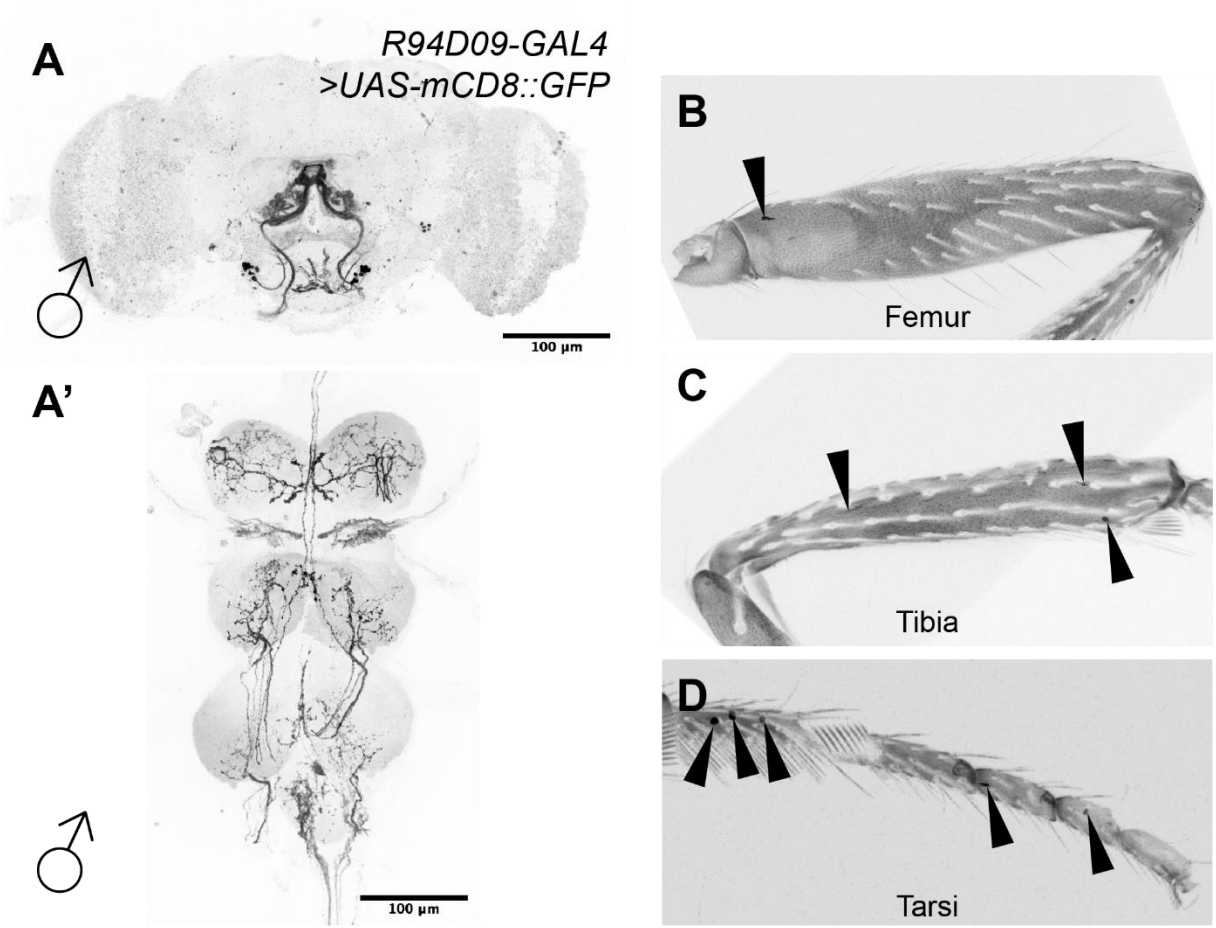

Figure 2-16: Central and peripheral nervous system expression of *R94D09-GAL4*.

(A & A') *R94D09-GAL4>UAS-mCD8::GFP* marks cell bodies in the gnathal ganglion and VLP in the central brain, and in the abdominal ganglion and accessory mesothoracic neuropil of the ventral nervous system. Projections into the VNS from peripheral tissues such as the legs and genitalia are clearly visible, with some projections in the cervical connective, although it is not clear whether these are ascending, descending, or both. **(B-D)** Expression of *R94D09-GAL4>UAS-mCD8::GFP* in the legs of male flies marks a singular femoral bristle neuron in each leg, **(C)** 2-3 tibia bristle neurons, and **(D)** 4-5 bristle neurons in the proximal segments of the tarsi. A further bristle neuron within each of the distal tarsal segments are also labelled. Scale bars are 100µm in all panels.

2.5.6 Alternative Genital Disc-expressing Enhancer Traps

Looking to further subdivide expression in MTS neurons, I identified a collection of enhancer traps that have been shown to express in the imaginal discs (Jory *et al*. 2012). Within this collection of 672 lines that express in at least one imaginal disc, 52 were found to express in the male genital disc but not the female. Of these, only 34 did not show expression in other imaginal discs structures like the legs (Table 2-3; Jory *et*

al. 2012). I reasoned that this collection might provide an excellent means for identifying drivers to MTS and examined the expression pattern of each of these lines in combination with *UAS-mCD8::GFP.* The resulting expression revealed that of the 34 lines screened; three showed expression in sensilla neurons; *73E12, 93D05* and *92B02*.

Table 2-3: Genital disc expressing lines from Jory *et al.* (2012).

Stock numbers relate to the Bloomington *Drosophila* Stock Centre (BDSC). Sequence locations are from FlyBase *D.melanogaster* release 6.32 and are for the loci which were cloned to develop the drivers. For examination, all transgenes are inserted into the third chromosome insertion site *attP2* (Markstein *et al*. 2008).

Line	BDSC #	Associated Gene	Sequence Location	Genital Exp?
GMR73E12	39823	*α2-adrenergic-like octopamine receptor (Octα2R)*	3R:18,836,917..18,840,614	Yes
GMR93D05	47223	*beaten path Vc (beat-Vc)*	3R:12,768,213..12,772,092	Yes
GMR92B02	40602	*beaten path Ic (beat-Ic)*	2L:15,986,889..15,989,682	Yes
GMR89C10	46878	*beaten path VI (beat-VI)*	3R:28,411,043..28,414,785	No
GMR83B11	46744	*Grunge (Gug)*	3L:8,458,842..8,462,019	No
GMR65H10	49614	*Tachykinin-like receptor at 99D (TkR99D)*	3R:29,955,189..29,956,568	No
GMR91G02	47176	*sidestep VIII (side-VIII)*	2R:20,434,312..20,437,234	No
GMR73E11	48317	*α2-adrenergic-like octopamine receptor (Octα2R)*	3R:18,840,008..18,843,750	No
GMR75D08	48323	*abrupt (ab)*	2L:11,219,699..11,223,184	No
GMR78A08	39986	*CG31859*	2L:12,594,708..12,598,170	No
GMR92H09	40634	*beaten path Ia (beat-Ia)*	2L:16,056,306..16,059,249	No

GMR87A08	40473	*Ecdysone-induced protein 93F (Eip93F)*	3R:21,926,730..21,929,966	No
GMR81E09	40118	*BarH1 (B-H1)*	X:17,352,542..17,354,699	No
GMR64H02	48232	*CASK*	3R:21,823,529..21,827,443	No
GMR85E08	46804	*spalt major (salm)*	2L:11,453,242..11,457,101	No
GMR87C08	40483	*spalt-related (salr)*	2L:11,394,036..11,397,012	No
GMR88C11	48629	*CG11247*	3L:21,721,026..21,724,164	No
GMR64G06	39317	*short neuropeptide F receptor (sNPF-R)*	3L:20,089,637..20,093,425	No
GMR88E08	46856	*empty spiracles (ems)*	3R:13,914,726..13,917,774	No
GMR81H03	47106	*NFAT nuclear factor (NFAT)*	X:13,634,466..13,636,954	No
GMR38A10	48134	*rhomboid (rho)*	3L:1,440,657..1,443,795	No
GMR84B06	47793	*Ionotropic receptor 68a (Ir68a)*	3L:11,236,599..11,240,241	No
GMR16F09	48736	*no ocelli (noc)*	2L:14,451,817..14,454,838	No
GMR15E10	48697	*sine oculis (so)*	2R:7,426,193..7,430,128	No
GMR78D09	39994	*CG34355*	3R:23,844,783..23,845,038	No
GMR37H08	49970	*Sarcoplasmic calcium-binding protein 2 (Scp2)*	3R:16,580,830..16,583,627	No
GMR84G01	48380	*spalt-related (salr)*	2L:11,359,028..11,361,047	No
GMR38F06	45254	*Protein tyrosine phosphatase 61F (Ptp61F)*	3L:1,443,158..1,446,973	No
GMR88G08	40528	*empty spiracles (ems)*	3R:13,929,027..13,932,185	No

GMR87B02	41316	*Ecdysone-induced protein 93F (Eip93F)*	3R:21,924,542..21,927,724	No
GMR89C03	46875	*beaten path VI (beat-VI)*	3R:28,423,343..28,426,466	No
GMR94A10	47246	*CG46339*	3R:26,921,815..26,924,674	No
GMR81D03	48365	*BarH1 (B-H1)*	X:17,339,489..17,342,836	No
GMR89B01	40541	*beaten path VI (beat-VI)*	3R:28,398,360..28,402,016	No

73E12-GAL4 expression is unique amongst the lines identified in this thesis as it primarily labels bristle neurons in ventral cercal bristles (Figure 1-20 A&A', mean=8±1, n=10) as well as one or two epandrial and surstylar bristle neurons. In the central nervous system, *73E12* expression is broad. There are a large number of cells in the brain, particularly in the optic lobe as well as the AOTU, VLP and lateral accessory lobe (Figure 1-20B; Ito *et al*. 2014). VNS expression is similarly broad, with *73E12* cells visible at the surface of all thoracic neuromeres, with the highest concentration located in the mesothoracic neuromere and accessory mesothoracic neuropil (Figure 1-20C; Court *et al*. 2017).

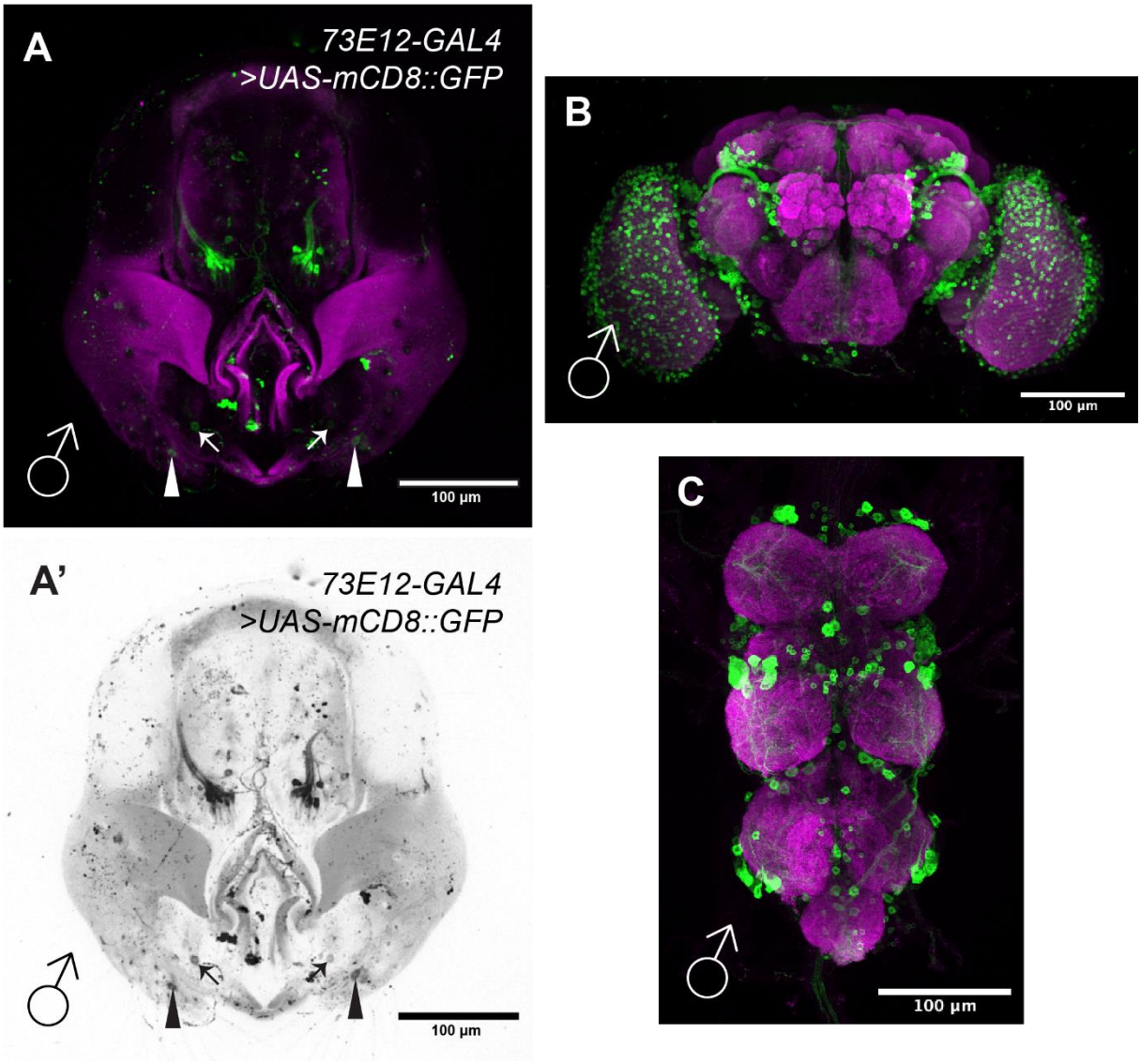

Figure 2-17: *73E12-GAL4* expression in the male genitalia and central nervous system.

(A) In the male genitalia *73E12-GAL4* labels 8±1 cercal bristle neurons and 1 to 2 epandrial (arrowheads) and surstylar bristle (arrows) neurons. **(B&C)** In the male central nervous system *73E12-GAL4* labels broad swathes of neural cells in the optic lobes, AOTU, AVLP and all thoracic neuromeres. In A, magenta represents the cuticle, whilst in B-C magenta is the neuropil stain nC82, and green represents *73E12-GAL4* driven GFP expression.

While *93D05* expression can be identified in the male genitalia, the labelled cells appear to be subcuticular, albeit a significantly smaller number and size of subcuticular cells than previously observed in *42D02-GAL4* males (Figure 2-18, Figure 2-11). As *93D05* does not provide genetic access to MTS, this line was not investigated further.

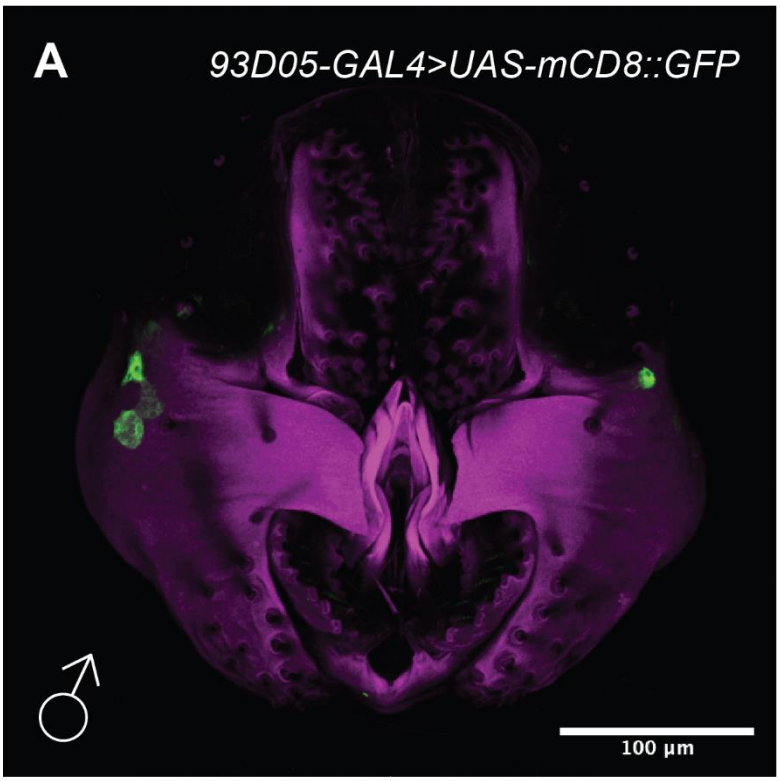

Figure 2-18: *93D05-GAL4* expression in the male genitalia.

93D05-GAL4>UAS-mCD8::GFP labels a small number of subcuticular cells on the lateral borders of the male genitalia. No labelling of MTS neurons was observed (n = 10).

Lastly, *92B02* labelled a handful of surstylar MTS neurons. The position of these neurons within the surstyli was surprisingly variable amongst individuals, so combined with its broader expression in the thoracic neuromeres, and the optic lobes and saddle in the central brain, this line was not suitable for behavioural experiments.

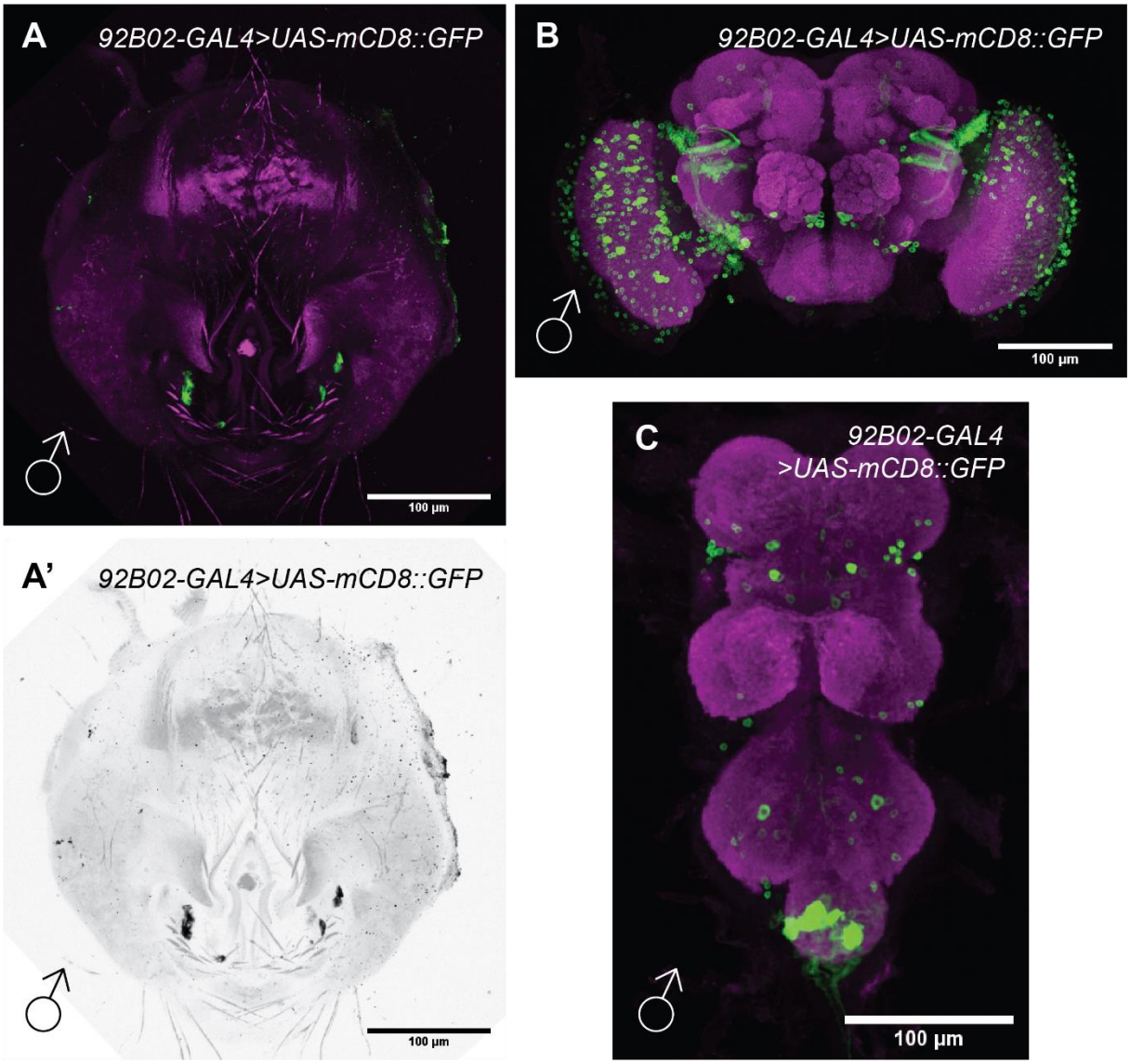

Figure 2-19: *92B02-GAL4* expression in the male genitalia and central nervous system.

(A) *92B02-GAL4>UAS-mCD8::GFP* labels neurons in the male surstyli, labelling ~4 neurons, and **(B & C)** the male brain and VNS, particularly in the abdominal ganglion and optic lobes.

2.6 Alternative Sources of MTS Drivers

As a final addition to the screening efforts presented within this chapter, two split-GAL4 hemi-drivers – *R20G10-p65AD* and *R23F02-p65AD* - were found within the Goodwin group, somewhat serendipitously, via an NBLAST screen (Costa *et al*. 2016) to identify drivers to *dsx*$^{+}$ pC2l neurons in the female brain (T. Nojima, personal communication). The first of these, *R20G10-p65AD*, is a ~3kb promoter fusion derived from regulatory sequences of the nicotinic Acetylcholine Receptor α3 gene (*nAChR α3*) and produces clearly dimorphic expression patterns when intersected against *dsx (dsx*^{DBD}*∩R20G10-p65AD)*. For example, in females *R20G10-p65AD∩dsx*^{DBD} drives *UAS-mCD8::GFP* to label a large number of Abg neurons that project extensively within the Abg, as well as the pC2l neurons themselves that project extensively in the superior lateral protocerebrum (SLP) and ventrolateral protocerebrum (VLP; Tetsuya Nojima, unpublished).

In males however, there are no cells labelled in the brain or VNS, and only projections into the abdominal ganglion are visible (Figure 2-20 A & B). These projections appear extremely similar in both position and morphology to the dye-labelled surstylar bristle neurons from Pavlou *et al*. (2016; compare Figure 1-23 panels C&D), thus we examined the genitalia of *dsx*^{DBD}*∩R20G10-p65AD>UAS-mCD8::GFP* males. Here, *dsx*^{DBD}*∩R20G10-p65AD* exclusively drives transgene expression in 6 surstylar bristle neurons per side located at the distal tip, and no other neurons (Figure 2-20 E&E'), making *dsx*^{DBD}*∩R20G10-p65AD* the ‘cleanest’ intersectional combination that we have identified for driving transgene expression in surstylar bristle neurons.

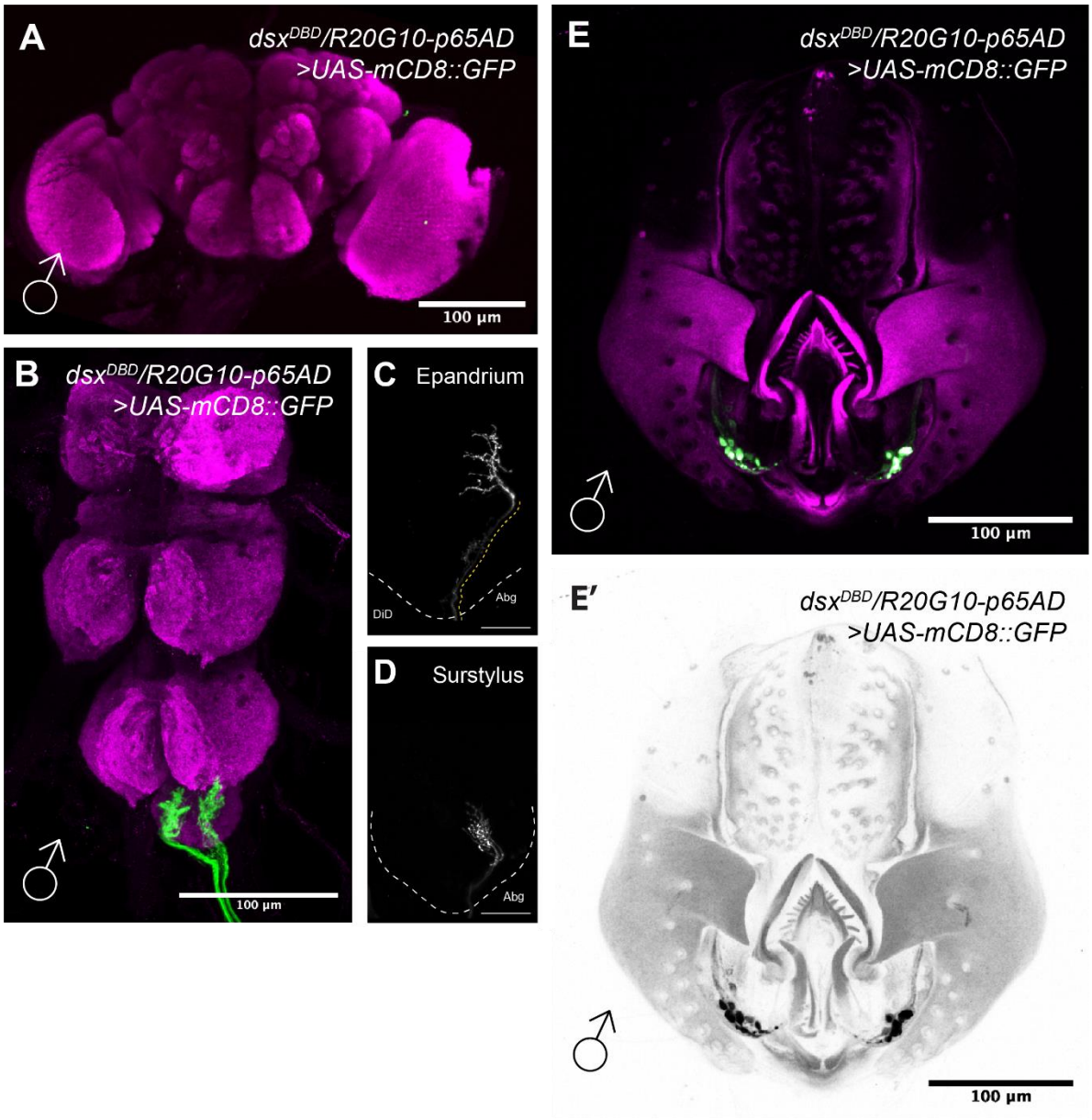

Figure 2-20: *R20G10-p65AD∩dsx^{DBD}>UAS-mCD8::GFP* labels only 6 surstylar bristle neurons in the male genitalia.
(A) There is no expression of *R20G10-p65AD∩dsx^{DBD}* in the male brain or cell bodies in the VNS **(B)**, although there are projections into the abdominal ganglion from the posterior. These projections share a distinctly similar morphology to back-filled surstyli bristle neurons from Pavlou *et al*. (2016; **C & D**). **(E & E')** In the male genitalia *R20G10-p65AD∩dsx^{DBD}>UAS-mCD8::GFP* labels 6 surstylar bristle neurons per side. Scale bars A-C are 100µm and 25 µm D-F.

Although we could not identify any projections into the thoracic neuromeres from other peripheral tissues like the legs and wings, we double-checked these regions to confirm the restricted nature of *dsx^{DBD}∩R20G10-p65AD*. Fortuitously, we did not observe any *dsx^{DBD}∩R20G10-p65AD* neurons innervating leg bristle neurons or other peripheral tissues of the male fly (Figure 1-24).

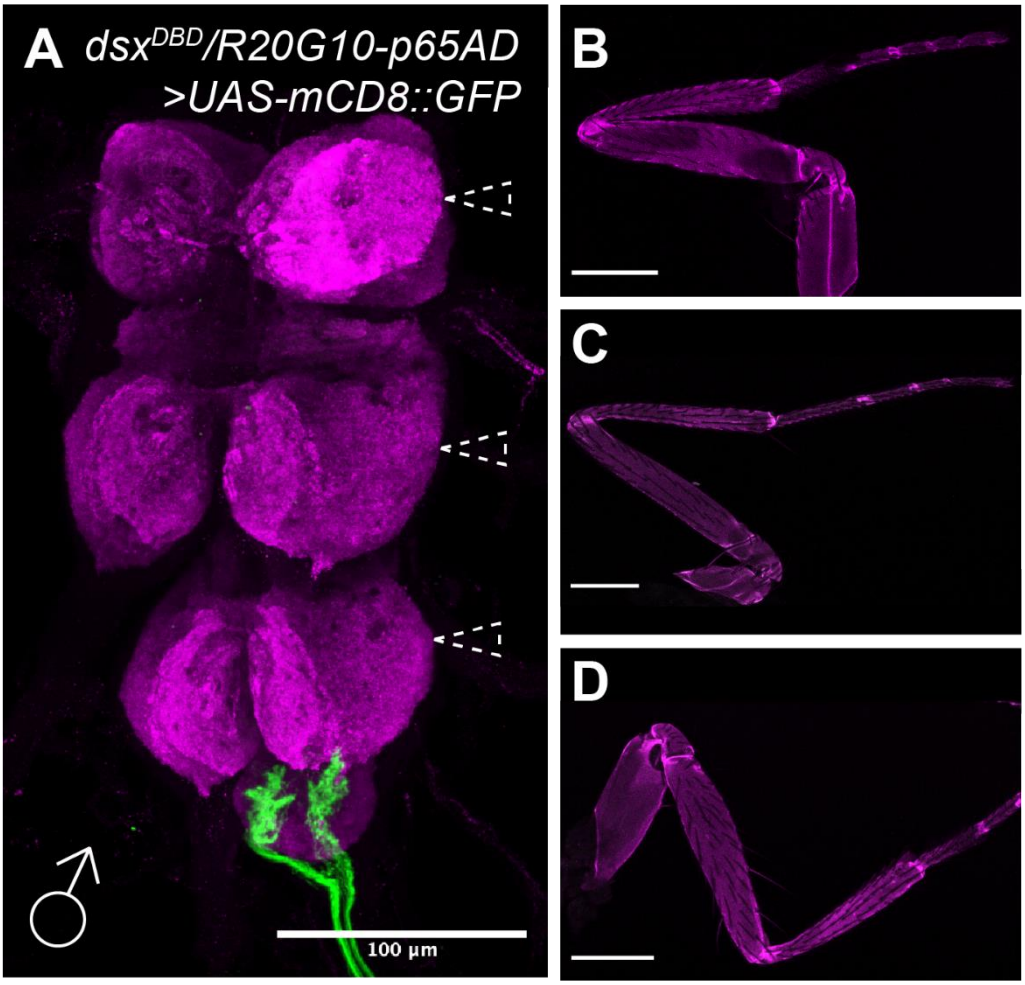

Figure 2-21: *dsx^{DBD}∩∩R20G10-p65AD* does not express in peripheral tissues.

(A) *R20G10-p65AD∩dsx^{DBD}>UAS-mCD8::GFP* male VNS showing characteristic surstyli neuron projections in the Abg and lack of inputs from peripheral organs (dashed arrowheads). **(B-D)** lack of labelling in the legs. Scale bar in A is 100µm and 200µm in B-D.

The second driver, *R23F02-p65AD,* is a promoter fusion line which drives expression under the control of ~3kb of regulatory sequence of *CG13229*, a 7-transmembrane G

protein-coupled receptor, which was noted as a potentially useful line for this study not because it labels any genital bristle neurons but because it may label neurons downstream of the MTS, and possibly act to combine sensory feedback from peripheral cells in multiple regions of the flies body. Combining *R23F02-p65AD* with *dsx^{DBD}* (*dsx^{DBD}∩R23F02-p65AD;* Figure 2-22) and computationally co-registering *dsx^{DBD}∩R23F02-p65AD* and *dsx^{DBD}∩R20G10-p65AD* expression in the male indicates that the putative output sites of surstylar bristle neurons may overlap with *dsx^{DBD}∩R23F02-p65AD* cells in the Abg (Figure 2-22 D). I will use both of these lines as part my 'genetic toolkit' to functionally test the role of MTS in attachment, detachment and mating posture. Should surstylar bristle neurons such as those labelled by *dsx^{DBD}∩R20G10-p65AD* be connected to *dsx^{DBD}∩R23F02-p65AD* neurons, then I would hypothesise that the artificial activation or inactivation of these two populations should result in similar or identical phenotypes, as it likely that some or all of the sensory information perceived by MTS neurons is incorporated downstream in cells such as those labelled by *dsx^{DBD}∩R23F02-p65AD,* and later incorporated into the control of other motor circuits.

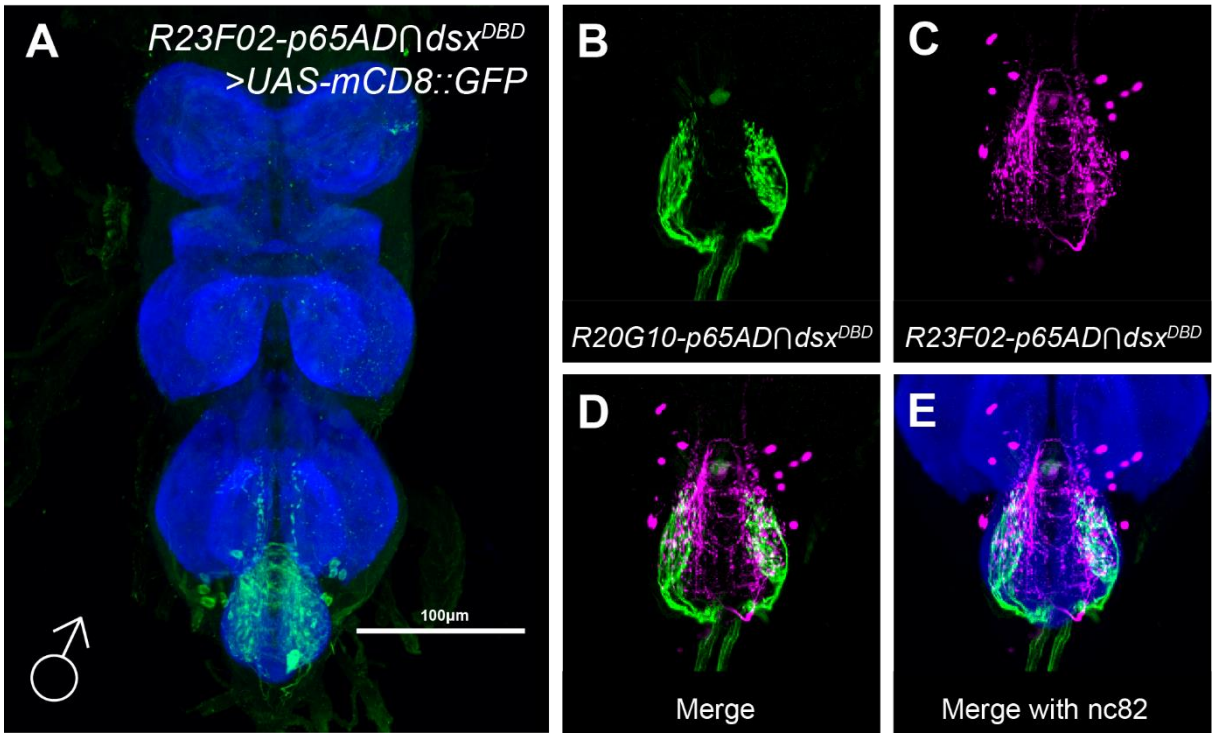

Figure 2-22: *dsx^{DBD}∩23F02-p65AD>UAS-mCD8::GFP* labels a set of abdominal ganglion interneurons that may connect with *dsx^{DBD}∩20G10-p65AD* cells.

(A) *dsx^{DBD}∩23F02-p65AD>UAS-mCD8::GFP* expression in the central nervous system is limited to a set of 9 abdominal ganglion interneurons. **(B)** Computationally co-registering both *dsx^{DBD}∩20G10-p65AD* projections with those of *dsx^{DBD}∩23F02-p65AD* **(C)** reveals putative synaptic overlap between the two **(D&E)** suggesting a functional connection.

2.7 Approach

While this style of targeted screen does not maximise the chances of finding every possible driver or hemidriver combination that labels our cells of interest, it has nonetheless proven to be an excellent method for rapidly developing a genetic toolkit that can later be refined. In future studies it may be possible to lean more heavily on the *de novo* generation of drivers that express in desirable spatiotemporal patterns, but by leveraging the increasing number of stocks present in curated public collections, we have shown that it is now more possible than ever to identify suitable lines for behavioural manipulation. Furthermore, whilst techniques like RNA-sequencing of the target cell(s) remain unparalleled in their ability to establish gene expression profiles

in all tissue types, these techniques are currently time and resource intensive, and the identification of driver lines that label MTS neurons provides an excellent insight into the most important aspects of their underlying physiology with much less technical investment. In our hands this approach has been successful in providing us with several lines which can be further refined, or used immediately in behavioural experiments, and these data provide an invaluable resource that can be used in concert with gene expression profiles to further target subsets of MTS neurons in the future.

2.8 Conclusion

In this chapter, I have described a screen of publicly available lines to identify the best tools available for specifically targeting transgene expression to genital bristle neurons. The relative contribution of the various developmental genes, mechanosensitive ion channels and enhancer traps that drive expression in these cells is varied, and this screen has enabled a deeper characterisation of the different drivers so that the most appropriate lines can be carried forward for behavioural analysis.

Some of the lines identified here have spatially restricted expression, such as *R20G10* and *R23F02*, and thus are suitable for immediate use in behavioural experiments. Most lines however, exhibit expression more broadly, particularly in cases such as *nompC-GAL4* and *94D09-GAL4* which show expression in surstylar bristle neurons as well as many additional neurons in the peripheral and central nervous system. Interpreting aberrant phenotypes upon artificially modifying the activity of these neurons would be

complicated by their broader expression, limiting our ability to causally link the sensory function of genital bristle neurons to any phenotypes we observed.

I will next present my efforts to further refine these driver lines by developing split-Gal4 hemi-drivers for *nompC, Piezo, ChAT* and *94D09*. These efforts will be described in chapter 3 and are accompanied with characterisation of the novel lines and comparison to their progenitors where applicable. Ultimately the identification and further development of drivers to specifically target MTS neurons lays the groundwork for behavioural manipulations as these novel tools will be used in combination with dsx^{DBD}, *R20G10* and/or *R23F02* to gain the most precise and reproducible expression possible.

3 Generating Novel Intersectional Tools

3.1 Introduction

In chapter 2, I identified several genetic drivers and split-hemidrivers that may be used to gain genetic access to genital bristle neurons. Identifying these 'hits' – i.e. lines that express in our cells of interest – serves as the first step towards precisely expressing transgenes that manipulate the activity of these neurons. However, while classifying the lines that mark genital bristle neurons aides in building our understanding of the underlying circuitry for incorporating external mechanical stimuli into motor circuits, in many cases, these drivers are too broadly expressed for behavioural experiments, and manipulating the function of this population would only cause a syndrome of effects that confound our interpretation of results. To address this issue, one can develop novel split-hemidriver lines to refine the set of labelled neurons.

In accordance with previous studies examining mechanosensation in the fly, we have identified that genital bristle neurons express both *nompC* and *Piezo*, but do not express *pickpocket* or the chordotonal organ markers *inactive* and *nanchung. Piezo* is a nociceptive, or painful touch-responsive ion channel (Kim *et al*. 2012), while *nompC* is sensitive to significantly lower magnitudes of force (Yan *et al*. 2013), suggesting that it is *nompC* through which stimuli arising from attempted copulation and attachment are transduced. Furthermore, the results of chapter 2 support the notion that genital bristle neurons are capable of modulating motor circuits in the abdominal ganglion, and that their number and position is functionally relevant as evidenced by the higher density of innervated bristles in areas which contact the female during copulation (Jagadeeshan and Singh 2006). We have also identified that these neurons are likely cholinergic and *engrailed*-positive as they express a *ChAT* reporter and the *engrailed* promoter fusion; *R94D09*. However, as I have alluded to, these lines either express in

additional mechanosensory organs or other central brain neurons, so using these GAL4 lines alone would not be sufficiently restricted to draw causal relationships between genital bristle sensilla and copulation behaviour.

To overcome these limitations, I will present within this chapter the development of novel split-GAL4 hemidrivers for *nompC, Piezo, ChAT,* and *R94D09*. I will then show that by combining two of these intersectional tools, it is possible to restrict transgene expression to a much-reduced number of neurons whilst retaining genital bristle neuron labelling.

3.1.1 Intersectional Strategies

As stated in chapter 2, directing transgene expression to a specific spatially restricted population of neurons requires the employment of intersectional strategies. With the development of GAL80, Flippase recombinase, LexA/LexAop and QF/QUAS expression systems, there are at least four strategies that can be used alongside GAL4 drivers.

However, these approaches do have their limitations. GAL80, for example, must be expressed at a sufficiently high level before it can prevent GAL4-mediated transcriptional activation (Traven *et al*. 2006) and predicting the dosage of GAL80 when developing new tools is at best inaccurate. On the other hand, the use of FLP in intersectional strategies often results in imprecise expression patterns, most likely due to the excision of the *FRT-stop-FRT* cassette in cells where both promoters are active

at some point in development, resulting in the persistent activation of UAS-reporter/effector transgenes into later stages (Bohm *et al*. 2010).

Alternatively, one can leverage ternary methods like the split-GAL4 system in which each functional half of the GAL4 protein is placed under the control of a separate promoter and fused with a heterodimerising leucine zipper (Luan *et al*. 2006). In this way, only in the cells in which both promoters are active is the full GAL4 protein recapitulated (Luan *et al*. 2006). This restricted active domain of GAL4 can then be used in conjunction with a multitude of UAS-transgenes and with other binary and ternary expression methods.

Compared to other methods, the split-GAL4 system has few drawbacks. Although initially *UAS* transgenes were expressed at slightly lower levels when using split-GAL4 compared to binary GAL4 (Luan *et al*. 2006), this has been overcome by utilising VP16 or p65 activation domains over the GAL4 activation domain, endowing the system with the ability to drive much higher levels of transgene expression (Luan *et al*. 2006).

For this study, I have developed novel hemidrivers for the split-GAL4 system for several reasons. Firstly, as I have stated the level of expression is reliably high, and so transgene expression for anatomical characterization and behavioural manipulations will be robust.

Secondly, I wanted to use existing split-drivers like dsx^{DBD} in combination with those presented in this chapter. dsx^{DBD} faithfully recapitulates *dsx* expression and expresses in the full complement of surstylar neurons – the most behaviourally relevant genital bristle neurons – including those innervating long surstylar bristles which have previously been shown to affect mating posture (Acebes 2003).

Lastly, the adoption of the split-GAL4 system by many different *Drosophila* groups around the world has resulted in a plethora of UAS-reporter/effector lines, allowing me to perform both anatomical characterization and functional analysis by simply crossing two animals together.

For these reasons, the development of novel hemidrivers within this chapter has focused on developing split-GAL4 hemidrivers. These will allow me to utilise dsx^{DBD} (Pavlou *et al*. 2016) for intersection, and later on the artificial activation and inhibition of MTS neurons. More specifically I have made split-GAL4 AD drivers relating to *nompC, Piezo, ChAT* and the *engrailed* enhancer *R94D09.*

The generation of these novel tools requires a significant amount of time and labour, with no guarantee that the resulting transgenic animal will recapitulate the expression of the GAL4 progenitor. For these reasons and the continued utility of our lines in later studies, I have utilized two methods when developing our novel split-GAL4 lines: the Trojan-MiMIC system for *nompC, Piezo, ChAT* lines, and site-specific transgene integration into the attP2 landing site for my *R94D09* variant as this site is where the original GAL4 element is located.

These two methods have allowed me to precisely target the insertion of both DBD and AD split halves (in separate animals) so that they can be used in combination with almost any other split-hemidriver. Furthermore, they are located in a genomic position that is best suited to either A) capturing endogenous gene expression patterns, or B) producing reliable expression with minimum interference from the surrounding chromatin (Markstein *et al*. 2008), thereby increasing the likelihood of a successful outcome.

3.1.2 Site-specific Integration via φC31

As outlined in chapter 2 of this thesis, the φC31 phage integrase mediates recombination between bacterial *(attB)* and phage *(attP)* attachment sites (Groth *et al*. 2004; Groth and Calos 2004). The *attB* and *attP* sequences do not naturally exist within the *Drosophila* genome, and therefore any animal that has been modified to contain one of these sequences can later be injected with a construct carrying the concomitant site for high-frequency integrations targeted to that locus. Many hundreds of these sites have been randomly mobilised throughout the *Drosophila* genome to allow researchers to insert constructs into distinct loci. However, a handful of these sites, for example, *attP2* on the 3rd chromosome and *attP40* on the 2nd chromosome have seen large-scale adoption as the insertion site of choice because they provide high levels of induced expression but practically zero 'leakiness' – basal ectopic expression resulting from the influence of the surrounding chromatin (Markstein *et al*. 2008). The Janelia FlyLight collection of GMR lines (Jenett *et al*. 2012; Pfeiffer *et al*. 2008) utilises *attP2* for inserting all promoter fusion lines, and as such I have targeted the insertion of my promoter fusion constructs to this site to recapitulate the expression of the original line.

The further development of recombinase-mediated cassette exchange (RMCE) utilises a similar approach, but instead flanks the donor sequence with φC31 recombination sites (Bateman *et al*. 2006) to enable the clean exchange of donor and target sequences. This RMCE method provides the framework for the MiMIC system (Venken *et al*. 2011), which I have used to develop split-hemidrivers for *nompC, Piezo* and *ChAT.*

3.1.3 The Trojan-MiMIC system

The MiMIC (*Minos*-mediated integration cassette) system (Venken *et al*. 2011) utilises the *Minos* transposon carrying a cassette with six elements: Two inverted attP recombination sites at either side of the cassette, a splice acceptor followed by stop codons in all three reading frames, the coding sequence for enhanced GFP (eGFP), an SV40 polyadenylation signal, and a *yellow* body colour marker (Venken *et al*. 2011).

The inverted attP sites flanking the cassette allow for the exchange of the intervening sequence via RMCE (Bateman *et al*. 2006), resulting in the removal of the *yellow*$^{+}$ marker so that exchange events can be readily identified. For this study, we have used donor sequences developed by Diao *et al.* (2015) known as 'Trojan exons'. These contain a splice acceptor followed by the coding sequence of the T2A peptide and an effector transgene such as the GAL4 DNA binding domain or P65 activation domain (Diao and White 2012). By inserting these trojan exons into MiMIC landing sites residing within 'coding introns' (i.e. introns between coding exons), the cassettes act to trap both endogenous transcription and translation of the target gene. The viral T2A peptide contains a motif (Donnelly *et al*. 2001) that ultimately causes the ribosome to skip between two codons without forming a peptide bond, and the nascent product is divided into two parts – the endogenous gene product up until the skipped T2A amino acid, and a second product formed after the T2A, the effector transgene. This method allows one to express any protein, e.g. GAL4 or it's functional halves, only in cells where the target gene is expressed and where it is translated into protein form, thereby providing the highest likelihood of capturing the actual expression pattern of the target gene.

Results

3.2 Generating Trojan-MiMIC lines

For this thesis. I have developed Trojan-MiMIC lines relating to *nompC, Piezo* and *ChAT*. As the first step in this process, I identified a MiMIC insertion within each of these genes that was positioned between two coding exons common to all isoforms so that the cassette could effectively capture the highest levels of expression. In the case of *nompC* and *Piezo,* two such insertions were available, and so we converted both to activation domain hemidrivers to examine their expression. The MiMIC sites we chose are outlined in Table 3-1.

Table 3-1: MiMIC insertion sites converted for use within this study.

Genomic Coordinates as per FlyBase Genome release 6.33. Reading frame of insertion and the isoforms captured is as reported by the Gene Disruption Project.

Affected Gene	MiMIC insertion	Reading Frame and isoform capture	Coordinates
nompC	*Mi{MIC}nompC^{MI12787}*	nompC-RA:0, nompC-RD:0, nompC-RE:0, nompC-RF:0	2L:5,347,437..5,347,437
	Mi{MIC}nompC^{MI03523}	nompC-RA:1, nompC-RD:1, nompC-RE:1, nompC-RF:1	2L:5,361,413..5,361,413
Piezo	*Mi{MIC}Piezo^{MI04294}*	Piezo-RE:1, Piezo-RF:1, Piezo-RG:1, Piezo-RH:1, Piezo-RI:1, Piezo-RJ:1, Piezo-RK:1, Piezo-RL:1, Piezo-RM:1	2L:8,182,217..8,182,217

	Mi{MIC}Piezo^{MI04189}	Piezo-RE:0, Piezo-RF:0, Piezo-RG:0, Piezo-RH:0, Piezo-RI:0, Piezo-RJ:0, Piezo-RK:0, Piezo-RL:0, Piezo-RM:0, Piezo-RN:0	2L:8,176,213..8,176,213
ChAT	*MI{MIC}ChAT*^{MI04508}	ChAT-RA:0, ChAT-RB:0	3R:18,727,608..18,727,608

BestGene Inc. injected flies that were transgenic for these insertion sites and a source of φC31 integrase, with pBS-KS-attB2-SA-T2A-p65AD-Hsp70 (Diao *et al*. 2015) - a plasmid containing a splice acceptor, T2A and p65 activation domain in one of three reading frames. Transformation was directed towards the locus through the specificity of φC31-mediated RMCE. BestGene reported a transformation efficiency of ~15%.

3.2.1 *nompC*$^{MI12787\text{-}AD}$ and *nompC*$^{MI03523\text{-}AD}$

Of the two *nompC* lines I developed, *nompC*$^{MI12787\text{-}AD}$ showed genital expression (Figure 3-1 A&A'), while *nompC*^{MI03523} did not show any that we could identify (data not shown). We reasoned that this difference is likely due to variation in the strength of transcriptional capture between the two insertion sites.

Labelling 54±2 bristle neurons per side (median±(range/2), n=5), *nompC*$^{MI12787\text{-}AD}$*∩elav*^{DBD}*>UAS-mCD8::GFP* labels more MTS neurons than *nompC-GAL4* in both the cercus and epandrium (see Figure 3-1 D for statistical comparison), suggesting that this MiMIC line may more faithfully capture the endogenous expression pattern of

nompC in these regions, or alternatively that *nompC*$^{MI12787\text{-}AD}$∩*elav*^{DBD} more strongly drives expression of the reporter. Both *nompC*$^{MI12787\text{-}AD}$∩*elav*^{DBD} and *nompC-GAL4* lines label the same number of cells in the surstyli (Figure 3-1 D) confirming that this novel hemidriver can provide an excellent means for the intersection and functional manipulation of surstylar bristles.

When examining expression in the central nervous system (Figure 3-1 B&C), we identified ramifications in the antennal mechanosensory motor centre (AMMC) in the central brain, projections in all thoracic neuromeres, the nerve trunks leading into the Abg from the posterior, and those projecting into the VNS from other peripheral tissues such as the legs and wings.

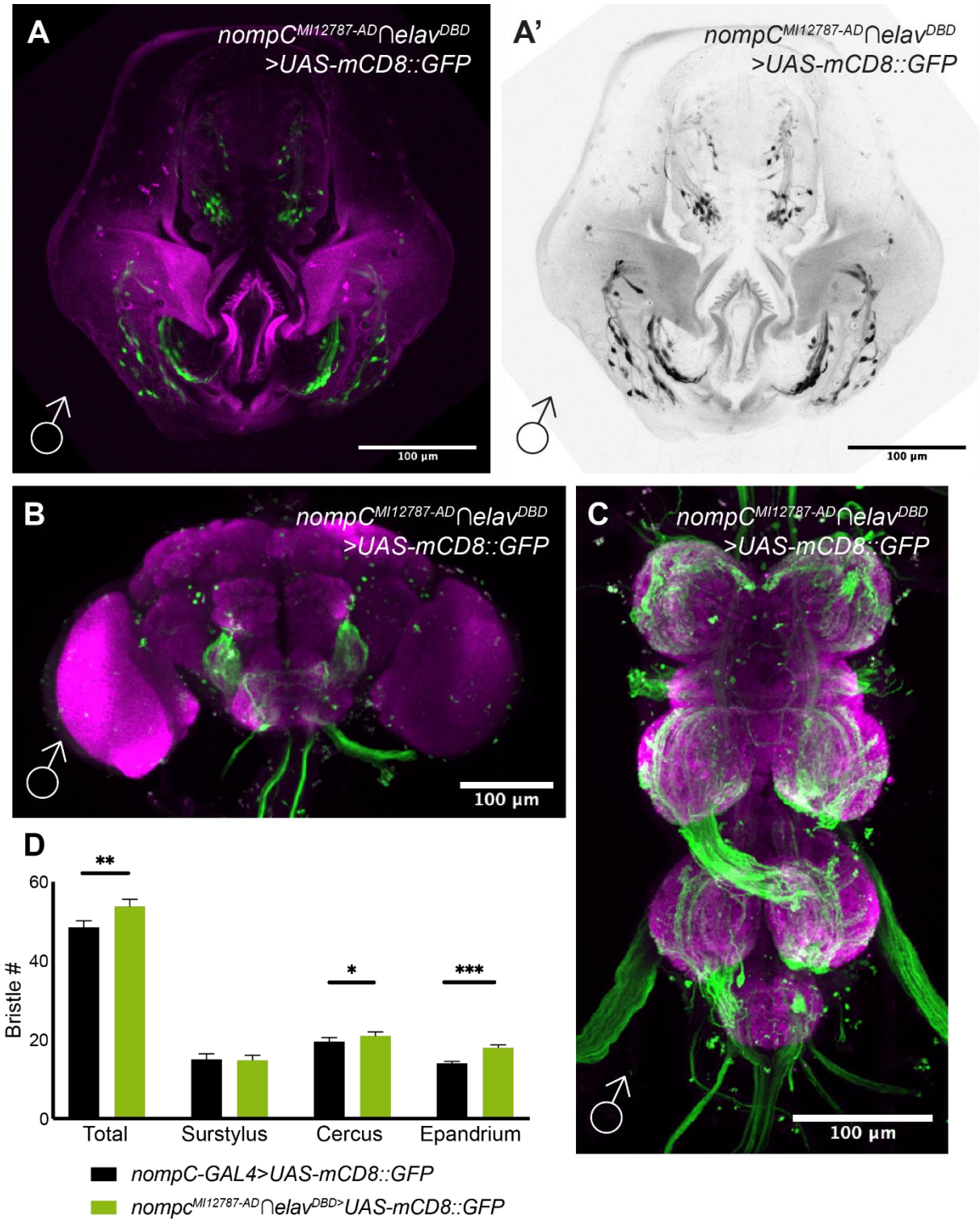

Figure 3-1: *nompC$^{MI12787\text{-}AD}$∩elav^{DBD}>UAS-mCD8::GFP* expression in male genitalia and central nervous system.

(A & A') Maximal Z-projection of *nompC$^{MI12787\text{-}AD}$∩elav^{DBD}* male genitalia shows extensive labelling of MTS neurons (54±2, median±(range/2)). MTS are labelled in the surstylus (15±2), cercus (21±1) and epandrium (18±1). **(B)** In the forebrain no cell bodies were labelled but ramifications of the AMMC are clearly visible. **(C)** In the VNS projections can primarily be seen in the abdominal nerve trunk and nerve trunks leading to the legs and wings. **(D)** Comparing the number and position of *nompC$^{MI12787\text{-}AD}$∩elav^{DBD}* labelled cells to those labelled by *nompC-GAL4* we identified that a greater total number of MTS neurons are labelled ($t(13)=5.56$, $p<0.01$) by the MiMIC line. Specifically, this difference in number arises from

the cercus (t(13)=2.52, p<0.05) and epandrium (t(13)=11.64, p<0.0001) of *nompC*$^{MI12787\text{-}AD}$∩*elav*^{DBD} males but labelling of surstylar bristles was consistent between the two lines (t(13)=0.255, p=0.8). Scale bar is 100µm in all panels. P<0.05 (*), P<0.01 (**), P<0.0001 (***).

3.2.2 *Piezo*$^{MI04294\text{-}AD}$ and *Piezo*$^{MI04189\text{-}AD}$

Of the two *Piezo* lines I have developed; *Piezo*$^{MI04294\text{-}AD}$ and *Piezo*$^{MI04189\text{-}AD}$, both show labelling of genital bristle neurons when combined with *elav*^{DBD}*;UAS-mCD8::GFP* (Figure 3-2). Specifically, *Piezo*$^{MI04294\text{-}AD}$∩*elav*^{DBD} labels 51±2 bristle neurons per side, with 15±2 of these being located in the claspers (n=5, Figure 3-2 A). The number of cells labelled by this MiMIC line is consistent with those labelled by *Piezo-GAL4* in all regions of the genitalia (see figure Figure 3-2 C for statistical comparison).

Conversely, *Piezo*$^{MI04189\text{-}AD}$∩ *elav*^{DBD}*>UAS-mCD8::GFP* labelled 40 bristle neurons per side (n=5, Figure 3-2 B), a significantly smaller number of labelled cells than *Piezo-GAL4* (see Figure 3-2 D) due to a reduced number of cells in the surstylus and cercus, but not the epandrium. However, it is not clear whether this number truly reflects a difference in the number of cells which express the UAS transgene as the strength of labelling produced by *Piezo*$^{MI04189\text{-}AD}$∩*elav*^{DBD} is significantly weaker than both *Piezo-GAL4* and *Piezo*$^{MI04294\text{-}AD}$∩*elav*^{DBD} (Figure 3-2 A). For clarity, *Piezo*$^{MI04189\text{-}AD}$ and *Piezo*$^{MI04294\text{-}AD}$ images are shown in black and white. Due to this low level of expression, I decided to continue with only *Piezo*$^{MI04294\text{-}AD}$ for my future experiments as the reduced expression of *Piezo*$^{MI04189\text{-}AD}$ is likely to result in the insufficient expression of transgenes designed to manipulate neural activity if used for behavioural experiments.

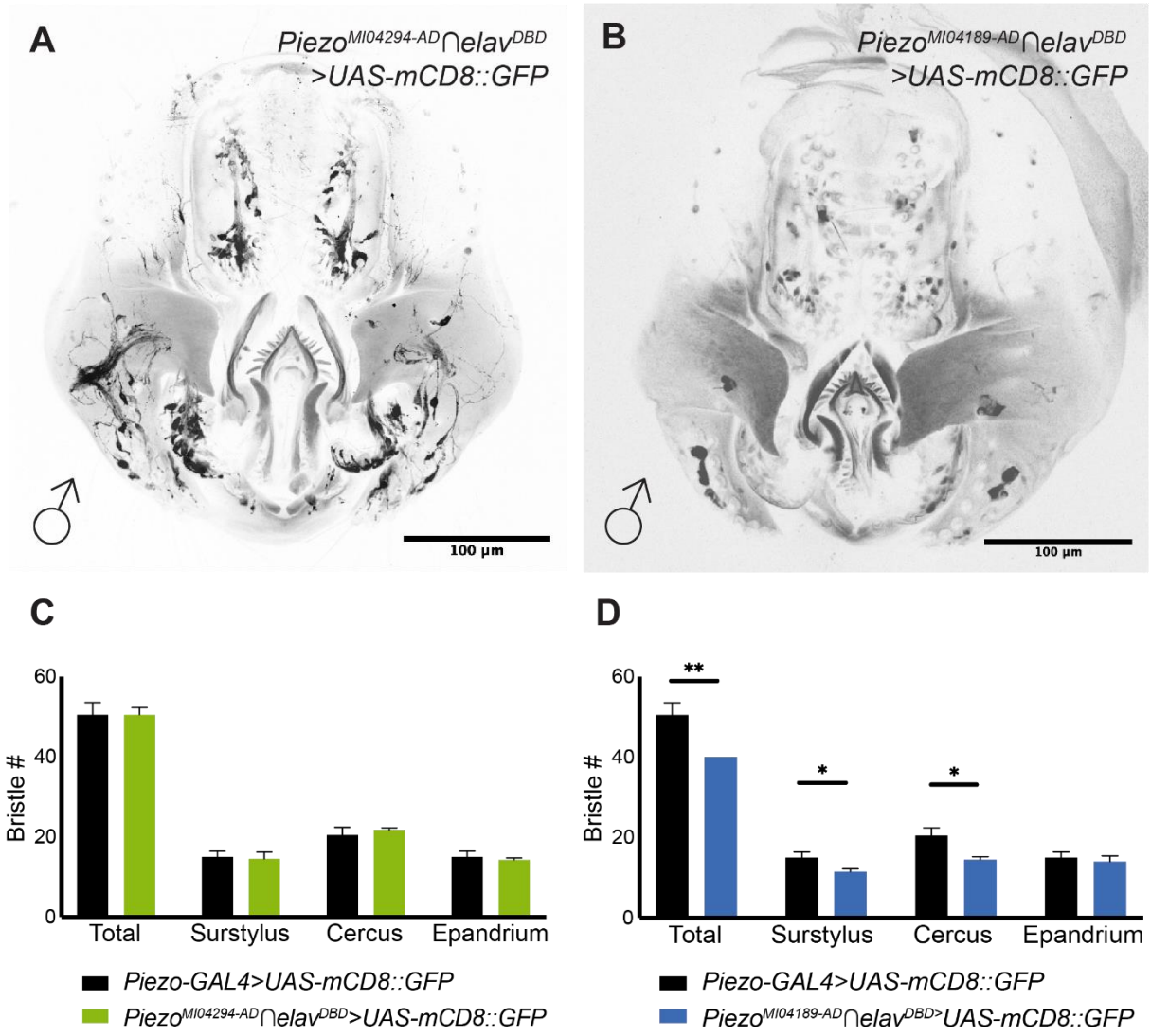

Figure 3-2: *Piezo$^{MI04294\text{-}AD}$∩elav^{DBD}>UAS-mCD8::GFP* and *Piezo$^{MI04189\text{-}AD}$∩elav^{DBD}>UAS-mCD8::GFP* expression in the male genitalia.

(A) Maximal Z-projection of whole mount male genitalia shows labelling of MTS neurons in the male genitalia of *Piezo$^{MI04294\text{-}AD}$∩elav^{DBD}* and **(B)** *Piezo$^{MI04189\text{-}AD}$∩elav^{DBD}* animals. **(C)** Statistical comparison of *Piezo$^{MI04294\text{-}AD}$∩elav^{DBD}* labelled cells against *Piezo-GAL4* indicates that there is no statistically significant difference in the total cell number ($t(13)=0$, $p>0.99$) or in any specific region; surstylus ($t(13)=0.45$, $p>0.05$), cercus ($t(13)=1.26$, $p>0.05$), epandrium ($t(13)=1$, $p>0.05$). **(D)** When comparing *Piezo$^{MI04189\text{-}AD}$∩elav^{DBD}* cells to *Piezo-GAL4* a significantly smaller total proportion of neurons are labelled ($t(13)=4.67$, $p<0.01$) due to a reduction in the number of labelled surstylar ($t(13)=3.17$, $p<0.05$) and cercal bristles ($t(13)=4.09$, $p<0.05$). There is no difference in *Piezo$^{MI04189\text{-}AD}$∩elav^{DBD}* and *Piezo-GAL4* epandrial bristles ($t(13)=0.82$, $p>0.05$). Scale bar is 100µm in all panels. P<0.05 (*), P<0.01 (**), P<0.0001 (***).

3.2.3 ChAT$^{MI04508\text{-}AD}$

When combining *elav^{DBD};UAS-mCD8::GFP* with our *ChAT MiMIC* line *ChAT$^{MI04508\text{-}AD}$*, we found it labelled 46±5 bristle neurons per side, including 18±1 in the surstyli (n=5, Figure 3-3).

The number of labelled neurons in the genitalia is comparable to *ChAT-GAL4* except in the epandrium where it labels a slightly reduced number of cells (see Figure 3-3 for statistical comparison), making this an excellent addition to our genetic toolkit for targeting genital bristle neurons. This is not without its' issues; however, as it has not yet been tested whether this insertion is hypomorphic for *ChAT,* which if true, would hinder its utility for behavioural experiments.

Nevertheless, although a deeper characterisation is required to fully appreciate the accuracy of *ChAT$^{MI04508\text{-}AD}$* expression in the rest of the nervous system, this line could provide an excellent tool for neurotransmitter specific manipulation of neural circuits. Furthermore, should *ChAT$^{MI04508\text{-}AD}$* insertions be found to significantly reduce the level of *ChAT* products in a given cell, this line could prove useful for the study of reduction or loss-of-function assays on cholinergic circuits.

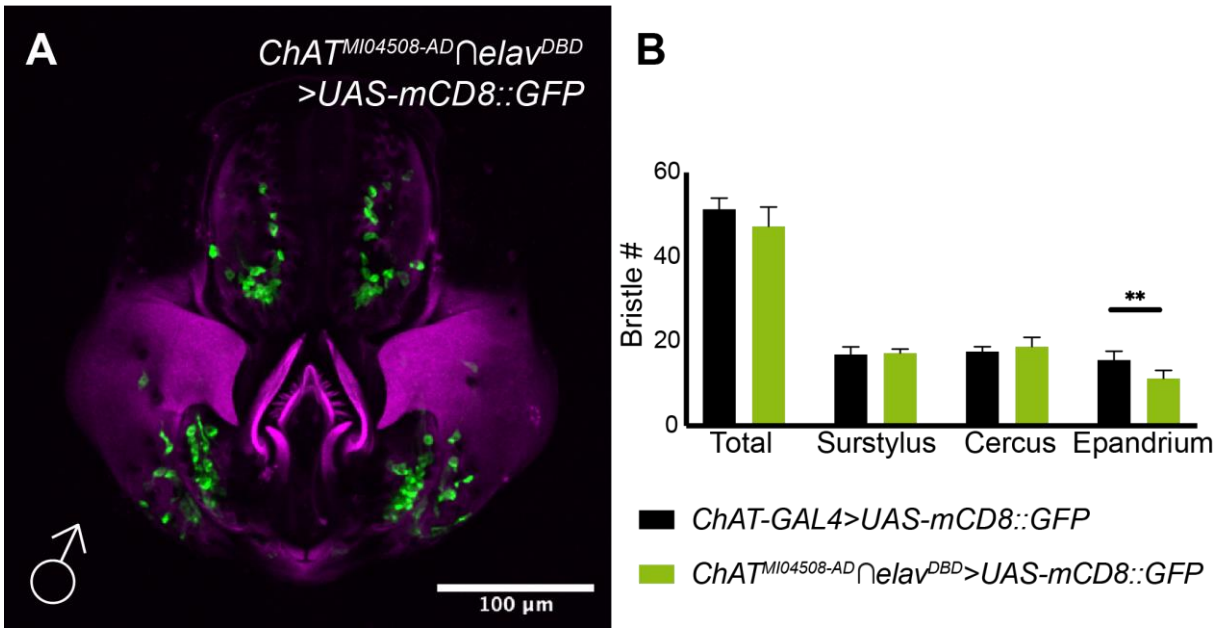

Figure 3-3: *ChAT$^{MI04508\text{-}AD}$∩elav^{DBD}>UAS-mCD8::GFP* labels MTS neurons in the male genitalia

(A) Maximal Z-projection of whole mount *ChAT$^{MI04508\text{-}AD}$∩elav^{DBD}* male genitalia highlights labelling of MTS in the surstyli, epandria and cercal lobes. **(B)** Statistical comparison of *ChAT$^{MI04508\text{-}AD}$∩elav^{DBD}* cells with *ChAT-GAL4* labelled cells reveals that the number of neurons marked is consistent between the two drivers in the surstyli (t(13)=0.36, p>0.05) and cercus (t(13)=1.29, p>0.05), but is slightly reduced in the epandrium (t(13)=3.56, p<0.01). Scale bar is 100µm. P<0.05 (*), P<0.01 (**), P<0.0001 (***).

3.3 Modifying Janelia FlyLight Drivers

The last split-hemidrivers I have developed to genetically target clasper bristle neurons are split-GAL4 AD and DBD variants of *R94D09-GAL4,* which I discussed in chapter 2. To best reproduce the expression of this promoter fusion of *engrailed,* I adapted the protocol outlined by Pfeiffer *et al*. (2008). The process of developing this novel *R94D09* split-GAL4 driver is outlined in methods section 7.4.8.

Theoretically, these split-GAL4 variants of *R94D09* should express identically to the original GAL4.

3.3.1 R94D09$^{AD/DBD}$ expression

Having developed *R94D09^{DBD},* I imaged its' expression in the male genitalia and central nervous system by combining it with *elav^{VP16AD};UAS-mCD8::GFP* (*R94D09^{DBD}∩elav^{VP16AD}>UAS-mCD8::GFP).* These images revealed the same expression pattern as the original *R94D09-GAL4* in the male genitalia and the central nervous system (Figure 3-4 A-B) where cell bodies could be identified in the GNG and Saddle, with projections forming a characteristic hairpin loop in the central complex (Ito *et al*. 2014).

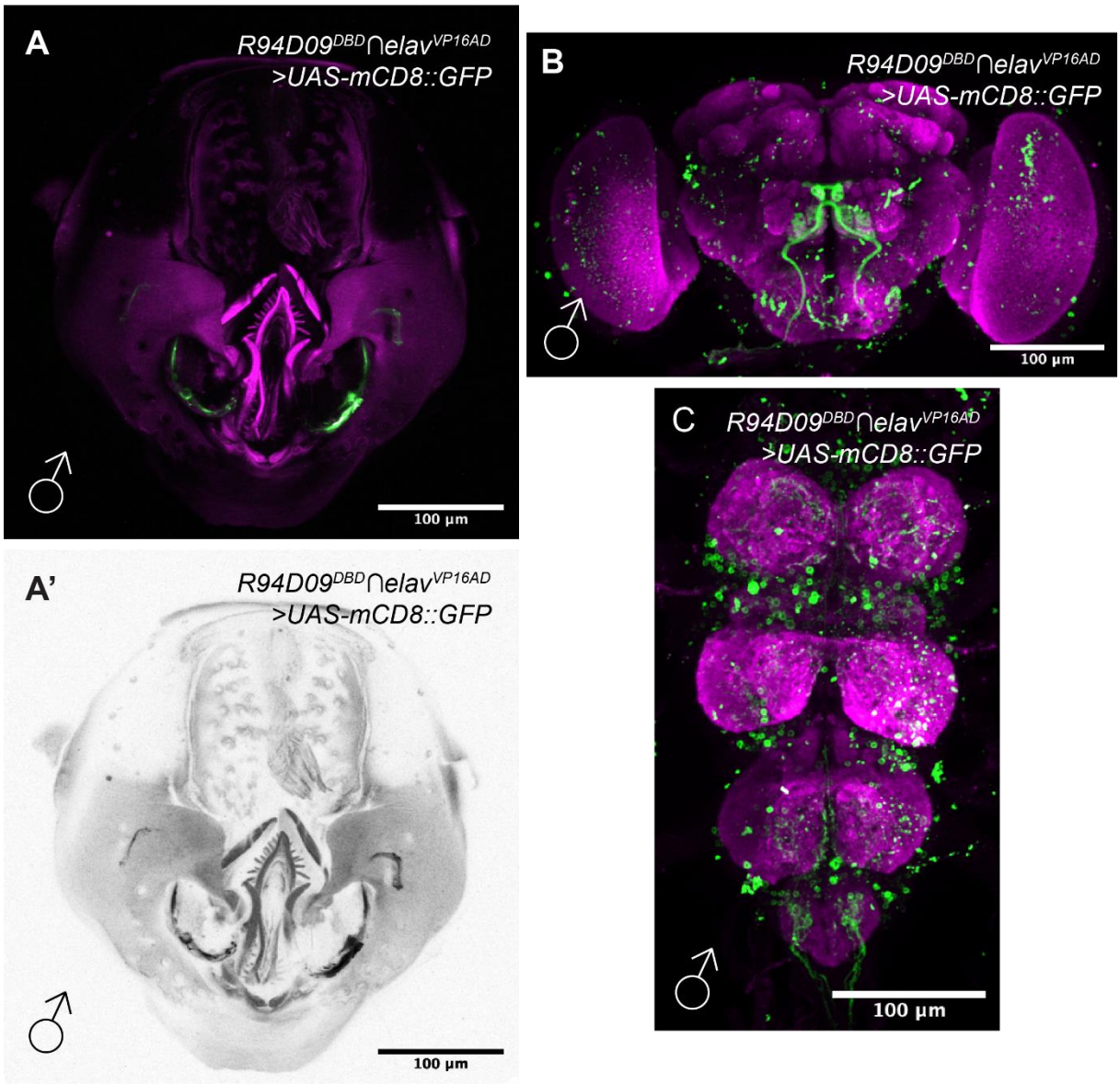

Figure 3-4: *R94D09^{DBD}∩elav^{VP16AD}* expression in the male genitalia and central nervous system.

(A & A') In the male genitalia *R94D09^{DBD}∩elav^{VP16AD}>UAS-mCD8::GFP* labels 6 surstylar bristle neurons per side, the same number as *R94D09-GAL4* (t(18)=1, P>0.05). The nerve fibre in which all ascending projections from the surstyli are collated is visible in the epandrial posterior lobes. **(B)** In the forebrain *R94D09^{DBD}* expression is consistent with the GAL4 line, marking cells in the gnathal ganglion and VLP and projections with a characteristic hairpin structure around the foramen and posterior to the antennal lobes. **(C)** In the VNS *R94D09^{DBD}* marks projections into the Abg from the genitalia as expected, but unlike *R94D09-GAL4* a large number of cell bodies are marked in the VNS, particularly in the accessory mesothoracic neuromere. Scale bar is 100µm in all panels.

Curiously, *R94D09^{DBD}∩elav^{VP16AD}* labels cell bodies in the adult VNS, particularly in the prothoracic, accessory and mesothoracic neuromeres, which were not seen with *R94D09-GAL4*. This 'extra' expression is curious considering that the UAS reporter remained the same between GAL4 and DBD drivers, so it is likely that variation between these two lines is caused by the differing strengths of basal promoters used in the GAL4 and DBD vectors or potentially the stability of these proteins compared to the original GAL4 line. Nevertheless, *R94D09^{DBD}* may still provide an excellent tool for targeting transgene expression to genital bristle neurons when combined with drivers that do not exhibit expression in the brain and VNS. For example *nompC$^{MI12787-AD}$* (see section 3.2.1). Therefore, the intersection of two lines such as these would only overlap in peripheral tissues like genital bristle neurons and not elsewhere.

3.3.2 *nompC$^{MI12787-AD}$∩R94D09^{DBD}* Combination Reduces Expression Outside Terminal Sensilla

To examine whether the intersection of *nompC$^{MI12787-AD}$* and the *R94D09* drivers I have developed might provide a high level of spatial restriction, I combined *nompC$^{MI12787-AD}$* and *R94D09^{DBD}* to drive *UAS-mCD8::GFP.* As predicted, the resulting expression marked cells in the surstyli (Figure 3-5 A&A') and the characteristic morphology of clasper neuron axonal arbors is visible in the Abg (Figure 3-5 C). Some projections were still visible in the GNG, presumably projecting into the brain from cells in the labellum, antennae or maxillary palps (Figure 3-5 B) although the number was drastically reduced compared to *R94D09* labelled cells either as the GAL4 form or when combined with the pan-neuronal *elav^{DBD}.*

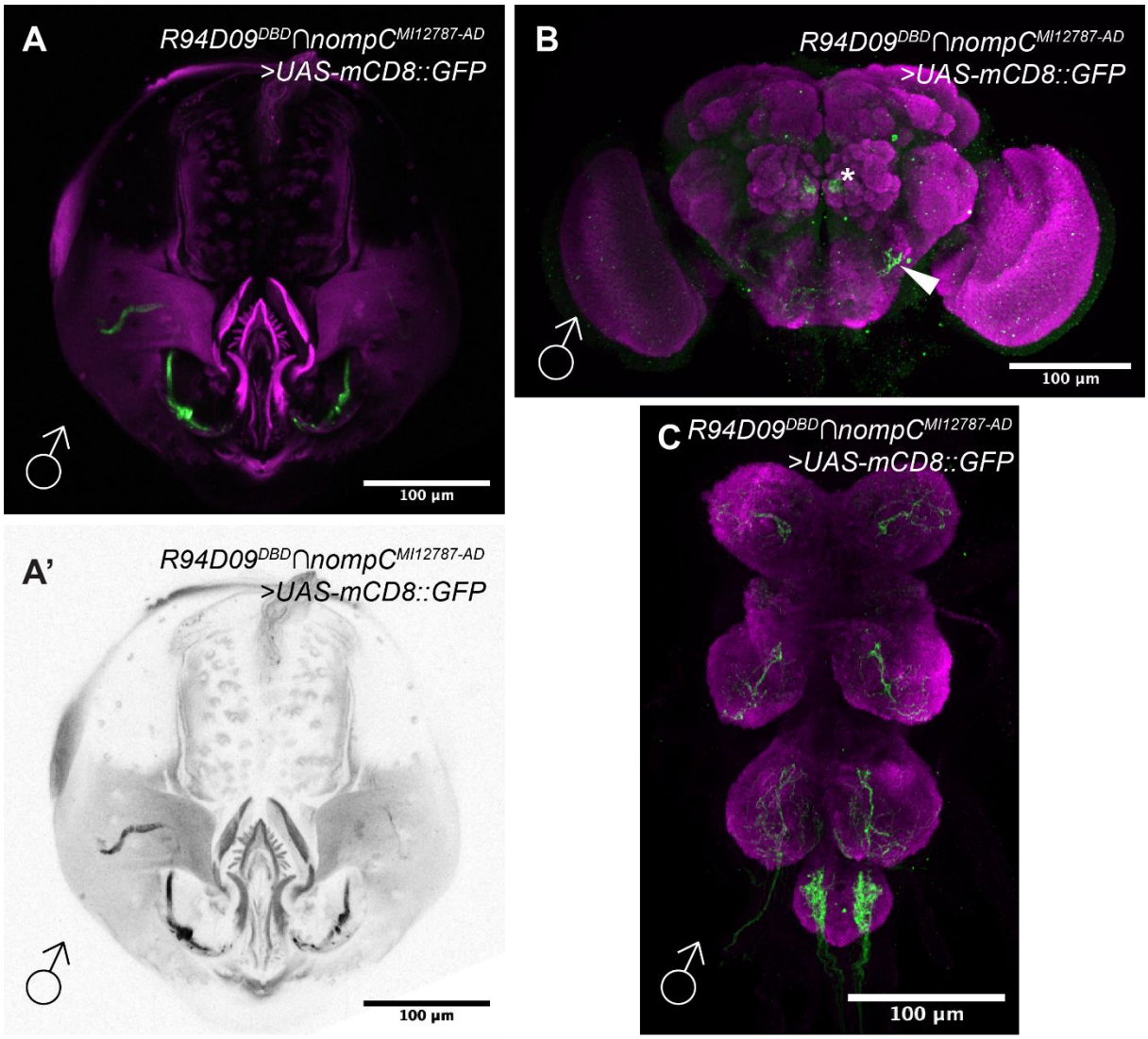

Figure 3-5: *R94D09^{DBD}∩nompC$^{MI12787-AD}$* expression in the male genitalia and central nervous system

(A) In the male genitalia *R94D09^{DBD}∩nompC$^{MI12787-AD}$>UAS-mCD8::GFP* labels 6 MTS neurons in the distal tip of the surstyli, consistent with the expression of the original *R94D09-GAL4* (t(18)=0.56, p>0.05). **(B)** In the brain the majority of *R94D09* expression is removed due to the lack of *nompC* expression in the central nervous system, However, some faint projections in the AMMC (white arrowhead) are visible, as are two small regions of projections which lie posterior of the antennal lobe. These likely originate from mechanosensory cells in the johnston's organs. **(C)** In the ventral nervous system no cell bodies are labelled but projections in the abdominal ganglion from the genitalia are clearly visible, as are projections into each thoracic neuromere from the legs (see Figure 3-6). Scale bar is 100µm in all panels.

Lastly, although some projections were still visible in the thoracic neuromeres, closer inspection revealed that these originate from a handful of chordotonal organ neurons and a single distal tibia bristle neuron in each leg (Figure 3-6). No other expression was identified in *nompC$^{MI12787-AD}$∩94D09^{DBD}* animals (data not shown).

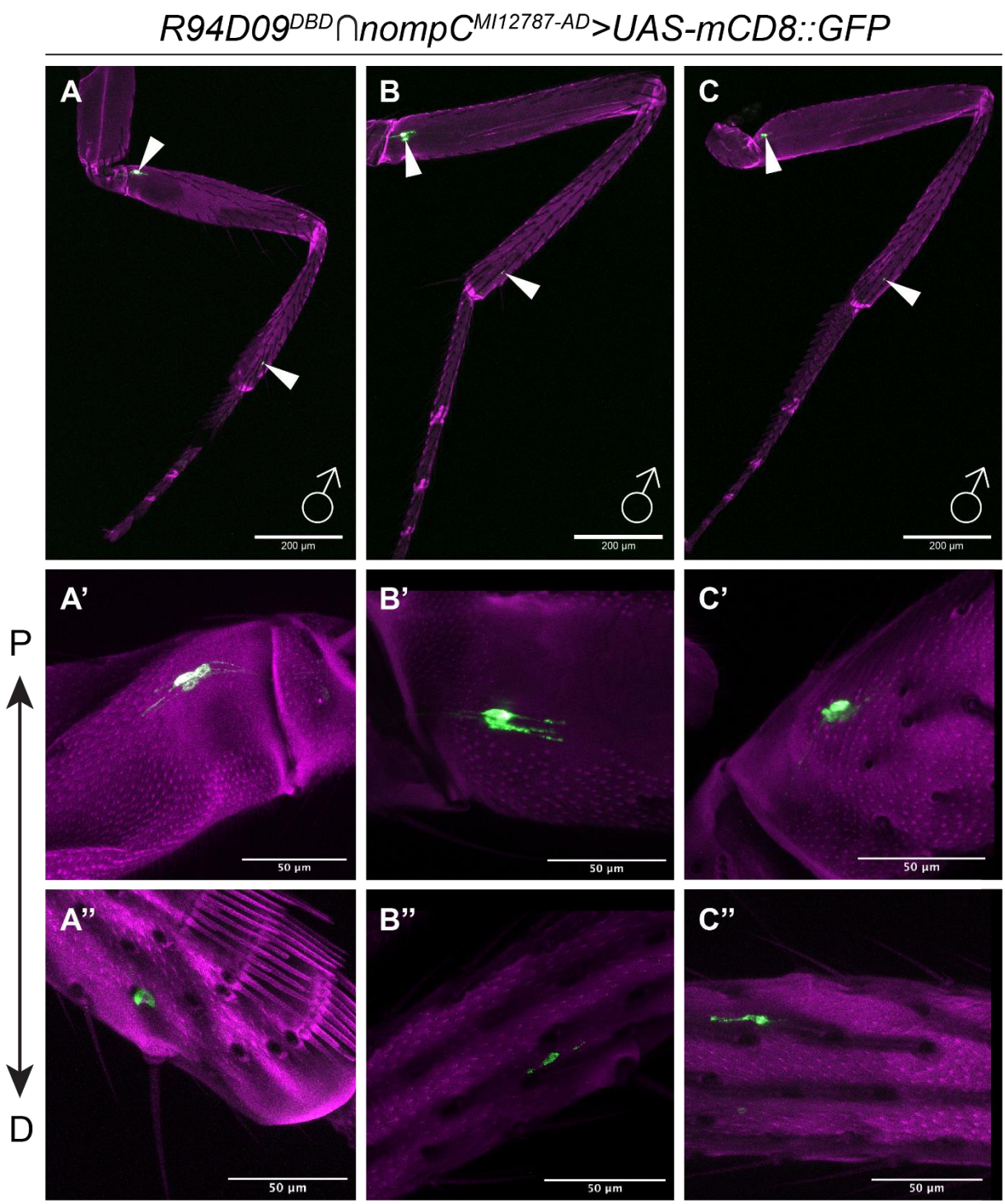

Figure 3-6: : *R94D09^{DBD}∩nompC$^{MI12787-AD}$>UAS-mCD8::GFP* expression in the periphery

Projections into the thoracic neuromeres originate from cells in the 1st, 2nd and 3rd pairs of legs (**A-C**, respectively). Specifically, these projections originate from 2-3 femoral chordotonal organs per leg (prime panels) and a single bristle neuron in the tibia (double prime panels). Arrowheads in panels A-C indicate the position of cell bodies in the panels below. P = proximal, D = distal. Scale bars are 200µm in panels A-C and 50µm in A'-C''.

3.4 Experimental applications of drivers from this study

While it is possible that the chordotonal neuron expression of *nompC*$^{MI12787\text{-}AD}$∩*94D09*^{DBD} may confound our results, only a subset of femoral chordotonal neurons are labelled per leg. Therefore, other than *R20G10-p65AD* reported in the previous chapter, this combination provides the most tightly restricted genetic access to bristle sensilla in the surstyli that this study has identified. In the following chapter I will utilise these drivers (*R20G10-p65AD*∩*dsx*^{DBD}, *R23F02-p65AD*∩*dsx*^{DBD} and *nompC*$^{MI12787\text{-}AD}$∩*94D09*^{DBD}) to manipulate MTS function using a number of transgenes under UAS control.

3.5 Conclusion

In this chapter I have presented the development of novel split-GAL4 hemi-driver lines by inserting p65AD and GAL4 DNA-binding transgenes under the transcriptional and translational control of the mechanosensitive ion channels; *nompC* and *Piezo* and the cholinergic neuron marker *ChAT*. Due to the nature of these trojan exons and the intronic position of MiMIC landing sites (Diao *et al*. 2015; Venken *et al*. 2011) these lines theoretically intersect all cells which express their respective target gene, providing an excellent resource for manipulating both peripheral and central neural circuits and highlighting the functionality of a targeted screen for genetic drivers such as we have employed. In the next chapter, I will use these lines to functionally assess sensory feedback from genital bristle sensilla in the context of copulation and to expand our understanding of the circuitry governing genital attachment and mating posture.

4 Functional Assessment of MTS

4.1 Introduction

Functional annotation of a circuit, or the component neurons within a circuit, can be achieved by using genetically encoded transgenes to silence (to determine necessity), artificially activate (to determine sufficiency), and image neural activity (to determine that context and stimuli which activate the neurons). The combination of these three ultimately allows one to draw causal links between neurons, their activity patterns, and their respective behavioural outputs. In this chapter I will present data resulting from the artificial activation and inhibition of MTS neurons and in chapter 5 I will present some data relating to imaging MTS neuron activity under specific stimuli.

To quantify the mating behaviour of *Drosophila,* several metrics have been developed to gain a sense of the general motivation and ability of a male to court and achieve successful copulation. Perhaps the most widely used, which was particularly well suited to experimental setups where the researcher would manually score recorded assays, is the courtship index (CI; Taylor *et al*. 1994). This is given as a number between 0 and 1, representing the percentage of time in the first ten minutes of an assay where the male is courting the female. Courtship behaviours are defined here as; orientation, following, tapping, and wing extension before attempted copulation (as per; Villella *et al*. 1997). Other informative metrics include, but are not limited to, courtship initiation – the time elapsed between the introduction of the male and the first display of courtship behaviours, copulation duration, the percentage of mating pairs, wing extension, and the fertility of females mated in these assays (for a more in depth description of each metric, see methods section 7.5.4).

Previous works such as Pavlou *et al*. (2016) and Acebes (2003), looking at adaptive motor control in relation to *Drosophila* copulation have thus far used these metrics, or simply the proportion of males achieving copulation within one hour. For example, Pavlou and colleagues showed that silencing *dsx∩VGlut* motor neurons pre-copulation resulted in the abolition of successful matings in one hour and drastically reduced CI compared to genetic controls. On the other hand, silencing *dsx∩Gad1* abdominal ganglion neurons pre-copulation produces little to no change in CI but reduces the number of successful copulations by over 75% Silencing these same neurons *in copulo* drastically increased the duration of copulation and leads to a 'stuck' phenotype where the male seemed unable to detach. For a discussion of the tools available for artificially manipulating neural activity, see sections 1.3.3 and 1.3.4.

With the introduction of machine-learning based automated behavioural analysis, new avenues through which to quantify behaviour, such as measuring the distance or angle between the two animals at any given frame in a video, have become more reliable and feasible on large sample sizes (for a more in depth description of the training and use of these tools, see section 7.5). As I will highlight in this chapter though, no singular automated analysis pipeline is currently able to extract all the information required to describe abnormal mating posture and calculate metrics like CI. Therefore, for the experiments performed here, particularly later experiments using *R20G10* and *R23F02,* I have adopted a two-step strategy using the Caltech Multiple Walking Fly Tracker (Ctrax; Branson *et al*. 2009) and Janelia Automatic Animal Behaviour Annotator (JAABA; Kabra *et al*. 2013) for determining all but the mating position of the male, and then performed an analysis using DeepLabCut (Mathis *et al*. 2018; Nath *et al*. 2019) on just the frames where the pair are copulating to determine any effect of

activating or silencing MTS neurons on mating posture. Unfortunately, in some cases this limited the number of videos which could be analysed, as this process necessitates the removal of ‘wall frames’, i.e. those frames in a video where the flies are positioned on the wall of the chamber, as these measurements would be inaccurate. Despite the small reduction in sample size that occurs as a result of removing these videos from the analysis, I reasoned that this was acceptable as a manual measurement would also be inaccurate in these cases.

Lastly, some researchers have suggested that the female can actively determine the quality of a mate *in copulo* and then bias her reproductive output through preferential sperm storage (Bressac and Hauschteck-Jungen 1996; Eberhard 1996; Schnakenberg *et al*. 2012). This process is often referred to as the sensory lock-and-key hypothesis (Eberhard 1992), an area of cryptic female choice, which suggests that females need to be presented with the correct combination of stimuli, at the appropriate levels (a sort of sensory goldilocks zone) before fully accepting a mate. To examine the possibility that abnormal mating postures caused by the artificial activation or inactivation of MTS neurons can lead a female to become less receptive *in copulo*, and therefore produce fewer offspring, we looked at two metrics; the movement of the female during copulatory bouts, and the number of eggs produced by that female every 48 hours for 10 days post-copulation.

4.1.1 Summary of work so far

Before presenting data associated with manipulating MTS function, it is worth recapping the progress in this thesis up to this point. I have established a toolkit of drivers that can be used to genetically access spatially restricted MTS neurons and in

the process of screening these lines I have identified that MTS neurons in all three main regions of the male genitalia are cholinergic, express the transcription factor *dsx* and the mechanosensitive ion channels *nompC* and *Piezo*. Curiously, the density of innervated bristles within a region appears to be highest in the ventral region of each segment, or on the distal tip of the surstyli, and bristles located in a dorsal position more basally in the surstyli are less likely to be innervated. A small number of surstylar bristle neurons are also labelled by *R94D09* and *R20G10*, two promotor fusion lines derived from putative regulatory regions of *engrailed* and *nAChR α3,* respectively. The latter of these two is the most restricted of all the lines I have identified as it is restricted to surstylar MTS neurons alone. Lastly, I have identified *R23F02,* which when combined with dsx^{DBD} (*R23F02-p65AD∩*dsx^{DBD}), labels a subset of abdominal ganglion interneurons that are putatively downstream of MTS neurons in the terminalia.

In most cases, the expression of drivers relating to these genes can be identified in multiple regions of the animal, in particular other sensilla on the legs, which limits their usefulness for behavioural experiments as the role of MTS neurons cannot be tested in isolation. To overcome these drawbacks, I have developed split-Gal4 hemidrivers for nompC, *Piezo, ChAT* and *R94D09* which can be used in a combinatorial fashion to target MTS cells. These can now be used for the functional analysis of genital bristles in freely behaving male flies, and for confirming the role of bristles on the male genitalia as mechanosensory cells in fixed preparations.

In this chapter I will present the outcomes of artificially activating or inhibiting the action of MTS neurons labelled by either *R94D09*^{DBD}*∩nompC*$^{MI12787\text{-}AD}$, *R20G10-*

p65AD∩dsx^{DBD} or *R23F02-p65AD∩dsx^{DBD},* as well as a discussion on the development of more robust methodologies for quantifying abnormal mating posture.

Results

4.2 Behavioural Analysis of *R94D09^{DBD}∩nompC$^{MI12787-AD}$*

The first line on which I performed behavioural analysis was *R94D09^{DBD}∩nompC$^{MI12787-AD}$.* The original lines that these two hemidrivers are developed from were first identified as labelling MTS cells in chapter 2, and then later developed into split-Gal4 hemidriver variants in chapter 3, validating the targeted screen approach for finding novel tools for genetic access to MTS neurons.

To maximise the likelihood that I could identify a phenotype arising from silencing these cells, I used *UAS-TNT* (*R94D09^{DBD}∩nompC$^{MI12787-AD}$>UAS-TNT*) to chronically silence the 6 surstylar bristle neurons as well as 2-3 femoral chordotonal organ neurons and single tibia bristle neuron per leg, that this driver combination labels.

When paired with a single virgin female, *R94D09^{DBD}∩nompC$^{MI12787-AD}$>UAS-TNT* males mated at levels intermediate between the two parental controls (Figure 4-1C) and exhibited high levels of courtship that were indistinguishable from both genetic controls (Figure 4-1D). The duration of copulation was also unaffected (Figure 4-1E), although the time to copulation (Figure 4-1F) was slightly increased in the experimental animal compared to the driver control (+;*R94D09^{DBD}∩nompC$^{MI12787-AD}$;*+). The wing index of experimental males was also slightly increased compared to driver control males (Figure 4-1G). Taken together, these data indicate that *R94D09^{DBD}∩nompC$^{MI12787-AD}$* males' ability to court and terminate copulation are

unaffected by silencing surstylar bristle neurons. However, the increased time to copulation suggests that they may have a reduced ability to attach to the female and begin copulation. Recording the number of attempts a male makes before achieving a mechanical interlock (Figure 4-1H) reveals that whilst not statistically significant, experimental males tend to make slightly more attempts, on average, before successfully attaching to the female.

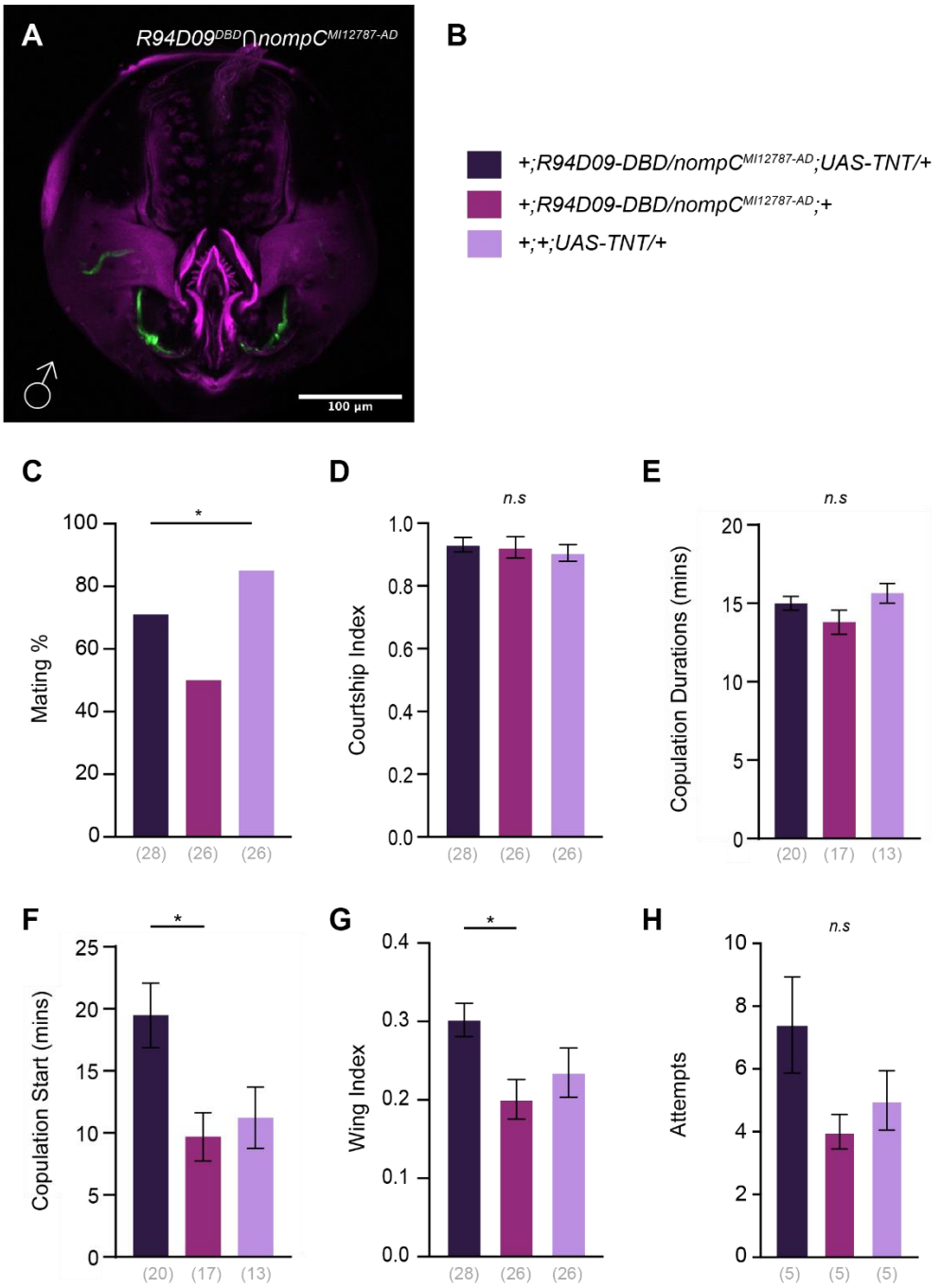

Figure 4-1: Mating analysis of *R94D09^{DBD}∩nompC$^{MI12787-AD}$>UAS-TNT* males.

(A) *R94D09^{DBD}∩nompC$^{MI12787-AD}$* labels 6 surstylar bristle neurons per side. **(B)** Genotypes and legend for figures shown in this panel. **(C)** *TNT* control males actually exhibited a slightly higher mating percentage than other genotypes (Fisher's exact test: p=0.041). **(D)** *R94D09^{DBD}∩nompC$^{MI12787-AD}$>UAS-TNT* males exhibit normal levels of CI compared to genetic controls. **(E)** The duration of copulatory bouts is unaffected by silencing *R94D09^{DBD}∩nompC$^{MI12787-AD}$* neurons. **(F)** The time to the start of copulation is significantly greater in experimental animals compared to driver control males (one-way ANOVA with Bonferroni correction: t(47)=2.76, p<0.05) and only slightly insignificant compared to effector control males (t(47)=2.48, p=0.051). **(G)** The wing index of *R94D09^{DBD}∩nompC$^{MI12787-AD}$* is also slightly increased compared to driver controls (t(77)=2.98, p<0.05). **(H)** Increased time to the start of copulation appears to be due to an inability of males to attach as experimental makes slightly more attempts before achieving genital interlock. Errors bars are standard error of the mean. * (p<0.05), ** (p<0.01), ***

($p<0.001$). Only significant results are indicated for the bars immediately underneath the edges of the line. Other comparisons are non-significant.

4.2.1 Postural Analysis of *R94D09^{DBD}∩nompC$^{MI12787-AD}$* Males *in copulo*

Despite there being no significant effect of silencing *R94D09^{DBD}∩nompC$^{MI12787-AD}$* cells on CI, copulation duration or termination of copulation, when watching the recordings of these assays it is clear that *R94D09^{DBD}∩nompC$^{MI12787-AD}$>UAS-TNT* males exhibit an abnormal mating posture compared to controls. Typically the male of *Drosophila melanogaster* will adopt a stereotypical 'delta wing' position where his body is in close alignment to the females, and her wings are pulled to each side of the male thorax using his sex combs (Figure 4-2Ai). In *R94D09^{DBD}∩nompC$^{MI12787-AD}$>UAS-TNT* males, the male is noticeably angled to one side of the female midline (Figure 4-2Aii) and he often seems unable to grasp the female properly, leading to him laying backwards for short periods of time (Figure 4-2Aiii) and varying his body position much more throughout the copulatory bout. At first, I tried to quantify these effect on mating posture by recording the angle between the male and female heads *in copulo* from recordings analysed with Ctrax and JAABA. However, I noticed that in many cases, the reported angle did not agree with a manual measurements taken at the same time point. To address this, I trained a DeepLabCut (DLC) model to mark the position of the male and female head and abdomen for each frame in which the pair was copulating (for more information regarding the DLC model see section 7.5.3) and extracted this angle data to calculate a mean and median mating angle.

This analysis revealed that *R94D09^{DBD}∩nompC$^{MI12787-AD}$>UAS-TNT* males exhibit a significantly greater mean and median mating angle compared to controls (Figure

4-2D&E), suggesting that these animals rely on feedback from MTS neurons to detect contact with the female genitalia during attachment, but also rely on this information, presumably in concert with other proprioceptive signals, to maintain their posture throughout copulation.

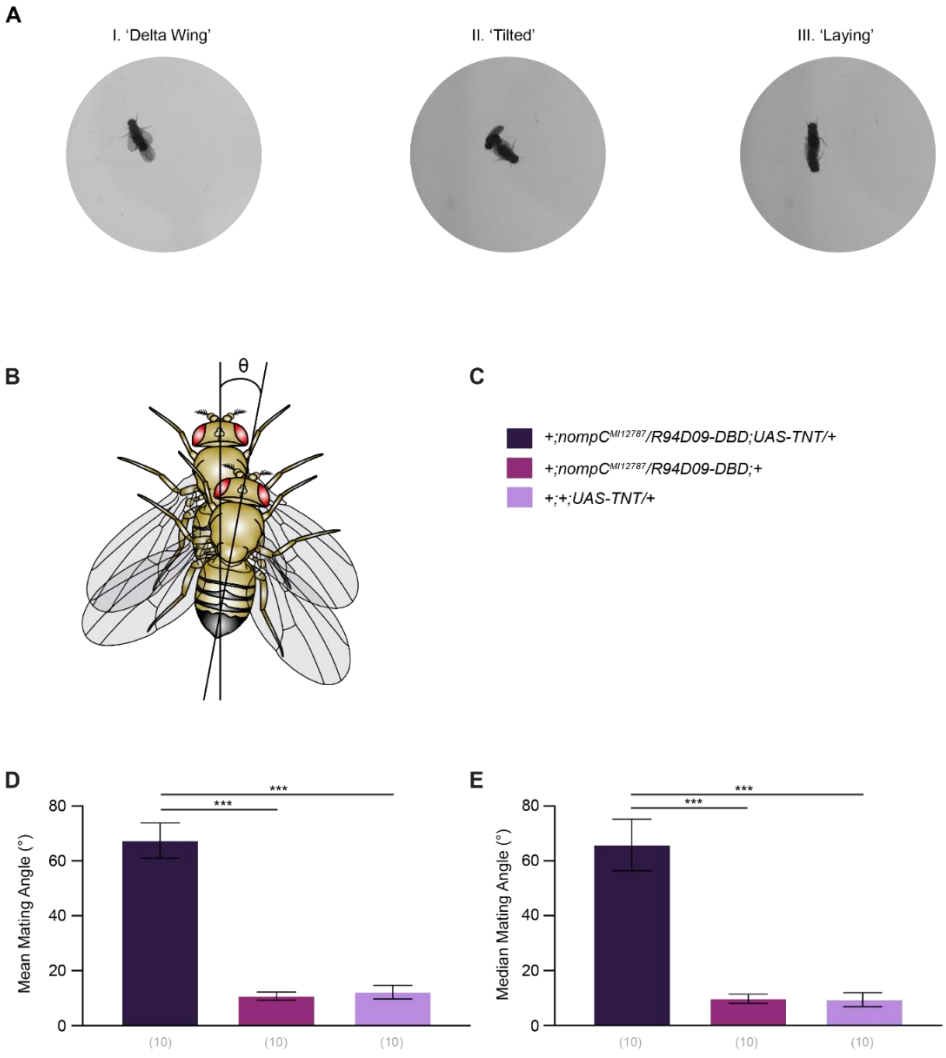

Figure 4-2: Mating posture analysis of *R94D09^{DBD}∩nompC$^{MI12787-AD}$* males.

(Ai) Typically, copulating males adopt a 'delta wing' position but **(Aii)** *R94D09^{DBD}∩nompC$^{MI12787-AD}$* males often exhibit a 'tilted' position and even **(Aiii)** lay backwards with a facing angle that completely opposes the female for short period. **(B)** Cartoon illustrating how mating angle is calculated between two copulating flies. Image adapted from (Sanchez-Alcaniz *et al*. 2017). **(C)** Genotypes and legend for the data presented. **(D)** Mean mating angle of *R94D09^{DBD}∩nompC$^{MI12787-AD}$* males is greatly increased compared to both driver (one-way ANOVA with Bonferroni correction; $t(27)=8.9$, $p<0.001$) and effector control males ($t(27)=9.29$, $p<0.001$). **(E)** Similarly, Median mating angle of *R94D09^{DBD}∩nompC$^{MI12787-AD}$*

males is greatly increased compared to both controls ($t(27)=6.3$, $p<0.01$ and $t(27)=6.7$, $p<0.001$, respectively). Grey numbers indicate sample sizes. Error bars are standard error of the mean. * ($p<0.05$), ** ($p<0.01$), *** ($p<0.001$). Only significant results are indicated for the bars immediately underneath the edges of the line. Other comparisons are non-significant.

4.2.2 Receptivity of Females Paired with *R94D09^{DBD}∩nompC$^{MI12787\text{-}AD}$>UAS-TNT* males

When viewing recordings of *R94D09^{DBD}∩nompC^{MI12787}* males paired with *CantonS* females, we believed that we could see a higher level of female rejection behaviour and movement during copulation. To quantify this and any direct impact on the number of eggs sired by males with silenced *R94D09^{DBD}∩nompC^{MI12787}* neurons, we recorded the number of eggs produced by females in the 10 days following mating, as well as the total distance they travelled during the first ten minutes of copulation (Figure 4-3).

Recording the number of eggs a female produced over the 10-days post-mating highlighted that females did not produce a different number depending on the genotype of the male they mated (Figure 4-3B). These values were highly variable within genotypes however and may therefore mask any true difference in the number of eggs produced. Nonetheless, from our data alone we cannot support the notion that females preferentially hold the sperm of males based on their copulatory experience.

Measuring the movement of the copulating pairs revealed females mated to *R94D09^{DBD}∩nompC$^{MI12787\text{-}AD}$>UAS-TNT* males do not exhibit a significantly higher degree of movement than females mated with control males. Using female movement as an indirect measure of rejection, these results suggest that there is little effect on female rejection behaviour resulting from the abnormal mating position that the male

often exhibits, however future experiments using multiple males may unveil a higher level of rejection behaviour from the female.

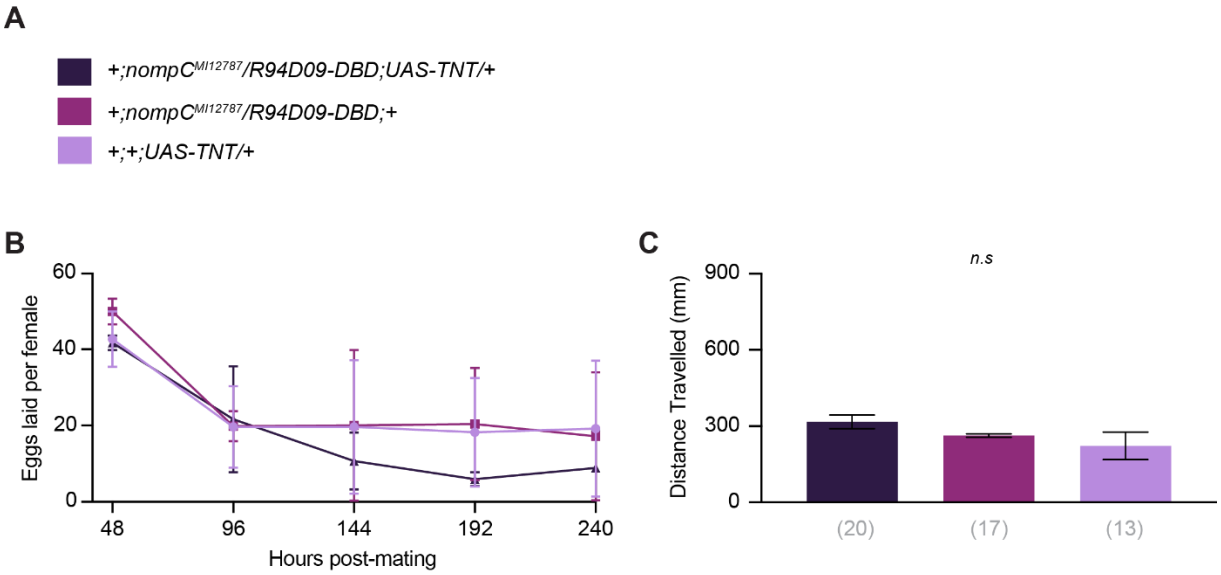

Figure 4-3: Analysis of female egg production and movement during copulation when mated with *R94D09^{DBD}∩nompC$^{MI12787\text{-}AD}$* males and relevant controls.

(A) Genotypes and legend for data presented in this figure. **(B)** Egg production every 48 hours over 10 days from females mated with *R94D09^{DBD}∩nompC$^{MI12787\text{-}AD}$* males or relevant genetic controls showed no significant effect at any time point. **(C)** The total distance moved during the first ten minutes of copulation by females mated to experimental or control males. These results show no significant effect on female movement or rejection behaviour. Grey numbers indicate sample sizes. Error bars are standard error of the mean. * (p<0.05), ** (p<0.01), *** (p<0.001).

4.3 Behavioural Analysis of *R20G10-p65AD∩dsx^{DBD}*

To assess the impact of perturbing surstylar bristle neurons labelled by *R20G10-p65AD∩dsx^{DB,}* I first drove expression of CsChrimson in these cells (*R20G10-p65AD∩dsx^{DBD}>UAS-CsChrimson*) to determine their sufficiency for inducing abnormal mating phenotypes. Later, to assess the impact of inactivating these cells, I

artificially silenced them using UAS-*shibire^{ts}* (*R20G10-p65AD∩dsx^{DBD}>UAS-shibire^{ts}*) to determine their necessity for genital attachment and mating posture.

For inactivation experiments with this and all lines shown in this thesis, assays performed at a restrictive temperature of 31°C were performed alongside assays at a permissive temperature of 23°C to aid in identifying the effects of *shibire*-mediated inhibition over genetic background effects. Similarly, for optogenetic experiments where cells are activated using CsChrimson, assays were performed both on animals which had been aged on retinal food, as is required for consistent activation of the channel, and on animals of the same genotype that were raised on standard cornmeal-agar food to identify any effect of low-level activation of the channel due to naturally occurring levels of retinal in the fly. For more details on animal collection, aging and retinal food see methods sections 7.1 and 7.5.

4.3.1 Artificial Activation of *R20G10-p65AD∩dsx^{DBD}* Neurons

To test the requirement of *R20G10-p65AD∩dsx^{DBD}* neurons for proper mating posture, I activated them using *UAS-CsChrimson* (*R20G10-p65AD∩dsx^{DBD}>UAS-CsChrimson*).

This manipulation did not significantly affect CI or wing extension (Figure 4-4C&D) and the time to the start of copulation was statistically similar between all genotypes and between conditions (Figure 4-4E), although it is worth noting the caveat of small sample sizes in this analysis. On the other hand, the duration of copulation (Figure 4-4F) was significantly longer in experimental males (*R20G10-p65AD∩dsx^{DBD}>UAS-*

CsChrimson), perhaps indicating that these males have problems detaching from the female. Despite these metrics reporting more or less normal levels of courtship, we found that only 40% of *R20G10-p65AD∩dsx^{DBD}>UAS-CsChrimson* males were able to copulate within the observation period, compared to 70% and 60% of the *dsx*/*Chrimson* controls and driver controls, respectively (Figure 4-4G). For assays performed on animals which were not provided supplemental retinal, males mated in 65% (*R20G10-p65AD∩dsx^{DBD}>UAS-CsChrimson* and driver control males) and 75% (dsx/chrimson control) of assays, highlighting that this reduction in successful copulations was a direct result of activating *R20G10-p65AD∩dsx^{DBD}* surstylar bristle neurons.

To further examine the cause of this reduction in successful matings, I examined the number of attempts each male makes before achieving copulation. Interestingly, this analysis highlighted that *R20G10-p65AD∩dsx^{DBD}>UAS-CsChrimson* males made, on average, a greater number of attempts at mating before successfully attaching to the female (Figure 4-4H), strongly suggesting that the activation of surstylar MTS neurons negatively impacts the males ability to attach to the female.

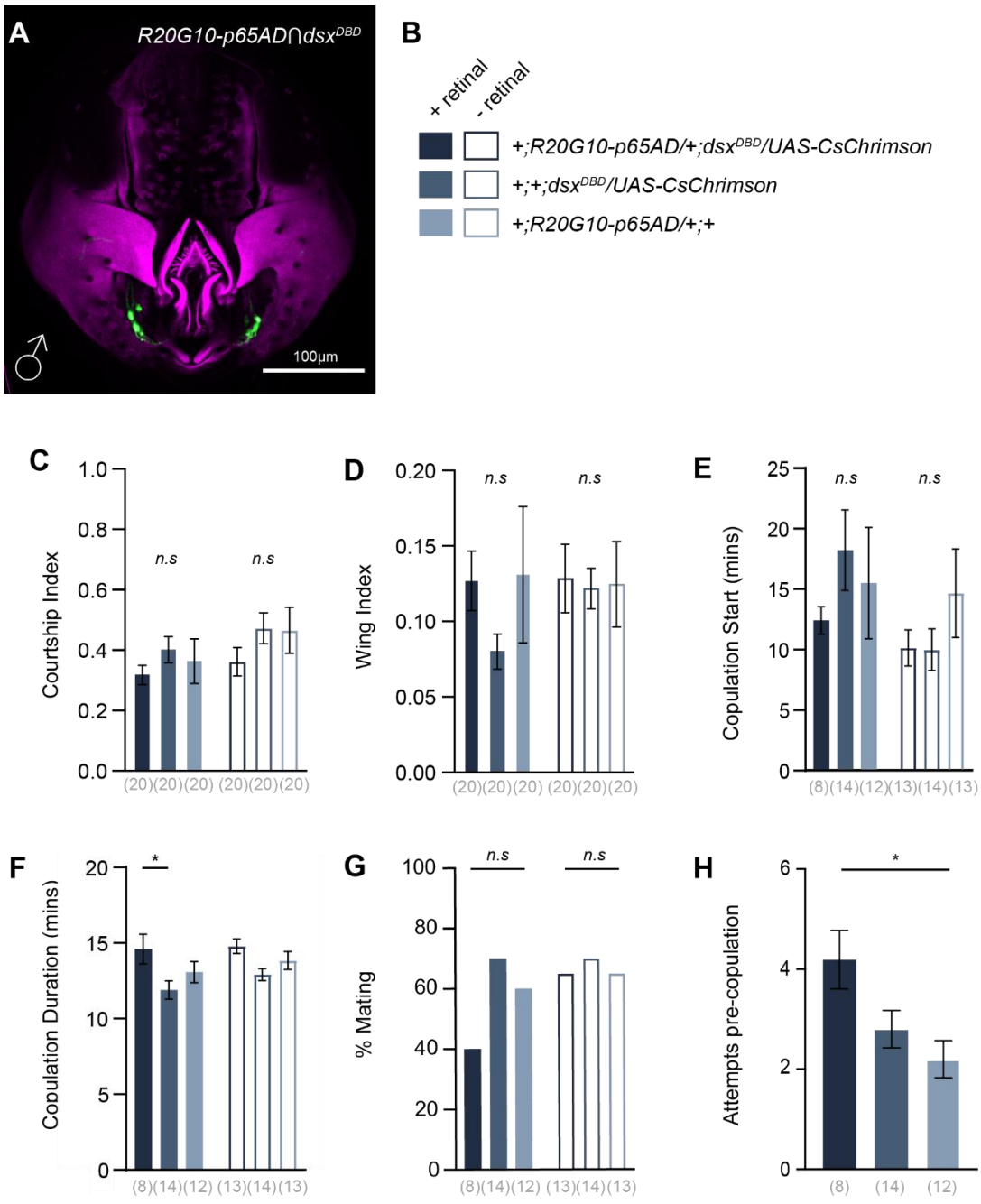

Figure 4-4: Mating analysis of *R20G10-p65AD∩dsx^{DBD}>UAS-CsChrimson* males.

R20G10-p65AD∩dsx^{DBD} labels 6 surstylar MTS neurons per side. **(B)** Genotypes and legend for the data presented in this panel. **(C)** The courtship index of *R20G10-p65AD∩dsx^{DBD}>UAS-CsChrimson* males and relevant genetic controls is not affected by optogenetic activation. **(D)** Wing extension is also unaffected, as is **(E)** the time to the start of copulation, although these values may be impacted by a low number of copulating pairs. **(F)** Duration of copulatory bouts is slightly reduced in dsx/Chrimson control males compared to experimental animals in the supplemental retinal condition (one-way ANOVA with Bonferroni correction, $t(22)=2.94$, $p<0.05$). **(G)** Despite some difference in the mating percentage of experimental males, this difference was not significant at these sample sizes in either condition (Fisher's exact test, $p=0.149$ (+retinal), $p=0.9277$ (-retinal). **(H)** *R20G10-p65AD∩dsx^{DBD}>UAS-CsChrimson* males make a greater number of attempts, on average, to copulate before achieving a successful genital interlock ($t(28)=2.18$, $p<0.05$), suggesting that these males have a reduced ability to attach to the female. Grey numbers indicate sample sizes. Error bars are standard error of the mean. * ($p<0.05$), ** ($p<0.01$), *** ($p<0.001$). Only significant results are indicated for the bars immediately underneath the edges of

the line. Other comparisons are non-significant. For panel G, controls were combined on a within-condition basis and compared against the experimental condition.

4.3.1.1 Postural Analysis of *R20G10-p65AD∩dsx^{DBD}>UAS-CsChrimson* Males

A DLC analysis of the males position during copulation reveals that whilst *R20G10-p65AD∩dsx^{DBD}>UAS-Chrimson* males do spend some time during copulation in a normal ‘delta wing’ position, they exhibit much more movement of their position and a mean mating angle of as high as 63° (Figure 4-5B). Without the supplementation of retinal the highest mean mating angle is 31°, with an average across all assays of 13°, well within the range of genetic controls. Taken together with our data from section 4.3.1, it is clear that the artificial activation of *R20G10-p65AD∩dsx^{DBD}* surstylar bristle neurons is sufficient to induce errors in the males’ ability to form genital attachments and maintain a proper body position during copulation.

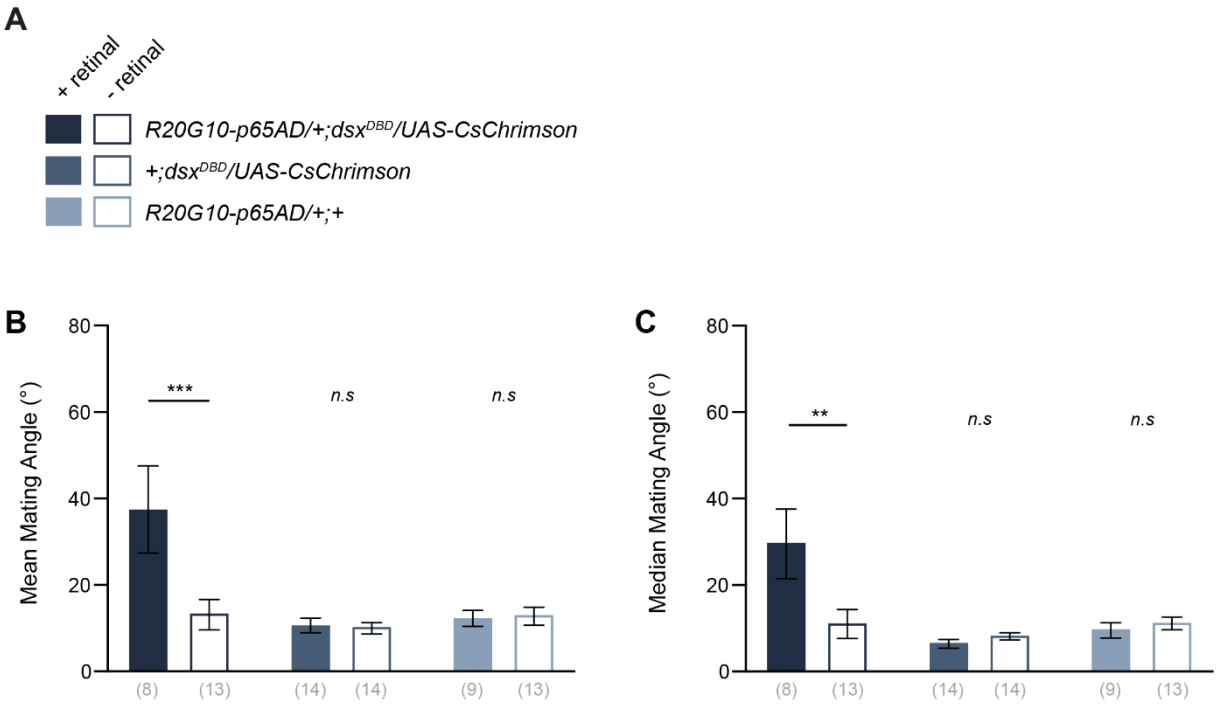

Figure 4-5: Mating posture analysis of *R20G10-p65AD∩dsx^{DBD}>UAS-Chrimson* males.

(A) Genotypes and legend for data presented in this figure. **(B&C)** Mean and median mating angles, respectively, of *R20G10-p65AD∩dsx^{DBD}>UAS-Chrimson* males is greatly increased by the supplementation of retinal in experimental animals but not controls ($t(36)=4.08$, $p<0.001$ and $t(36)=3.88$, $p<0.01$, respectively). Error bars are standard error of the mean. Grey numbers indicate sample sizes. * ($p<0.05$), ** ($p<0.01$), *** ($p<0.001$).

4.3.1.2 Female Receptivity Toward *R20G10-p65AD∩dsx^{DBD}>UAS-CsChrimson* Males

Assaying at the number of eggs laid by females mated to *R20G10-p65AD∩dsx^{DBD}* males (Figure 4-6B&D), we can see that without retinal supplementation (Figure 4-6D), females mated to males of all genotypes laid 30-40 eggs in the first 48 hours post-copulation, 10-15 after 96 hours and then drastically reduced to less than ten on the following days.

On the other hand, when provided supplemental retinal (Figure 4-6B), our data suggests that whilst the genotype of the male partner does not seem to significantly influence the number of eggs laid in each 48 hour period, females mated in this

condition continued to lay more than 20 eggs per 48-hour period until 144 hours post-eclosion and whilst this effect does not appear to be related to sensory feedback it is worth noting as it may alter the outcome of similar experiments when raising animals on retinal.

Similar to when looking at the influence of *R94D09^{DBD}∩nompC$^{MI12787\text{-}AD}$* neurons, analysis of female movement during copulation (Figure 4-6C&E) does not support the idea that manipulating surstylar MTS function during copulation leads the female exhibiting more rejection, as we found that activating *R20G10-p65AD∩dsx^{DBD}* neurons in the surstyli does not impact the amount of movement a female exhibits during copulation, although the analysis of these findings may be underpowered due to the low sample size of this study. Lastly, it is important to note that movement is only one aspect of female rejection (and is ultimately the rejection behaviour most easily quantified by our analysis) so a closer assessment of how often females exhibit behaviours like kicking would help to clarify whether female receptivity is impacted by the activation of *R20G10-p65AD∩dsx^{DBD}* neurons.

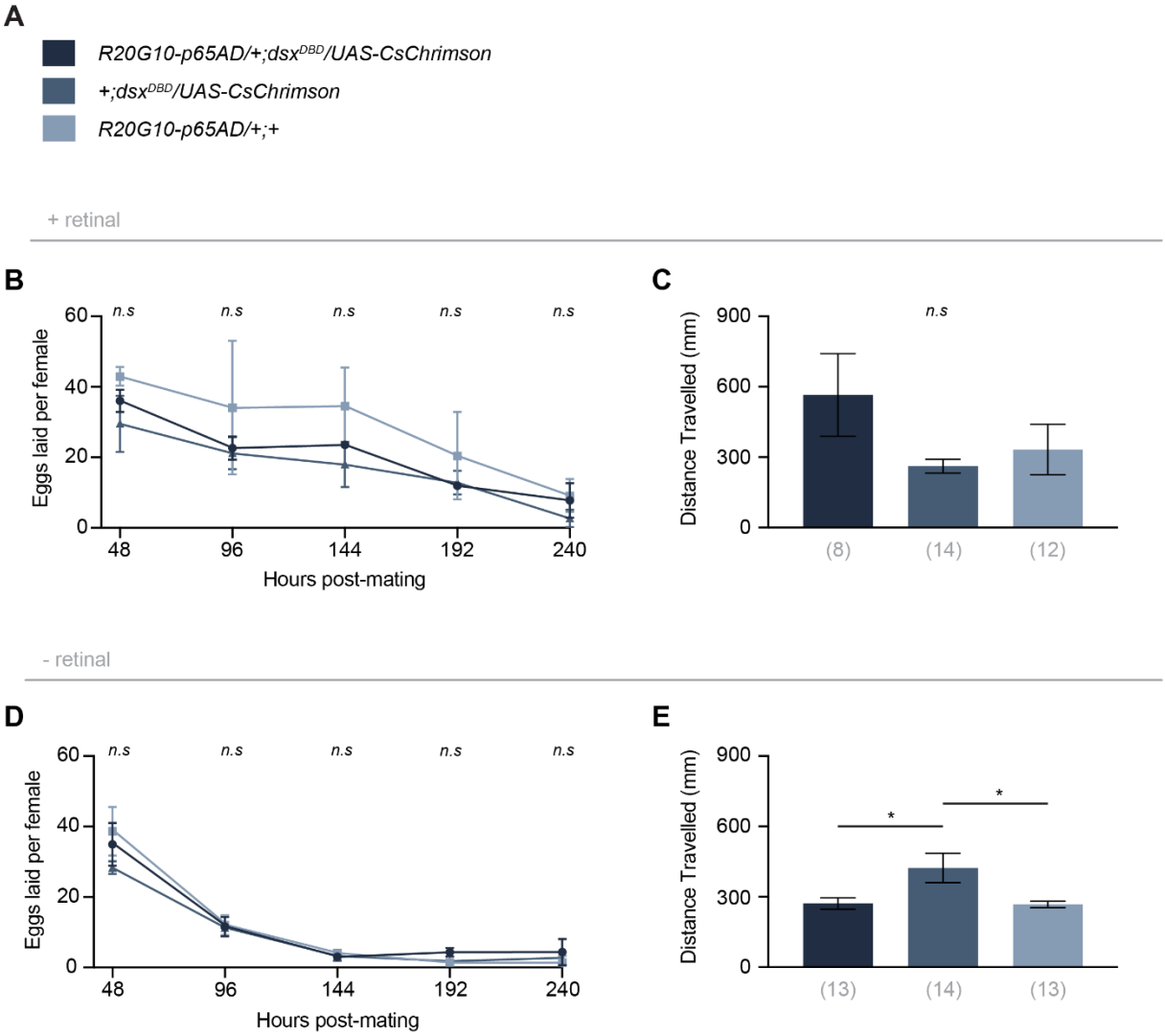

Figure 4-6: Female receptivity toward *R20G10-p65AD∩dsx^{DBD}>UAS-CsChrimson* males

(A) Genotypes and legend for the data presented in this figure. **(B)** The number of eggs laid by females mated to *R20G10-p65AD∩dsx^{DBD}>UAS-CsChrimson* or control males over 10 days was statistically invariable in the experimental condition. **(C)** Female movement during the first ten minutes of copulation was also unaffected by the activation of *R20G10-p65AD∩dsx^{DBD}* neurons. **(D)** Similar to the +retinal experimental condition, no effect of male genotype on female egg laying was seen with males raised on normal food. **(E)** Movement of the female was slightly increased when mated with *dsx/Chrimson* males compared to both experimental and driver control-mated females (one-way ANOVA with Bonferroni correction; (t(37)=2.61, p=0.038 and t(37)=2.68, p=0.032, respectively), although this effect was minor. Error bars are standard error of the mean, grey numbers indicate sample sizes. * (p<0.05), ** (p<0.01), *** (p<0.001).

4.3.2 Artificial Inactivation of *R20G10-p65AD∩dsx^{DBD}* Neurons

Following on our experiments artificially activating *R20G10-p65AD∩dsx^{DBD}* neurons, I next wanted to test their necessity for attachment and mating posture by silencing them with *UAS-shibire^{ts}.*

In our hands, *R20G10-p65AD∩dsx^{DBD}>UAS-shibire^{ts}* males placed at 31°C were almost entirely unable to achieve copulation throughout the one-hour observation period (Figure 4-7B). Specifically, of the 20 *R20G10-p65AD∩dsx^{DBD}>UAS-shibire^{ts}* males assayed at the restrictive temperature, only one male copulated with the CS female. At the permissive temperature of 23°C however, 85-90% of males in all genotypes were able to copulate within the one-hour observation. We recorded a lower percentage of copulating pairs for all genotypes at the restrictive temperature, perhaps indicating that copulation is less likely at this higher temperature. However, the effect is most pronounced in the experimental genotype (*R20G10-p65AD∩dsx^{DBD}>UAS-shibire^{ts}*) and so I am confident that this reduction is at least in part due to the perturbation of surstylar MTS function.

Despite this low level of mating, comparing the CI and wing index of males (Figure 4-7C&D) revealed that all genotypes courted equally, both when compared against males assayed at the same temperature and between permissive and restrictive temperatures, suggesting that the inability of *R20G10-p65AD∩dsx^{DBD}>UAS-shibire^{ts}* to copulate is not a result of insufficient courtship display.

Comparing the duration of copulation for those animals which did mate, reveals that within a temperature condition, males of all genotypes copulate for a similar amount of time (Figure 4-7E). The time to the start of copulation was also unaffected by silencing *R20G10-p65AD∩dsx^{DBD}* neurons (Figure 4-7F).

To better establish the underlying cause of this reduction in successful mating at 30°C, I quantified the number of attempts each male makes within the first 15 minutes of the assay (Figure 4-7D). I chose to quantify attempts for 15 minutes as this is a little longer than it takes for the upper quartile of males at the permissive temperature to achieve copulation, and so I reasoned that this period of time would contain the majority of attempts, and that the male would remain motivated throughout. When looking at the number of attempts made in this period, I found that experimental males (*R20G10-p65AD∩dsx^{DBD}>UAS-shibire^{ts}*) actually made a greater number of attempts than both genetic controls, strongly indicating that the silencing of *R20G10-p65AD∩dsx^{DBD}* surstylar bristles does not influence the males ability to attempt copulation, but severely reduces his ability to form and maintain genital attachment.

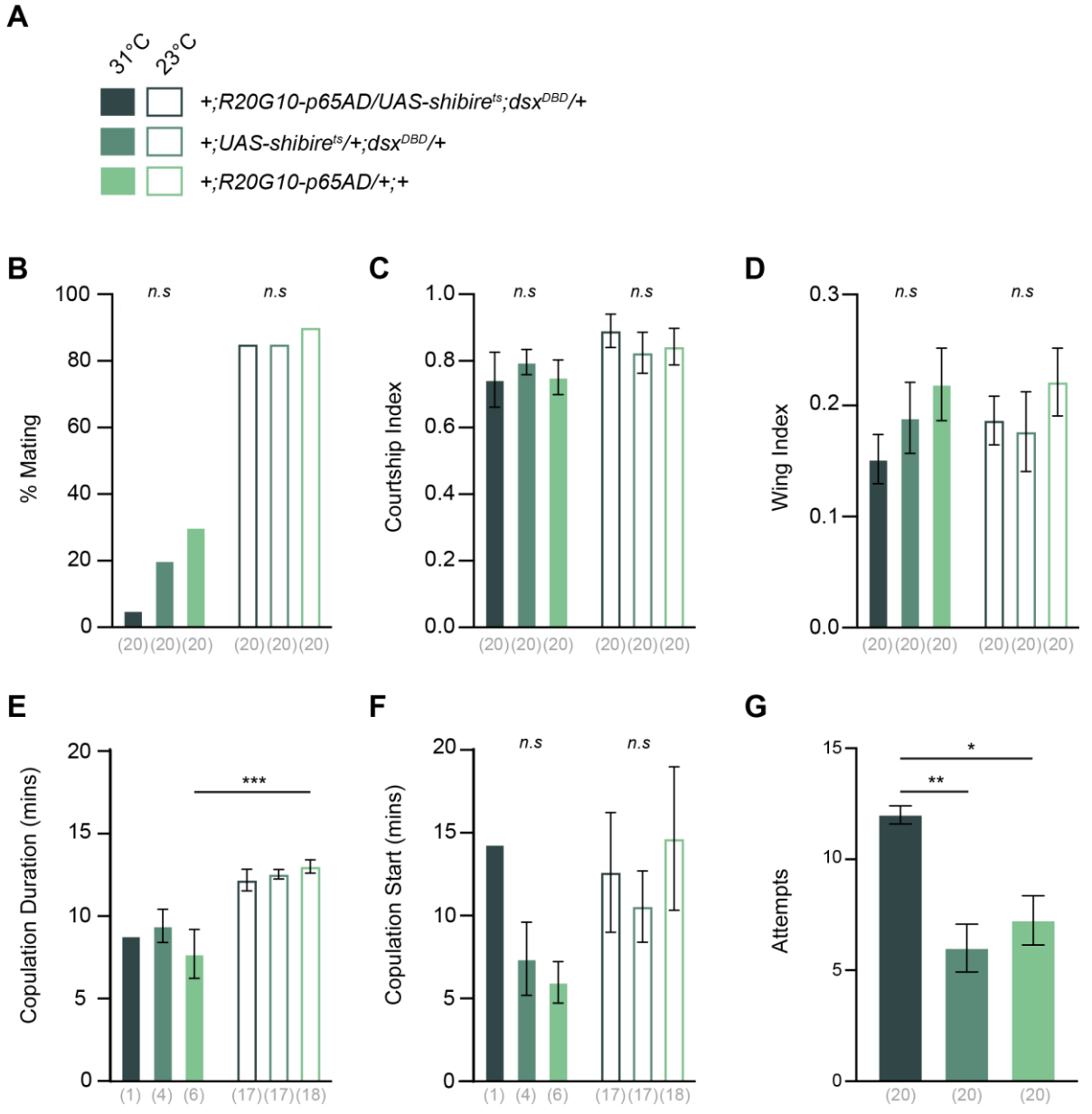

Figure 4-7: Mating analysis of *R20G10-p65AD∩dsx^{DBD}>UAS-shibire^{ts}* males.

Genotypes and legend for the data presented in this figure. **(B)** Males assayed at the restrictive temperature of 31°C mated in a drastically lower proportion of assays. This effect was seen for males of all genotypes and was not statistically different between them (Fisher's exact test, p=0.1). At the permissive temperature, all genotpyes mated equally (Fisher's exact test, p=0.865) **(C)** The courtship index of *R20G10-p65AD∩dsx^{DBD}>UAS-shibire^{ts}* and control males was unaffected, as was the wing index **(D)**. **(E)** Copulation duration was indifferent between all genotypes except the driver control which showed significantly shorter copulations at the restrictive temperature ($t(57)=5.22$, $p<0.001$). **(F)** The time taken to the start of copulation was statistically indifferent across all genotypes and conditions. **(G)** On average, *R20G10-p65AD∩dsx^{DBD}>UAS-shibire^{ts}* males make a greater number of attempts before successfully attaching to a female than both dsx/Shibire control males ($t(21)=4.59$, $p<0.01$) and *R20G10-p65AD* males ($t(21)=3.63$, $p<0.05$). Error bars are standard error of the mean, grey numbers indicate sample sizes. * ($p<0.05$), ** ($p<0.01$), *** ($p<0.001$). Only significant results are indicated for the bars immediately underneath the edges of the line. Other comparisons are non-significant. For panel B, controls were combined on a within-condition basis and compared against the experimental animal.

4.3.2.1 Postural Analysis of *R20G10-p65AD∩dsx^{DBD}>UAS-shibire^{ts}* Males

Despite the near abolition of copulation in *R20G10-p65AD∩dsx^{DBD}>UAS-shibire^{ts}* males, a DLC analysis of the individual which was able to mate revealed that mating posture was strongly affected, with an average mating angle of 45° (Figure 4-8B). Much like males in which *R94D09^{DBD}∩nompC$^{MI12787\text{-}AD}$* cells were artificially silenced (see section 4.2.1), this male not only tilted his abdomen to one side of the female midline during copulation, but would lose grasp of the females wings, leading to him falling backwards off of the female without releasing genital attachment. The low number of successful copulations means that there is insignificant statistical power to compare the mating angle of males assayed at 30°C, but a clear effect on mating posture is visible when reviewing recordings.

Males assayed at 23°C, of which a much greater number can be measured, showed no difference in mating angle between all three genotypes (Figure 4-8B&C). Altogether, the effects on mating posture of silencing *R20G10-p65AD∩dsx^{DBD}* cells are similar if not identical to the effects of activating these cells, strongly supporting the notion that sensory feedback from MTS neurons is necessary for achieving a proper mating posture.

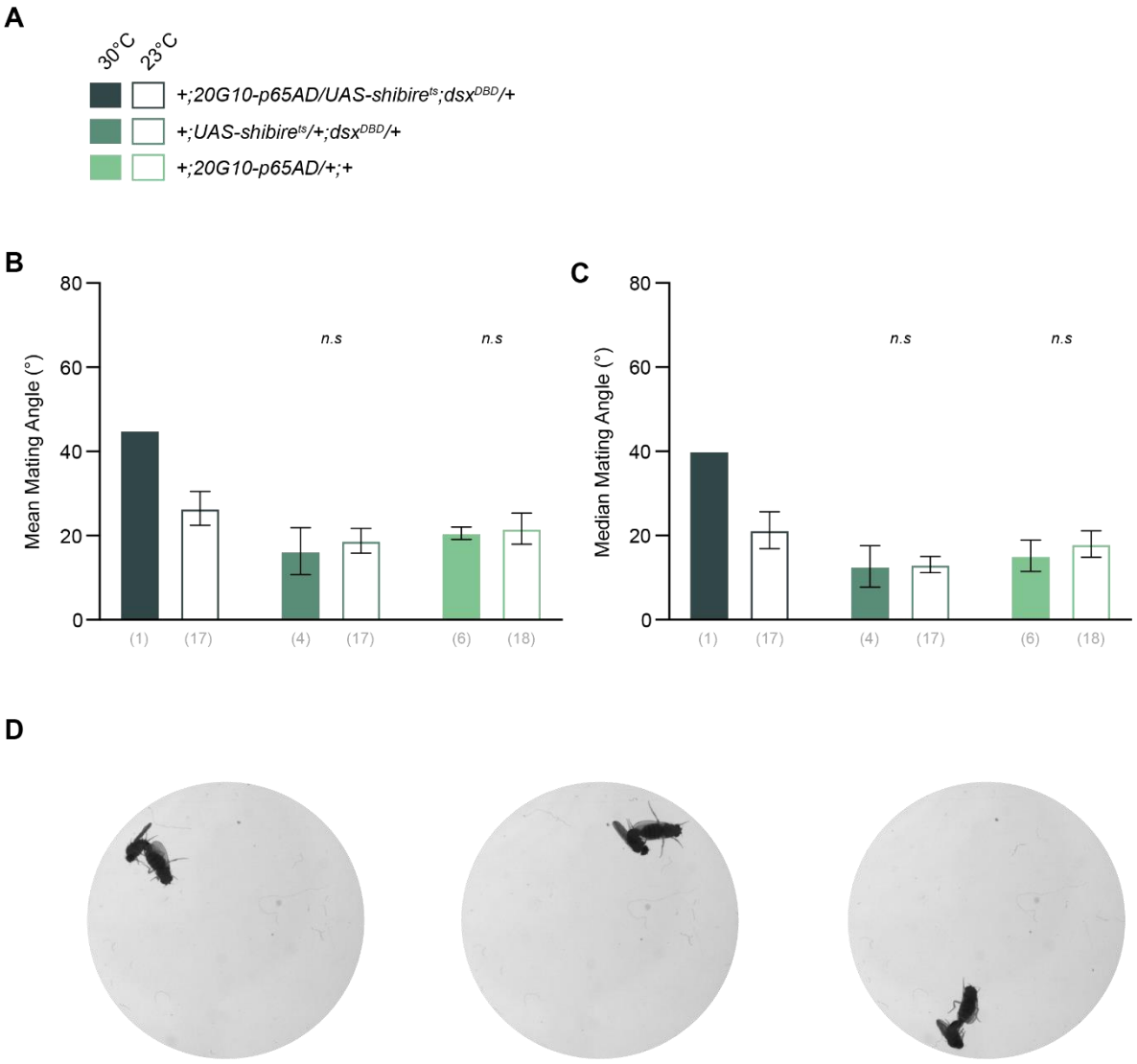

Figure 4-8: Mating posture analysis of *R20G10-p65AD∩dsx^{DBD}>UAS-shibire^{ts}* males.

(A) Genotypes and legend for the data presented in this figure. Whilst the low mating rate of *R20G10-p65AD∩dsx^{DBD}>UAS-shibire^{ts}* males make statistical analysis of the mean **(B)** and median **(C)** mating angle obsolete, a clear effect can be seen in the experimental animals assayed at the restrictive temperature that is not seen for the genetic controls. **(D)** Reviewing the recordings of these assays reveals that silencing surstylar MTS neurons is sufficient to induce aberrant mating postures where the male either tilts to one side of the female or loses his grasp entirely. Error bars are standard error of the mean, grey numbers indicate sample sizes. * ($p<0.05$), ** ($p<0.01$), *** ($p<0.001$).

4.3.2.2 Female Receptivity Toward *R20G10-p65AD∩dsx^{DBD}>UAS-shibire^{ts}* Males

Owing to the low level of successful matings from *R20G10-p65AD∩dsx^{DBD}>UAS-shibire^{ts}* males at 31°C, analysis of the number of eggs laid by females mated in this assay, and the movement of these females during copulation has low statistical power. Nonethless, looking solely at data collected from those females who were mated in this experiment, we see that under the restrictive temperature, females mated with *R20G10-p65AD∩dsx^{DBD}>UAS-shibire^{ts}* produced drastically lower numbers of eggs in the first 48 hours (Figure 4-9B). At the 96-hour timepoint, however, this number is indistinguishable from the number of eggs produced by females mated to control males. Females mated to *R20G10-p65AD∩dsx^{DBD}>UAS-shibire^{ts}* males or control males at the permissive temperature of 23°C laid statistically similar numbers of eggs over 10 days post-eclosion (Figure 4-9D), except for in the first 48 hours when females mated with dsx/Shibire control males laid a greater number of eggs than both experimental and *R20G10-p65AD*-mated females. Beyond the first 48 hours, as with those females mated at the restrictive temperature, no difference in the eggs sired by males of either genotype can be found in our data.

Lastly, looking at female movement during copulation reveals that at the restrictive temperature, no effect on female movement was found as a result of silencing these surstylar MTS neurons. These results are consistent with our previous experiments activating these neurons, but more experiments are needed to confirm these findings. Whilst these data support the notion that proprioceptive feedback from MTS neurons aide the male in forming genital attachment, we cannot support the notion that females exhibit higher levels of movement based on their copulatory experience, although they

do raise the interesting possibility that there is a short term reduction in egg laying as a result of mating with males that receive improper sensory feedback from *R20G10-p65AD∩dsx^{DBD}* neurons.

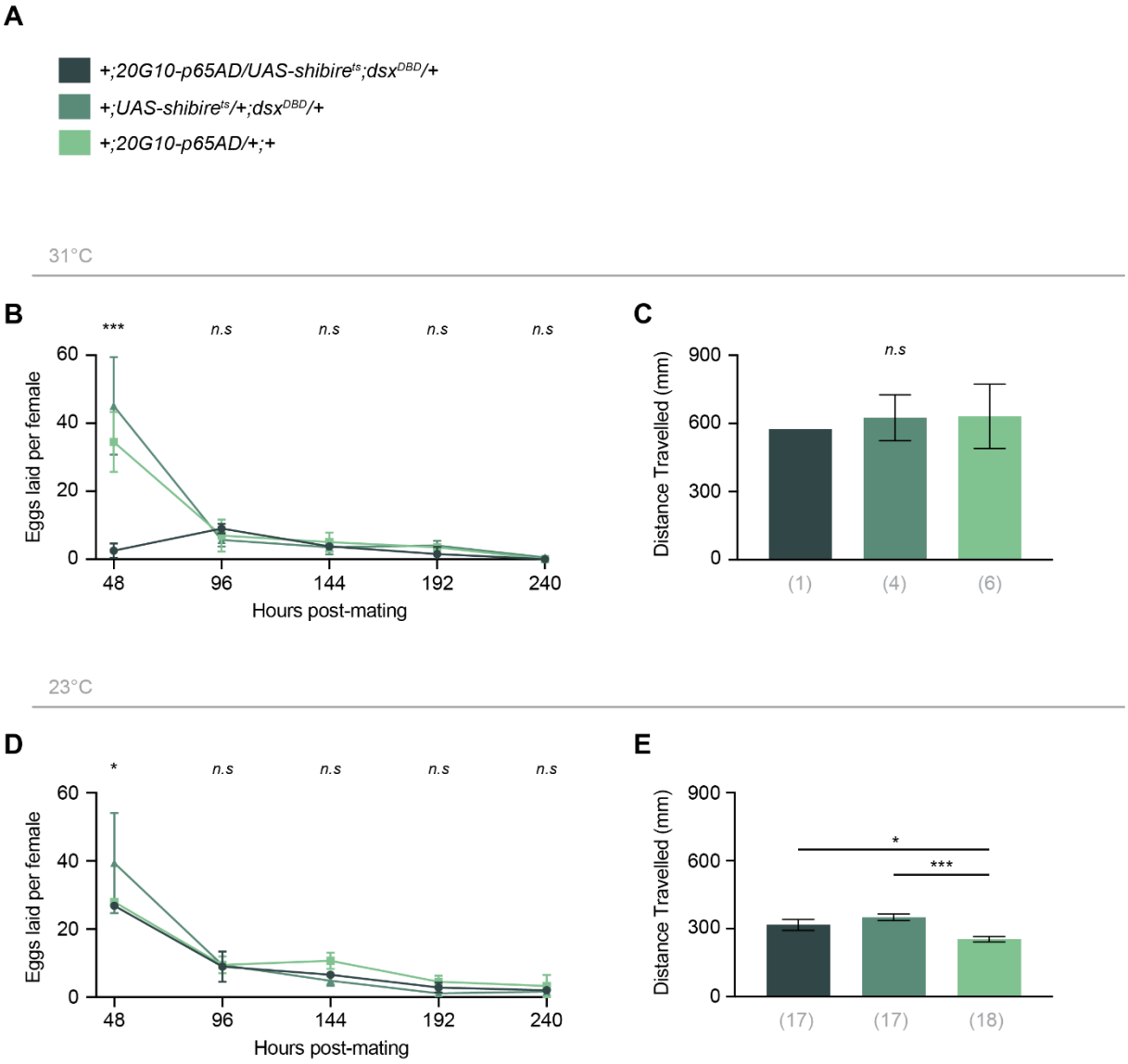

Figure 4-9: Female receptivity toward *R20G10-p65AD∩dsx^{DBD}>UAS-shibire^{ts}* males.

(A) Genotypes and legend for the data presented in this figure. **(B)** Female egg laying assay for females mated at the restrictive temperature indicate that females mated to partners with silenced *R20G10-p65AD∩dsx^{DBD}* MTS neurons produce significantly fewer eggs in the first 48 hours compared to both *dsx/Shibire* control males ($t(15)=8.98$, $p<0.001$) and *R20G10-p65AD* males ($t(15)=6.742$, $p<0.001$) although the statistical power of these tests is limited by only one pair having mated in the experimental condition. **(C)** No effect on female movement was identified in females mated at the restrictive temperature, although this is again limited by the singular mating pair. **(D)** At the permissive temperature the only difference in egg production is also seen in the first 48 hours where females mated to *dsx/Shibire* control males produced a greater number of eggs than both experimental-mated

(t(15)=2.97, p<0.05) and *R20G10-p65AD-mated* females (t(15)=2.71, p<0.05). **(E)** Analysing the movement of females during copulation under the restrictive temperature revealed a slight increase in the movement of females mated with *dsx/shibire* control males compared to both experimental (t(49)=2.59, p=0.038) and driver control males (t(49)=3.95, p<0.001), although this effect may be a result of statistical noise. Scale bars are standard deviation, grey numbers indicate sample sizes. * (p<0.05), ** (p<0.01), *** (p<0.001).

4.4 Behavioural Analysis of *R23F02-p65AD∩dsx^{DBD}*

Following on from the experiments in sections 4.3 which highlight the importance of *R20G10-p65AD∩dsx^{DBD}* MTS neurons for achieving and maintaining a proper copulatory body position, I performed behavioural assays on *R23F02-p65AD∩dsx^{DBD}* using both *UAS-shibire^{ts}* and *UAS-CsChrimson* in the same manner. If my hypothesis that these abdominal ganglion interneurons labelled by *R23F02-p65AD∩dsx^{DBD}* do receive input from MTS neurons, such as those labelled by *R20G10-p65AD∩dsx^{DBD}*, then I would expect that the effects on behaviour of artificially activating or inhibiting *R23F02-p65AD∩dsx^{DBD}* should be similar to those arising from the activation or inhibition of *R20G10-p65AD∩dsx^{DBD}* neurons.

4.4.1 Artificial Activation of *R23F02-p65AD∩dsx^{DBD}* Neurons

Artificial activation of the abdominal ganglion interneurons labelled by *R23F02-p65AD∩dsx^{DBD}* with CsChrimson (*R23F02-p65AD∩dsx^{DBD}>UAS-CsChrimson*) drastically reduced the proportion of males achieving copulation within one hour compared to controls (Figure 4-10C, 35% of experimental males compared to 70-75% of control males) but did not cause any significant effects on CI or wing extension that can be attributed to the activation of *R23F02-p65AD∩dsx^{DBD}* cells (Figure 4-10D&E).

The duration of copulation was longer for experimental males, indicating that these animals have difficulty detaching at the end of copulation (Figure 4-10F), yet despite their apparent inability to detach, looking at the time to starting copulation we saw no difference between the genotypes or between conditions, suggesting that these males do not struggle to attach to the female (Figure 4-10G). Taken together with our data regarding the duration of copulation, it is possible that *R23F02-p65AD∩dsx^{DBD}* cells are important for detaching from the female. More experiments, especially a characterization of the neurotransmitter used by these cells will aid in understanding the mechanism by which *R23F02-p65AD∩dsx^{DBD}* neurons impact detachment.

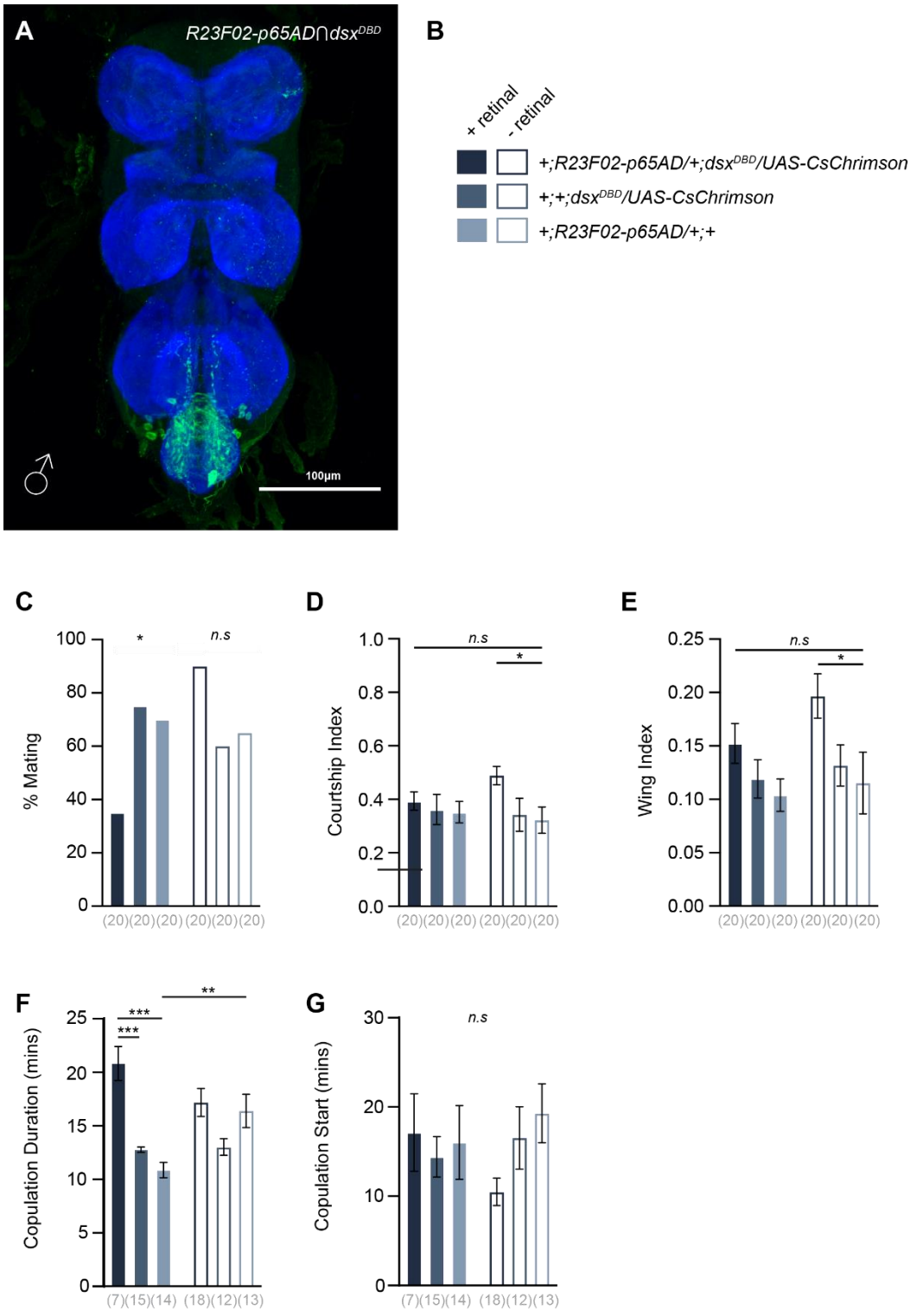

Figure 4-10: Mating analysis of *R23F02-p65AD∩dsx^{DBD}>UAS-CsChrimson* males.

R23F02-p65AD∩dsx^{DBD} labels a subset of abdominal ganglion interneurons in the male, approximately 9 cells per side. **(B)** Genotype and legend for the data presented in this figure. **(C)** The proportion of mating males was reduced in males with activated *R23F02-p65AD∩dsx^{DBD}* neurons compared to genetic controls (Fishers exact test, p=0.0108). In the -retinal condition, all genotypes mate equally (Fisher's exact test, p=0.0785). Inactivated males were not significantly effected (p=0.07). **(D)** No effect between conditions was seen on courtship index or **(E)** wing index, although *R23F02-p65AD* control males showed reduced CI and WI compared to experimental males in the no retinal condition (t(114)=2.52, p<0.05, and t(114)=2.82, p<0.05, respectively). **(F)** Experimental males exhibited a much

longer duration of copulation compared to both *dsx/Chrimson* control and *R23F02-p65AD* control males ($t(73)=5.24$, $p<0.001$, and $T(73)=6.36$, $p<0.001$, respectively) and *R23F02-p65AD* males in the + retinal condition copulated for significantly less time than the same genotype in the -retinal condition ($t(73)=3.25$, $p<0.01$). **(G)** Time to start of copulation was unaffected. Error bars are standard error of the mean. Grey numbers indicate sample sizes. * ($p<0.05$), ** ($p<0.01$), *** ($p<0.001$). Only significant results are indicated for the bars immediately underneath the edges of the line. Other comparisons are non-significant. For panel C, controls were combined on a within-condition basis and compared against the experimental animal.

4.4.1.1 Postural Analysis of *R23F02-p65AD∩dsx^{DBD}>UAS-CsChrimson* Males

Males in which *R23F02-p65AD∩dsx^{DBD}* cells have been activated with *UAS-CsChrimson* exhibit a much greater average mating angle, reminiscent of what we identified when activating *R20G10-p65AD∩dsx^{DBD}* neurons but with a higher average mating angle. This effect was not seen in males that had not been raised on supplemental retinal, indicating that this effect is a direct result of optogenetic activation and that ectopic activation of *R23F02-p65AD∩dsx^{DBD}* neurons in the abdominal ganglion is sufficient to induce an aberrant mating posture.

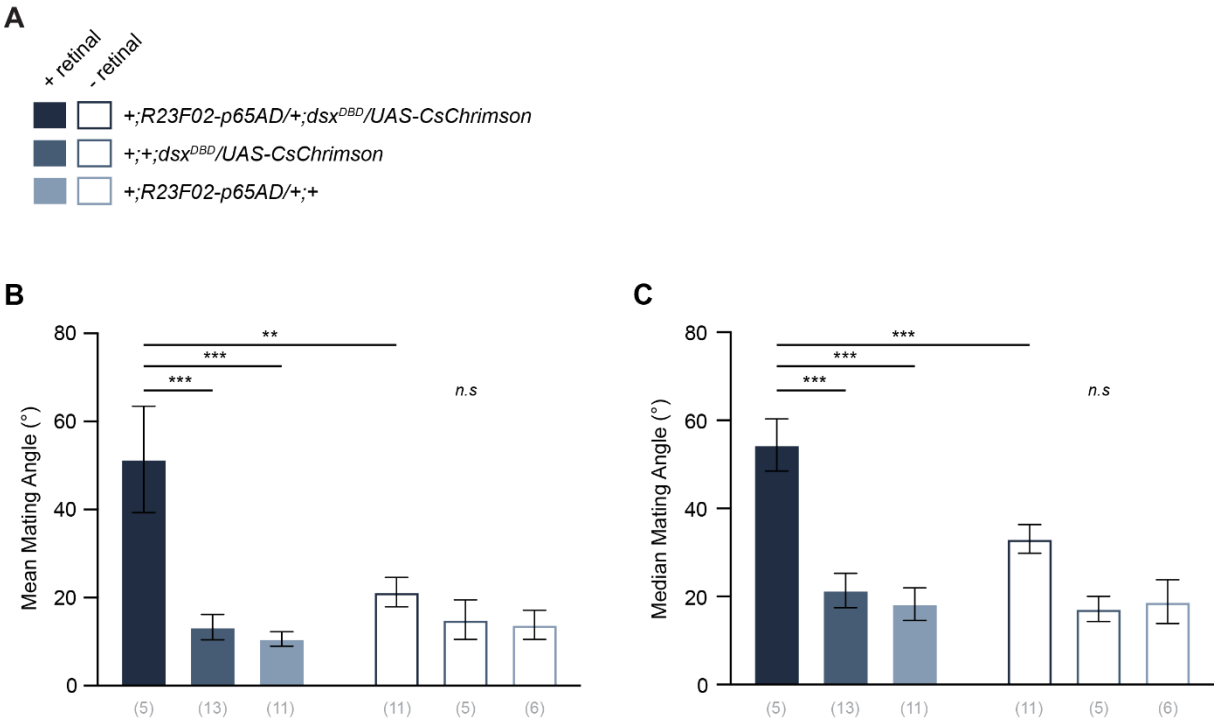

Figure 4-11: Mating posture analysis of *R23F02-p65AD∩dsx^{DBD}>UAS-CsChrimson* males.
(A) Genotypes and legend for the data presented in this figure. **(B)** *R23F02-p65AD∩dsx^{DBD}>UAS-CsChrimson* raised on supplemental retinal showed a significantly greater mean mating angle compared to both *dsx/Chrimson* controls (t(45)=5.18, p<0.001) and *23F02-p65AD* control (t(45)=2.32, p<0.001) but this effect was not seen when animals were not provided supplemental sources of retinal. **(C)** Calculating the median mating angle also highlights this effect against *dsx/Chrimson* control males (T(45)=5.18, p<0.001) and *23F02-p65AD* control males (t(45)=6.29, p<0.001), as well as against males raised without retinal (t(45)=4.65, p<0.001). Error bars are standard error of the mean, * (p<0.05), ** (p<0.01), *** (p<0.001).

4.4.1.2 Female Receptivity Toward R23F02-p65AD∩dsx^{DBD}>UAS-CsChrimson Males

Females mated to *R23F02-p65AD∩dsx^{DBD}>UAS-CsChrimson* males and the respective parental controls did not lay significantly more or less eggs over a ten day period in in either condition (Figure 4-12B&D).

Similarly, assessing female movement during copulation with *R23F02-p65AD∩dsx^{DBD}* males and the relevant controls revealed no significant effect of activating these abdominal ganglion interneurons in either the +retinal, or -retinal condition (Figure

4-12C&E). These results are once again consistent with our findings from the manipulation of *R20G10-p65AD∩dsx^{DBD}* surstylar neurons and indicate that at least in a 1-on-1 setting, the aberrant copulatory experience (due to altered mating posture) a female receives does not influence her movement or egg laying output. However, as noted in section 4.3.1.2, movement during copulation is only a proxy for female acceptance behaviour and an analysis focusing solely on these behaviours would provide a much more detailed insight into any changes in female behaviour as a result of activation *R23F02-p65AD∩dsx^{DBD}* neurons.

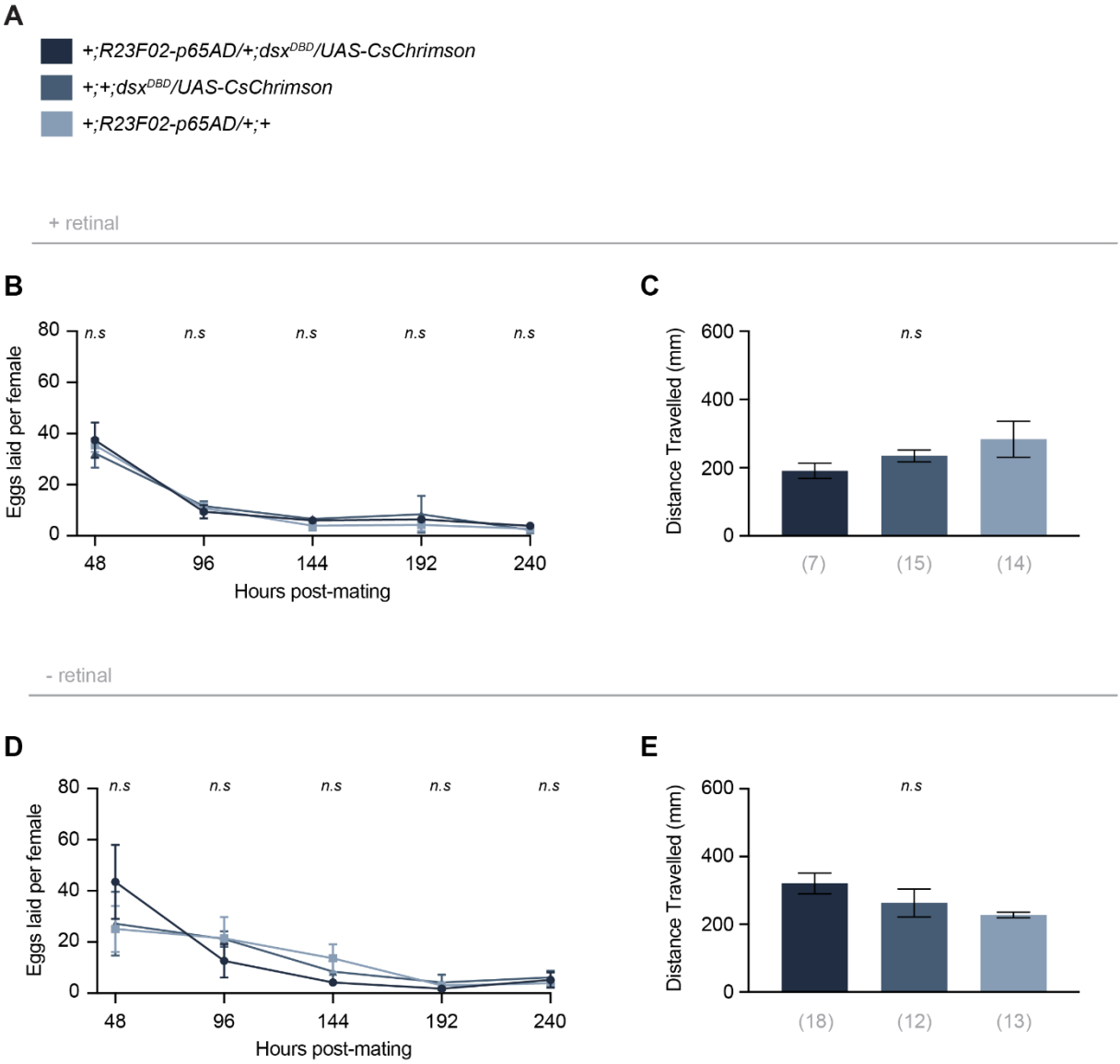

Figure 4-12: Female Receptivity toward *R23F02-p65AD∩dsx^{DBD}* males.
(A) Genotypes and legend for the data presented in this figure. **(B)** The number of eggs laid by females mated to either genotype was indifferent over 10 days post-mating in the experimental condition. **(C)** Female movement was also unaffected in the experimental condition. **(D)** When assaying females mated with -retinal males, we once again identified no statistically significant effect on egg production. **(E)** There was no identifiable difference in female movement in the no retinal condition. Error bars are standard deviation. Grey numbers indicate sample sizes. * (p<0.05), ** (p<0.01), *** (p<0.001).

4.4.2 Artificial Inactivation of *R23F02-p65AD∩dsx^{DBD}* Neurons

To assess the impact of silencing *R23F02-p65AD∩dsx^{DBD}* abdominal ganglion neurons, I once again utilised *UAS-shibire^{ts}.*

At the restrictive temperature of 31°C, *R23F02-p65AD∩dsx^{DBD}>UAS-shibire^{ts}* males showed a 5-10% reduction in the proportion of successful copulations. On the other hand, the experimental male actually showed an increased likelihood of mating at the permissive temperature (Figure 4-13B). Males with silenced *R23F02-p65AD∩dsx^{DBD}* neurons also exhibited normal levels of CI and wing extension (Figure 4-13C&D). The duration of copulation as well as the time to copulation is also unaffected (Figure 4-13E&F).

At the permissive temperature of 23°C, the time to copulation and the duration of copulatory bouts were unaffected, but surprisingly the experimental line exhibited greater CI than both driver control males (*+/23F02-p65AD;+*) and *R23F02-p65AD* control males (Figure 4-13C).

Between the conditions, we identified a reduction in CI for both genetic controls and the copulation duration of *23F02-p65AD* control males. These effects are consistent with the notion that males at lower temperature are less active, rather than the inhibition of *R23F02-p65AD∩dsx^{DBD}* causing these effects.

Lastly, effector control males (*+/dsx^{DBD};+/UAS-shibire^{ts}*) showed reduced wing extension at the permissive temperature, this is again likely a result of reduced activity, or may be due to some low-level leakage of the *UAS-shibire^{ts}* transgene (Figure 4-13D).

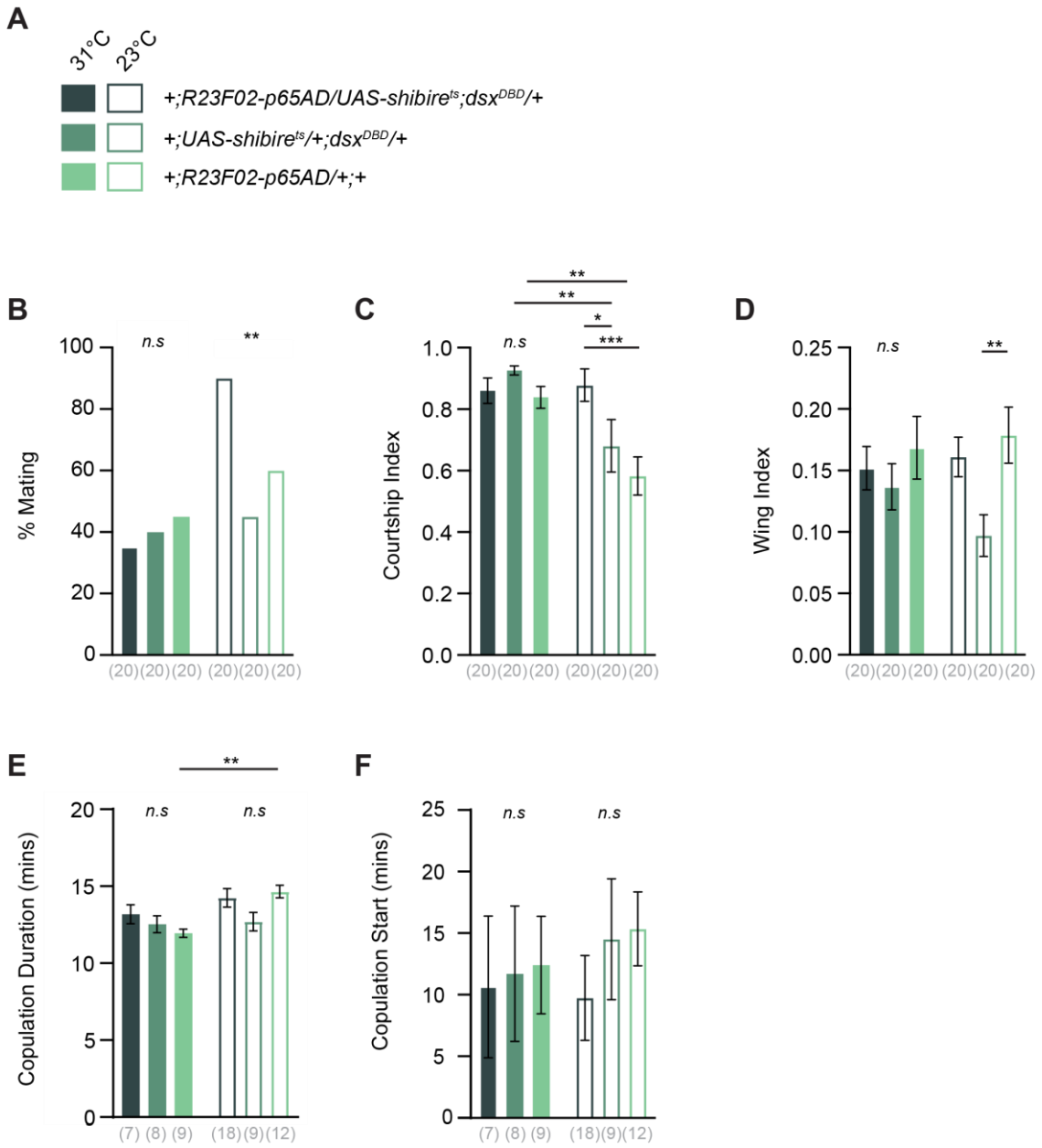

Figure 4-13: Mating analysis of *R23F02-p65AD∩dsx^{DBD}>UAS-shibire^{ts}* males.

Genotypes and legend for the data presented in this figure. **(B)** Experimental males placed at 31°C had a similar percentage mating chance to controls (Fisher's exact test, p=0.8119), but interestingly in the control (23°C) condition, males mated notably more (Fisher's p=0.0043). **(C)** The courtship index of *R23F02-p65AD∩dsx^{DBD}>UAS-shibire^{ts}* males was unaffected at the restrictive temperature but significantly reduced in driver control males at the permissive temperature. **(D)** Wing extension was unaffected at the restrictive temperature, but significantly reduced between controls at the permissive temperature (t(114)=3.05, p<0.01). **(E)** Duration of copulation was only significantly affected between temperature regimes in *23F02-p65AD* controls (t(57)=3.29, p<0.01). **(F)** Time to the start of copulation was not affected either within or between conditions. Error bars are standard error of the mean, grey numbers indicate sample sizes. * (p<0.05), ** (p<0.01), *** (p<0.001). Only significant results are indicated for the bars immediately underneath the edges of the line. Other comparisons are non-significant. For panel B, controls were combined on a within-condition basis and compared against the experimental animal.

4.4.2.1 Postural Analysis of *R23F02-p65AD∩dsx^{DBD}>UAS-shibire^{ts}* Males

Analysing the mating angle of *R23F02-p65AD∩dsx^{DBD}>UAS-shibire^{ts}* males highlights that similarly to when these neurons were activated, these males adopted an aberrant mating posture where the male leans to one side of the female. Combined with our results from activating these neurons (section 4.4.1), these results indicate that not only are *R23F02-p65AD∩dsx^{DBD}* cells necessary for proper mating posture, but manipulating their activity is sufficient to induce aberrant postural phenotypes.

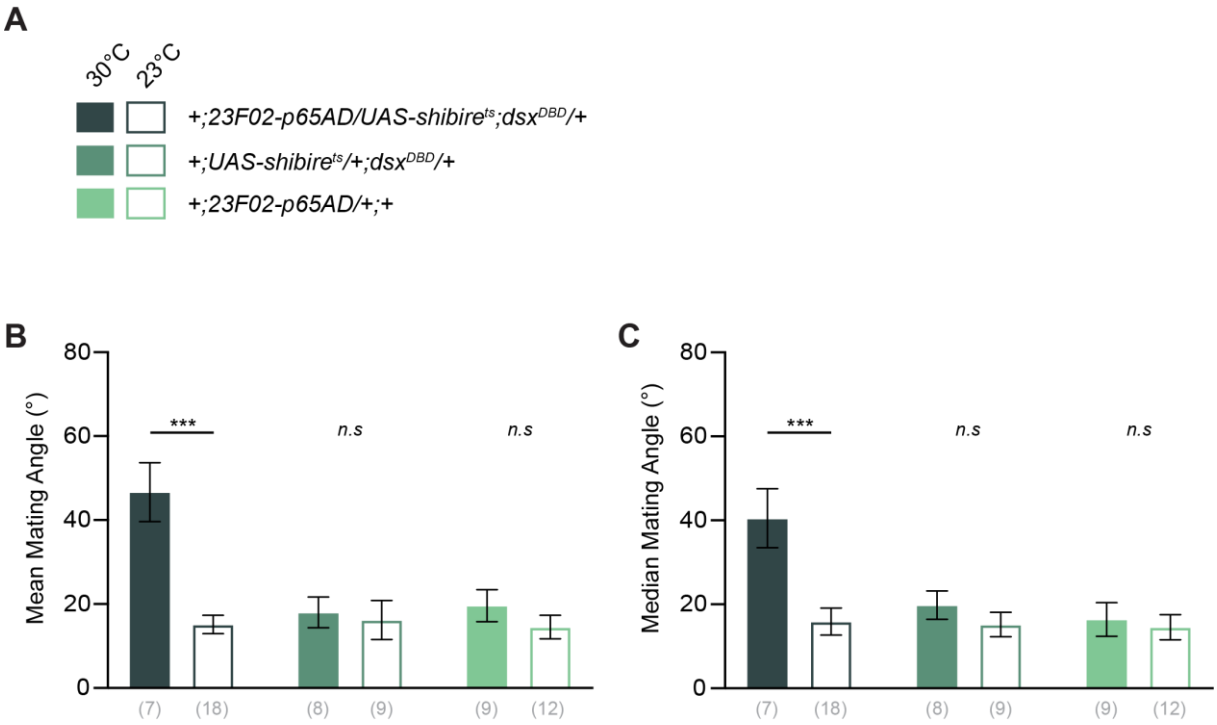

Figure 4-14: Mating posture analysis of *R23F02-p65AD∩dsx^{DBD}>UAS-shibire^{ts}* males.

(A) Genotypes and legend for the data presented in this figure. **(B)** Mean mating angle of experimental males is significantly increased for males assayed at the restrictive temperature ($t(57)=5.94$, $p<0.001$) but not affected in any of the control lines. **(C)** Median mating angle was similarly affected in experimental animals only ($t(57)=4.55$, $p<0.001$). Error bars are standard error of the mean, * ($p<0.05$), ** ($p<0.01$), *** ($p<0.001$).

4.4.2.2 Female Receptivity Toward *R23F02-p65AD∩dsx^{DBD}>UAS-shibire^{ts}* Males

Comparing the number of eggs produced by females mated at the restrictive temperature showed no difference in their egg laying output depending on the genotype of the male they mated with (Figure 4-15B). At the permissive temperature, the only difference in egg laying we saw was in the first 48 hours, where females mated to *dsx/shibire* controls produced fewer eggs (Figure 4-15D).

Interestingly, comparing the numbers of eggs laid by females in different conditions (permissive or restrictive temp) reveals that females who mated at 31°C produced far more eggs in the first 48 hours compared to those mated at 23°C. Kaliss and Graubard (1936) reported that females who are mated and allowed to lay at temperatures greater than those they were raised in, produce a greater number of eggs compared to those who are raised, mate in, and lay eggs at the same temperature, so it is possible that the difference in temperature during mating assays caused this short-term difference in egg production.

Analysing female movement during copulation does not indicate any effect in either condition (Figure 4-15C&E), a finding that is consistent with the effects of activating this same population.

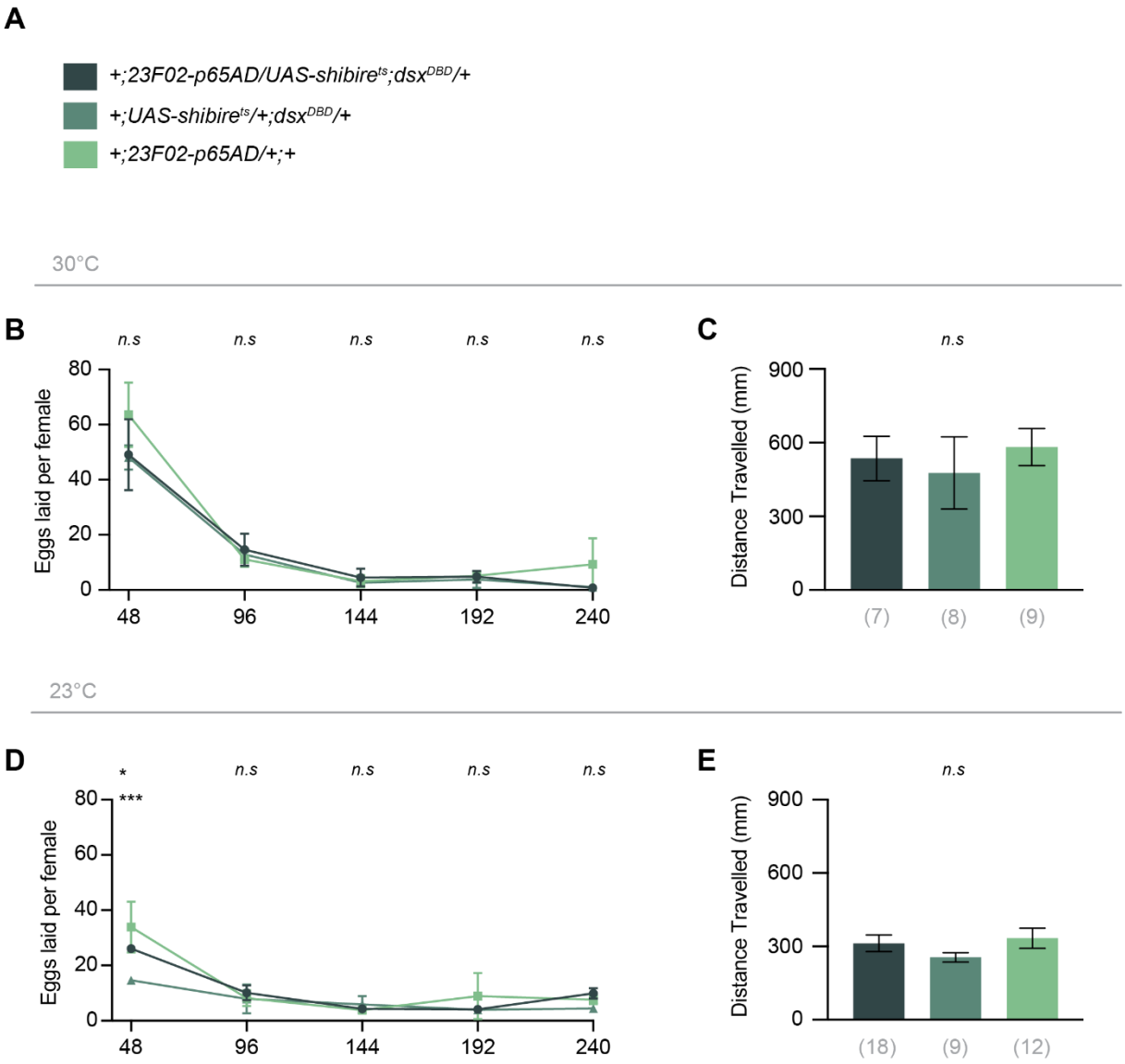

Figure 4-15: Female receptivity toward *R23F02-p65AD∩dsx^{DBD}>UAS-shibire^{ts}* males.

(A) Genotypes and legend for data presented in this figure. **(B)** Analysis of the number of eggs sired by males of each genotype at the restrictive temperature revealed no difference at any time point. **(C)** No effect on female movement during the first ten minutes of copulation was found as a result of silencing *R23F02-p65AD∩dsx^{DBD}* neurons. **(D)** At the permissive temperature eggs produced by females mated to *dsx/shibire* control males were significantly less than those produced by females mated to either experimental ($t(15)=2.04$, $p<0.05$) or *R23F02-p65AD* controls ($t(15)=5.05$, $p<0.001$). **(E)** As with females mated at 31°C, no effect on movement was seen at the permissive temperature. Error bars are standard error of the mean, grey numbers indicate sample sizes. * ($p<0.05$), ** ($p<0.01$), *** ($p<0.001$).

4.5 Concluding Remarks

The experiments presented in this chapter were intended to assess the impact of perturbing MTS neuron function in the terminalia and putative downstream neurons.

After extensively characterizing the phenotypic effects of both silencing and activating surstylar MTS neurons, as well as a population of abdominal ganglion interneurons that we hypothesize lie downstream of external sensory cells, it is clear that male flies rely on sensory feedback from external bristles to properly form genital attachments. Sensory lock and key theory would suggest that these abnormal matings would result in females producing fewer offspring fathered by those males, but from our data we cannot support this notion. Despite this, it may be the case that these 1-on-1 mating assays are unable to identify any differences in egg production as females are not presented with the opportunity to preferentially use the sperm of another male, and may therefore simply wait a short period of time before resuming normal egg production. This is a trend that we saw in section 4.3.2.2 in particular.

In terms of testing the possibility that *R23F02* neurons lie downstream of *R20G10* MTS neurons, the near phenocopy of aberrant mating posture when manipulating these two populations supports this notion, and in the next chapter I will further examine this possibility using functional calcium imaging.

Interestingly, whilst both activating and inhibiting the function of *R20G10-p65AD∩dsx^{DBD}* bristle neurons lead to aberrant mating posture, and in some cases a reduced ability to form genital attachments, little or no effect on the duration of copulation was identified, suggesting that feedback from these bristles is not necessary when detaching the surstyli. On the other hand, activating *R23F02-p65AD∩dsx^{DBD}* interneurons not only affected mating posture, but also significantly increased the duration of copulation, suggesting that these neurons not only receive input form MTS neurons but also signal to motor neurons involved in controlling the timing of detachment. Alternatively, they may be linked to an internal ‘clock’ controlling the

timing of detachment. Further experiments looking at the downstream partners of *R23F02-p65AD∩dsx^{DBD}* cells will help to further expand the circuit model.

5 Imaging MTS Neuron Activity and Identifying Downstream Partners

5.1 Introduction

In the previous chapter I have presented a series of data that highlight the importance of MTS neurons, and the sensory feedback they provide, for the formation of proper genital attachment and the maintenance of mating posture. By genetically targeting MTS neurons and putative downstream neurons in the abdominal ganglion, this work has provided the most precise manipulation of their function that is currently available. The results of these manipulations are consistent with previous works where the bristles were removed from the cuticle (e.g. Acebes 2003), and morphological observations that posited the bristles of the male genitalia, especially those on the surstyli, are sensitive to mechanical stimuli. Furthermore, our data in chapter 2 has shown that the neurons innervating these bristles are potentially sensitive to mechanical stimuli due to their expression of the ion channels *nompC* and *Piezo*. Despite this, there is little physiological evidence to complement these findings and show conclusively that MTS neurons convey this stimulus to motor circuits in the VNS. Secondly, whilst our behavioural data, combined with the anatomical overlap of *R20G10-p65AD∩dsx^{DBD}* and *R23F02-p65AD∩dsx^{DBD}* neurites in the abdominal ganglion indicate that *R23F02-p65AD∩dsx^{DBD}* likely receive input from MTS neurons, we cannot confirm this on the basis of the existing evidence alone.

Therefore, to address more directly whether stimulation of the MTS neurons labelled by *R20G10-p65AD∩dsx^{DBD}* leads to the activation of *R23F02-p65AD∩dsx^{DBD}* neurons, I will record the activity of these two populations during mechanical stimulation of the surstyli, using a reporter for calcium influx; GCaMP6s (Chen *et al*. 2013). Recording calcium transients in *R23F02-p65AD∩dsx^{DBD}* cells that are closely associated with the onset of stimulation to the genitalia, will provide an excellent line of evidence supporting the functional connection between the two populations.

Lastly, following on from our calcium imaging data I will present some data that attempt to expand our current circuit model using the anterograde transsynaptic labelling technology; *trans*-Tango (Talay *et al*. 2017). The technical aspects of *trans*-Tango are discussed in more detail in section 5.1.2, but in essence this technology will allow us to visualise, within the same animal, a population of neurons we have defined with a GAL4 or split-GAL4 driver, and all of their downstream synaptic partners in an unbiased manner. By using this tool we can not only visualise the synaptic partners of *R20G10-p65AD∩dsx^{DBD}* neurons in the central nervous system, but should we find evidence that supports the notion they are directly connected to *R23F02-p65AD∩dsx^{DBD}* cells, then we can also use *trans*-Tango with this driver combination to examine their connections to other regions of the nervous system. This process will allow us to shed light on how signals from peripheral MTS neurons are combined and integrated with other circuits.

5.1.1 Visualising Neural Activity

To detect whether neurons are active during a given behaviour or in response to a known stimulus, it is possible to precisely record the electrical activity of individual neurons using classical electrophysiological approaches, or to express genetically encoded calcium indicators that can be measured as a proxy for neural activity. Electrophysiological recordings are in many ways the gold standard for measuring neural activity and provide unparalleled, precise information about the firing of action potentials within a given neuron. However, even the most technically gifted physiologists cannot record from more than a few neurons at a time, and the size of *Drosophila* neurons, plus the tendency for signal quality to decline over time, makes

electrophysiological recordings inefficient in many experimental paradigms. Furthermore, in the case of MTS neurons, which have small cell bodies located just beneath the cuticle of flexible structures like the surstyli, achieving direct contact with the neuron itself is near impossible, as the cuticle would have to first be stabilized and punctured. To overcome some of these limitations, extracellular methods for recording bristle neuron activity have been developed that rely on clipping the bristle and then covering the tip with a glass recording pipette containing a high K+ saline solution. This saline solution mimics the mechanoreceptor lymph and preserves the mechanosensory responses (Grunert and Gnatzy 1987; Kernan *et al*. 1994; Tuthill and Wilson 2016).

Despite these advances, however, such recordings are still only feasible on the larger mechanosensory bristles of the legs, making light-based visualisations of neural activity an indispensable tool when aiming to record the activity of MTS neurons.

Another method for identifying neural activity is to optically record a calcium-respondent reporter, as the fusion of neurotransmitter-containing vesicles with the presynaptic membrane occurs once the neuron depolarizes and the opening of voltage-gated Ca2+ channels causes a local influx of calcium ions (Jaffe *et al*. 1992; Muller and Connor 1991). The local concentration of Ca2+ ions is dependent on the intensity of neural activation, thus making Ca2+ dynamics within a cell an excellent indicator of activity (Pologruto *et al*. 2004; Tian *et al*. 2009). Genetically encoded calcium indicators (GECIs) provide a robust light-based method to visualize and record these changes in calcium concentration, and thereby infer the activity of a given population of neurons.

GECIs are comprised of a calcium binding element which undergoes Ca2+-dependent conformational change, and a reporter in the form of a fluorescent protein which is

modulated by the conformation of the calcium-binding element. Many groups have developed fluorescence based GECIs with varying dynamic ranges and kinetics, with the most highly developed being the GCaMPs (for a review regarding the construction and optimization of GECIs, see; Mank and Griesbeck 2008).

Expressing GCaMP proteins using various targeted expression system strategies has allowed researchers to identify which neurons are activated during the performance of many different behaviours (Flood *et al*. 2013; Min *et al*. 2013; Pavlou *et al*. 2016) and are even being utilised within some technologies for recording activity in freely behaving, rather than tethered animals (Grover *et al*. 2016).

In this chapter, I will utilise the hemidriver combination *R20G10-p65AD∩dsx*^{DBD} to direct expression of the recombinant calcium sensor GCaMP6s to surstylar bristle neurons (Chen *et al*. 2013). I will then record changes in calcium concentration at their neurites in the Abg at the onset of mechanical stimulation of the bristle using 2-photon imaging. As a control I will record the same output sites during the stimulation of abdominal segment A6 (Figure 5-1). By doing this, I would expect to see a drastic change in fluorescence brought about by a touch stimulus to the surstyli, and due to the highly restricted nature of the driver combination (*R20G10-p65AD∩dsx*^{DBD}), we can be sure that we are only recording the activity of the surstylar neurons alone. Secondly, before moving on to attempting to identify downstream neurons in this circuit, I will perform the same experiment with GCaMP6s being expressed in *R23F02-p65AD∩dsx*^{DBD} cells in order to investigate the potential that these neurons may receive input from MTS neurons.

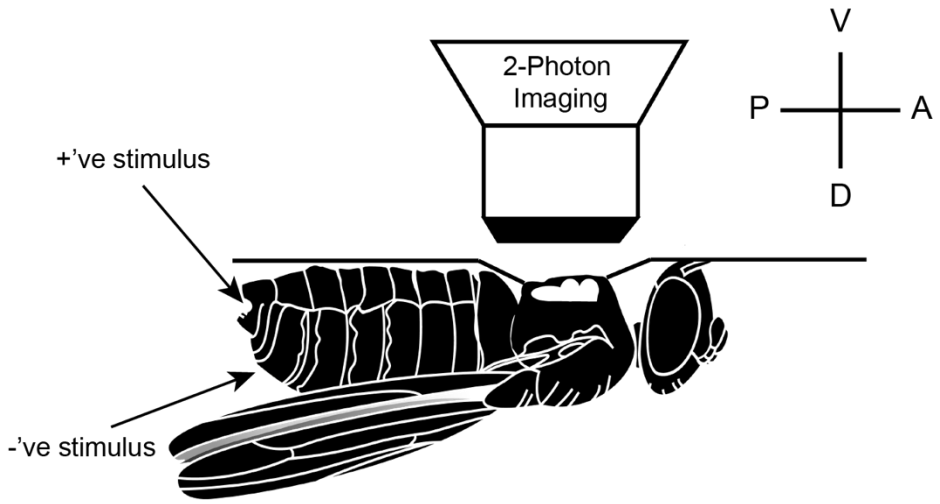

Figure 5-1: Cartoon showing calcium imaging setup for recording responses to genital stimulation in *R20G10-p65AD∩dsx^{DBD}* and *R23F02-p65AD∩dsx^{DBD}* cells.
To record GCaMP6s responses in the abdominal ganglion, the fly was mounted, ventral side down onto a small dish with an opening cut into the thorax for 2-photon imaging. Positive stimuli (+'ve) where directed onto the surstyli, whilst control stimuli (-'ve) were directed to abdominal segment A6. V – ventral, D – dorsal, P – posterior, A – anterior.

5.1.2 Examining Synaptic Connectivity

To identify the downstream synaptic partners of a user-defined population of neurons, one can use the recently developed transsynaptic labelling system, *trans*-Tango (Talay *et al*. 2017).

Until the development of this technology, the availability of tools for transsynaptic labelling similar to the viral methods commonly used in vertebrates (Callaway and Luo 2015; Lo and Anderson 2011; Zingg *et al*. 2017), have been absent in *Drosophila*, with the main system for identifying synaptic connections for a defined set of cells being GRASP (GFP reconstitution across synaptic partners; Feinberg *et al*. 2008; Macpherson *et al*. 2015). The GRASP system allows the researcher to visualise punctate staining of GFP at the interface of two neurons by expressing two halves of the protein; one in a specific set of neurons and the other in putative synaptic partner

neurons, thus enabling the reconstitution of the functional fluorescent protein where they come into contact. However, this method only labels synapses rather than whole cells so cannot identify the projections of the postsynaptic cell. Alternatively, one could use photo-activatable GFP, that can be expressed pan-neuronally and photo-activated in precise regions to enable labelling of potentially connected cells (Clowney *et al*. 2015; Datta *et al*. 2008; Patterson and Lippincott-Schwartz 2002; Ruta *et al*. 2010). This method enables the labelling of neural processes and in theory a high degree of spatial specificity can be achieved, but it requires an invasive process, can label unrelated cells, and does not report connectivity.

The *trans*-Tango system overcomes all of these limitations; the specificity of labelling is restricted entirely to postsynaptic partners of a defined 'donor' neuron population, the entirety of the donor and postsynaptic cell(s) can be visualized, and the entire system is genetically encoded negating the need for invasive procedures, with the added benefit that the system provides genetic access to the postsynaptic cell, which with further development could be used to manipulate the function of downstream cells.

The system requires three components: (1) a GAL4 or split-GAL4 driver, (2) a reporter allele containing a membrane-trafficked GFP variant (*UAS*-myrGFP) to mark presynaptic neurons, and a membrane-associated RFP (mtdTomato) under QF control (*QUAS-mtdTomato(3xHA)*) to mark postsynaptic neurons, and (3) the *trans*-Tango allele containing three fusions proteins; a receptor fusion, hArr::TEV, and a ligand fusion (Talay *et al*. 2017).

The receptor fusion encodes the human Glucagon Receptor (hGCGR) fused with a cleavage site for the TEV protease (TEVcs) that links to the transcription factor; QF (Barnea *et al*. 2008; Potter *et al*. 2010). The entire construct (hGCGR::TEVcs::QF)

is placed under the control of the *neuronal Synaptobrevin* promoter to drive its' expression in all neural cells (*nSyb*-hGCGR::TEVcs::QF).

The second fusion protein, human β-Arrestin2 fused to the N1A protease from the Tobacco Etch Virus (hArr:TEV) is also expressed pan-neuronally under the *elav* promotor (*elav*-hArr:TEV), such that all cells are primed for QF-dependent expression of the *QUAS-mtdTomato(3xHA)* postsynaptic label (Barnea *et al*. 2008; Talay *et al*. 2017).

Lastly, the ligand fusion is expressed in a GAL4-dependent pattern chosen by the researcher. It is tethered to the synaptic membrane by its fusion to the transmembrane and cytoplasmic domains of the *Drosophila* synaptic protein Neurexin1 (dNRXN1) via a spacer developed from the extracellular domain of the cell adhesion molecule ICAM1 (hGCG::hICAM1::dNRXN1). At synapses where the ligand is absent, the QF transcription factor remains tethered to the receptor and is unable to regulate the expression of the *QUAS*-mtdTomato reporter. At synapses which oppose the GAL4 labelled population however, hGCG binds its receptor, triggering the expression of the postsynaptic label as QF is released to translocate into the nucleus.

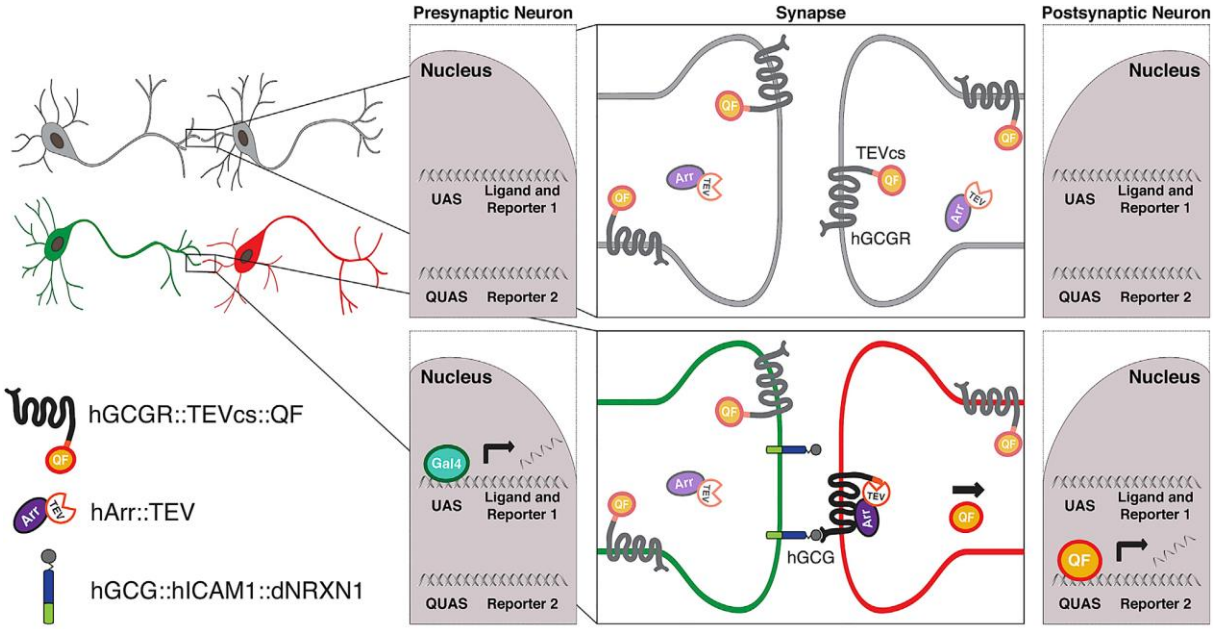

Figure 5-2: Diagrammatic representation of *trans*-Tango system.
In *trans*-Tango, all neurons express the components of the Tango signalling pathway (Barnea *et al*. 2008) (*hGCGR::TEVcs::QF* and *hArr::TEV*), rendering them competent for the QF-dependent expression of reporter 2 (*QUAS-RFP,* red). The pathway is transsynaptically activated by membrane-tethered glucagon (*hGCG::hICAM1::dNRXN1*) with the expression of this ligand fusion, and GFP (green) being dependent on a GAL4 driver supplied by the researcher. In the absence of the glucagon ligand, *hGCGR* does not undergo cleavage by *hArr::TEV* and therefore the QF transcription factor remains at the membrane. When activated, the receptor fusion is cleaved by *hArr::TEV*, allowing QF to enter the nucleus and promote expression of the red postsynaptic label. Image taken for (Talay *et al*. 2017).

Results

5.2 Functional Calcium Imaging Supports Mechanosensory Role of Surstylar MTS

To directly establish the sensory modality of genital bristles, particularly those in the surstyli, I expressed GCaMP6s (UAS-GCaMP6s; Chen *et al*. 2013) in the 6 surstylar bristle neurons labelled by *R20G10-p65AD∩dsx^{DBD}* (*R20G10-p65AD∩dsx^{DBD}>UAS-GCaMP6s*) and stimulated the bristles of the surstyli with a small wire attached to a micromanipulator. At the same time, we imaged the neurites of *R20G10-p65AD∩dsx^{DBD}* in the abdominal ganglion to detect calcium influx brought about

through mechanical stimulation (Figure 5-3A). As a negative control, we stimulated abdominal segment A6 and imaged the same region.

We identified strong increases in GCaMP fluorescence immediately following genital stimulation but not during abdominal stimulation, supporting the notion that they are mechanosensory and transduce the sensory signal to the Abg. Looking at recordings from individual animals, clear spikes in fluorescence can be seen that correlate closely with mechanical stimulation of the surstyli (Figure 5-3B). This effect was also clear when averaging the responses across multiple animals (n=10; Figure 5-3C), with a mean increase in fluoresecence (ΔF/F) of ~20%, rising to ~30%. This is a similar increase in fluorescence as was reported by Pavlou *et al*. (2016) when stimulating the genitalia and recording *dsx∩VGlut and dsx∩Gad1* neurons in the Abg. Conversely, mechanical stimulation of abdominal segment A6 lead to no discernible calcium transients in individual recordings, or when averaging across multiple recordings (n=10; Figure 5-3C&D, respectively), although some minor changes (<10% ΔF/F) in fluorescence were detected, likely as a result of abdominal stimulation pushing the base of the genitalia against the dish in which the fly was mounted, or as artifacts caused by movement of the sample.

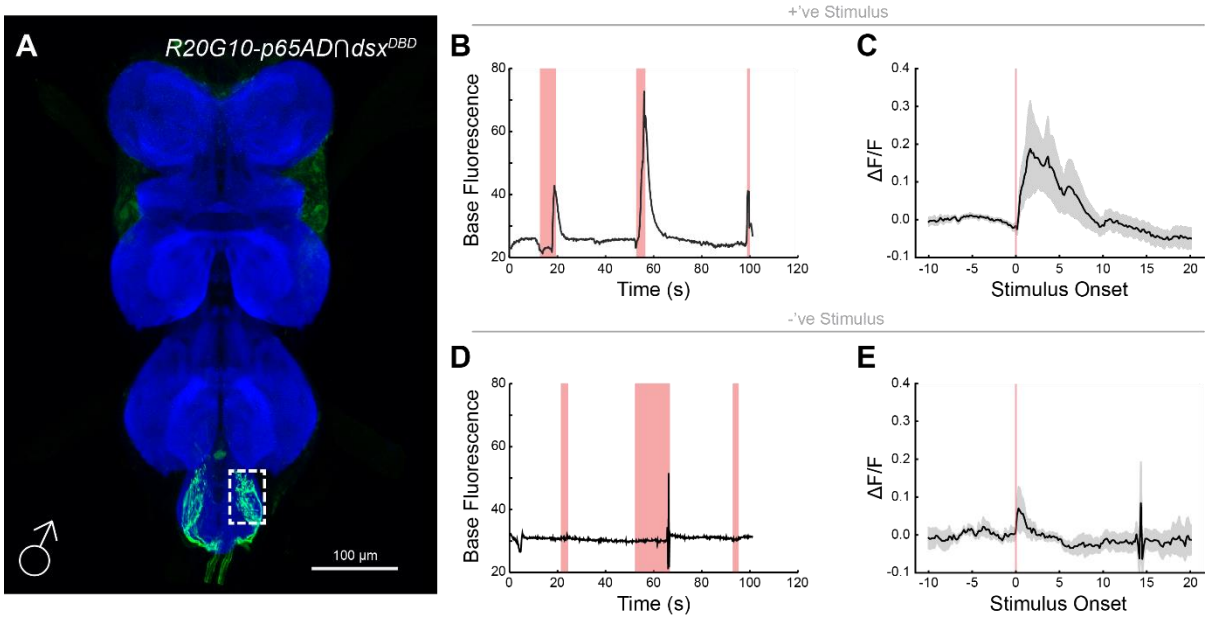

Figure 5-3: Recording calcium transients in *R20G10-p65AD∩dsx^{DBD}* neurites in the abdominal ganglion during genital stimulation.
R20G10-p65AD∩dsx^{DBD} labels 6 surstylar bristles neurons per side, with putative outputs in the abdominal ganglion **(A)**. To record calcium transients resulting from the mechanical stimulation of these surstylar neurons, we expressed GCaMP6s in these cells (*R20G10-p65AD∩dsx^{DBD}-UAS-GCaMP6s)* and recorded changes in calcium fluourescence at their neurites in the Abg. White box in panel A indicates the region recorded from. 'positive' stimuli, i.e. stimuli directed towards the surstyli induce rapid spikes in calcium fluorescence at the onset of stimuli. **(B)** A representative recording from a single male fly. Each animal was stimulated three times and averaging these responses **(C)** reveals that on average, a ~20% increase in calcium fluorescence was brought about by the stimulus, indicating an activation of *R20G10-p65AD∩dsx^{DBD}* neurons. On the other hand, control stimuli directed towards the abdomen of the fly, which were applied to the same animals as +'ve stimuli, did not elicit spikes in calcium fluorescence in individual animals **(D)** or when averaged across all recordings **(E)**, indicating that abdominal stimulation does not activate *R20G10-p65AD∩dsx^{DBD}* neurons. Pink lines indicate the onset of the touch.

5.3 Functional Imaging of *R23F02∩dsx* Cells Highlights a Possible Downstream Partner of MTS Neurons

To test the hypothesis that *R23F02-p65AD∩dsx^{DBD}* neurons in the Abg receive inputs from *R20G10-p65AD∩dsx^{DBD}* surstylar bristles, we repeated the same calcium imaging experiment reported in the previous section (5.2), whilst driving GCaMP6s expression in *R23F02-p65AD∩dsx^{DBD}* cells (*R23F02-p65AD∩dsx^{DBD}>UAS-GCaMP6s;* Figure 5-4A). Imaging the mass of *R23F02-p65AD∩dsx^{DBD}* neurites in the Abg whilst

stimulating the genitalia revealed that these cells are indeed responsive to mechanical stimulation of the surstyli (Figure 5-4B&C), but not the abdomen (Figure 5-4D&E). Averaging all recordings taken during stimulation of the genitalia (Figure 5-4C) reveals an average ΔF/F of ~15% associated with stimulation, a lesser but nonetheless noticeable effect compared with recordings taken from the projections of surstylar neurons themselves. On the other hand, averaging recordings in which the abdomen was stimulated (Figure 5-4E) shows almost no change from baseline.

Whilst we cannot rule out the possibility that these two populations communicate via intermediate 2nd order cells, the strong correlation of calcium influx to the onset of stimulus supports the notion that they receive mechanosensory signals from MTS neurons. The smaller change in fluorescence compared to our recordings from *R20G10-p65AD∩dsx^{DBD}* may indicate that only a subset of *R23F02-p65AD∩dsx^{DBD}* cells are responsive to genital stimulation. Further subdivision of the *R23F02-p65AD∩dsx^{DBD}* population, i.e. on the basis of their neurotransmitter usage, may provide a clearer view of which cells in this group are responsive to mechanical stimulation of the genitalia.

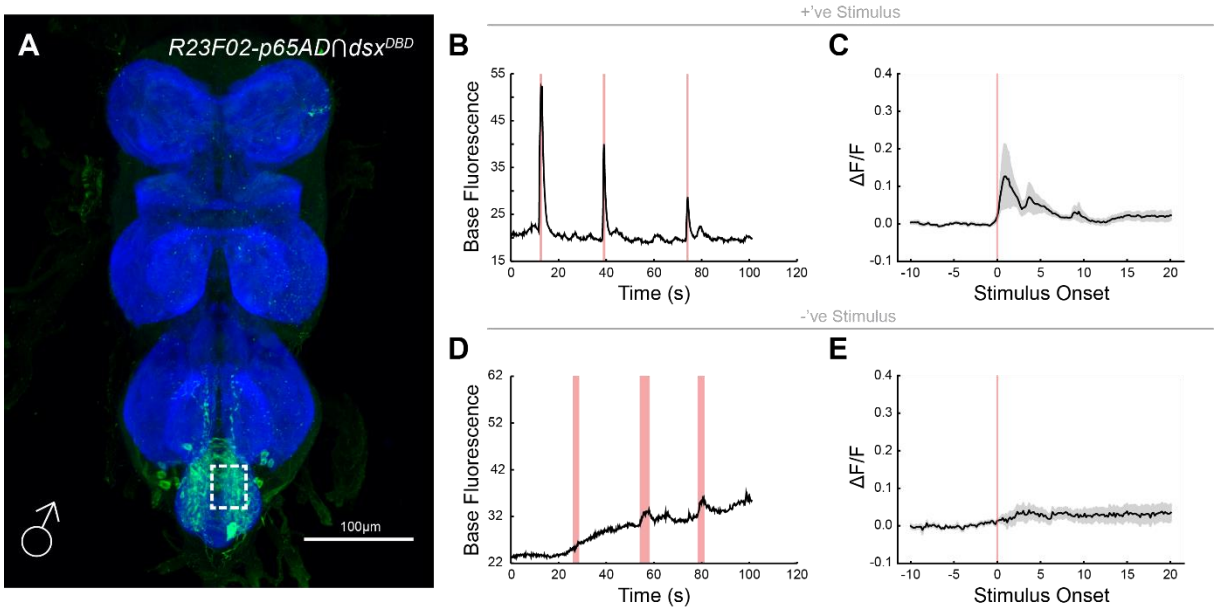

Figure 5-4: Recording calcium transients in *R23F02-p65AD∩dsx^{DBD}* neurites in the abdominal ganglion during genital stimulation.
(A) *R23F02-p65AD∩dsx^{DBD}* labels 9 abdominal ganglion interneurons on each side of the Abg. To record calcium transients in *R23F02-p65AD∩dsx^{DBD}* cells that result from the mechanical stimulation of the surstyli, we expressed GCaMP6s in these cells (*R23F02-p65AD∩dsx^{DBD}-UAS-GCaMP6s)* whilst touching the surstyli with a small wire and recording changes in calcium fluourescence in the Abg. White box in panel A indicates the region recorded from. 'positive' stimuli, i.e. stimuli directed towards the surstyli induce rapid spikes in calcium fluorescence at the onset of stimuli. **(B)** shows a representative recording from a single male fly. Each animal was stimulated three times and averaging these responses across all recordings (n=10) **(C)** reveals that on average, a ~15% increase in calcium fluorescence was brought about by the stimulus, indicating an activation of *R23F02-p65AD∩dsx^{DBD}* neurons. Control stimuli directed towards the abdomen of the fly did not elicit spikes in calcium fluorescence in individual animals **(D)** or when averaged across all recordings **(E)**, indicating that abdominal stimulation does not activate *R23F02-p65AD∩dsx^{DBD}* neurons. Pink lines indicate the onset of the touch.

5.4 Expanding the circuit model

In the process outlined in this work I have identified means to genetically access MTS neurons, refined these drivers to allow access to my cells of interest without also labelling cells elsewhere in the animal, and shown how they can be utilised for manipulating the function of MTS neurons in freely behaving male *Drosophila*. Lastly, in the data presented in this chapter I have shown unequivocally that MTS neurons are activated by mechanical stimuli and that they transmit this signal into the abdominal ganglion where it is passed on to at least a subset of abdominal ganglion interneurons

labelled by *R23F02-p65AD∩dsx^{DBD}.* In the following sections I will present my data from experiments using both *R20G10-p65AD∩dsx^{DBD}* and *R23F02-p65AD∩dsx^{DBD}* in combination with the *trans*-Tango system (see section 5.1.2) to visualise the downstream synaptic partners of these two populations. These results, in combination with data presented throughout this thesis, provide strong lines of evidence from which to infer the circuit structure that incorporates MTS signals into other sensorimotor pathways, and enable us to answer questions such as; are the motor programs for genital attachment/detachment and the maintenance of mating posture located entirely within the ventral nervous system, or do they relay onto regions of the central brain.

5.4.1 Postsynaptic partner of *R20G10-p65AD∩dsx^{DBD}* bristle neurons

Looking to identify synaptic partners to *R20G10-p65AD∩dsx^{DBD}* neurons in the surstyli, I crossed *R20G10-p65AD∩dsx^{DBD}* with flies containing the *trans*-Tango components (see section 5.1.2). After staining the CNS of flies containing all the required elements, I was able to visualise both *R20G10-p65AD∩dsx^{DBD}* neural processes in the Abg and their synaptic partners (Figure 5-5). To determine whether these partner neurons send projections to the forebrain, the entire nervous system was dissected intact. We did not see any projections in the cervical connective, indicating that synaptic partners of *R20G10-p65AD∩dsx^{DBD}* neurons do not project to the brain (Figure 5-5A).

Looking at the VNS (Figure 5-5B-H), we can see that *R20G10-p65AD∩dsx^{DBD}* neurons enter the Abg from the posterior and spread their axonal arbors across the medial layer of the abdominal ganglion (Figure 5-5B&C). Here they form synapses with a mass of neurites which extend across all layers of the Abg (Figure 5-5D&E). An overlay of first order *R20G10-p65AD∩dsx^{DBD}* cells and their synaptic partners is shown in Figure

5-5F&G. The cell bodies of these synaptic partner neurons, as well as the majority of their processes are contained within the abdominal ganglion, although a higher exposure image (Figure 5-5H) reveals that they also send projections from the Abg into all of the thoracic neuromeres, strongly suggesting that they receive input from, and pass on signals to, other motor circuits in the legs, wing and halteres.

From these results, we believe it is likely that the postsynaptic neurons are capable of integrating mechanosensory information from a variety of different areas of the fly's body to enable the fine control of multiple limbs during movement. Interestingly, Tsubouchi *et al*. (2017) have shown that external sensory bristles on the dorsal and ventralmost abdomen also send their projections to a medial layer of the abdominal ganglion, although it appears from our data that MTS neurons in the surstyli have a large part of their axonal arbor located slightly more towards the ventral side of the Abg than other bristle neurons. On the other hand, the postsynaptic cells have their processes spread across the depth of the Abg, suggesting that they also incorporate input from abdominal sensory bristles, genital sensory bristles, and likely also some chordotonal organs on the ventral midline that have outputs in the dorsal edge of the Abg (Tsubouchi *et al*. 2017).

Whilst the morphology and cell body position of these postsynaptic neurons is partially similar to *R23F02-p65AD∩dsx^{DBD}* cells, there are a handful of differences in the morphology of the two populations. The most obvious difference being that *R23F02-p65AD∩dsx^{DBD}* does not label projections from the abdominal ganglion into the more anterior thoracic neuromeres. Combined with our calcium imaging data (see section 5.3), this suggests that surstylar bristle neurons do not only form synaptic connections with *R23F02-p65AD∩dsx^{DBD}* cells, but they may instead connect to all, or a subset of

R23F02-p65AD∩dsx^{DBD} neurons, as well as to neurons which project to other thoracic neuromeres. Alternatively, surstylar MTS neurons may connect to *R23F02-p65AD∩dsx^{DBD}* cells via a 2nd order group of neurons. In order to determine which of these is the case, an experiment where the stimulation of surstylar MTS neurons is controlled optogenetically would be required, as in this paradigm the duration of the stimulus can be controlled so precisely that the response time of *R23F02-p65AD∩dsx^{DBD}* neurons can be used to determine if they are directly or indirectly connected to MTS neurons labelled by *R20G10∩dsx^{DBD}*.

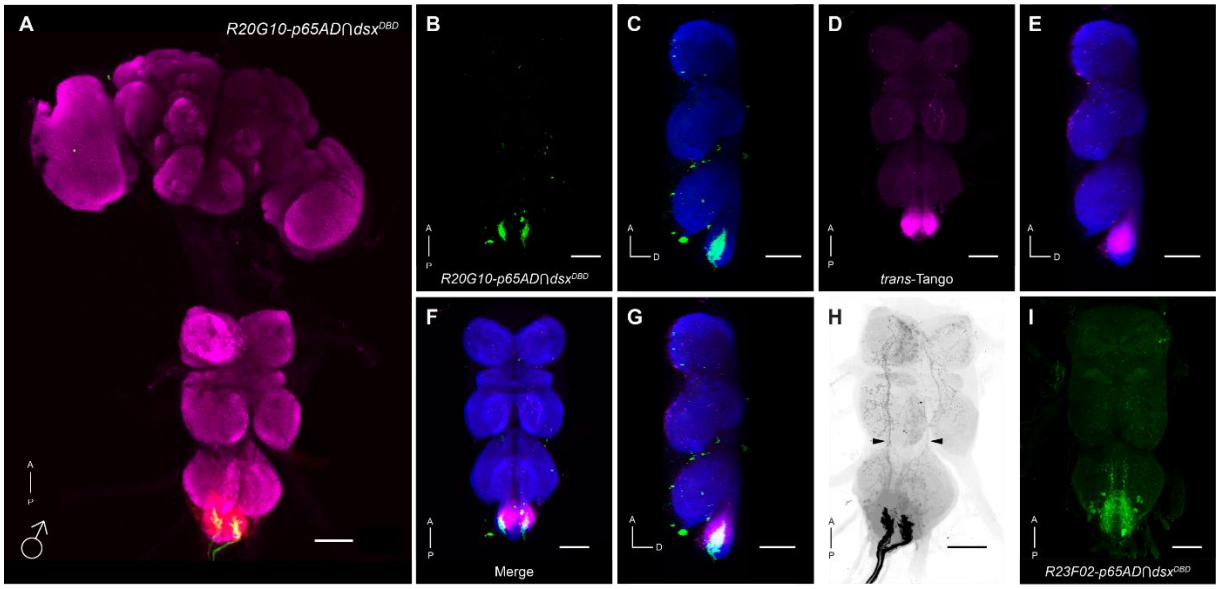

Figure 5-5: Postsynaptic partners of *R20G10-p65AD∩dsx^{DBD}* neurons.
(A) Whole-mount dissection of adult male CNS indicates that neurons postsynaptic to *R20G10-p65AD∩dsx^{DBD}* do not project into the brain but do form synaptic connections in the Abg. **(B-C)** Focusing on the VNS, the axonal arbors of surstylar MTS neurons project to a medial layer of the Abg where they connect to **(D&E)** postsynaptic partner cells in the Abg, labelled by trans-*Tango*. **(F-G)** Showing both colour channels (MTS neurons and their postsynaptic partners) shows a large interface between the two populations in the medial layer of the Abg. **(H)** Closer inspection of these postsynaptic cells reveals two anterior projections into the thoracic neuromeres and confirms the lack of projections in the cervical connective. **(I)** *R23F02-p65AD∩dsx^{DBD}* projections show some but not complete anatomical similarity to trans-*Tango* labelled cells in D&E. Scale bars are 50µm in all panels. A – Anterior, P – Posterior, D – Dorsal.

5.4.2 Postsynaptic partners of *R23F02-p65AD∩dsx^{DBD}* abdominal ganglion neurons

Combining *R23F02-p65AD∩dsx^{DBD}* with *trans*-Tango (Figure 5-6) reveals that *R23F02-p65AD∩dsx^{DBD}* neurons (Figure 5-6B&C) form synaptic contacts with a number of cells located in the abdominal ganglion (Figure 5-6D&E). No cell bodies could be identified in other regions of the nervous system. The majority of postsynaptic processes are contained within the abdominal ganglion, covering the depth of the neuropil (Figure 5-6E), although interestingly, two bilaterally symmetric processes pass through the centre of the VNS, cross the midline in the mesothoracic and prothoracic neuropils (Figure 5-6D, and white arrowheads in Figure 5-6F) and traverse the cervical connective into the brain where they form extensive ramifications into the antennal mechanosensory motor complex (AMMC), gnathal ganglion and periesophageal neuropils, with the AMMC in particular being known to incorporate both auditory and mechanosensory signals (Kamikouchi *et al*. 2006). In our hands we were only able to weakly label these projections, but closer inspection and staining of multiple animals has shown these projections to be bilaterally symmetrical.

As we did not see these projections to the central brain when examining the postsynaptic partners to *R20G10-p65AD∩dsx^{DBD}* neurons, it is clear that these projection neurons are not directly connected with surstylar bristle neurons. What is more likely, however, is that the postsynaptic cells of *R20G10-p65AD∩dsx^{DBD}* combine mechanosensory signals from multiple regions of the animals body, and these neurons (which may be a subset of *R23F02-p65AD∩dsx^{DBD}* although we cannot show this conclusively) then synapse onto 3rd-order neurons to project this information anteriorly.

Once these signals have reached the brain they can then inform descending motor control.

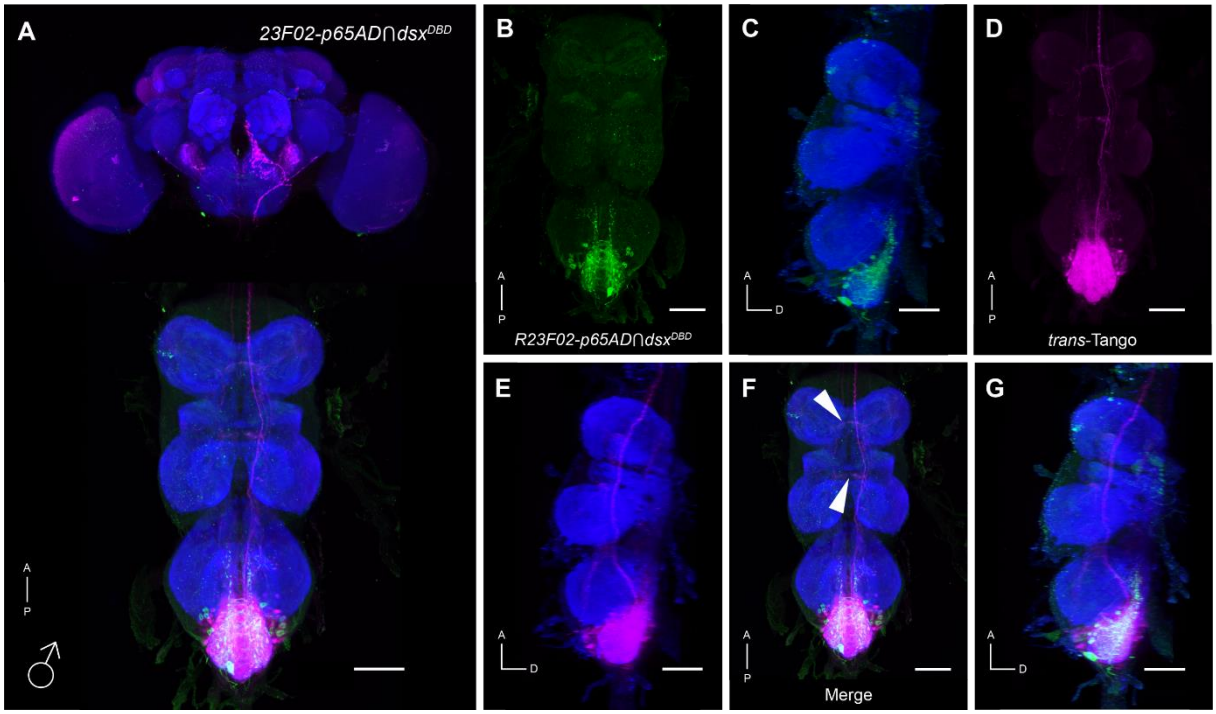

Figure 5-6: Postsynaptic partners of *R23F02-p65AD∩dsx^{DBD}* neurons
(A) Combining *R23F02-p65AD∩dsx^{DBD}* with *trans*-Tango reveals extensive postsynaptic labelling in the Abg and projections to the forebrain. **(B)** In the VNS, *R23F02-p65AD∩dsx^{DBD}* neurons have neurites extending throughout the Abg with the highest density of processes located slightly to the dorsal side. **(C)** Lateral view showing *R23F02-p65AD∩dsx^{DBD}* neurites. **(D&E)** The postsynaptic partners of *R23F02-p65AD∩dsx^{DBD}* neurons also have processes in all layers of the Abg, as well as projections that traverse the midline to the brain where they innervate the AMMC and periesophageal ganglia (shown in A). These projections cross the midline in the meso- and prothoracic neuromeres (**F**, white arrowheads). **(F&G)** Both channels imaged in a single animal show the overlap of *R23F02-p65AD∩dsx^{DBD}* neurons and their synaptic partners. Scale bars are 50µm in all panels. A – Anterior, P – Posterior, D – Dorsal.

5.5 Concluding remarks and future experiments

In this short chapter I have shown our experiments using calcium imaging to visualise the conditions under which MTS neurons are activated and to highlight possible synaptic connections between MTS neurons labelled by *R20G10-p65AD∩dsx^{DBD}* and abdominal ganglion interneurons labelled by *R23F02-p65AD∩dsx^{DBD}*. Following on

from these experiments, I used *trans*-Tango (Talay *et al*. 2017) to establish whether we could find further evidence to support a connection between these two populations, as well as to reveal their synaptic connections to all other neurons in an unbiased manner. Altogether, the outcome of these experiments, combined with our behavioural data suggests that whilst *R23F02-p65AD∩dsx^{DBD}* neurons do have an impact on mating behaviour and posture, and do receive input relating to the mechanical stimulation of the genitalia, the most likely situations are either that the two populations of cells are linked through an intermediate set of neurons, or that only a subset of *R23F02-p65AD∩dsx^{DBD}* neurons are connected directly with surstylar neurons. Whilst neural connectivity is often difficult to predict from anatomical data alone, and would require electron microscopy or more precise electrophysiology to show conclusively, the position of the neurites that are postsynaptic to *R20G10-p65AD∩dsx^{DBD}* do not extend as far to the dorsal side of the Abg as the projections of *R23F02-p65AD∩dsx^{DBD}.* Furthermore, our data showing that neurons postsynaptic to *R23F02-p65AD∩dsx^{DBD}* have processes that extend across all the thoracic neuromeres suggests that they collate mechanosensory information from multiple different regions of the flies body and then communicate that information to neurons which project to the brain, and in particular the AMMC. One possible set of experiments for future investigation might be to stimulate bristles on other regions of the fly and see whether they also elicit responses in *R23F02-p65AD∩dsx^{DBD}* neurons.

Lastly, in order to perform an experiment to more conclusively link the two populations, I cloned the *R23F02* sequence to make a set of *LexA* drivers to these neurons. This would enable us to drive CsChrimson in the surstylar neurons so that they can be activated for precise periods of time, whilst simultaneously recording GCaMP

fluoresecence in the Abg. Ultimately this may allow us to determine whether they are physiologically connected by looking at the timing of calcium transients in relation to the onset of the stimulus. It would also enable more thorough investigations into the physiological properties of the cells by, for example, applying a consistent stimulus and looking at the rate at which these neurons become sensitized to it, a trait which is common in mechanosensory neurons, particular in the auditory system. Unfortunately, these experiments were not completed in time to be included in this work and will be carried out in the future.

6 Summary Discussion

6.1 Investigative Summary

In this work I have aimed to quantify the contribution of mechanosensory bristles on the male genitalia, to copulation. This process began by carefully screening through a number of publicly available drivers and then, when needed, developing novel intersectional tools that provide genetic access to MTS neurons. Thus allowing me to precisely manipulate their function *in vivo.* Performing these manipulations during well-defined assays for *Drosophila* reproductive behaviour and examining the behavioural effects arising from the artificial activation or inhibition of these neurons, then enables us to tie the function of these bristles to a behavioural output. At the same time, they can be used in combination with neural imaging techniques to study the context in which the neurons are active and to identify downstream partners.

For my screening efforts, I focused particularly on lines that relate to genes with known roles in mechanosensation, as well as a handful of promotor fusion lines from the 'FlyLight' GMR collection (Jenett *et al*. 2012; Pfeiffer *et al*. 2008).

Interestingly, despite the longstanding belief that these bristles are mechanosensory, we identified that only a proportion of the bristles adorning the male genitalia express *dsx* and a mechanosensory ion channel such as *nompC.* This leads to the question of whether all of the bristles on the male genitalia are in fact sensory at all. Previous studies have shown that whilst *Pox neuro* (*Poxn*) - a marker for chemosensory neurons - does have some influence on the morphology of the surstyli and epandrial lobes, there is no labelling of bristle neurons, suggesting that they are also not innervated by chemosensory neurons (Boll and Noll 2002). Using a pan-neuronal marker like *elav-GAL4* or *nSyb-GAL4* will ultimately allow us to confidently say whether those bristles

which do not appear to have a *dsx* or mechanosensory-positive neuron associated with them, are innervated or not.

In many cases the lines which were initially screened and found to express in MTS neurons were too broad for use in behavioural experiments. Therefore, with some lines, most importantly with *nompC,* I utilised the Trojan-MiMIC system (Venken *et al*. 2011) to insert a transcriptional and translational trap into an intronic region of the gene, thereby allowing me to faithfully recapitulate it's expression. I then intersected *nompC^{MI12787}* against the expression of another novel line; *R94D09^{DBD}* to enable the directed expression of transgenes under UAS control to MTS neurons, with little labelling outside of the genitalia.

R94D09^{DBD} was developed by cloning the existing *R94D09* element and combining it into a p65AD vector, before reinserting it back into the same genomic position using recombinase-mediated cassette exchange. This combination, as well as two promotor fusion lines; *R20G10,* derived from *nicotinic Acetylcholine Receptor α3* (*nAChRα3*), and *R23F02,* derived from ~1kb of sequence at the 3' end of *CG13229* (a 7-transmembrane GPCR) form the basis of the lines which I then manipulated in behavioural assays when combined with *dsx^{DBD}* (Pavlou *et al*. 2016).

The artificial activation of MTS neurons (*R94D09^{DBD}∩nompC^{MI12787}* and *R20G10-p65AD∩dsx^{DBD}* driver combinations) using CsChrimson (Klapoetke *et al*. 2014), and their artificial inhibition using tetanus toxin or *shibire^{ts}* (Kitamoto 2001; Sweeney *et al*. 1995) highlights how these sensory bristles are important for both the initiation of genital coupling and mating posture. This was shown by both the proportion of males which copulated, the time to copulation, and the consistent movement of the male outside of a typical 'delta wing' position during copulation. We identified little or no

demonstrable effects on other metrics for *Drosophila* courtship like CI, or the duration of copulation, when manipulating the action of these neurons.

Conversely, performing these same manipulations on a population of abdominal ganglion interneurons labelled by the promotor fusion line *R23F02,* also influenced the rate of mating and the posture of the male during copulation. Interestingly, though, when activating these neurons, the duration of copulation was significantly increased, suggesting that these neurons link to motor neurons controlling the detachment of the genitalia, or alternatively, to an internal 'clock' mechanism that controls the timing of copulatory bouts.

Following on from behavioural experiments, I used the same lines to drive expression of the calcium reporter GCaMP6s (Chen *et al*. 2013) in both MTS neurons (*R20G10-p65AD∩dsx^{DBD}*) and the abdominal ganglion neurons labelled by *R23F02-p65AD∩dsx^{DBD}.* Our data showing the responsiveness of both of these populations to mechanical stimulation is the most precise assessment of the sensory nature of genital bristles that we are aware of, and highlights the potential that *R23F02-p65AD∩dsx^{DBD}* neurons receive inputs from the periphery. Lastly, using the *trans*-Tango system to identify the synaptic partners of both *R20G10* and *R23F02* populations, we have shown that surstylar bristle neurons form extensive synaptic contacts with a large number of cells in the Abg. Closer inspection of these postsynaptic cells reveals that although some of these neurons may be the same as those labelled by *R23F02-p65AD∩dsx^{DBD},* it is likely that only a subset of the total *R23F02* population is directly connected to MTS neurons originating from the surstyli, as the position of *trans*-Tango labelled neurites is markedly different (although slightly overlapping) to *R23F02-p65AD∩dsx^{DBD}* neurites in the Abg. Furthermore, *trans*-Tango labels postsynaptic

neurons that send projections into the more anterior neuromeres, potentially to receive input from motor neurons innervating the legs, wings, and halteres. These projections are not visible when looking at *R23F02-p65AD∩dsx^{DBD}* neurons alone.

Lastly, viewing the synaptic partners of *R23F02-p65AD∩dsx^{DBD}* neurons, revealed two interesting facts. Firstly, these neurons contact a large number of cells locally in the Abg, although it is difficult to accurately count the number of postsynaptic neurons due to the strength of the RFP reporter. Perhaps more importantly, however, two bilaterally symmetric projections are seen ascending from the Abg to the AMMC in the forebrain, thus indicating that at least some signals received by *R23F02-p65AD∩dsx^{DBD}* neurons have the potential to be incorporated into higher-processing centres that receive mechanosensory signals from multiple regions of the fly. These findings are summarised in the simplified circuit diagram are shown in Figure 6-1.

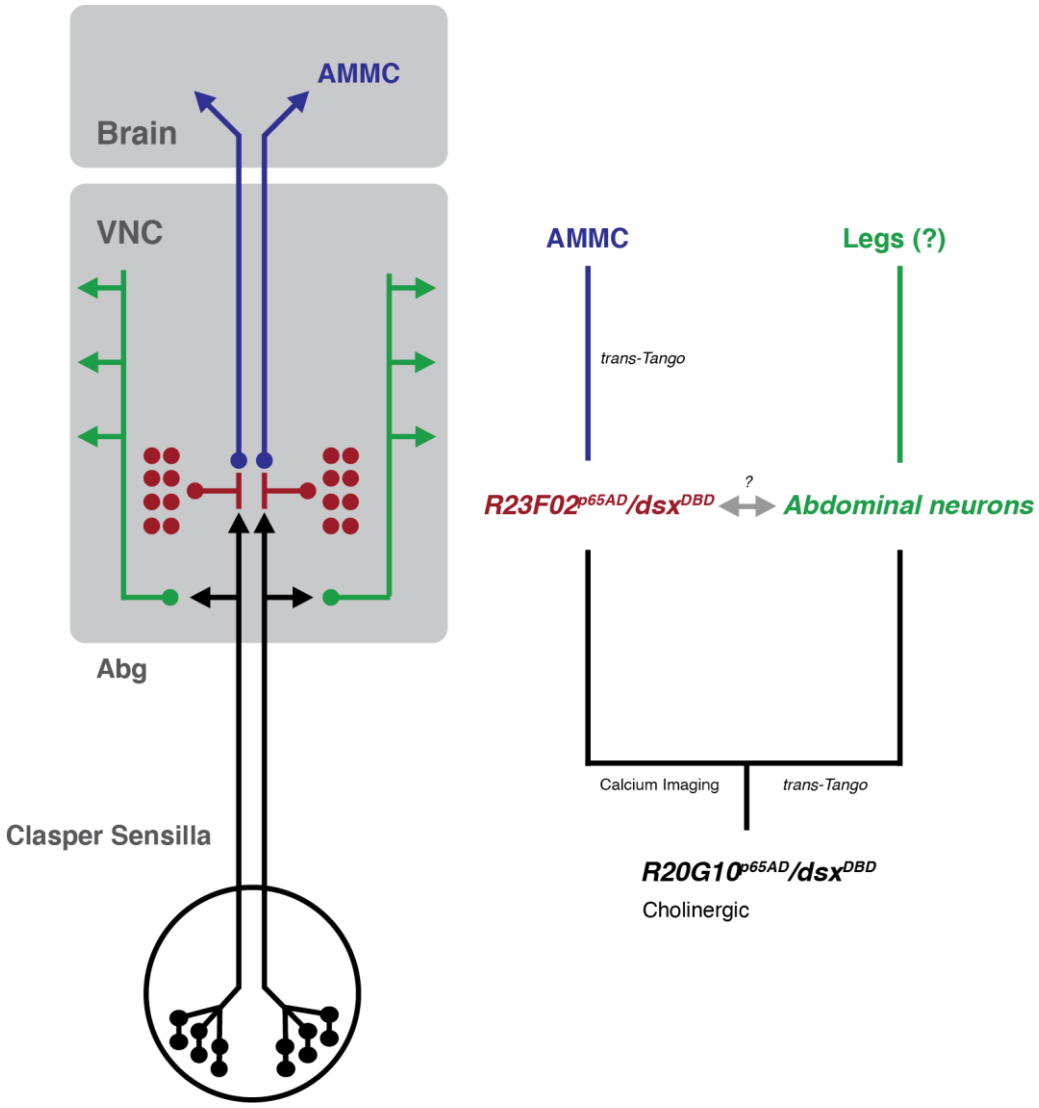

Figure 6-1: Putative circuit diagram linking MTS neurons to downstream elements.
Six surstylar bristle neurons per side labelled by *R20G10-p65AD∩dsx^{DBD}* (black) have been shown to pass mechanical stimuli to *R23F02-p65AD∩dsx^{DBD}* cells (red) in the Abg via calcium imaging. These MTS neurons are also directly connected with neurons that innervate the other thoracic neuromeres and potentially receive input from leg mechanoreceptors (green). We are unable to confirm whether *R20G10* and *R23F02* are directly connected, but trans-*Tango* labelling confirms that *R23F02-p65AD∩dsx^{DBD}* cells do synapse onto a population of neurons in the Abg, some of which project to the AMMC in the forebrain. Whilst the polarity of some of these neurons is unclear, this circuit can enable the coordination of motor signals between the periphery, different limbs, and likely also send information regarding the activity of the circuit to the forebrain where it may be influenced by, or alter the animals internal state.

Altogether, this behavioural and anatomical investigation into the role of MTS neurons in *Drosophila* reproductive behaviour has highlighted many new avenues to better understand how sensory signals from the periphery are utilised for adaptive motor control. We have shown, using targeted genetic tools for the first time, how these

sensory bristles influence attempted copulation and copulation itself, the likelihood of successful reproduction, their sensitivity to mechanical stimuli, and ultimately how these signals might signal to downstream neurons to inform motor programs elsewhere in the animal.

6.2 Future Experiments

Looking forward, a handful of important next experiments are required for this project. As a first step, examining the expression of a pan-neuronal marker like *elav-GAL4* or *nSyb-GAL4*, would provide concrete evidence to support or disprove the idea that not all genital bristles are innervated. Another straightforward next step, requiring a few genetic crosses, would be to reduce the transcript levels of genes such as *nompC* and *ChAT* in MTS neurons using RNAi. Should these genes be required for the proper function of MTS neurons as we expect, then a behavioural phenotype akin to those we have reported using *UAS-shibire^{ts}* should be found. This process will not only confirm our findings that MTS neurons express these genes, but may also provide an insight into whether it is one channel alone, or perhaps multiple channels working in concert, that are required for the proper maintenance of body position. Several RNAi stocks are available for *nompC* in particular from the Transgenic RNAi Project (TRiP) and have already be shown to effectively knock down transcripts in live animals (e.g. Turner *et al*. 2016)

The reagents outlined and developed in this thesis also create several new avenues of research. For example, whilst we have shown that the majority of MTS neurons are cholinergic, it is not clear what neurotransmitter the cells labelled by *R23F02-*

p65AD⁀dsx^{DBD} use for signaling. *R23F02-p65AD,* or the novel *R23F02-LexA* developed at the end of this work (see section 7.4.9) can be used in combination with a number of neurotransmitter specific hemidrivers to identify neurotransmitter expression in this population, and any potential heterogeneity therein.

Whilst annotation of *CG13229* (from which *R23F02* is derived) is currently limited, the protein shows similarity to class A G-protein coupled receptors, which bind to several neuropeptides with known roles in *Drosophila* arousal and sexual behaviour. Including, for example, sex-peptide (Kubli 1996; Yapici *et al*. 2008) and corazonin (Hou *et al*. 2018; Zer-Krispil *et al*. 2018).

Currently, *CG13229* is considered an 'orphan receptor' and its' ligand is unknown, although it shares strong sequence homology with both *Myosuppressin receptor 1* and *2* (Hewes and Taghert 2001; Yapici *et al*. 2008) which have the primary roles of controlling neurotransmitter release in motor neurons and negatively regulating muscle contraction, respectively. Identifying the ligand(s) of *CG13229* could provide insights into how this circuit is modulated by the action of neuropeptides when the animal is attempting to mate, and the *R23F02-LexA* we have developed could prove invaluable for imaging these neurons under exposure to various neuropeptides.

Interestingly, Looking at the single-cell data for the adult Drosophila VNS developed in our lab (Allen *et al*. 2019), we can see that *CG13229* colocalizes with a small number of cells expressing the vesicular monoamine transporter *Vmat*, and some serotonergic neurons as marked by the expression of *Tryptophan hydroxylase* (*Trh*). Furthermore, it is a marker for a handful of neuronal clusters in the VNS. Amongst these, cluster 84 is a peptidergic cluster which shows high expression levels of several neuropeptides and their precursors, including (but not limited to) *Leucokinin, FMRFamide, Pigment-*

dispersing factor (Pdf), and *proctolin.* These, alongside *Myosuppressin* would be excellent candidates for studies looking at the sensitivity of *R23F02-p65AD∩dsx*^{DBD} cells and general mating posture when exposed to neuropeptides.

The functions of neuropeptides expressed in this cluster are numerous, but intriguingly, *proctolin* has been shown to modulate the sensitivity of motorneurons to fast-acting neurotransmitters (Anderson *et al*. 1988), whilst *pdf* expression in the brain has been shown to regulate the duration of mating depending on the presence of a rival male (Kim *et al*. 2013). Whilst this information from the single cell atlas requires further testing and verification, it highlights the possibility that *R23F02-p65AD∩dsx*^{DBD} neurons release neuropeptides on the basis of both the internal state of the animal and/or the sensory input they receive from the periphery. This may allow a higher degree of sensitivity within motor neurons required for genital attachment and detachment. The presence of the *CG13229* GPCR on *R23F02-p65AD∩dsx*^{DBD} neurons themselves may enable these neurons to respond to their own neuropeptide release in a closed feedback loop.

In some cases, it should be possible to overexpress or reduce the level of these neuropeptides in *R23F02-p65AD∩dsx*^{DBD} neurons to assay the effect on reproductive behaviour. To this end, the reagents I have discussed or developed in this thesis provide an excellent means to target transgenes for manipulating expression levels to these neurons.

R23F02-LexA can also be used in a complex intersectional strategy using *R20G10-p65AD, R23F02-p65AD, dsxDBD, dsxFLP, UAS-CsChrimson* and a flippable GCaMP (e.g. *LexAop>stop>GCaMP6s*) to precisely control the activation of surstylar MTS neurons with optogenetics, whilst recording calcium transients in the Abg. The ability that this experimental setup provides to temporally control the stimulus will allow us to

better determine the connectivity between *R23F02* and *R20G10* neurons, as well as establish the rate at which MTS neurons adapt to a controlled stimulus – a hallmark of mechanosensory neurons in multiple phyla. In studies of tactile hairs in other insect species, two types are present: rapidly and slowly adapting. In comparison, recordings from bristles on the notum of *Drosophila* as well as the head of blowflies have thus far only identified slowly adapting bristles (Chadha and Cook 2012; Corfas and Dudai 1990; Theis 1979).

As a final point, if someone were to expand the 'genetic toolkit' for targeting MTS neurons, then the data I have presented points towards a handful of extremely promising candidates. An *Abdominal-B* split-Gal4 line would be highly useful when combined with *nompC*^{MI12787} and could potentially label all surstylar bristles as opposed to the subset which is labelled by *R20G10-p65AD∩dsx*^{DBD}. Alternatively, the opportunities that an *AbdB*^{DBD} line would provide to intersect neurons in the abdominal ganglion are extensive, as *AbdB* is near exclusively expressed in the abdominal ganglion.

Altogether, the results from this thesis as well as the further experiments I have recommended here can be combined to tell a compelling story about the requirement of sensory feedback for *Drosophila* copulation, and to help build our understanding of the component properties and underlying neural substrates of such circuits.

7 Materials and methods

7.1 Fly husbandry

Several methods for raising *Drosophila* stocks were used in this thesis depending on the experiments being undertaken. Regardless of all other variables, fly stocks were kept on a 12h:12h light:dark cycle. Stocks raised for activation experiments in chapter 4 were kept covered with a box to reduce exposure to ambient light, but were still moderately illuminated during 'lights on'. Unless mentioned specifically, flies were kept at 25°C and ~50% relative humidity.

Collection of flies was performed under CO_2 anaesthetic at room temperature with a paintbrush and stereomicroscope.

Three types of fly food were used. Their compositions are as follows:

Yellow food – The primary food media for flies reared for experiments in chapters 2 and 3, inactivation experiments in chapter 4 and calcium imaging experiments in chapter 5.

This food contains (per litre): H_2O; 1L, Agar; 7.9g, Yeast; 27.5g, Cornmeal; 52g, Dextrose; 110g, Ethanol; 9.2ml, Tegosept; 2.4g.

Brown food - A more nutrient dense media, which was used for the longer-term storage of stocks at ~18°C. Contains (per litre): H_2O; 1L, Agar; 6.75g, Yeast; 25g, Cornmeal; 62.5g, Molasses; 0.0375 litres, Acid; 4.2ml, Ethanol; 7ml, Tegosept; 1.4g.

This media was also used to rear flies used in *trans-Tango* experiments (chapter 5). They were crossed and reared on this more dense media as it is better suited to being kept at ~18°C. This lower rearing temperature has long been known to reduce the lethality associated with driving high levels of *trans-Tango* transgenes and preventing 'leaky' ectopic expression (Talay *et al*. 2017).

When retrieving stock strains from the 18°C storage area for use in experiments, these flies were always kept for a minimum of one generation in the 25°C Environmentally Controlled Room (ECR) before collecting the virgin flies for genetic crosses.

Retinal food – The primary food source for flies used in activation experiments in chapter 4. Contains all the same components as yellow food with the addition of a 100mM stock of *All-trans-retinal* diluted 1:100 in fresh food. These are then poured into vials, allowed to set, and used for rearing.

7.1.1 Wild-type strain

The wild-type strain used and referred to in this work was Canton-Special (Canton-S; CS). Virgin females used in behavioural experiments were *CantonS* raised on standard yellow food at 25°C.

7.1.2 Drosophila melanogaster stocks

A description of all the *Drosophila melanogaster* stocks used in the course of this work are described in Table 7-1. The stocks genotype, source and a short description are provided for each. A full description of all mutations and balancer chromosomes used can be found in FlyBase (http://www.flybase.org).

Table 7-1: Drosophila stocks used in this study
"*w**" and "*y**" indicates that the precise allele of *w* or *y* is unknown.

Strain/Genotype	Description	Reference
Isogenised Strains		
Canton-Special (Canton-S; CS)	Isogenic 'wild-type' strain	Flybase.
Balancer Chromosome Strains		
w;if/CyO;Sb/TM3, Ser*	Isogenised to CS, provides a balancer for 2nd and 3rd chromosomes as well as visible markers for the non-balancer chromsome	Flybase.
+;+;TM3, Sb, Ser/TM6B, Tb, Hu, e	Isogenised to CS. Third Multiple series of chromosome balancers (TM). *TM3* with dominant markers *Sb* and *Ser*, and *TM6B* with dominant markers *Tb, Hu, e*.	Flybase.
w+;ES/CyO,TM3, Sb	Isogenised to CS. A fused second and third chromosome opposed by the 2nd chromosome balancer *CyO* and 3rd	Flybase.

	chromosome balancer *TM3, Sb*. Ensures that within a genetic cross, either both, or neither chromosomes will be balanced in the offspring	
w;wg^{Sp-1}/CyO;Dr/TM3, Sb*	Balancer chromosomes for 2nd and 3rd (*CyO* and *TM3, Sb)* accompanied by the visible genetic markers *wg^{Sp-1} (sternopleural*) and *Drop* on the homologous chromosome.	
GAL4, Split-GAL4 and LexA drivers		
y^{1}w;PBac{nompC-GAL4.P}VK00014*	Isogenised to CS from parental strain *y^{1}w*;PBac{nompC-GAL4.P}VK00014;Df(3L)Ly, sensLy-1/TM6C, Sb*	Cheng *et al*. (2010)
w;+;P{Piezo-GAL4.1.0}III*	1kb promoter fusion from *Piezo* cloned into pPTGAL vector.	Kim *et al*. (2012)
w;P{nan-GAL4.K}2;+*	1kb promoter fusion cloned from *nanchung.* May be segregating *CyO* and/or *TM6B.*	Kim *et al*. (2003)
w;P{w[+mC]=ppk-GAL4.G}2;+*	Replacement of *ppk-eGFP* (Grueber *et al*. 2003) with GAL4.	Grueber *et al*. (2007)
w;P{iav-GAL4.K}3*	~3kb promoter fusion of sequence cloned from 5' end of *iav*.	Kwon *et al*. (2010)

w;ChAT-T2A-GAL4/Tm6B*	GAL4 coding sequence fused with *ChAT* via T2A viral peptide	(Diao and White 2012)
w;+;dsx$^{GAL4\text{-}DBD}$/TM3, Sb, Ser*	GAL4 DNA-binding domain element inserted into *doublesex* locus via ends-in HR.	(Pavlou *et al*. 2016)
w;+;Pw[+mC]=elav-VP16.AD}G3A1*	VP16 transactivation domain-leucine zipper fusion for split-GAL4. Driven under the control of the *elav* promoter. Located on the 3rd chromosome.	(Luan *et al*. 2006)
fru^{GAL4}/TM3, Sb, Ser	GAL4 knock-in at the *fru* locus by homologous recombination. Labels all *fruitless*-expressing neurons.	(Stockinger *et al*. 2005)
y^{1}w*;P{GawB}Abd-B^{LDN}/TM6B, Tb	P-*lacZ* replacement to P-*Gal4* inserted into *Abd-B* locus on the third chromosome.	(de Navas *et al*. 2006)
w^{1118};P{y[+t7.7] w[+mC]=GMR94D09-GAL4}attP2	Expresses GAL4 under the control of DNA near *engrailed.*	(Jenett *et al*. 2012)
w^{1118};P{y[+t7.7]w[+mC]=R20G10-p65.AD}attP40	Expresses the p65 activation domain under control of sequences in/near *nAChRalpha3*.	(Dionne *et al*. 2018)
w^{1118};P{y[+t7.7]w[+mC]=R23F02-p65.AD}attP40	Expresses the p65 activation domain under control of sequences in/near *CG13229*.	(Dionne *et al*. 2018)
***dsx* promoter fusions (section 2.5.3)**		

w^{1118}; P{y[+t7.7] w[+mC]=GMR40F04-GAL4}attP2	Fragment of *dsx* genomic DNA fused with *Drosophila* synthetic core promoter and GAL4. Sequence location: 3R:7,970,268..7,973,286	(Jenett *et al*. 2012)
w^{1118}; P{y[+t7.7] w[+mC]=GMR42B01-p65.AD}attP40	Fragment of *dsx* genomic DNA fused with *Drosophila* synthetic core promoter and GAL4. Sequence location: 3R:7,967,735..7,971,550	(Jenett *et al*. 2012)
w^{1118}; P{y[+t7.7] w[+mC]=GMR42C06-GAL4}attP2	Fragment of *dsx* genomic DNA fused with *Drosophila* synthetic core promoter and GAL4. Sequence location: 3R:7,962,625..7,966,507	(Jenett *et al*. 2012)
w^{1118}; P{y[+t7.7] w[+mC]=GMR39E06-GAL4}attP2	Fragment of *dsx* genomic DNA fused with *Drosophila* synthetic core promoter and GAL4. Sequence location: 3R:7,960,790..7,962,578	(Jenett *et al*. 2012)
w^{1118}; P{y[+t7.7] w[+mC]=GMR40F03-GAL4}attP2	Fragment of *dsx* genomic DNA fused with *Drosophila* synthetic core promoter and GAL4. Sequence location: 3R:7,956,762..7,959,777	(Jenett *et al*. 2012)

w^{1118}; P{y[+t7.7] w[+mC]=GMR42D04-GAL4}attP2	Fragment of *dsx* genomic DNA fused with *Drosophila* synthetic core promoter and GAL4. Sequence location: 3R:7,953,942..7,957,854	(Jenett *et al*. 2012)
w^{1118}; P{y[+t7.7] w[+mC]=GMR41A01-GAL4}attP2	Fragment of *dsx* genomic DNA fused with *Drosophila* synthetic core promoter and GAL4. Sequence location: 3R:7,951,729..7,954,994	(Jenett *et al*. 2012)
w^{1118}; P{y[+t7.7] w[+mC]=GMR42A11-GAL4}attP2	Fragment of *dsx* genomic DNA fused with *Drosophila* synthetic core promoter and GAL4. Sequence location: 3R:7,949,001..7,952,795	(Jenett *et al*. 2012)
w^{1118}; P{y[+t7.7] w[+mC]=GMR68D03-GAL4}attP2	Fragment of *dsx* genomic DNA fused with *Drosophila* synthetic core promoter and GAL4. Sequence location: 3R:7,946,411..7,949,735	(Jenett *et al*. 2012)
w^{1118}; P{y[+t7.7] w[+mC]=GMR41F06-GAL4}attP2	Fragment of *dsx* genomic DNA fused with *Drosophila* synthetic core promoter and GAL4. Sequence location: 3R:7,944,266..7,947,896	(Jenett *et al*. 2012)

w^{1118}; P{y[+t7.7] w[+mC]=GMR42D02-GAL4}attP2	Fragment of *dsx* genomic DNA fused with *Drosophila* synthetic core promoter and GAL4. Sequence location: 3R:7,941,579..7,945,482	(Jenett *et al*. 2012)
w^{1118}; P{y[+t7.7] w[+mC]=GMR41D01-GAL4}attP2	Fragment of *dsx* genomic DNA fused with *Drosophila* synthetic core promoter and GAL4. Sequence location: 3R:7,938,919..7,942,427	(Jenett *et al*. 2012)
w^{1118}; P{y[+t7.7] w[+mC]=GMR42G02-lexA}attP40	Fragment of *dsx* genomic DNA fused with *Drosophila* synthetic core promoter and GAL4. Sequence location: 3R:7,930,618..7,934,708	(Jenett *et al*. 2012)
w^{1118}; P{y[+t7.7] w[+mC]=GMR40A05-GAL4}attP2	Fragment of *dsx* genomic DNA fused with *Drosophila* synthetic core promoter and GAL4. Sequence location: 3R:7,925,287..7,927,810	(Jenett *et al*. 2012)
Genital disc drivers (section 2.5.6)		
w^{1118}; P{y[+t7.7] w[+mC]=GMR73E12-GAL4}attP2	Fragment of α2-adrenergic-like octopamine receptor (Octα2R) genomic DNA fused with Drosophila synthetic core promoter and GAL4.	Jory *et al*. (2012)

	Sequence location: 3R:18,836,917..18,840,614	
w[1118]; P{y[+t7.7] w[+mC]=GMR93D05-GAL4}attP2	Fragment of beaten path Vc (beat-Vc) genomic DNA fused with Drosophila synthetic core promoter and GAL4. Sequence location: 3R:18,836,917..18,840,614	Jory *et al*. (2012)
w[1118]; P{y[+t7.7] w[+mC]=GMR92B02-GAL4}attP2	Fragment of beaten path Ic (beat-Ic) genomic DNA fused with Drosophila synthetic core promoter and GAL4. Sequence location: 2L:15,986,889..15,989,682	Jory *et al*. (2012)
w[1118]; P{y[+t7.7] w[+mC]=GMR89C10-GAL4}attP2	Fragment of beaten path VI (beat-VI) genomic DNA fused with Drosophila synthetic core promoter and GAL4. Sequence location: 3R:28,411,043..28,414,785	Jory *et al*. (2012)
w[1118]; P{y[+t7.7] w[+mC]=GMR83B11-GAL4}attP2	Fragment of Grunge (Gug) genomic DNA fused with Drosophila synthetic core promoter and GAL4. Sequence location: 3L:8,458,842..8,462,019	Jory *et al*. (2012)

w[1118]; P{y[+t7.7] w[+mC]=GMR65H10-GAL4}attP2	Fragment of Tachykinin-like receptor at 99D (TkR99D) genomic DNA fused with Drosophila synthetic core promoter and GAL4. Sequence location: 3R:29,955,189..29,956,568	Jory *et al*. (2012)
w[1118]; P{y[+t7.7] w[+mC]=GMR91G02-GAL4}attP2	Fragment of sidestep VIII (side-VIII) genomic DNA fused with Drosophila synthetic core promoter and GAL4. Sequence location: 2R:20,434,312..20,437,234	Jory *et al*. (2012)
w[1118]; P{y[+t7.7] w[+mC]=GMR73E11-GAL4}attP2	Fragment of α2-adrenergic-like octopamine receptor (Octα2R) genomic DNA fused with Drosophila synthetic core promoter and GAL4. Sequence location: 3R:18,840,008..18,843,750	Jory *et al*. (2012)
w[1118]; P{y[+t7.7] w[+mC]=GMR75D08-GAL4}attP2/TM3, Sb[1]	Fragment of *abrupt (ab)* genomic DNA fused with Drosophila synthetic core promoter and GAL4. Sequence location: 2L:11,219,699..11,223,184	Jory *et al*. (2012)
w[1118]; P{y[+t7.7] w[+mC]=GMR78A08-GAL4}attP2	Fragment of CG31859 genomic DNA fused with Drosophila	Jory *et al*. (2012)

	synthetic core promoter and GAL4. Sequence location: 2L:12,594,708..12,598,170	
w[1118]; P{y[+t7.7] w[+mC]=GMR92H09-GAL4}attP2	Fragment of beaten path Ia (beat-Ia) genomic DNA fused with Drosophila synthetic core promoter and GAL4. Sequence location: 2L:16,056,306..16,059,249	Jory *et al*. (2012)
w[1118]; P{y[+t7.7] w[+mC]=GMR87A08-GAL4}attP2	Fragment of Ecdysone-induced protein 93F (Eip93F) genomic DNA fused with Drosophila synthetic core promoter and GAL4. Sequence location: 3R:21,926,730..21,929,966	Jory *et al*. (2012)
w[1118]; P{y[+t7.7] w[+mC]=GMR81E09-GAL4}attP2	Fragment of BarH1 (B-H1) genomic DNA fused with Drosophila synthetic core promoter and GAL4. Sequence location: X:17,352,542..17,354,699	Jory *et al*. (2012)
w[1118]; P{y[+t7.7] w[+mC]=GMR64H02-GAL4}attP2	Fragment of *CASK* genomic DNA fused with Drosophila synthetic core promoter and GAL4.	Jory *et al*. (2012)

	Sequence location: 3R:21,823,529..21,827,443	
w[1118]; P{y[+t7.7] w[+mC]=GMR85E08-GAL4}attP2/TM3, Sb[1]	Fragment of *spalt major (salm)* genomic DNA fused with Drosophila synthetic core promoter and GAL4. Sequence location: 2L:11,453,242..11,457,101	Jory *et al*. (2012)
w[1118]; P{y[+t7.7] w[+mC]=GMR87C08-GAL4}attP2	Fragment of *spalt-related (salr)* genomic DNA fused with Drosophila synthetic core promoter and GAL4. Sequence location: 2L:11,394,036..11,397,012	Jory *et al*. (2012)
w[1118]; P{y[+t7.7] w[+mC]=GMR88C11-GAL4}attP2	Fragment of *CG11247* genomic DNA fused with Drosophila synthetic core promoter and GAL4. Sequence location: 3L:21,721,026..21,724,164	Jory *et al*. (2012)
w[1118]; P{y[+t7.7] w[+mC]=GMR64G06-GAL4}attP2	Fragment of *short neuropeptide F receptor (sNPF-R)* genomic DNA fused with Drosophila synthetic core promoter and GAL4. Sequence location: 3L:20,089,637..20,093,425	Jory *et al*. (2012)

w[1118]; P{y[+t7.7] w[+mC]=GMR88E08-GAL4}attP2	Fragment of *empty spiracles (ems)* genomic DNA fused with Drosophila synthetic core promoter and GAL4. Sequence location: 3R:13,914,726..13,917,774	Jory *et al*. (2012)
w[1118]; P{y[+t7.7] w[+mC]=GMR81H03-GAL4}attP2	Fragment of *NFAT nuclear factor (NFAT)* genomic DNA fused with Drosophila synthetic core promoter and GAL4. Sequence location: X:13,634,466..13,636,954	Jory *et al*. (2012)
w[1118]; P{y[+t7.7] w[+mC]=GMR38A10-GAL4}attP2	Fragment of *rhomboid (rho)* genomic DNA fused with Drosophila synthetic core promoter and GAL4. Sequence location: 3L:1,440,657..1,443,795	Jory *et al*. (2012)
w[1118]; P{y[+t7.7] w[+mC]=GMR84B06-GAL4}attP2/TM3, Sb[1]	Fragment of *Ionotropic receptor 68a (Ir68a)* genomic DNA fused with Drosophila synthetic core promoter and GAL4. Sequence location: 3L:11,236,599..11,240,241	Jory *et al*. (2012)
w[1118]; P{y[+t7.7] w[+mC]=GMR16F09-GAL4}attP2	Fragment of *no ocelli (noc)* genomic DNA fused with Drosophila synthetic core promoter and GAL4.	Jory *et al*. (2012)

	Sequence location: 2L:14,451,817..14,454,838	
w[1118]; P{y[+t7.7] w[+mC]=GMR15E10-GAL4}attP2	Fragment of *sine oculis (so)* genomic DNA fused with Drosophila synthetic core promoter and GAL4. Sequence location: 2R:7,426,193..7,430,128	Jory *et al*. (2012)
w[1118]; P{y[+t7.7] w[+mC]=GMR78D09-GAL4}attP2	Fragment of *CG34355* genomic DNA fused with Drosophila synthetic core promoter and GAL4. Sequence location: 3R:23,844,783..23,845,038	Jory *et al*. (2012)
w[1118]; P{y[+t7.7] w[+mC]=GMR37H08-GAL4}attP2	Fragment of *Sarcoplasmic calcium-binding protein 2 (Scp2)* genomic DNA fused with Drosophila synthetic core promoter and GAL4. Sequence location: 3R:16,580,830..16,583,627	Jory *et al*. (2012)
w[1118]; P{y[+t7.7] w[+mC]=GMR84G01-GAL4}attP2	Fragment of *spalt-related (salr)* genomic DNA fused with Drosophila synthetic core promoter and GAL4. Sequence location: 2L:11,359,028..11,361,047	Jory *et al*. (2012)

w[1118]; P{y[+t7.7] w[+mC]=GMR38F06-GAL4}attP2	Fragment of *Protein tyrosine phosphatase 61F (Ptp61F)* genomic DNA fused with Drosophila synthetic core promoter and GAL4. Sequence location: 3L:1,443,158..1,446,973	Jory *et al*. (2012)
w[1118]; P{y[+t7.7] w[+mC]=GMR88G08-GAL4}attP2	Fragment of *empty spiracles (ems)* genomic DNA fused with Drosophila synthetic core promoter and GAL4. Sequence location: 3R:13,929,027..13,932,185	Jory *et al*. (2012)
w[1118]; P{y[+t7.7] w[+mC]=GMR87B02-GAL4}attP2	Fragment of *Ecdysone-induced protein 93F (Eip93F)* genomic DNA fused with Drosophila synthetic core promoter and GAL4. Sequence location: 3R:21,924,542..21,927,724	Jory *et al*. (2012)
w[1118]; P{y[+t7.7] w[+mC]=GMR89C03-GAL4}attP2	Fragment of *beaten path VI (beat-VI)* genomic DNA fused with Drosophila synthetic core promoter and GAL4. Sequence location: 3R:28,423,343..28,426,466	Jory *et al*. (2012)
w[1118]; P{y[+t7.7] w[+mC]=GMR94A10-GAL4}attP2	Fragment of *CG46339* genomic DNA fused with Drosophila	Jory *et al*. (2012)

	synthetic core promoter and GAL4. Sequence location: 3R:26,921,815..26,924,674	
w[1118]; P{y[+t7.7] w[+mC]=GMR81D03-GAL4}attP2	Fragment of *BarH1 (B-H1)* genomic DNA fused with Drosophila synthetic core promoter and GAL4. Sequence location: X:17,339,489..17,342,836	Jory *et al*. (2012)
w[1118]; P{y[+t7.7] w[+mC]=GMR89B01-GAL4}attP2	Fragment of *beaten path VI (beat-VI)* genomic DNA fused with Drosophila synthetic core promoter and GAL4. Sequence location: 3R:28,398,360..28,402,016	Jory *et al*. (2012)
Trojan-MiMIC insertion lines		
y[1]w[*];Mi{y[+mDint2]=MIC}nompC[MI12787]/SM6A	MiMIC insertion site located within an intron of *nompC.* Can be targeted for replacement via RMCE.	(Nagarkar-Jaiswal *et al*. 2015)
y[1]w[*];Mi{y[+mDint2]=MIC}nompC[MI03523]	MiMIC insertion site located within an intron of *nompC.* Can be targeted for replacement via RMCE. May be segregating SM6A	(Nagarkar-Jaiswal *et al*. 2015)

y^{1}w*;Mi{y[+mDint2]=MIC}Piezo^{MI04294}	MiMIC insertion site located within an intron of *Piezo.* Can be targeted for replacement via RMCE. May be segregating SM6A	(Nagarkar-Jaiswal *et al*. 2015)
y^{1}w*;Mi{y[+mDint2]=MIC}Piezo^{MI04189}	MiMIC insertion site located within an intron of *Piezo.* Can be targeted for replacement via RMCE. May be segregating SM6A	(Nagarkar-Jaiswal *et al*. 2015)
y^{1}w*;Mi{y[+mDint2]=MIC}ChAT^{MI04508},CG7715 ^{MI04508}/TM3, Sb^{1}, Ser^{1}	MiMIC insertion site located within an intron of *ChAT* and *CG7715.* Can be targeted for replacement via RMCE.	(Nagarkar-Jaiswal *et al*. 2015)
UAS Reporter/Effector Strains		
w*;P{w[+mC]=UAS-mCD8::GFP}LL5/Cyo	Gal4-repsonsive transgene expression a fusion protein of mouse CD8 lymphocyte marker and Green Fluorescent Protein (mCD8::GFP). Labels all cell membranes and is well concentrated in neural processes.	(Lee and Luo 1999)
w;P{w[+mC]=UAS-TeTxLC.tnt}G2*	Also referred to as UAS-TNT. A GAL4 responsive transgene expressing tetanus neurotoxin light chain.	(Sweeney *et al*. 1995)

w⁺;+;dsx^{DBD},UAS-CsChrimson/TM3, Ser	Recombinant between *dsx^{DBD}* and *csChrimson* for intersection and activation of *dsx* neurons.	(Pavlou *et al*. 2016) Flybase.
w⁺;UAS-shi^{TS}/CyO;dsx^{DBD}/TM3, Ser	double balanced line containing *dsx^{DBD}* and *shibire^{ts}* for inactivation of *dsx* neurons.	Flybase.
w^{1118};P{y[+t7.7w[+mC]=20XUAS-IVS-GCaMP6s}attP40	GAL4 driven GCaMP6s. Placed under multiple *UAS* elements to improve expression level.	(Chen *et al*. 2013)
w;trans-Tango;+*	trans-*Tango* signalling components combined into single allele. Located in *attP40.*	(Talay *et al*. 2017)
w;+;UAS-myrGFP, QUAS-mtdTomato(3xHA)*	trans-*Tango* effector components. Located in *su(Hw)attP8*.	(Talay *et al*. 2017)
w; P{y[+t7.7] w[+mC]=13XLexAop2-IVS-myr::GFP}attP2*	*LexA* driven membrane-bound GFP variant.	Flybase.

7.2 Dissection and Imaging

7.2.1 Primary and secondary antibodies

The primary and secondary antibodies used in this study and their concentrations during staining steps are listed in tables Table 7-2 and Table 7-3, respectively.

Table 7-2: Primary antibodies used in this study

Antibody	Description	Dilution	Source
Anti-Green Fluorescent Protein (anti-GFP)	Polyclonal antibody against GFP with Rabbit IgG.	1:1000	Abcam
Anti-brp (nC82)	Monoclonal against bruchpilot (marks neuropil) with Mouse IgG.	1:10	Developmental Studies Hybridoma Bank (DSHB), Univ of Iowa.
Anti-HA	Monoclonal against human influenza Hemagglutinin with Rat IgG.	1:1000	Invitrogen Molecular Probes.

Table 7-3: Secondary antibodies used in this study

Antibody	Description	Dilution	Source
Goat anti-rabbit IgG Alexa Fluor 488	Goat polyclonal against rabbit IgG conjugated to Alexa Fluor 488	1:500	Invitrogen Molecular Probes
Goat anti-mouse IgG Alexa Fluor 546	Goat polyclonal against mouse IgG conjugated to Alexa Fluor 546	1:500	Invitrogen Molecular Probes
Goat anti-mouse IgG Alexa Fluor 633	Goat polyclonal against mouse IgG conjugated to Alexa Fluor 633	1:500	Invitrogen Molecular Probes
Goat anti-rat IgG Alexa Fluor 633	Goat polyclonal against rat IgG conjugated to Alexa Fluor 633	1:500	Invitrogen Molecular Probes

7.2.2 Whole-mount dissection of adult CNS

Adult flies were aged for at least 5 days prior to dissection. After lightly anaesthetising flies by placing their vial into an ice bucket, flies were immersed in ethanol for 5 seconds and then transferred to a dissecting dish containing ~1mL phosphate-buffered saline (PBS; 137 mM NaCl, 2.7 mM KCl, 10mM Na_2HP0_4, 2 mM KH_2PO_4). Legs and wings were removed using No. 5 dissection forceps (Dumont, Switzerland). The head capsule was left attached to the thorax and the brain exposed by removing the proboscis. Reaching through the cavity left by the excision of the proboscis, the trachea and large air sacs of the head capsule were removed. The head capsule was then torn apart by pulling at the lower corner of each eye, revealing the brain attached to the body via the cervical connective.

At this point, the abdomen was removed, the animal positioned ventral side up and forceps were used to cut the thoracic cuticle along both sides from posterior/caudal to anterior/cephalic. The ventral cuticle was then lifted away to reveal the ventral nerve system (VNS) attached to the brain, and both organs were transferred to ice cold PBS before washes and fixation. To begin fixation, the ice cold PBS was pipetted off and samples were washed once in 0.5% PBT (1xPBS, 0.5% Triton X-100). The samples were agitated by pipetting up and down during this first wash. They were then incubated on ice with 4% paraformaldehyde in PBS for 20 minutes, washed three times (20 minutes per wash) in 0.5% PBT at room temperature and eventually incubated at 4°C overnight in PTN (PBS with 10% (w/v) normal goat serum).

The following day, samples were washed 3 times in 0.5% PBT and left to incubate for 48 hours at 4°C in PTN containing appropriate primary antibodies (see Table 7-2 and Table 7-3). After two days, the solution was pipetted off, samples were washed 3 times

for 1 hour each in PBT and incubated for a further 24 hours at 4°C in PTN containing the appropriate fluor-conjugated secondary antibody.

Finally, they were washed another 3 times (for 1 hour each) in PBT and stored in 70% glycerol at 4°C for at least one day until imaging.

7.2.3 Whole-mount dissection of adult male terminalia and legs

Flies which were to have their genitalia or legs dissected and imaged were anaesthetised and placed in PBS as mentioned in section 7.2.2. The legs and wings were left intact and can be held to stabilise the fly with the ventral side facing upwards. A sharp pair of No. 5 forceps can then be inserted horizontally between the hypandrium and abdomen, allowing the terminalia to be torn free. Once the terminalia are detached, any remaining gut can easily be removed with the forceps. Lastly, the terminalia were placed so their caudal face pointed downwards, and with some light pressure from above, dissection scissors were used to remove the hypandrial phragma and phallopodeme, thus allowing the whole structure to be lay flat when turned back. At this point, the legs which are to be imaged can be removed easily with the forceps.

The male genitalia and legs were not stained prior to imaging as we found this typically reduced rather than amplified the fluorescent signal. Therefore, a simple process was employed prior to imaging where the sample received one 20 minute wash in 0.5% PBT, a 30 minute fixation in 4% PFA on ice, and a final 20 minute wash with PBT before they were then mounted in 70% glycerol for immediate confocal imaging.

7.2.4 Confocal Microscopy

Whole mount samples were imaged using a Leica TCA SP5 confocal microscope with 10x, 20x, 40x (oil immersion) and 63x (oil/water immersion) objective lenses and 'white light laser'. Alexa fluor-488-conjugated secondary antibodies are excited at 488 nm and emit at ~519 nms. Alexa fluor-546-conjugated antibodies are excited at 546 nm and emit at ~573 nms. Alexa fluor-633-conjugated antibodies are excited at 632 nms and emit at ~647 nms.

For imaging the male terminalia, GFP was excited at 488 nms whilst the cuticle counter stain was achieved by exciting at 488 nms and capturing emission at 633 nms. A background subtraction was then performed to remove the small amount of GFP signal captured at 633 nms (see section 7.2.5).

For images of the central nervous system, GFP was imaged at 488 nms, whilst the neuropil stain was imaged at 633 nms.

For imaging trans-*Tango* animals, GFP was imaged at 488 nms, the neuropil was imaged at 546 nms, and the postsynaptic signal was imaged at 633 nms.

When imaging multiple fluorophores in a single sample, each wavelength was sequentially scanned at each optical section to excite the fluorophores independently and prevent cross-excitation. Optical sections were imaged at 1 µm intervals.

7.2.5 Image processing

Confocal images were processed using Imaris (Bitplane Scientific, Zurich, Switzerland) and FIJI (Schindelin *et al*. 2012; Schindelin *et al*. 2015). For images of the male genitalia, a background subtraction was performed on the two images using a 50 pixel

rolling ball radius to remove the small amount of signal from the GFP molecule that was captured at 633 nms when imaging the cuticle. All images were then transformed into ‘maximum Z-stack projections’ with each optical section stacking onto the previous to form a single image.

3-dimensional projections were also formed using FIJI’s own interpolation process to fill in gaps between sections when viewed laterally. The brightness, colour and contrast of images was also modified if needed using FIJI. Finally the images were saved into a .png format and figures were assembled using Adobe Illustrator CC 2017 (Adobe Systems Inc, San Jose, CA).

7.2.6 Cell counts

For counting the number of cells labelled in a given sample, the confocal .lif format image was loaded into Imaris (Bitplane Scientific, Zurich, Switzerland). This allowed for better 3D manipulation of the image and allowed for the easier identification of individual cell bodies.

7.3 Molecular protocols

7.3.1 Strains and plasmids

The *Eschericia coli* strains used in this study were the chemically competent strains; One Shot™ TOP10 and Subcloning Efficiency™ DH5α (ThermoFisher Scientific). Their genotypes are listed in Table 7-4.

Table 7-4: *E. coli* strains used in this study.

Name	Genotype	Source
One Shot™ TOP10	*F- mcrA Δ(mrr-hsdRMS-mcrBC) Φ80lacZΔM15 Δ lacX74 recA1 araD139 Δ(araleu)7697 galU galK rpsL (StrR) endA1 nupG*	ThermoFisher Scientific
Subcloning Efficiency™ DH5α	F- Φ80*lac*ZΔM15 Δ(*lac*ZYA-*arg*F) U169 *rec*A1 *end*A1 *hsd*R17(r_{k^-}, m_{k^+}) *pho*A *sup*E44 *thi*-1 *gyr*A96 *rel*A1 λ^-	ThermoFisher Scientific

Plasmids used in this study, other than those whose construction is described specifically in other sections of this thesis, are listed in Table 7-5.

Table 7-5: Plasmids used in this study.

Name	Description	Source
pBPp65ADZpUw	Plasmid containing two inverted *attR* sites for the insertion of *attL* flanked amplicons via RMCE and *attB* for the insertion of the plasmid into *attP* genomic landing sites. Used for development of *R94D09^{p65AD}*.	Pfeiffer *et al*. (2010)
pBPZpGAL4DBDUw	Plasmid containing two inverted *attR* sites for the	Pfeiffer *et al*. (2010)

	insertion of *attL* flanked amplicons via RMCE and *attB* for the insertion of the plasmid into *attP* genomic landing sites. Used for the development of *R94D09^{DBD}*.	
pCR™8/GW/TOPO®	Used for the development of entry clones during *R94D09$^{p65AD/DBD}$* development. Includes 3' T-overhangs and covalently bonded Topoisomerase for direct integration of dA-tailed products and *att* sites for Gateway cloning.	ThermoFisher Scientific.
PBS-KS-attb1-2-PT-SA-SD-0-T2A-p65ADZpUw-HSP70	Insert vector for creating p65AD hemidrivers from MiMIC lines with inserts into coding introns in Phase 0	Diao *et al*. (2015)

7.3.2 Culture Media

The culture media used in this study was made using Sigma Luria Bertani (LB) broth tablets at a ratio of 2 tablets per 100mL of water.

7.3.3 Antibiotics

Where appropriate, antibiotics were added to culture media for plasmid selection. All plasmids used in this study (Table 7-5) were Carbenicillin or Spectinomycin resistant. Antibiotics were added to liquid LB broth at room temperature and to molten LB+agar at ~50°C. Final concentrations of all antibiotics used were 100 µg/mL.

Antibiotics were purchased from Sigma-Aldrich.

7.3.4 Bacterial transformation

Plasmid vectors which were to be grown into larger quantities with *E. coli* were transformed in the following manner:

Starting by thawing the cells on ice, 1-100ng of plasmid DNA (post-QIAGEN cleanup) was added to the cells and mixed gently. Once mixed, the cells were incubated on ice for 30 minutes, then heat shocked at 42°C for exactly 30 seconds.

Following this, working aseptically, 100-500µl of SOC media (Invitrogen, Carlsbad, CA) was added. The amount can be varied depending on the viability of transformed cells. This was shaken for 1 hour at 37°C and then 10-20µl was spread onto agar plates with appropriate selective antibiotic.

7.3.5 Isolation of plasmid DNA from *E.coli*

After colony selection with a pipette tip, 3ml LB broth with appropriate antibiotic were inoculated. These cultures were grown in a 37°C shaker incubator for 24 hours. Following this incubation period, plasmid DNA for sequencing and cloning was isolated

using the QIAprep spin miniprep kit (QIAGEN, Hilden, Germany) according to the manufacturer's instruction. In most cases, 2.4ml of the culture was used for the miniprep whilst the remaining 600μl was retained for making a glycerol stock that was retained at -80°C.

7.4 Molecular biology protocols

7.4.1 DNA extraction

Two methods were used for DNA extraction depending on the task at hand. For diagnostic PCRs where the fidelity of the amplified sequence wasn't vital, I used a 'quick and dirty' method where flies were crushed in a solution containing 10mM Tris-Cl (pH 8.2), 1mM EDTA, 25mM NaCl and 200μg/ml of fresh Proteinase K. After incubating in this solution at 37°C for 30 minutes to 1 hour, the Proteinase K is inactivated at 95°C for 1-2 minutes and the DNA is ready for use in PCR.

For applications requiring higher quality DNA, such as when cloning the original *R94D09* fragment to develop a split hemidriver, I used the QIAGEN spin-column DNA extraction kit as per the manufacturers instructions.

7.4.2 Polymerase chain reaction (PCR)

MyTaq Red Mix (Bioline, London, England) was used for diagnostic PCRs such as for checking the presence/absence of transgenes in a fly stock or verifying the identity of

a plasmid. A typical 15μl reaction using MyTaq included; 6.25μl MyTaq Red Mix, 5.75μl dH_2O, 1μl each of forward and reverse primer (100μM stock) and 1μl of template DNA (ranging from ~20-100ng/μl). Reactions were performed under the following conditions - 95°C for 3 minutes, thirty cycles of; 95°C for 30 seconds, 60°C (may vary with primer T_m) for 30 seconds then 72°C for 30 seconds per kb of desired product, and then a final 5 minute extension period at 72°C and holding at 12°C until ready for use or storage.

For applications which required higher fidelity amplification, such as when modifying driver lines in chapter 3.3, Phusion high fidelity polymerase (New England Biolabs, Ipswich, MA) was used. A typical 50μl reaction using Phusion includes; 0.5μl Phusion polymerase, 1μl 10mM dNTPs, 10μl Phusion high-fidelity buffer, 2.5μl of both forward and reverse primer and 1μl of DNA (ranging from ~20-100ng/μl) with dH_2O making up the rest of the volume. Such a reaction was typically run under these conditions - 98°C for 1 minute, followed by 30 cycles of; 98°C for 10 seconds, 60°C for 30 secs and 72°C for 30 seconds per kb of desired product, before a final extension at 72°C for three minutes and holding at 12°C.

7.4.2.1 Primer design

Primers used in this study were designed with the aid of Geneious® 10.1.3 (Biomatters Ltd).

Geneious 10.1.3 uses Primer3 (Untergasser *et al*. 2012) to calculate the T_m of primers. This was used to inform the annealing temperature in PCR reactions using those

primers, although in many cases a standard annealing temperature of 60°C was sufficient. A description of the primers used in this study can be found in Table 7-6.

Table 7-6: Primers used throughout this study.

Name	Sequence	Use
Trojan-MiMIC primers		
Insert.F (18660.F)	ACCCCGCAAGTTCACTTCAA	Vector-specific primer lying just outside of trojan exon cassette. Paired with locus-specific primers to identify insert orientation.
Insert.R (18660.R)	GTTGGTTTCGGAGCAGGAGG	Vector-specific primer lying just outside of trojan exon cassette. Paired with locus-specific primers to identify insert orientation.
nompC^{MI12787}_Fwd1 (58601.F)	AGCAATGGCGACAAGAAGGA	For genotyping *nompC^{MI12787}* lines. When combined with Insert.R, will produce a 1.5kb product when the insert is in the '+' orientation. When paired with Insert.F, will produce a product in the presence of '-' orientation inserts.
nompC^{MI12787}_Rev1 (58601.R)	AAACCGAATGCCACCAAAGC	For genotyping *nompC^{MI12787}* lines. When combined with Insert.F, will produce a 1.3kb product for '+' orientation inserts. When paired

		with Insert.R, will produce a product in '-' orientation inserts.
nompC^{MI03523}_Fwd1 (37009.F)	CCCTCGCCTTGCTAGTTTCA	For genotyping *nompC^{MI03523}* lines. When paired with Insert.R, will produce a 1.5kb product for '+' orientation insers. When paired with Insert.F, will produce a 1.45kb product for '-' oriented products.
nompC^{MI03523}_Rev1 (37009.R)	TTTTGGAGAGTGCGGGTGAG	For genotyping *nompC^{MI03523}* lines. When paired with Insert.F, will produce a 1.5kb product for '+' orientation inserts. When paired with Insert.R, will produce a 1.55kb product for '-' orientation inserts.
Piezo^{MI04294}_Fwd1 (37433.F)	GCACCAACAGTACGCAGAAG	For genotyping *Piezo^{MI04294}* lines. When paired with Insert.R, will produce a 1.5kb product for '+' orientation inserts. When paired with Insert.F, will produce a 1.4kb product for '-' orientation inserts.
Piezo^{MI04294}_Rev1 (37433.R)	GCAGCATGGCCTAAACACAG	For genotyping *Piezo^{MI04294}* lines. When paired with Insert.F, will produce a 1.45kb product for '+' orientation inserts. When paired with Insert.R, will produce a 1.5kb product for '-' orientation inserts.
Piezo^{MI04189}_Fwd1	ATGAACCGACTGAGACGACG	For genotyping *Piezo^{MI04189}* lines.

(44680.F)		When paired with Insert.R, will produce a 1.4kb product for '+' orientation inserts. When paired with Insert.F, will produce a 1.3kb product in '-' orientation inserts.
Piezo^{MI04189}_Rev1 (44680.R)	ATGAATCCTCCCACGCTGAC	For genotyping *Piezo^{MI04189}* lines. When paired with Insert.F, will produce a 1.6kb product for '+' orientation inserts. When paired with Insert.R, will produce a 1.7kb product for '-' orientation inserts.
ChAT^{MI04508}_Fwd1 (37817.F)	TGTGCTTATCTTGCCGACCT	For genotyping *ChAT^{MI04508}* lines. When paired with Insert.R, will produce a 1.6kb product for '+' orientation inserts. When paired with Insert.F, will produce a 1.5kb product for '-' orientation inserts.
ChAT^{MI04508}_Rev1 (37817.R)	GTCGCCAGCCCACTATATCC	For genotyping *ChAT^{MI04508}* lines. When paired with Insert.F, will produce a 1.65kb product for '+' orientation inserts. When paired with Insert.R, will produce 1.7kb product for '-' orientation inserts.
***R94D09* split-hemidriver primers**		
Amp.R	ATAATACCGCGCCACATAGC	Vector-specific primer for genotyping *R94D09-p65AD/DBD* flies. Combined with D09_R1,

		produces a 768bp product in both *R94D09-p65AD* and *R94D09-DBD* flies.
D09_R1	TTCATTGGCGGGTGAAAGAA	Sequence-specific primer for genotyping both *R94D09-p65AD* and *R94D09-DBD* flies. Produces a 768bp product when combined with Amp.R.
D09_Fwd	ACCGCCATGCCGAATGAAAAACAAC	Sequence-specific primer for genotyping both *R94D09-p65AD* and *R94D09-DBD* flies. Combined with D09_R2 will produce a 1024bp product when paired with D09_R2.
D09_R2	GGTGTTGGCATTCGCTAAAC	Sequence-specific primer for genotyping both *R94D09-p65AD* and *R94D09-DBD* flies. Produces a 1024bp product when combined with D09_Fwd.
D09_F1	TGTGGGTCACAACTCTTTGG	Sequence-specific primer for genotyping both *R94D09-p65AD* and *R94D09-DBD* flies. Produces a 976bp product when paired with D09_R3.
D09_R3	GCGGCATTTTATGGACGCAT	Sequence-specific primer for genotyping both *R94D09-p65AD* and *R94D09-DBD* flies. Produces a 976bp product when combined with D09_F1.

D09_F2	GTAATTTGGGCACGTGAAGC	Sequence-specific primer for genotyping both *R94D09-p65AD* and *R94D09-DBD* flies. Produces a 581bp product when paired with D09_R4.
D09_R4	CTGGCCATAGGGAAACGAAA	Sequence-specific primer for genotyping both *R94D09-p65AD* and *R94D09-DBD* flies. Produces a 581bp product when paired with D09_F2.
D09_F3	TGCTGGCTGCTTTTCGTTTC	Sequence-specific primer for genotyping both *R94D09-p65AD* and *R94D09-DBD* flies. Produces a 862bp product when paired with D09_R5.
D09_R5	GCCATTTTGTGAGCGTGTGT	Sequence-specific primer for genotyping both *R94D09-p65AD* and *R94D09-DBD* flies. Produces a 862bp product when paired with D09_F3.
D09_F4	ATCATGTCCTGTCAATGGGC	Sequence-specific primer for genotyping both *R94D09-p65AD* and *R94D09-DBD* flies. Produces a 959bp product when paired with D09_Rev.
D09_Rev	CACAGGATAGTCGGTTGTGTCGAAG	Sequence-specific primer for genotyping both *R94D09-p65AD* and *R94D09-DBD* flies. Produces a

		959bp product when paired with D09_F4.
D09_F5	ATCTTGGTGAAAGTGCAGCA	Sequence-specific primer for genotyping *R94D09-DBD* flies only. Produces a ~1000bp product when paired with DBD.R.
DBD.R	CGGCATATGTCACACGCTTG	Sequence-specific primer for genotyping *R94D09-DBD* flies only. Produces a ~1000bp when paired with D09_F5.
D09_F6	ACTTAGCTCACTGGCTACCA	Sequence-specific primer for genotyping *R94D09-p65AD* flies only. Produces a 789bp product when paired with D09_R6.
D09_R6	GTTCGCTTCCGCTTTTCTTC	Sequence-specific primer for genotyping *R94D09-p65AD* flies only. Produces a 789bp product when paired with D09_F6.
D09_F7	AGACGCATACCAAACGGTAC	Sequence-specific primer for genotyping *R94D09-p65AD* flies only. Produces a 696bp product when paired with AD.R.
AD.R	CCGGGATTCCCTGATTCAAG	Sequence-specific primer for genotyping *R94D09-p65AD* flies only. Produces a 696bp product when paired with D09_F7.

***R23F02-LexA* sequencing primers**

F02_Fwd	GCGAGCCTACAACAGCATCCATGGA	Sequence-specific primer which binds the *R23F02* sequence and extends across the right-most breakpoint (attR2) of *R23F02-nlsLexA* cassettes.
F02_Rev	GGGCGTCTTGGCCATTTCCTTTCTG	Sequence-specific primer which binds the *R23F02* sequence and extends across the left-most breakpoint (attR1) of *R23F02-nlsLexA* cassettes.
PQE30_Fwd	CCCGAAAAGTGCCACCTG	Vector specific primer which sequences across the left-most breakpoint (attR1) of *23F02-nlsLexA* cassettes.

7.4.3 Gel electrophoresis

To visualize DNA fragments, they were run on agarose (Cambridge Reagents Ltd., Barton Upon Humber, UK) gels containing 0.1μg/ml EtBr. The MyTaq Red Mix used for many reactions already contains a loading dye, but other samples were mixed with a loading dye (New England Biolabs, Ipswich, MA) at a 1:6 ratio before being loaded into an agarose gel containing 1x TAE (40 mM Tris/AcOH (pH 8.2), 20mM NaOAc, 1mM EDTA). Various agarose concentrations were used, depending on the size of the fragment to be resolved, but most common was 1% (w/v). Gels were run from 1 to 1.5 hours at voltages ranging from 90-120 mV. DNA size marking ladders were either 100bp+ or 1kb+ (NBS Biologicals, Huntingdon, UK).

7.4.4 Visualization of gels

A UVIdoc HD2 (UVItec, Cambridge, UK) transilluminator was used to visualise DNA in agarose gels by UV fluorescence induced at short wave (254 nm) or long wave (385 nm). A Sony CCD camera captured and saved an image of the illuminated gel onto the UVIdoc hardware, whilst a Sony UP-D897MD digital thermal printer was used to print the saved images.

7.4.5 Gel Extraction

Size-selected DNA fragments were excised from their gels using a clean razor blade on a long-wave UV transilluminator to reduce the likelihood of UV-induced DNA damage in these fragments. Purification of the fragment from the gel matrix as well as any remaining salt or enzyme was performed using the QIAquick gel extraction kit (QIAGEN, Hilden, Germany).

7.4.6 Quantification of total DNA in a sample

The amount of DNA in a given sample was estimated by taking Optical Density (O.D.) measurements at a 260nm wavelength using a NanoDrop 2000 spectrophotometer (ThermoFisher Scientific, Waltham, MA).

7.4.7 DNA sequencing

DNA sequencing was carried out by Source Bioscience (Nottingham, UK) using Sanger sequencing SpeedREAD™ technology. They required 5ul per reaction of sample at a concentration of 100ng/ul for plasmid DNA and 10ng/ul for PCR products. Primers used for sequencing were provided at 3.2pmol/ul and are detailed in Table 7-6.

7.4.8 Developing *R94D09* split-hemidrivers

For the development of *R94D09*-p65AD/DBD a subcloning process was required. After amplifying the target region from a *y; cn bw sp* stock (from which the original element was cloned) with Phusion polymerase (see primers in section 7.4.2.1), the product was incubated with *dATP* and *Taq* polymerase for 20 minutes at 72°C to add 3' A overhangs. This product was then cleaned up using a QIAGEN PCR cleanup kit (QIAGEN, Hilden, Germany) and incubated with *pCR™8/GW/TOPO®* for 30 minutes at room temperature. Following this, 2µl of reaction mixture was transformed into TOP10 cells. After establishing a stable culture of *pCR™8/GW/TOPO®-R94D09* cells in a 3 mL liquid culture, a glycerol stock was made with 800 µL and the remaining culture was miniprepped with a QIAprep Spin Miniprep Kit. The R94D09 element was then recombined into one of two split-GAL4 vectors via a Gateway™ cloning reaction. Briefly, this reaction required the incubation of 200 ng pCR™8/GW/TOPO®-R94D09 with 100 ng of either pBPp65ADZpUw or pBPZpGAL4DBDUw and 4 µL Gateway™ LR Clonase™ II Enzyme mix (ThermoFisher Scientific, Waltham, MA) at 25°C overnight. Reactions were halted after 24 hours by adding 2 µL Proteinase K and incubating at 37°C for 20 minutes before 2 µL of the reaction mixture was transformed

into TOP10 cells. After growing this culture and miniprepping the final product, these vectors were sequenced to ensure the element had been properly inserted into the destination vector before being sent to BestGene Inc (Chino Hills, CA) for injection.

7.4.9 Developing *R23F02-LexA* driver

During the course of this work we have developed a *LexA* variant of *R23F02-p65AD.* This process was similar to that used when making *R94D09-p65AD/DBD* (previous section). After inserting the *R23F02* element into pCR™8/GW/TOPO® a Gateway™ LR reaction was used to recombine it into pBPnlsLexA::P65UW (Pfeiffer *et al*. 2010). It was then transformed into OneShot TOP10 cells, miniprepped and sent for sequence verification by Source Bioscience

7.4.10 Developing Trojan-MiMIC drivers

The injection of 'Trojan exon' cassettes was performed by BestGene Inc (Chino Hills, CA). Prior to injection, we identified one or more attP insertion sites in our genes of interest using the *Drosophila* Gene Disruption Project Database (http://flypush.imgen.bcm.tmc.edu/). Flies homozygous for these insertion sites were then ordered by BestGene and crossed to a source of germline φC31 integrase. The resulting offspring were then injected with PBS-KS-attb1-2-PT-SA-SD-0-T2A-P65ADZpuw-Hsp70 which we provided. After maturing, these injected flies were crossed to a suitable balancer and genotype using primers listed in table 2-1. As this recombination event is non-directional, a PCR strategy using two primer pairs was used to identify insertions in the correct orientation relative to the target gene. We also

repeated this verification after receiving the flies. These primers are also listed in table 2-1.

7.5 Behavioural Analysis

7.5.1 Courtship assays

Individual virgin males and females were collected and aged for 5 days post-eclosion at 25°C. Males were kept individually during this time, whilst females were housed in groups of 3. Courtship assays were performed at 25°C except for inactivation assays (sections 4.3.2 and 4.4.2) when experiments were performed at a permissive temperature of 23°C and a restrictive temperature of 31°C.

For optogenetic experiments, assays were performed at 25°C, but in the dark to minimise ambient light exposure. Experimental animals (+retinal condition) were illuminated throughout the observation period with 10 ms ON:OFF pulses containing 50 Hz flashes of red LED light, whilst control animals (-retinal) where assayed without illumination.

Males and females were individually introduced into a round courtship chamber (20mm diameter x 2mm) with a retractable divider. 20 chambers were arranged in a 4x5 plate constructed from custom cut acrylic (https://southernacrylics.co.uk/) which was mounted in a 3D printed support and backlit with a FLFL-Si200-IR24 infrared backlight (http://www.falcon-illumination.com/productdetail_FLFL.php). One-hour courtship assays were recorded using a Basler ace A2440-75um camera with a 35mm VIS-NIR fixed focal length lens and a UB/VIS cut-off filter from Edmund Optics (https://www.edmundoptics.co.uk/). Uncompressed videos in .avi format were

recorded at 25 frames per second, 2400x1600 resolution, and 8-bit grayscale using LabVIEW (https://www.ni.com/en-gb/shop/labview.html).

7.5.2 Automated behaviour tracking and annotation

Uncompressed .avi videos were converted µFMF video format using *any2ufmf* software (http://ctrax.sourceforge.net/any2ufmf.html). µFMF video files were tracked with the Caltech FlyTracker (http://www.vision.caltech.edu/Tools/FlyTracker/) with the following settings: num_chunks=1, num_cores=1, max_minutes=60, save_JAABA=1. Once tracked, courtship behaviours were annotated using the Janelia Automatic Animal Behaviour Annotator (JAABA; Kabra *et al*. 2013). JAABA classifiers were trained for the following behaviours:

- '*Approaching*' – focal fly was approaching the other fly (TP = 96.8%, FN = 3.2%, TN = 98.5%, FP = 1.5%, nP = 2715, nN = 16169).
- '*Facing*' – the focal flies head was oriented towards the other fly, while not being on the opposite side of the chamber (TP = 100.0%, FN = 0.0%, TN = 95.2%, FP = 4.8%, nP = 4490, nN = 7937).
- '*Contact*' – the leg, proboscis, or head of the focal fly contacted any part the other fly (TP = 93.9%, FN = 6.1%, TN = 98.1%, FP = 1.9%, nP = 2684, nN = 10789).
- '*Circling*' – the focal fly walked sideways while facing and being close to the other fly (TP = 71.6%, FN = 28.4%, TN = 98.5%, FP = 1.5%, nP = 638, nN = 9746).

- '*Turning*' – the focal fly turned their body to orient towards the other fly while not moving forward (TP = 89.6%, FN = 10.4%, TN = 96.6%, FP = 3.4%, nP = 414, nN = 1540).
- '*Wing extension*' – the focal fly extended a wing beyond their body (TP = 98.3%, FN = 1.7%, TN = 98.6%, FP = 1.4%, nP = 1575, nN = 10926).

(TP – true positive, FN – false negative, TN – true negative, FN – false negative, nP – number of annotated positive frames, nN – number of annotated negative frames).

Classifiers were applied to the tracking data using the '*JAABADetect*' function.

7.5.3 Postural analysis with DeepLabCut

To extract information regarding the male and female body position during copulation, we employed DeepLabCut (DLC) version 2.1.6.2 (Mathis *et al*. 2018). Raw .avi files were cropped into several smaller videos containing a singular chamber and converted into MP4 format using FFmpeg. These videos were then cropped to contain only those frames where we deemed the pair to be *in copulo before* analysis with our DLC model.

To train the DLC model, I manually labelled the male and female head and thorax position in 200 frames taken from videos of wild-type, *R94D09*^{DBD}∩*nompC*$^{MI12787\text{-}AD}$*>UAS-TNT* and *R20G10-p65AD*∩*dsx*^{DBD}*>UAS-shibire*^{ts} males. This dataset was used to train for 300,000 iterations. To test the model, I then compared an automated DLC analysis (p-cutoff 0.6) of a novel video, with manual labelling of the same points. This comparison revealed a testing error of ±2.83 pixels but was noticeably poor at marking the desired points in the most extreme cases (such as those shown in Figure 4-2Aii-iii).

We then further supplemented the training dataset with 50 frames of these extreme cases and re-trained the model for a further 200,000 iterations. This resulted in a testing error of ±2.89 pixels across the entire copulatory bout, but a more reliable labelling of points during extreme cases of abnormal mating posture.

Lastly, we noted that cases where the copulating pair are on the edge of the chamber often produced erroneous measurements. To remedy this, only measurements taken when the ‘thorax’ marker is at least half the body length of the fly from the chambers edge were used.

7.5.4 Metrics

When reporting *Drosophila* reproductive behaviour assays in this thesis, the following metrics are used:

Male behaviour metrics:

Courtship Index (CI): The proportion of time in the first ten minutes of an assay where the male is exhibiting any of the behaviours classified by JAABA. CI can include or exclude the male facing the female as a courtship behaviour. For this study, orientation towards the female was included when calculating CI indices.

Time to copulation:

The time between the removal of the chamber divider and copulation. In practice the start time of copulation is typically 3 seconds after the initial attachment as this ensures that instances where the male immediately detaches from the female are not counted.

Percentage Mating:

The proportion of flies, per genotype, which achieved copulation within the 1 hour observation.

Wing Index:

The proportion of time in the one hour assay where a male is unilaterally extending a wing beyond 30°.

Copulation Duration:

The total time for which the male and female are copulating. Bouts beginning close to the end of the assay are not counted to avoid skewing the results.

Attempts made:

The number of times a male bends his abdomen anteriorly with surstyli open in order to copulate with the female.

Female behaviour metrics:

Offspring sired (10 days):

Mated females are collected post-mating and placed in groups of 5 into empty bottles capped with a grape-juice agar plate. The centre of this agar plate has a small amount of yeast paste to stimulate laying. Every 2 days for the proceeding 10, the caps were

replaced and eggs/larvae present on it were counted. This value is then divided by the number of females to calculate an average number of eggs produced each 48 hours.

Distance travelled during copulation:

Used as a proxy for female receptivity during copulation, this is simply the total distance (in milimetres) that a copulating pair travels during the first ten minutes of copulation. This metric is only calculated for the first ten minutes to minimise the effect that changes to the duration of copulation might have on this value.

7.6 *In vivo* Calcium imaging

For experiments where we recorded transient calcium currents in response to a mechanical stimulus, flies were raised at 25°C on yellow food and then kept for up to one week at room temperature to increase GCaMP signal. Once ready for imaging, flies were anaesthetized on ice and their legs were removed so that the ventral thorax could be positioned over a small hole of approximately 1 mm in a 3D-printed dish used to hold the fly during imaging. Once properly aligned on this dish, the fly was fixed in place using eicosane wax (Sigma Aldrich, St. Louis, MO) on the wings and abdomen. The sample was then turned over and the ventral cuticle was carefully removed using fine forceps under a small amount of carbogen bubbled (95% O_2, 5% CO_2) imaging solution (103mM NaCl, 3mM KCl, 5mM TES, 26mM NaHCO3, 1mm NaH2PO4, 1.5mM CaCl2, 4mM MgCl2, 10mM Trehalose, 10mM glucose, osmolarity adjusted to 275 mmol/Kg).

Following the removal of the cuticle, the tracheal tubules which cover the surface of the abdominal ganglion were removed and the specimen was mounted onto a Scientifica 2-photon microscope ready for imaging and stimulation.

To stimulate MTS neurons, a 0.5 mm tungsten minutien pin (Fine Science Tools, Heidelberg, Germany) attached to a Scientifica micromanipulator was slowly moved towards the male genitalia, targeting the surstyli in particular. Gentle contact between the pin and genital bristles was made with particular effort being made to move the bristles from their resting position towards the dorsal side. Typically, each sample was stimulated on the terminalia three times and the abdomen three times. GCaMP6s fluorescence was recorded from the Abg throughout. GCaMP6s signals were recorded using ScanImage 3.8 software (Pologruto *et al*. 2003) whilst touches were recorded using a Guppy PRO F-031B camera (Allied Vision, Stadtroda, Germany) with a 842 nm blocking edge BrightLine® short-pass filter (Semrock Inc, Rochester, NY). After recording, the two videos were aligned and changes in GCaMP fluorescence from a user specified ROI encompassing the target neurites was calculated using a series of custom MATLAB (MathWorks, Natick, MA) scripts available at https://github.com/AR2202/2-photon. Individual recordings could then be averaged and aligned to the stimulus onset using custom scripts also available at https://github.com/AR2202/2-photon.

7.7 Statistical Analysis

Statistical analyses were performed in GraphPad Prism 9.0.1 (https://www.graphpad.com/). For comparisons of cell counts such as those reported in chapter 2 an unpaired t-test was performed between the ‘ground-truth’ exterior bristle count and the number of labelled cells in that region. For the comparisons between multiple driver lines such as those reported in Figure 2-9, a one-way ANOVA with Bonferroni correction for multiple comparisons was used. To analyse the behavioural experiments reported in chapter 4, a one-way ANOVA with Bonferroni correction was used for all tests except when looking for differences in the mating percentage of each genotype. In these cases, datapoints from control males were combined and then compared against the experimental condition using a Fisher’s exact test.

8 Bibliography

Acebes, A. (2003), Species-Specific Effects of Single Sensillum Ablation on Mating Position in Drosophila, *Journal of Experimental Biology,* 206 (17), 3095-3100.

Adams, M. D., Clelniker, S. E., Holt, R. A., Evans, C. A., Gocayne, J. D., Amanatides, P. G., . . . and Venter, J. C. (2000), The Genome Sequence of Drosophila Melanogaster, *Science,* 287, 2185-2195.

Akam, M. (1998), Hox Genes: From Master Genes to Micromanagers, *Current Biology,* 8, 676-678.

Allen, A. M., Neville, M. C., Birtles, S., Croset, V., Treiber, C. D., Waddell, S., and Goodwin, S. F. (2019), A Single-Cell Transcriptomic Atlas of the Adult Drosophila Ventral Nerve Cord, *bioRxiv*.

An, W., Cho, S., Ishii, H., and Wensink, P. C. (1996), Sex-Specific and Non-Sex-Specific Oligomerization Domains in Both of the Doublsex Transcription Factors from Drosophila Melanogaster, *Molecular and Cellular Biology,* 16, 3106-3111.

Anand, A., Villella, A., Ryner, L. C., Carlo, T., Goodwin, S. F., Song, H. J., . . . Taylor, B. J. (2001), Molecular Genetic Dissection of the Sex-Specific and Vital Functions of the Drosophila Melanogaster Sex Determination Gene Fruitless, *Genetics,* 158 (4), 1569-1595.

Anderson, M. D. S., Halpern, M. E., and Keshisian, H. (1988), Identification of the Neuropeptide Transmitter Proctolin in Drosophila Larvae: Characterization of Muscle Fiber-Specific Neuromuscular Endings, *The Journal of Neuroscience,* 8, 242-255.

Asahina, K., Watanabe, K., Duistermars, B. J., Hoopfer, E., Gonzalez, C. R., Eyjolfsdottir, E. A., . . . Anderson, D. J. (2014), Tachykinin-Expressing Neurons Control Male-Specific Aggressive Arousal in Drosophila, *Cell,* 156 (1-2), 221-235.

Ashburner, M., Golic, K. G., and Hawley, R. S. (2005), *Drosophila: A Laboratory Handbook* (II edn.; Cold Spring Harbor, New York, US: Cold Spring Harbor Laboratory Press).

Baines, R. A., Uhler, J. P., Thompson, A., Sweeney, S. T., and Bate, M. (2001), Altered Electrical Properties in Drosophila Neurons Developing without Synaptic Transmission, *The Journal of Neuroscience,* 21 (5), 1523-1531.

Barnea, G., Strapps, W., Herrada, G., Berman, Y., Ong, J., Kloss, B., . . . Lee, K., J. (2008), The Genetic Design of Signalling Cascades to Record Receptor Activation, *PNAS,* 105 (1), 64-69.

Bateman, J. R., Lee, A. M., and Wu, C. T. (2006), Site-Specific Transformation of Drosophila Via Phic31 Integrase-Mediated Cassette Exchange, *Genetics,* 173 (2), 769-777.

Bell, L. R., Maine, E. M., Schedl, P., and Cline, T. W. (1988), Sex-Lethal, a Drosophila Sex Determination Switch Gene, Exhibits Sex-Specific Rna Splicing and Sequence Similarity to Rna Binding Proteins, *Cell,* 55 (6), 1037-1046.

Bellen, H. J., O'Kane, C. J., Wilson, C., Grossniklaus, U., Pearson, R. K., and Gehring, W. J. (1989), P-Element-Mediated Enhancer Detection: A Versatile Method to Study Development in Drosophila, *Genes Dev,* 3, 1288-1300.

Bier, E., Vaessin, H., Shepherd, S., Lee, K., McCall, K., Barbel, S., . . . Jan, Y. N. (1989), Searching for Pattern and Mutation in the Drosophila Genome with a F-Lacz Vector, *Genes Dev,* 3, 1273-1287.

Billeter, J. C., Rideout, E. J., Dornan, A. J., and Goodwin, S. F. (2006a), Control of Male Sexual Behavior in Drosophila by the Sex Determination Pathway, *Curr Biol,* 16 (17), R766-776.

Billeter, J. C., Villella, A., Allendorfer, J. B., Dornan, A. J., Richardson, M., Gailey, D. A., and Goodwin, S. F. (2006b), Isoform-Specific Control of Male Neuronal Differentiation and Behavior in Drosophila by the Fruitless Gene, *Curr Biol,* 16 (11), 1063-1076.

Bloch Qazi, M. C. and Wolfner, M. F. (2003), An Early Role for the Drosophila Melanogaster Male Seminal Protein Acp36de in Female Sperm Storage, *J Exp Biol,* 206 (Pt 19), 3521-3528.

Bohm, R. A., Welch, W. P., Goodnight, L. K., Cox, L. W., Henry, L. G., Gunter, T. C., . . . Zhang, B. (2010), A Genetic Mosaic Approach for Neural Circuit Mapping in Drosophila, *Proc Natl Acad Sci U S A,* 107 (37), 16378-16383.

Boll, W. and Noll, M. (2002), The Drosophila Pox Neuro Gene: Control of Male Courtship Behavior and Fertility as Revealed by a Complete Dissection of All Enhancers, *Development,* 129 (24), 5667-5681.

Boyden, E. S., Zhang, F., Bamberg, E., Nagel, G., and Deisseroth, K. (2005), Millisecond-Timescale, Genetically Targeted Optical Control of Neural Activity, *Nat Neurosci,* 8 (9), 1263-1268.

Brand, A. H. and Perrimon, N. (1993), Targeted Gene Expression as a Means of Altering Cell Fates and Generating Dominant Phenotypes, *Development,* 118, 401-415.

Branson, K., Robie, A. A., Bender, J., Perona, P., and Dickinson, M. H. (2009), High-Throughput Ethomics in Large Groups of Drosophila, *Nat Methods,* 6 (6), 451-457.

Brent, R. and Ptashne, M. (1985), A Eukaryotic Transcriptional Activator Bearing the DNA Specificity of a Prokaryotic Repressor, *Cell,* 43, 729-736.

Bressac, C. and Hauschteck-Jungen, E. (1996), Drosophila Subobscura Females Preferentially Select Long Sperm for Storage and Use, *Journal of Insect Physiology,* 42, 323-328.

Burtis, K. C. and Baker, B. S. (1989), Drosophila Doublesex Gene Controls Somatic Sexual Differentiation by Producing Alternatively Spliced Mrnas Encoding Related Sex-Specific Polypeptides, *Cell,* 56, 997-1010.

Burtis, K. C., Coschigano, K. T., Baker, B. S., and Wensink, P. C. (1991), The Doublesex Proteins of Drosophila Melanogaster Bind Directly to a Sex-Specific Yolk Protein Gene Enhancer, *The EMBO Journal,* 10 (9), 2577-2582.

Bussell, J. J., Yapici, N., Zhang, S. X., Dickson, B. J., and Vosshall, L. B. (2014), Abdominal-B Neurons Control Drosophila Virgin Female Receptivity, *Curr Biol,* 24 (14), 1584-1595.

Cachero, S., Ostrovsky, A. D., Yu, J. Y., Dickson, B. J., and Jefferis, G. S. (2010), Sexual Dimorphism in the Fly Brain, *Curr Biol,* 20 (18), 1589-1601.

Callaway, E. M. and Luo, L. (2015), Monosynaptic Circuit Tracing with Glycoprotein-Deleted Rabies Viruses, *J Neurosci,* 35 (24), 8979-8985.

Camara, N., Whitworth, C., and Van Doren, M. (2008), The Creation of Sexual Dimorphism in the Drosophila Soma, *Current Topics in Developmental Biology,* 83, 65-107.

Carpenter, F. W. (1905), The Reactions of the Pomace Fly (Drosophila Ampelophila Loew) to Light, Gravity, and Mechanical Stimulation, *The American Naturalist,* 39 (459), 157-171.

Carvalho, G. B., Kapahi, P., Anderson, D. J., and Benzer, S. (2006), Allocrine Modulation of Feeding Behavior by the Sex Peptide of Drosophila, *Curr Biol,* 16 (7), 692-696.

Chadha, A. and Cook, B. (2012), Dissection of Gain Control Mechanisms in Drosophila Mechanotransduction, *J Neurosci,* 32 (38), 13052-13061.

Chan, Y.-B. and Kravitz, E. A. (2007), Specific Subgroups of Frum Neurons Control Sexually Dimorphic Patterns of Aggression in Drosophila Melanogaster, *PNAS,* 104 (49), 19577-19582.

Chen, T. W., Wardill, T. J., Sun, Y., Pulver, S. R., Renninger, S. L., Baohan, A., . . . Kim, D. S. (2013), Ultrasensitive Fluorescent Proteins for Imaging Neuronal Activity, *Nature,* 499 (7458), 295-300.

Cheng, L. E., Song, W., Looger, L. L., Jan, L. Y., and Jan, Y. N. (2010), The Role of the Trp Channel Nompc in Drosophila Larval and Adult Locomotion, *Neuron,* 67 (3), 373-380.

Cho, S. and Wensink, P. C. (1997), DNA Binding by the Male and Female Doublsex Proteins of Drosophila Melanogaster, *The Journal of Biological Chemistry,* 272, 3185-3189.

Clough, E., Jimenez, E., Kim, Y. A., Whitworth, C., Neville, M. C., Hempel, L. U., . . . Oliver, B. (2014), Sex- and Tissue-Specific Functions of Drosophila Doublesex Transcription Factor Target Genes, *Dev Cell,* 31 (6), 761-773.

Clowney, E. J., Iguchi, S., Bussell, J. J., Scheer, E., and Ruta, V. (2015), Multimodal Chemosensory Circuits Controlling Male Courtship in Drosophila, *Neuron,* 87 (5), 1036-1049.

Clyne, J. D. and Miesenbock, G. (2008), Sex-Specific Control and Tuning of the Pattern Generator for Courtship Song in Drosophila, *Cell,* 133 (2), 354-363.

Cohen, B., Wimmer, E. A., and Cohen, S. M. (1991), Early Development of Leg and Wing Primordia in the Drosophila Embryo, *Mechanisms of Development,* 33, 229-240.

Connolly, K. and Cook, R. (1973), Rejection Responses by Female Drosophila Melanogaster: Their Ontogeny, Causality and Effects Upon the Behaviour of the Courting Male, *Behaviour,* 44, 142-166.

Cook, K. R., Parks, A. L., Jacobus, L. M., Kaufman, T. C., and Matthews, K. A. (2010), New Research Resources at the Bloomington Drosophila Stock Center, *Fly (Austin),* 4 (1), 88-91.

Cordero, C. and Eberhard, W., G. (2003), Female Choice of Sexually Antagonistic Male Adaptations: A Critical Review of Some Current Research, *Journal of Evolutionary Biology,* 16, 1-6.

Corfas, G. and Dudai, Y. (1990), Adaptation and Fatigue of a Mechanosensory Neuron in Wild-Type Drosophila and in Memory Mutants, *The Journal of Neuroscience,* 10 (2), 491-499.

Costa, M., Manton, J. D., Ostrovsky, A. D., Prohaska, S., and Jefferis, G. S. (2016), Nblast: Rapid, Sensitive Comparison of Neuronal Structure and Construction of Neuron Family Databases, *Neuron,* 91 (2), 293-311.

Court, R., Namiki, S., Armstrong, J. D., Börner, J., Card, G. M., Costa, M., . . . Williams, D. (2017), A Systematic Nomenclature for the Drosophila Ventral Nervous System, *bioRxiv*.

Croset, V., Treiber, C. D., and Waddell, S. (2018), Cellular Diversity in the Drosophila Midbrain Revealed by Single-Cell Transcriptomics, *Elife,* 7.

Daniels, R. W., Gelfand, M. V., Collins, C. A., and DiAntonio, A. (2008), Visualizing Glutamatergic Cell Bodies and Synapses in Drosophila Larval and Adult Cns, *J Comp Neurol,* 508 (1), 131-152.

Daniels, R. W., Collins, C. A., Gelfand, M. V., Dant, J., Brooks, E. S., Krantz, D. E., and DiAntonio, A. (2004), Increased Expression of the Drosophila Vesicular Glutamate Transporter Leads to Excess Glutamate Release and a Compensatory Decrease in Quantal Content, *J Neurosci,* 24 (46), 10466-10474.

Datta, S. R., Vasconcelos, M. L., Ruta, V., Luo, S., Wong, A., Demir, E., . . . Axel, R. (2008), The Drosophila Pheromone Cva Activates a Sexually Dimorphic Neural Circuit, *Nature,* 452 (7186), 473-477.

de Navas, L., Foronda, D., Suzanne, M., and Sanchez-Herrero, E. (2006), A Simple and Efficient Method to Identify Replacements of P-Lacz by P-Gal4 Lines Allows Obtaining Gal4 Insertions in the Bithorax Complex of Drosophila, *Mech Dev,* 123 (11), 860-867.

del Alamo, D., Terriente, J., and Diaz-Benjumea, F. J. (2002), Spitz/Egfr Signalling Via the Ras/Mapk Pathway Mediates the Induction of Bract Cells in Drosophila Legs, *Development,* 129 (8), 1975-1982.

del Valle Rodriguez, A., Didiano, D., and Desplan, C. (2012), Power Tools for Gene Expression and Clonal Analysis in Drosophila, *Nat Methods,* 9 (1), 47-55.

Demir, E. and Dickson, B. J. (2005), Fruitless Splicing Specifies Male Courtship Behavior in Drosophila, *Cell,* 121 (5), 785-794.

Diao, F. and White, B. H. (2012), A Novel Approach for Directing Transgene Expression in Drosophila: T2a-Gal4 in-Frame Fusion, *Genetics,* 190 (3), 1139-1144.

Diao, F., Ironfield, H., Luan, H., Diao, F., Shropshire, W. C., Ewer, J., . . . White, B. H. (2015), Plug-and-Play Genetic Access to Drosophila Cell Types Using Exchangeable Exon Cassettes, *Cell Rep,* 10 (8), 1410-1421.

Dionne, H., Hibbard, K. L., Cavallaro, A., Kao, J. C., and Rubin, G. M. (2018), Genetic Reagents for Making Split-Gal4 Lines in Drosophila, *Genetics,* 209 (1), 31-35.

Donnelly, M. L. L., Luke, G., Mehrota, A., Li, X., Hughes, L. E., Gani, D., and Ryan, M. D. (2001), Analysis of the Aphhovirus 2a/2b Polyprotein 'Cleavage' Mechanism Indicates Not a Proteolytic Reaction, but a Novel Translational Effect: A Putative Ribosomal 'Skip', *Journal of General Virology,* 82, 1013-1025.

Dubnau, J. and Tully, T. (1998), Gene Discovery in Drosophila: New Insights for Learning and Memory, *Annu Rev Neuroscience,* 21, 407-444.

Eberhard, W. G. (1992), Species Isolation, Genital Mechanics, and the Evolution of Species-Specific Genitalia in Three Forms of Mecrodactylus Beetles (Coleoptera, Scarabidae, Melolnthinae), *Evolution,* 46 (6).

Eberhard, W. G. (1996), *Female Control: Sexual Selection by Cryptic Female Choice* (Monographs in Behaviour and Ecology: Princeton University Press, Princeton NJ).

Eberhard, W. G. and Ramirez, N. (2004), Functional Morphology of the Male Genitalia of Four Species of <I>Drosophila</I>: Failure to Confirm Both Lock and Key and Male-Female Conflict Predictions, *Annals of the Entomological Society of America,* 97 (5), 1007-1017.

Effertz, T., Wiek, R., and Gopfert, M. C. (2011), Nompc Trp Channel Is Essential for Drosophila Sound Receptor Function, *Curr Biol,* 21 (7), 592-597.

Ejima, A., Nakayama, S., and Aigaki, T. (2001), Phenotypic Association of Spontaneous Ovulation and Sexual Receptivity in Virgin Females of Drosophila Melanogaster Mutants, *Behaviour Genetics,* 31, 437-444.

Ejima, A., Smith, B. P., Lucas, C., van der Goes van Naters, W., Miller, C. J., Carlson, J. R., . . . Griffith, L. C. (2007), Generalization of Courtship Learning in Drosophila Is Mediated by Cis-Vaccenyl Acetate, *Curr Biol,* 17 (7), 599-605.

Elgin, S. C. and Reuter, G. (2013), Position-Effect Variegation, Heterochromatin Formation, and Gene Silencing in Drosophila, *Cold Spring Harb Perspect Biol,* 5 (8), a017780.

Emerald, S. E. and Roy, J. K. (1998), Organising Activities of Engrailed, Hedgehog, Wingless and Decapentaplegic in the Genital Discs of Drosophila Melanogaster, *Dev Genes Evol,* 208, 504-516.

Erdman, S. E., Chen, H.-J., and Burtis, K. C. (1996), Functional and Genetic Characterization of the Oligomerization and DNA Binding Properties of the Drosophila Doublsex Proteins, *Genetics,* 144, 1639-1652.

Erlander, M. G. and Tobin, A. J. (1991), The Structural and Functional Heterogeneity of Glutamic Acid Decarboxylase: A Review, *Neurochemical Research,* 16, 215-226.

Estes, P. S., Ho, G. L. Y., Narayanan, R., and Ramaswami, M. (2009), Synaptic Localization and Restricted Diffusion of a Drosophila Neuronal Synaptobrevin -

Green Fluorescent Protein Chimera in Vivo, *Journal of Neurogenetics,* 13 (4), 233-255.

Estrada, B., Casares, F., and Sanchez-Herrero, E. (2003), Development of the Genitalia in Drosophila Melanogaster, *Differentiation,* 71, 299-310.

Estrada, B., Casares, F., Busturia, A., and Sanchez-Herrero, E. (2002), Genetic and Molecular Characterization of a Novel Iab-8 Regulatory Domain in the Abdominal-B Gene of Drosophila Melanogaster, *Development,* 129, 5195-5204.

Falk, R., Bleiser-Avivi, N., and Atidia, J. (1976), Labellar Taste Organs of Drosophila Melanogaster, *J Morphol,* 150 (2), 327-341.

Fan, P., Manoli, D. S., Ahmed, O. M., Chen, Y., Agarwal, N., Kwong, S., . . . Shah, N. M. (2013), Genetic and Neural Mechanisms That Inhibit Drosophila from Mating with Other Species, *Cell,* 154 (1), 89-102.

Feinberg, E. H., Vanhoven, M. K., Bendesky, A., Wang, G., Fetter, R. D., Shen, K., and Bargmann, C. I. (2008), Gfp Reconstitution across Synaptic Partners (Grasp) Defines Cell Contacts and Synapses in Living Nervous Systems, *Neuron,* 57 (3), 353-363.

Felsenberg, J., Barnstedt, O., Cognigni, P., Lin, S., and Waddell, S. (2017), Re-Evaluation of Learned Information in Drosophila, *Nature,* 544 (7649), 240-244.

Ferveur, J. F. (2005), Cuticular Hydrocarbons: Their Evolution and Roles in Drosophila Pheromonal Communication, *Behaviour Genetics,* 35, 279-295.

Fischer, J. A., Giniger, E., Maniatis, T., and Ptashne, M. (1988), Gal4 Activates Transcription in Drosophila, *Nature,* 332 (6167), 853-856.

Flood, T. F., Iguchi, S., Gorczyca, M., White, B., Ito, K., and Yoshihara, M. (2013), A Single Pair of Interneurons Commands the Drosophila Feeding Motor Program, *Nature,* 499 (7456), 83-87.

Gailey, D. A. and Hall, J. C. (1989), Behavior and Cytogenetics of Fruitless in Drosophila Melanogaster: Different Courtship Defects Caused by Separate, Closely Linked Lesions, *Genetics,* 121 (4), 773-785.

Gailey, D. A., Taylor, B. J., and Hall, J. C. (1991), Elements of the Fruitless Locus Regulate Development of the Muscle of Lawrence, a Male-Specific Structure in the Abdomen of Drosophila Melanogaster Adults, *Development,* 113 (3), 879-890.

Gao, S., Takemura, S. Y., Ting, C. Y., Huang, S., Lu, Z., Luan, H., . . . Lee, C. H. (2008), The Neural Substrate of Spectral Preference in Drosophila, *Neuron,* 60 (2), 328-342.

Gaszner, M. and Felsenfeld, G. (2006), Insulators: Exploiting Transcriptional and Epigenetic Mechanisms, *Nat Rev Genet,* 7 (9), 703-713.

Geyer, P. K., Spana, C., and Gorces, V. G. (1986), On the Molecular Mechanism of Gypsy-Induced Mutations at the Yellow Locus of Drosophila Melanogaster, *EMBO J,* 5 (10), 2657-2662.

Ghosh, N., Bakshi, A., Khandelwal, R., Rajan, S. G., and Joshi, R. (2019), The Hox Gene Abdominal-B Uses Doublesex(F) as a Cofactor to Promote Neuroblast Apoptosis in the Drosophila Central Nervous System, *Development,* 146 (16).

Gilchrist, A. S. and Partridge, L. (2000), Why It Is Difficult to Model Sperm Displacement in Drosophila Melanogaster: The Relation between Sperm Transfer and Copulation Duration, *Evolution,* 54, 534-542.

Gill, K. S. (1963), A Mutation Causing Abnormal Mating Behaviour, *Drosophila Information Service,* 38, 33.

Gomez-Marin, A. and Louis, M. (2012), Active Sensation During Orientation Behavior in the Drosophila Larva: More Sense Than Luck, *Curr Opin Neurobiol,* 22 (2), 208-215.

Goodwin, S. F., Taylor, B. J., Villella, A., Foss, M., Ryner, L. C., Baker, B. S., and Hall, J. C. (2000), Aberrant Splicing and Altered Spatial Expression Patterns in Fruitless Mutants of Drosophila Melanogaster, *Genetics,* 154, 725-745.

Griffith, L. C. and Ejima, A. (2009), Courtship Learning in Drosophila Melanogaster: Diverse Plasticity of a Reproductive Behavior, *Learn Mem,* 16 (12), 743-750.

Groth, A. C. and Calos, M. P. (2004), Phage Integrases: Biology and Applications, *J Mol Biol,* 335 (3), 667-678.

Groth, A. C., Fish, M., Nusse, R., and Calos, M. P. (2004), Construction of Transgenic Drosophila by Using the Site-Specific Integrase from Phage Phic31, *Genetics,* 166, 1775-1782.

Grover, D., Katsuki, T., and Greenspan, R. J. (2016), Flyception: Imaging Brain Activity in Freely Walking Fruit Flies, *Nat Methods,* 13 (7), 569-572.

Grueber, W. B., Ye, B., Moore, A. W., Jan, L. Y., and Jan, Y. N. (2003), Dendrites of Distinct Classes of Drosophila Sensory Neurons Show Different Capacities for Homotypic Repulsion, *Current Biology,* 13 (8), 618-626.

Grueber, W. B., Ye, B., Yang, C. H., Younger, S., Borden, K., Jan, L. Y., and Jan, Y. N. (2007), Projections of Drosophila Multidendritic Neurons in the Central Nervous System: Links with Peripheral Dendrite Morphology, *Development,* 134 (1), 55-64.

Grunert, U. and Gnatzy, W. (1987), K+ and Ca++ in the Receptor Lymph of Arthropod Cuticular Mechanoreceptors, *Journal of Comparative Physiology,* 161, 329-333.

Hall, J. C. (1979), Control of Male Reproductive Behaviour by the Central Nervous System of Drosophila, Dissection of a Courtship Pathway by Genetic Mosaics, *Genetics,* 92, 437-457.

Hampel, S., McKellar, C. E., Simpson, J. H., and Seeds, A. M. (2017), Simultaneous Activation of Parallel Sensory Pathways Promotes a Grooming Sequence in Drosophila, *Elife,* 6.

Hartenstein, V. and Posakony, J. W. (1990), A Dual Function of the Notch Gene in Drsosophila Sensillum Development, *Developmental Biology,* 142 (1), 13-30.

Hasemeyer, M., Yapici, N., Heberlein, U., and Dickson, B. J. (2009), Sensory Neurons in the Drosophila Genital Tract Regulate Female Reproductive Behavior, *Neuron,* 61 (4), 511-518.

Held, L. I., Jr. (2002), Bristles Induce Bracts Via the Egfr Pathway on Drosophila Legs, *Mech Dev,* 117 (1-2), 225-234.

Hewes, R. S. and Taghert, P. H. (2001), Neuropeptides and Neuropeptide Receptors in the Drosophila Melanogaster Genome, *Genome Res,* 11 (6), 1126-1142.

Hou, Q. L., Chen, E. H., Jiang, H. B., Yu, S. F., Yang, P. J., Liu, X. Q., . . . Smagghe, G. (2018), Corazonin Signaling Is Required in the Male for Sperm Transfer in the Oriental Fruit Fly Bactrocera Dorsalis, *Front Physiol,* 9, 660.

Ijspeert, A. J. (2014), Biorobotics: Using Robots to Emulate and Investigate Agile Locomotion, *Science,* 346 (6206), 196-203.

Inoue, K., Hoshijima, K., Sakamoto, H., and Shimura, Y. (1990), Binding of the Drosophila Sexlethal Gene Product to the Alternative Splice Site of Transformer Primary Transcript, *Nature,* 344, 461-463.

Isono, K. and Morita, H. (2010), Molecular and Cellular Designs of Insect Taste Receptor System, *Front Cell Neurosci,* 4, 20.

Ito, H., Fujitani, K., Usui, K., Shimizu-Nishikawa, K., Tanaka, S., and Yamamoto, D. (1996), Sexual Orientation in Drosophila Is Altered by the Satori Mutation in the Sex-Determination Gene Fruitless That Encodes a Zinc Finger Protein with a Btb Domain, *PNAS,* 93, 9687-9692.

Ito, K., Shinomiya, K., Ito, M., Armstrong, J. D., Boyan, G., Hartenstein, V., . . . Insect Brain Name Working, G. (2014), A Systematic Nomenclature for the Insect Brain, *Neuron,* 81 (4), 755-765.

Jackson, F. R., Newby, L. M., and Kulkarni, S. J. (1990), Drosophila Gabaergic Systems: Sequence and Expression of Glutamic Acid Decarboxylase, *Journal of Neurochemistry,* 54, 1068-1078.

Jaffe, D. B., Johnston, D., Lasser-Ross, N., Lisman, J. E., Miyakawa, H., and Ross, W. N. (1992), The Spread of Na + Spikes Determines the Pattern of Dendritic Ca2+ Entry into Hippocampal Neurons, *Nature,* 357, 244-246.

Jagadeeshan, S. and Singh, R. S. (2006), A Time-Sequence Functional Analysis of Mating Behaviour and Genital Coupling in Drosophila: Role of Cryptic Female Choice and Male Sex-Drive in the Evolution of Male Genitalia, *J Evol Biol,* 19 (4), 1058-1070.

Jallon, J.-M. (1984), A Few Chemical Words Exchanged by Drosophila During Courtship and Mating, *Behaviour Genetics,* 14, 441-478.

Jan, Y. N. and Jan, L. Y. (1993), 'The Peripheral Nervous System', *The Development of Drosophila Melanogaster* (1; New York: Cold Spring Harbor Laboratory Press), 1207-1244.

Jefferis, G. S., Potter, C. J., Chan, A. M., Marin, E. C., Rohlfing, T., Maurer, C. R., Jr., and Luo, L. (2007), Comprehensive Maps of Drosophila Higher Olfactory Centers: Spatially Segregated Fruit and Pheromone Representation, *Cell,* 128 (6), 1187-1203.

Jenett, A., Rubin, G. M., Ngo, T. T., Shepherd, D., Murphy, C., Dionne, H., . . . Zugates, C. T. (2012), A Gal4-Driver Line Resource for Drosophila Neurobiology, *Cell Rep,* 2 (4), 991-1001.

Jones, W. D. (2009), The Expanding Reach of the Gal4/Uas System into the Behavioural Neurobiology of Drosophila, *BMB Reports*, 705-712.

Jory, A., Estella, C., Giorgianni, M. W., Slattery, M., Laverty, T. R., Rubin, G. M., and Mann, R. S. (2012), A Survey of 6,300 Genomic Fragments for Cis-Regulatory

Activity in the Imaginal Discs of Drosophila Melanogaster, *Cell Rep,* 2 (4), 1014-1024.

Jursnich, V. A. and Burtis, K. C. (1993), A Positive Role in Differentiation for the Male Doublesex Protein of Drosophila, *Developmental Biology,* 155, 235-249.

Kabra, M., Robie, A. A., Rivera-Alba, M., Branson, S., and Branson, K. (2013), Jaaba: Interactive Machine Learning for Automatic Annotation of Animal Behavior, *Nat Methods,* 10 (1), 64-67.

Kaliss, N. and Graubard, M. A. (1936), The Effect of Temperature on Oviposition in Drosophila Melanogaster, *Biological Bulletin,* 70 (3), 385-391.

Kamikouchi, A., Shimada, T., and Ito, K. (2006), Comprehensive Classification of the Auditory Sensory Projections in the Brain of the Fruit Fly Drosophila Melanogaster, *J Comp Neurol,* 499 (3), 317-356.

Kamimura, Y. (2010), Copulation Anatomy of Drosophila Melanogaster (Diptera: Drosophilidae): Wound-Making Organs and Their Possible Roles, *Zoomorphology,* 129 (3), 163-174.

Kamimura, Y. (2012), Correlated Evolutionary Changes in Drosophila Female Genitalia Reduce the Possible Infection Risk Caused by Male Copulatory Wounding, *Behavioral Ecology and Sociobiology,* 66 (8), 1107-1114.

Kamimura, Y. and Mitsumoto, H. (2011), Comparative Copulation Anatomy of the Drosophila Melanogaster Species Complex (Diptera: Drosophilidae), *Entomological Science,* 14 (4), 399-410.

Keegan, L., Gill, G., and Ptashne, M. (1986), Separation of DNA Binding from the Transcription-Activating Function of a Eukaryotic Regulatory Protein., *Science,* 231 (4739), 699-704.

Kellum, R. and Schedl, P. (1991), A Position-Effect Assay for Boundaries of Higher Order Chromosomal Domains, *Cell,* 64, 941-950.

Kellum, R. and Schedl, P. (1992), A Group of Scs Elements Function as Domain Boundaries in an Enhancer-Blocking Assay, *Molecular and Cellular Biology,* 12, 2424-2431.

Kernan, M., Cowan, D., and Zuker, C. (1994), Genetic Dissection of Mechanosensory Transduction: Mechanoreception-Defective Mutations of Drosophila, *Neuron,* 12, 1195-1206.

Kim, Coste, B., Chadha, A., Cook, B., and Patapoutian, A. (2012), The Role of Drosophila Piezo in Mechanical Nociception, *Nature,* 483 (7388), 209-212.

Kim, Chung, Y. D., Park, D.-Y., Choi, S. K., Shin, D. W., Soh, H., . . . Kim, C. (2003), A Trpv Family Ion Channel Required for Hearing in Drosophila, *Nature,* 424.

Kim, W. J., Jan, L. Y., and Jan, Y. N. (2013), A Pdf/Npf Neuropeptide Signaling Circuitry of Male Drosophila Melanogaster Controls Rival-Induced Prolonged Mating, *Neuron,* 80 (5), 1190-1205.

Kimura, K., Ote, M., Tazawa, T., and Yamamoto, D. (2005), Fruitless Specifies Sexually Dimorphic Neural Circuitry in the Drosophila Brain, *Nature,* 438 (7065), 229-233.

Kimura, K., Hachiya, T., Koganezawa, M., Tazawa, T., and Yamamoto, D. (2008), Fruitless and Doublesex Coordinate to Generate Male-Specific Neurons That Can Initiate Courtship, *Neuron,* 59 (5), 759-769.

Kitamoto, T. (2001), Conditional Modification of Behaviour in Drosophila by Targeted Expression of a Temperature-Sensitive Shibire Allele in Defined Neurons, *Journal of Neurobiology,* 47, 91-92.

Klapoetke, N. C., Murata, Y., Kim, S. S., Pulver, S. R., Birdsey-Benson, A., Cho, Y. K., . . . Boyden, E. S. (2014), Independent Optical Excitation of Distinct Neural Populations, *Nat Methods,* 11 (3), 338-346.

Kohl, J., Ostrovsky, A. D., Frechter, S., and Jefferis, G. S. (2013), A Bidirectional Circuit Switch Reroutes Pheromone Signals in Male and Female Brains, *Cell,* 155 (7), 1610-1623.

Konopka, R. J. (1987), Genetics of Biological Rhythms in Drosophila, *Annu Rev Genet,* 21, 227-236.

Kopp, A. (2012), Dmrt Genes in the Development and Evolution of Sexual Dimorphism, *Trends Genet,* 28 (4), 175-184.

Kornberg, T., Siden, I., O'Farrell, P., and Simon, M. (1985), The Engrailed Locus of Drosophila: In Situ Localization of Transcripts Reveals Compartment Specific Expression, *Cell,* 40, 45-53.

Kubli, E. (1996), The Drosophila Sex-Peptide: A Peptide Pheromone Involved in Reproduction, *Advances in Developmental Biochemistry,* 4, 99-128.

Kubli, E. (2008), Sexual Behaviour: A Receptor for Sex Control in Drosophila Females, *Curr Biol,* 18 (5), R210-212.

Kuraishi, T., Kenmoku, H., and Kurata, S. (2015), From Mouth to Anus: Functional and Structural Relevance of Enteric Neurons in the Drosophila Melanogaster Gut, *Insect Biochem Mol Biol,* 67, 21-26.

Kwon, Y., Shen, W. L., Shim, H. S., and Montell, C. (2010), Fine Thermotactic Discrimination between the Optimal and Slightly Cooler Temperatures Via a Trpv Channel in Chordotonal Neurons, *J Neurosci,* 30 (31), 10465-10471.

Kyriacou, C. P. and Hall, J. C. (1980), Circadian Rhythm Mutations in Drosophila Melanogaster Affect Short-Term Fluctuations in the Male's Courtship Song, *PNAS,* 77 (11), 6729-6733.

Lai and Orgogozo, V. (2004), A Hidden Program in Drosophila Peripheral Neurogenesis Revealed: Fundamental Principles Underlying Sensory Organ Diversity, *Dev Biol,* 269 (1), 1-17.

Lai and Lee, T. (2006), Genetic Mosaic with Dual Binary Transcriptional Systems in Drosophila, *Nat Neurosci,* 9 (5), 703-709.

Laughton, A. and Gesteland, R. F. (1984), Primary Structure of the Saccharomyces Cerevisiae Gal4 Gene., *Molecular and Cellular Biology,* 4, 119-122.

Lawrence, P. A. and Johnston, P. (1984), The Genetic Specification of Pattern in a Drosophila Muscle, *Cell,* 36 (3), 775-782.

Lee, G., Foss, M., Goodwin, S. F., Carlo, T., Taylor, B. J., and Hall, J. C. (2000), Spatial, Temporal, and Sexually Dimorphic Expression Patterns of the Fruitless Gene in the Drosophila Central Nervous System, *J Neurobiol,* 43 (4), 404-426.

Lee, J., Moon, S., Cha, Y., and Chung, Y. D. (2010), Drosophila Trpn(=Nompc) Channel Localizes to the Distal End of Mechanosensory Cilia, *PLoS One,* 5 (6), e11012.

Lee, T. and Luo, L. (1999), Mosaic Analysis with a Repressible Cell Marker for Studies of Gene Function in Neuronal Morphogenesis, *Neuron,* 22, 451-461.

Lima, S. Q. and Miesenbock, G. (2005), Remote Control of Behavior through Genetically Targeted Photostimulation of Neurons, *Cell,* 121 (1), 141-152.

Liu, H. and Kubli, E. (2003), Sex-Peptide Is the Molecular Basis of the Sperm Effect in Drosophila Melanogaster, *PNAS,* 100, 9929-9933.

Lo, L. and Anderson, D. J. (2011), A Cre-Dependent, Anterograde Transsynaptic Viral Tracer for Mapping Output Pathways of Genetically Marked Neurons, *Neuron,* 72 (6), 938-950.

Luan, H., Peabody, N. C., Vinson, C. R., and White, B. H. (2006), Refined Spatial Manipulation of Neuronal Function by Combinatorial Restriction of Transgene Expression, *Neuron,* 52 (3), 425-436.

Ma, J. and Ptashne, M. (1987), The Carboxy Terminal 30 Amino Acids of Gal4 Are Recognized by Gal80, *Cell,* 50, 137-142.

Macpherson, L. J., Zaharieva, E. E., Kearney, P. J., Alpert, M. H., Lin, T. Y., Turan, Z., . . . Gallio, M. (2015), Dynamic Labelling of Neural Connections in Multiple Colours by Trans-Synaptic Fluorescence Complementation, *Nat Commun,* 6, 10024.

Mahr, A. and Aberle, H. (2006), The Expression Pattern of the Drosophila Vesicular Glutamate Transporter: A Marker Protein for Motoneurons and Glutamatergic Centers in the Brain, *Gene Expr Patterns,* 6 (3), 299-309.

Mamiya, A., Gurung, P., and Tuthill, J. C. (2018), Neural Coding of Leg Proprioception in Drosophila, *Neuron,* 100 (3), 636-650 e636.

Manev, H. and Dzitoyeva, S. (2010), Gaba-B Receptors in Drosophila, *Advances in Pharmacology,* 58, 453-464.

Mank, M. and Griesbeck, O. (2008), Genetically Encoded Calcium Indicators, *Chem. Rev.,* 108, 1550-1564.

Manoli, D. S., Foss, M., Villella, A., Taylor, B. J., Hall, J. C., and Baker, B. S. (2005), Male-Specific Fruitless Specifies the Neural Substrates of Drosophila Courtship Behaviour, *Nature,* 436 (7049), 395-400.

Markow, T., A. (1987), Behavioural and Sensory Basis of Courtship Success in Drosophila Melanogaster, *PNAS,* 84, 6200-6204.

Markstein, M., Pitsouli, C., Villalta, C., Celniker, S. E., and Perrimon, N. (2008), Exploiting Position Effects and the Gypsy Retrovirus Insulator to Engineer Precisely Expressed Transgenes, *Nat Genet,* 40 (4), 476-483.

Mathis, A., Mamidanna, P., Cury, K. M., Abe, T., Murthy, V. N., Mathis, M. W., and Bethge, M. (2018), Deeplabcut: Markerless Pose Estimation of User-Defined Body Parts with Deep Learning, *Nat Neurosci,* 21 (9), 1281-1289.

McNabb, S. L., Bakers, J. D., Agapite, J., Steller, H., Riddiford, L. M., and Truman, J. W. (1997), Disruption of a Behavioural Sequence by Targeted Death of Peptidergic Neurons in Drosophila, *Neuron,* 19, 813-823.

McRobert, S. P., Tompkins, L., Barr, N. B., Bradner, J., Lucas, D., Rattigan, D. M., and Tannous, A. F. (2003), Mutations in Raised Drosophila Melanogaster Affect Experience-Dependent Aspects of Sexual Behavior in Both Sexes, *Behaviour Genetics,* 33, 347-356.

Mellert, D. J., Knapp, J. M., Manoli, D. S., Meissner, G. W., and Baker, B. S. (2010), Midline Crossing by Gustatory Receptor Neuron Axons Is Regulated by Fruitless, Doublesex and the Roundabout Receptors, *Development,* 137 (2), 323-332.

Min, S., Ai, M., Shin, S. A., and Suh, G. S. (2013), Dedicated Olfactory Neurons Mediating Attraction Behavior to Ammonia and Amines in Drosophila, *Proc Natl Acad Sci U S A,* 110 (14), E1321-1329.

Morimura, S., Maves, L., Chen, Y., and Hoffmann, F. M. (1996), Decapentaplegic Overexpression Affects Drosophila Wing and Leg Imaginal Disc Development and Wingless Expression, *Dev Biol,* 177 (1), 136-151.

Muller, W. and Connor, J. A. (1991), Cholinergic Input Uncouples Ca2+ Changes from K+ Conducatance Activation and Amplifies Intradendritic Ca2+ Changes in Hippocampal Neurons, *Neuron,* 6 (6), 901-905.

Murphey, R. K., Possidente, D. R., Vandervorst, P., and Ghysen, A. (1989), Compartments and the Topography of Leg Afferent Projections in Drosophila, *The Journal of Neuroscience,* 9 (9), 3209-3217.

Nagarkar-Jaiswal, S., DeLuca, S. Z., Lee, P. T., Lin, W. W., Pan, H., Zuo, Z., . . . Bellen, H. J. (2015), A Genetic Toolkit for Tagging Intronic Mimic Containing Genes, *Elife,* 4.

Nagel, G., Szellas, T., Huhn, W., Kateriya, S., Adeishvili, N., Berthold, P., . . . Bamberg, E. (2003), Channelrhodopsin-2, a Directly Light-Gated Cation-Selective Membrane Channel, *PNAS,* 100 (24), 13940-13945.

Nagoshi, R. N., McKeown, M., Burtis, K. C., Belote, J. M., and Baker, B. S. (1988), The Control of Alternative Splicing at Genes Regulating Sexual Differentiation in D. Melanogaster, *Cell,* 53, 229-236.

Nath, T., Mathis, A., Chen, A. C., Patel, A., Bethge, M., and Mathis, M. W. (2019), Using Deeplabcut for 3d Markerless Pose Estimation across Species and Behaviors, *Nat Protoc,* 14 (7), 2152-2176.

Neville, M. C., Nojima, T., Ashley, E., Parker, D. J., Walker, J., Southall, T., . . . Goodwin, S. F. (2014), Male-Specific Fruitless Isoforms Target Neurodevelopmental Genes to Specify a Sexually Dimorphic Nervous System, *Curr Biol,* 24 (3), 229-241.

Nicolai, L. J. J., Ramaekers, A., Ramaekers, T., Drozdzecki, A., Mauss, A. S., Yan, J., . . . Hassan, B. A. (2010), Genetically Encoded Dendritic Marker Sheds Light on Neural Connectivity in Drosophila, *PNAS,* 107 (47), 20553-20558.

Olsen, S. R. and Wilson, R. I. (2008), Cracking Neural Circuits in a Tiny Brain: New Approaches for Understanding the Neural Circuitry of Drosophila, *Trends Neurosci,* 31 (10), 512-520.

Ostrovsky, A., Cachero, S., and Jefferis, G. (2013), Clonal Analysis of Olfaction in Drosophila: Image Registration, *Cold Spring Harb Protoc,* 2013 (4), 347-349.

Parks, A. L. and Muskavitch, M. A. T. (1993), Delta Function Is Required for Bristle Organ Determination and Morphogenesis in Drosophila, *Developmental Biology,* 157, 484-496.

Patterson, G. H. and Lippincott-Schwartz, J. (2002), A Photoactivatable Gfp for Selective Photolabelling of Proteins and Cells, *Science,* 297, 1873-1877.

Pavlou, H. J. and Goodwin, S. F. (2013), Courtship Behavior in Drosophila Melanogaster: Towards a 'Courtship Connectome', *Curr Opin Neurobiol,* 23 (1), 76-83.

Pavlou, H. J., Lin, A. C., Neville, M. C., Nojima, T., Diao, F., Chen, B. E., . . . Goodwin, S. F. (2016), Neural Circuitry Coordinating Male Copulation, *Elife,* 5.

Peabody, N. C., Pohl, J. B., Diao, F., Vreede, A. P., Sandstrom, D. J., Wang, H., . . . White, B. H. (2009), Characterization of the Decision Network for Wing Expansion in Drosophila Using Targeted Expression of the Trpm8 Channel, *J Neurosci,* 29 (11), 3343-3353.

Pfeiffer, B. D., Ngo, T. T., Hibbard, K. L., Murphy, C., Jenett, A., Truman, J. W., and Rubin, G. M. (2010), Refinement of Tools for Targeted Gene Expression in Drosophila, *Genetics,* 186 (2), 735-755.

Pfeiffer, B. D., Jenett, A., Hammonds, A. S., Ngo, T.-T., Misra, S., Murphy, C., . . . Rubin, G. M. (2008), Tools for Neuroanatomy and Neurogenetics in Drosophila, *PNAS,* 105 (28), 9715–9720.

Pologruto, T. A., Sabatini, B. L., and Svoboda, K. (2003), Scanimage: Flexible Software for Operating Laser Scanning Microscopes, *BioMedical Engineering OnLine,* 2.

Pologruto, T. A., Yasuda, R., and Svoboda, K. (2004), Monitoring Neural Activity and [Ca2+] with Genetically Encoded Ca2+ Indicators, *J Neurosci,* 24 (43), 9572-9579.

Potter, C. J., Tasic, B., Russler, E. V., Liang, L., and Luo, L. (2010), The Q System: A Repressible Binary System for Transgene Expression, Lineage Tracing, and Mosaic Analysis, *Cell,* 141 (3), 536-548.

Power, M. E. (1948), The Thoracico-Abdominal Nervous System of an Adult Insect Drosophila Melanogaster, *J Comp Neurol,* 88 (3), 347-409.

Ram, K. R. and Wolfner, M. F. (2007), Seminal Influences: Drosophila Acps and the Molecular Interplay between Males and Females During Reproduction, *Integr Comp Biol,* 47 (3), 427-445.

Rezaval, C., Nojima, T., Neville, M. C., Lin, A. C., and Goodwin, S. F. (2014), Sexually Dimorphic Octopaminergic Neurons Modulate Female Postmating Behaviors in Drosophila, *Curr Biol,* 24 (7), 725-730.

Rezaval, C., Pavlou, H. J., Dornan, A. J., Chan, Y. B., Kravitz, E. A., and Goodwin, S. F. (2012), Neural Circuitry Underlying Drosophila Female Postmating Behavioral Responses, *Curr Biol,* 22 (13), 1155-1165.

Rhyu, M. S., Jan, L., Y., and Jan, Y. N. (1994), Asymmetric Distribution of Numb Protein During Division of the Sensory Organ Precursor Cell Confers Distinct Fates to Daughter Cells, *Cell,* 76, 477-491.

Riabinina, O., Dai, M., Duke, T., and Albert, J. T. (2011), Active Process Mediates Species-Specific Tuning of Drosophila Ears, *Curr Biol,* 21 (8), 658-664.

Rice, David, J. R., Kamimura, Y., Masly, J. P., McGregor, A. P., Nagy, O., . . . Yassin, A. (2019), A Standardized Nomenclature and Atlas of the Male Terminalia of Drosophila Melanogaster, *Fly (Austin),* 13 (1-4), 51-64.

Rice, M. J. (1977), Blowfly Ovipositor Receptor Neurone Sensitive to Monovalent Cation Concentration, *Nature,* 268, 747-750.

Rideout, E. J., Billeter, J. C., and Goodwin, S. F. (2007), The Sex-Determination Genes Fruitless and Doublesex Specify a Neural Substrate Required for Courtship Song, *Curr Biol,* 17 (17), 1473-1478.

Rideout, E. J., Dornan, A. J., Neville, M. C., Eadie, S., and Goodwin, S. F. (2010), Control of Sexual Differentiation and Behavior by the Doublesex Gene in Drosophila Melanogaster, *Nat Neurosci,* 13 (4), 458-466.

Ritchie, M. G., Halsey, E., J., and Gleason, J. M. (1999), Drosophila Song as a Species-Specific Mating Signal and the Behavioural Importance of Kyriacou & Hall Cycles in D. Melanogaster Song, *Animal Behaviour,* 58, 1-9.

Robertson, H. M. (1988), Mating Asymmetries and Phylogeny in the Drosophila Melanogaster Species Complex, *Pacific Science,* 42, 72-80.

Robinett, C. C., Vaughan, A. G., Knapp, J. M., and Baker, B. S. (2010), Sex and the Single Cell. Ii. There Is a Time and Place for Sex, *PLoS Biology,* 8 (5), e1000365.

Royet, J. and Finkelstein, R. (1997), Establishing Primordia in the Drosophila Eye-Antennal Imaginal Disc: The Roles of Decapentaplegic, Wingless and Hedgehog, *Development,* 124 (23), 4793-4800.

Ruta, V., Datta, S. R., Vasconcelos, M. L., Freeland, J., Looger, L. L., and Axel, R. (2010), A Dimorphic Pheromone Circuit in Drosophila from Sensory Input to Descending Output, *Nature,* 468 (7324), 686-690.

Ryner, L. C., Goodwin, S. F., Castrillon, D. H., Anand, A., Villella, A., Baker, B. S., . . . Wasserman, S. A. (1996), Control of Male Sexual Behavior and Sexual Orientation in Drosophila by the Fruitless Gene, *Cell,* 87 (6), 1079-1089.

Sanchez-Alcaniz, J. A., Zappia, G., Marion-Poll, F., and Benton, R. (2017), A Mechanosensory Receptor Required for Food Texture Detection in Drosophila, *Nat Commun,* 8, 14192.

Sanchez-Herrero, E., Vernos, I., Marco, R., and Morata, G. (1985), Genetic Organization of Drosophila Bithorax Complex, *Nature,* 313 (5998), 108-113.

Sanicola, M., Sekelsky, J., Elson, S., and Gelbart, W. M. (1995), Drawing a Stripe in Drosophila Imaginal Disc: Negative Regulation of Decapentaplegic and Patched Expression by Engrailed, *Genetics,* 139, 745-756.

Sawamura, K. and Tomaru, M. (2002), Biology of Reproductive Isolation in Drosophila: Toward a Better Understanding of Speciation, *Population Ecology,* 44, 209-219.

Schilcher, F. V. (1976a), The Behaviour of Cacophony, a Courtship Song Mutant in Drosophila Melanogaster, *Behavioural Biology,* 17, 187-196.

Schilcher, F. V. (1976b), The Role of Auditory Stimuli in the Courtship of Drosophila Melanogaster, *Animal Behaviour,* 24, 18-26.

Schindelin, J., Rueden, C. T., Hiner, M. C., and Eliceiri, K. W. (2015), The Imagej Ecosystem: An Open Platform for Biomedical Image Analysis, *Mol Reprod Dev,* 82 (7-8), 518-529.

Schindelin, J., Arganda-Carreras, I., Frise, E., Kaynig, V., Longair, M., Pietzsch, T., . . . Cardona, A. (2012), Fiji: An Open-Source Platform for Biological-Image Analysis, *Nat Methods,* 9 (7), 676-682.

Schnakenberg, S. L., Siegal, M. L., and Bloch Qazi, M. C. (2012), Oh, the Places They'll Go: Female Sperm Storage and Sperm Precedence in Drosophila Melanogaster, *Spermatogenesis,* 2 (3), 224-235.

Schroeder, C. E., Wilson, D. A., Radman, T., Scharfman, H., and Lakatos, P. (2010), Dynamics of Active Sensing and Perceptual Selection, *Curr Opin Neurobiol,* 20 (2), 172-176.

Schweisguth, F., Gho, M., and Lecourtois, M. (1996), Control of Cell Fate Choices by Lateral Signalling in the Adult Peripheral Nervous System of Drosophila Melanogaster, *Developmental Genetics,* 18, 28-39.

Seeds, A. M., Ravbar, P., Chung, P., Hampel, S., Midgley, F. M., Jr., Mensh, B. D., and Simpson, J. H. (2014), A Suppression Hierarchy among Competing Motor Programs Drives Sequential Grooming in Drosophila, *Elife,* 3, e02951.

Shimono, K., Fujimoto, A., Tsuyama, T., Yamamoto-Kochi, M., Sato, M., Hattori, Y., . . . Uemura, T. (2009), Multidendritic Sensory Neurons in the Adult Drosophila Abdomen: Origins, Dendritic Morphology, and Segment- and Age-Dependent Programmed Cell Death, *Neural Dev,* 4, 37.

Shorey, H. H. (1962), Nature of the Sound Produced by Drosophila Melanogaster During Courtship, *Science,* 137, 677-678.

Siegel, R. W. and Hall, J. C. (1979), Conditioned Responses in Courtship Behaviour of Normal and Mutant Drosophila, *PNAS,* 7, 3430-3434.

Siwicki, K. K., Riccio, P., Ladewski, L., Marcillac, F., Dartevelle, L., Cross, S. A., and Ferveur, J. F. (2005), The Role of Cuticular Pheromones in Courtship Conditioning of Drosophila Males, *Learn Mem,* 12 (6), 636-645.

Sokolowski, M. B. (2001), Drosophila: Genetics Meets Behaviour, *Nat Rev Genet,* 2 (11), 879-890.

Spieth, H., T. (1974), Courtship Behaviour in Drosophila, *Annu Rev Entomology,* 19, 385-405.

Stockinger, P., Kvitsiani, D., Rotkopf, S., Tirian, L., and Dickson, B. J. (2005), Neural Circuitry That Governs Drosophila Male Courtship Behavior, *Cell,* 121 (5), 795-807.

Suster, M. L., Seugnet, L., Bate, M., and Sokolowski, M. B. (2004), Refining Gal4-Driven Transgene Expression in Drosophila with a Gal80 Enhancer-Trap, *Genesis,* 39 (4), 240-245.

Sweeney, S., Broadie, K., Keane, J., Niemann, H., and O'Kane, C. J. (1995), Targeted Expression of Tetanus Toxin Light Chain in Drosophila Specifically Eliminates Synaptic Transmission and Causes Behavioural Defects, *Neuron,* 14, 341-351.

Talay, M., Richman, E. B., Snell, N. J., Hartmann, G. G., Fisher, J. D., Sorkaç, A., . . . Barnea, G. (2017), Transsynaptic Mapping of Second-Order Taste Neurons in Flies by Trans -Tango, *Neuron*.

Taylor, B. J. (1989), Sexually Dimorphic Neurons in the Terminalia of Drosophila Melanogaster: I. Development of Sensory Neurons in the Genital Disc During Metamorphosis, *Journal of Neurogenetics,* 5 (3), 173-192.

Taylor, B. J., Villella, A., Ryner, L. C., Baker, B. S., and Hall, J. C. (1994), Behavioural and Neurobiological Implications of Sex-Determinging Factors in Drosophila, *Developmental Genetics,* 15, 275-296.

Theis, J. (1979), Mechanoreceptive Bristles on the Head of the Blowfly: Mechanics and Electrophysiology of the Macrochaete, *J. Comp. Physiol.,* 132, 55-68.

Thistle, R., Cameron, P., Ghorayshi, A., Dennison, L., and Scott, K. (2012), Contact Chemoreceptors Mediate Male-Male Repulsion and Male-Female Attraction During Drosophila Courtship, *Cell,* 149 (5), 1140-1151.

Tian, L., Hires, S. A., Mao, T., Huber, D., Chiappe, M. E., Chalasani, S. H., . . . Looger, L. L. (2009), Imaging Neural Activity in Worms, Flies and Mice with Improved Gcamp Calcium Indicators, *Nat Methods,* 6 (12), 875-881.

Ting, C. Y., Gu, S., Guttikonda, S., Lin, T. Y., White, B. H., and Lee, C. H. (2011), Focusing Transgene Expression in Drosophila by Coupling Gal4 with a Novel Split-Lexa Expression System, *Genetics,* 188 (1), 229-233.

Tiong, S., Bone, L. M., and Whittle, J. R. (1985), Recessive Lethal Mutations within the Bithorax-Complex in Drosophila, *Mol Gen Genet,* 200 (2), 335-342.

Tompkins, L., Siegel, R. W., Gailey, D. A., and Hall, J. C. (1983), Conditioned Courtship in Drosophila and Its Mediation by Association of Chemical Cues, *Behaviour Genetics,* 13 (6), 565-578.

Traven, A., Jelicic, B., and Sopta, M. (2006), Yeast Gal4: A Transcriptional Paradigm Revisited, *EMBO Rep,* 7 (5), 496-499.

Tsubouchi, A., Yano, T., Yokoyama, T. K., Murtin, C., Otsuna, H., and Ito, K. (2017), Topological and Modality-Specific Representation of Somatosensory Information in the Fly Brain, *Science,* 358, 615-623.

Turner, H. N., Armengol, K., Patel, A. A., Himmel, N. J., Sullivan, L., Iyer, S. C., . . . Cox, D. N. (2016), The Trp Channels Pkd2, Nompc, and Trpm Act in Cold-Sensing Neurons to Mediate Unique Aversive Behaviors to Noxious Cold in Drosophila, *Curr Biol,* 26 (23), 3116-3128.

Tuthill, J. C. and Wilson, R. I. (2016), Parallel Transformation of Tactile Signals in Central Circuits of Drosophila, *Cell,* 164 (5), 1046-1059.

Tuthill, J. C. and Azim, E. (2018), Proprioception, *Curr Biol,* 28 (5), R194-R203.

Untergasser, A., Cutcutache, I., Koressaar, T., Ye, J., Faircloth, B. C., Remm, M., and Rozen, S. G. (2012), Primer3--New Capabilities and Interfaces, *Nucleic Acids Res,* 40 (15), e115.

van der Goes van Naters, W. (2014), *Drosophila Phermones: From Reception to Perception*, in C. Mucignat-Caretta, *Neurobiology of Chemical Communication.* Taylor & Francis, Boca Raton, FL.

Vandervorst, P. and Ghysen, A. (1980), Genetic Control of Sensory Connections in Drosophila *Nature,* 286, 65-67.

Venken, K. J. and Bellen, H. J. (2005), Emerging Technologies for Gene Manipulation in Drosophila Melanogaster, *Nat Rev Genet,* 6 (3), 167-178.

Venken, K. J., Schulze, K. L., Haelterman, N. A., Pan, H., He, Y., Evans-Holm, M., . . . Bellen, H. J. (2011a), Mimic: A Highly Versatile Transposon Insertion Resource for Engineering Drosophila Melanogaster Genes, *Nat Methods,* 8 (9), 737-743.

Venken, K. J. T., Schulze, K. L., Haelterman, N. A., Pan, H., He, Y., Evans-Holm, M., . . . Bellen, H. J. (2011b), Mimic: A Highly Versatile Transposon Insertion Resource for Engineering Drosophila Melanogaster Genes, *Nature Methods,* 8 (9), 737-743.

Viktorinova, I. and Wimmer, E. A. (2007), Comparative Analysis of Binary Expression Systems for Directed Gene Expression in Transgenic Insects, *Insect Biochem Mol Biol,* 37 (3), 246-254.

Villella, A. and Hall, J. C. (1996), Courtship Anomalies Caused by Doublsex Mutation in Drosophila Melanogaster, *Genetics,* 143, 331-344.

Villella, A. and Hall, J. C. (2008), Neurogenetics of Courtship and Mating in Drosophila, *Advances in Genetics,* 62, 67-184.

Villella, A., Gailey, D. A., Berwald, B., Ohshima, S., Barnes, P. T., and Hall, J. C. (1997), Extended Reproductive Roles of the Fruitless Gene in Drosophila Melanogaster Revealed by Behavioral Analysis of New Fru Mutants, *Genetics,* 147, 1107-1130.

von Philipsborn, A. C., Liu, T., Yu, J. Y., Masser, C., Bidaye, S. S., and Dickson, B. J. (2011), Neuronal Control of Drosophila Courtship Song, *Neuron,* 69 (3), 509-522.

Walker, R. G., Willingham, A. T., and Zuker, C. S. (2000), A Drosophila Mechanosensory Transduction Channel, *Science,* 287, 2229-2234.

Wallrath, L., L. and Elgin, S., C,R. (1995), Position Effect Variegation in Drosophila Is Associated with an Altered Chromatin Structure, *Genes Dev,* 9, 1263-1277.

Waterbury, J. A., Jackson, L. L., and Schedl, P. (1999), Analysis of the Doublesex Female Protein in Drosophila Melanogaster: Role in Sexual Differentiation and Behavior and Dependence on Intersex, *Genetics,* 152, 1653-1667.

Williams, T. M., Selegue, J. E., Werner, T., Gompel, N., Kopp, A., and Carroll, S. B. (2008), The Regulation and Evolution of a Genetic Switch Controlling Sexually Dimorphic Traits in Drosophila, *Cell,* 134 (4), 610-623.

Yamamoto, M.-T. (2010), Drosophila Genetic Resource and Stock Center the National Bioresource Project, *Exp. Anim.,* 59, 125-138.

Yan, Z., Zhang, W., He, Y., Gorczyca, D., Xiang, Y., Cheng, L. E., . . . Jan, Y. N. (2013), Drosophila Nompc Is a Mechanotransduction Channel Subunit for Gentle-Touch Sensation, *Nature,* 493 (7431), 221-225.

Yang, C. H., Rumpf, S., Xiang, Y., Gordon, M. D., Song, W., Jan, L. Y., and Jan, Y. N. (2009), Control of the Postmating Behavioral Switch in Drosophila Females by Internal Sensory Neurons, *Neuron,* 61 (4), 519-526.

Yapici, N., Kim, Y. J., Ribeiro, C., and Dickson, B. J. (2008), A Receptor That Mediates the Post-Mating Switch in Drosophila Reproductive Behaviour, *Nature,* 451 (7174), 33-37.

Yassin, A. and Orgogozo, V. (2013), Coevolution between Male and Female Genitalia in the Drosophila Melanogaster Species Subgroup, *PLoS One,* 8 (2), e57158.

Yu, J. Y., Kanai, M. I., Demir, E., Jefferis, G. S., and Dickson, B. J. (2010), Cellular Organization of the Neural Circuit That Drives Drosophila Courtship Behavior, *Curr Biol,* 20 (18), 1602-1614.

Zavortink, M. and Sakonju, S. (1989), The Morphogenetic and Regulatory Functions of the Drosophila Abdominal-B Gene Are Encoded in Overlapping Rnas Transcribed from Separate Promotors, *Genes Dev,* 3, 1969-1981.

Zemelman, B., V., Nesnas, N., Lee, G., A., and Miesenböck, G. (2003), Photochemical Gating of Heterologous Ion Channels: Remote Control over Genetically Designated Populations of Neurons, *PNAS,* 100, 1352-1357.

Zer-Krispil, S., Zak, H., Shao, L., Ben-Shaanan, S., Tordjman, L., Bentzur, A., . . . Shohat-Ophir, G. (2018), Ejaculation Induced by the Activation of Crz Neurons Is Rewarding to Drosophila Males, *Curr Biol,* 28 (9), 1445-1452 e1443.

Zhang, L., Yu, J., Guo, X., Wei, J., Liu, T., and Zhang, W. (2020), Parallel Mechanosensory Pathways Direct Oviposition Decision-Making in Drosophila, *Curr Biol*.

Zhang, W., Yan, Z., Li, B., Jan, L. Y., and Jan, Y. N. (2014), Identification of Motor Neurons and a Mechanosensitive Sensory Neuron in the Defecation Circuitry of Drosophila Larvae, *Elife,* 3.

Zhang, W., Cheng, L. E., Kittelmann, M., Li, J., Petkovic, M., Cheng, T., . . . Jan, Y. N. (2015), Ankyrin Repeats Convey Force to Gate the Nompc Mechanotransduction Channel, *Cell,* 162 (6), 1391-1403.

Zingg, B., Chou, X. L., Zhang, Z. G., Mesik, L., Liang, F., Tao, H. W., and Zhang, L. I. (2017), Aav-Mediated Anterograde Transsynaptic Tagging: Mapping Corticocollicular Input-Defined Neural Pathways for Defense Behaviors, *Neuron,* 93 (1), 33-47.